Studies on poly (butylmethacrylate) with doped and undoped metal oxide nanoparticles

Thesis submitted to the
University of Calicut
in partial fulfilment of the requirements
for the award of the degree of

Doctor of Philosophy
in
Chemistry

by

SUHAILATH K

DEPARTMENT OF CHEMISTRY
UNIVERSITY OF CALICUT
KERALA-673635
2020

DEPARTMENT OF CHEMISTRY
UNIVERSITY OF CALICUT
THENHIPALAM, MALAPPURAM

KERALA-673 635

Dr. M.T Ramesan Tel: +91-9447837455
Asso. Professor E-mail: mtramesan@uoc.ac.in

Date: …….

Certificate

Certified that the research work embodied in the thesis entitled **"Studies on poly (butylmethacrylate) with doped and undoped metal oxide nanoparticles"** has been carried out by **Suhailath K** under my supervision at the Department of Chemistry, University of Calicut, Kerala and the same has not been submitted elsewhere previously for the award of any other degree or diploma.

University of Calicut **Dr. M.T Ramesan**

DEPARTMENT OF CHEMISTRY
UNIVERSITY OF CALICUT
THENHIPALAM, MALAPPURAM

KERALA-673 635

Dr. M.T Ramesan Tel: +91-9447837455
Asso. Professor E-mail: mtramesan@uoc.ac.in

Date: …….

Certificate

Certified that the research work embodied in the thesis entitled **"Studies on poly (butylmethacrylate) with doped and undoped metal oxide nanoparticles"** has been carried out by **Suhailath K** under my supervision at the Department of Chemistry, University of Calicut, Kerala. The contents of the thesis have been checked for plagiarism using the software 'Urkund' and the similarity index falls under permissible limit, and I further certify that the thesis or part has not previously formed the basis for the award of any degree, diploma or associate ship of any other University or Institute. The suggestions/corrections/recommendations/observations made by the adjudicators have been included in the revised thesis

University of Calicut **Dr. M.T Ramesan**

DEPARTMENT OF CHEMISTRY
UNIVERSITY OF CALICUT
THENHIPALAM, MALAPPURAM
KERALA-673 635

Dr. M.T Ramesan
Asso. Professor

Tel: +91-9447837455
E-mail: mtramesan@uoc.ac.in

Date: .....

Certificate

Certified that the research work embodied in the thesis entitled **"Studies on poly (butylmethacrylate) with doped and undoped metal oxide nanoparticles"** has been carried out by **Suhailath K** under my supervision at the Department of Chemistry, University of Calicut, Kerala. The contents of the thesis have been checked for plagiarism using the software 'Urkund' and the similarity index falls under permissible limit, and I further certify that the thesis or part has not previously formed the basis for the award of any degree, diploma or associate ship of any other University or Institute. The suggestions/corrections/recommendations/observations made by the adjudicators have been included in the revised thesis

University of Calicut

Dr. M.T Ramesan

Declaration

I hereby declare that the research work embodied in the thesis entitled **"Studies on poly (butylmethacrylate) with doped and undoped metal oxide nanoparticles"**, is based on the original research work carried out by me under the guidance of **Dr. M. T Ramesan**, Associate Professor, Department of Chemistry, University of Calicut, Kerala and the same has not been submitted elsewhere previously for the award of any other degree or diploma.

University of Calicut **Suhailath K**

Acknowledgment

There are many people who cheering with me throughout the research period, because of them only I fulfilled my dream successfully. So, it is my pleasure to express my sincere gratitude to them in words of acknowledgment.

First and foremost I express my heartfelt gratitude to my supervisor and mentor Dr. M. T Ramesan for his guidance and insights throughout the work. It has been a great privilege for me to work under a guide like him. He monitored my progress of work at correct time and encouraged with valuable suggestions and excellent comments throughout the course of my work that enabled me to complete the same.

I wish to express my thanks to Dr. A. I Yahya, Head of the Department and former heads Dr. P Raveendran and Dr. K Muraleedharan, for providing necessary facilities during the research period. I extend my sincere thanks to all the non-teaching staffs for their hard work, support and care.

Let me honestly thank my teachers in the Department of Chemistry, Dr. Gangadevi, Dr. P Purushothaman, Dr. Aravindankshan, Dr. V. M Abdul Mujeeb, Dr. Abraham Joseph, Dr. N. K Renuka, Dr. D Bahulayen, Dr. P Pradeepan, for their hearty support, advice, suggestions and motivation during my MSc as well as research period. Also I extend my gratitude to Dr. Suresh Babu and other guest faculties in the department for their kind support.

Words are not sufficient to express my gratitude to my beloved teacher, Dr. Muhammed Shafi. His words and constant advices inspired me to become in this position. He always encourage and motivate me in each of my steps by saying 'You deserve it'. I am also grateful to Dr.

Zubair, PSMO College, Tirurangadi for constant advice and support during my carrier.

I find no words to express my gratitude to my group members Jasnatha, Nihmatha and Jayakrishnan for the supporting atmosphere created by them. Special thanks to Parvathi and Sanker for helping and supporting me during the writing of thesis.

I am so much grateful to my friends Jini, Shamsi, Dipin, Anu, Shameera, Akhila, Ansi, Anjali, Roopasri, Varsha, Lijin, Deepak, Shiva, Anjitha, Anupama, Linda, Soumya, Arshad (List not complete) for the fun-filled atmosphere created by them during the research period. I extend my thanks to all my seniors, former and present MPhil scholars for their kind support and love.

I take this opportunity to thank Prof. P. P Pradyumnan, Department of Physics, University of Calicut, Dr. A Sujith, Associate Professor, NIT Calicut and their group members for providing their facilities and help for doing the analysis. I thank SAIF- STIC, Cochin and CSIF, University of Calicut for providing instrument facilities. Also I would like to acknowledge UGC, India for the fellowship.

Above all, I extremely grateful to my parents, sisters and brothers for their immense love and support. Special thanks to my husband, Jamsheer and my in-laws, especially sister in-law, Rajeenatha for the constant support and motivation. Further, I extend my deep sense of gratitude to all other family members for their support and prayer. Also, special thank to my cutie, Jazil Aimen, who came to us during the PhD period.

Suhailath K

..... To my beloved

Preface

Polymer composites are widely studied nowadays due to their extraordinary properties and, thus, they are more exploited in the development of many electrical and electronic devices. One of the thrilling achievements in this field is the development of electrically conducting polymer composites from insulating polymer and conducting filler. Such advanced materials find applications in conducting adhesives, electromagnetic shielding and sensors, etc. The most interesting aspect of these advanced materials is the drastic change in electrical, mechanical and chemical properties with the incorporation of even a very small amount of nanofillers. With the uniform dispersion of nanofiller and the resulting improvement in unique properties, the polymer nanocomposites open a new avenue in the field of electrical applications.

Poly (butylmethacrylate) (PBMA)/metal oxide nanocomposite got significant attention due to their immense mechanical and electrical properties coupled with light weight, flexible and transparent nature. Further, PBMA nanocomposites can easily developed with uniform morphology and so they are more interesting in both research and industrial filed. Recently, studies are going on developing the flexible electronic devices based on polymer nanocomposites. Polymers with light weight, transparent and can be made into flexible thin films are more promising in the field of flexible electronic devices. Thus, PBMA which is light weight, flexible and transparent, got considerable

attention in the field of flexible electronic devices owing to their interesting properties.

This thesis is mainly focused on the development of PBMA nanocomposites with different types of metal oxide nanoparticles possessing excellent mechanical and electrical properties and thus found applications in flexible electronic devices. And for developing the PBMA nanocomposites, titanium dioxide (TiO_2), cerium doped titanium dioxide (Ce-TiO_2), neodymium doped titanium dioxide (Nd-TiO_2), cerium dioxide (CeO_2) and neodymium dioxide (Nd_2O_3) nanoparticles are used as fillers. The thesis entitled "**Studies on poly (butylmethacrylate) with doped and undoped metal oxide nanoparticles**" is organised into 8 chapters. **Chapter 1** provide brief introduction about composites, different types of polymer matrixes, fillers and different synthetic strategies of polymer nanocomposites etc. Also this chapter presents the motivation and objectives of the current research problem. **Chapter 2** discuss the details of materials and the experimental procedure used for synthesis of various nanoparticles and the utilization of these nanoparticles as reinforcing filler in PBMA nanocomposites. This chapter also describe the various techniques used for the characterization of fabricated PBMA nanocomposites. **Chapter 3** presents the detailed discussion on the effect of TiO_2 nanoparticles on the structural, thermal, mechanical and electrical properties of PBMA nanocomposites. Moreover, the role of various parameters behind the enhanced tensile and DC conductivity of PBMA was analysed by employing different theoretical modelling studies. The effect of Ce doped TiO_2 nanoparticles on the structural,

thermal, mechanical, AC and DC conductivity of PBMA nanocomposites was described in **chapter 4.** This chapter also contain the theoretical modelling studies for tensile and DC conductivity properties. **Chapter 5** examines the effect of Nd doped TiO_2 nanoparticle on the structural, thermal, mechanical and electrical properties of PBMA nanocomposites. The applicability of different theoretical modelling for tensile and DC conductivity was also studied. **Chapter 6** describes the effect of CeO_2 nanoparticle loading on the structural, thermal, mechanical and electrical properties of PBMA nanocomposites. The theoretical modelling studies were done to explore the role of CeO_2 nanoparticle on enhancing the tensile and DC conductivity properties. The change in the structural, thermal, mechanical and electrical properties of PBMA nanocomposites by the incorporation of Nd_2O_3 nanoparticles was discussed in **chapter 7**. Different theoretical modelling studies were employed for predicting the mechanism behind the enhanced mechanical and electrical properties of PBMA nanocomposites. **Chapter 8** concludes the major findings of the studies and also provide some suggestion for future research.

Contents

CHAPTER 1
INTRODUCTION

Contents

1.2 General Introduction

Polymers are integral part of our day to day life. Tooth brushes, sandals, cloths, electronic devices, whatever material we come across in our daily life has a bond with polymers. Polymers are class of materials which constitute long chain macro-molecules with numerous repeating units called monomers. The structure of polymers is determined by the way in which the monomer units are combined together to form the polymer chain. So, depending on the mode of arrangement of monomers, polymers may be linear, branched or ladder like structure. As already coined, monomers are the building units of polymers, the properties of polymers greatly vary with the type of monomer present in it. There are two types of polymers, natural and synthetic polymers. Proteins, DNA, cellulose, starch, natural rubber are examples of natural polymers. However, the poor mechanical and thermal properties limit their applications and hence the uses of synthetic polymers are important. The easy as well as cost effective production coupled with lightweight and excellent mechanical properties of synthetic polymers replace the position of natural polymers from various applications. Further, the macromolecular structure of synthetic polymers enables them to perform in various fields which cannot be done by other synthetic materials. For last decades, polymeric materials are widely used in biomedical applications, automobile industries, domestic applications, construction fields, food packaging, developing flexible electronics etc. In biomedical fields they are utilized for drug delivery, developing artificial blood vessels, ligaments, tendons etc.

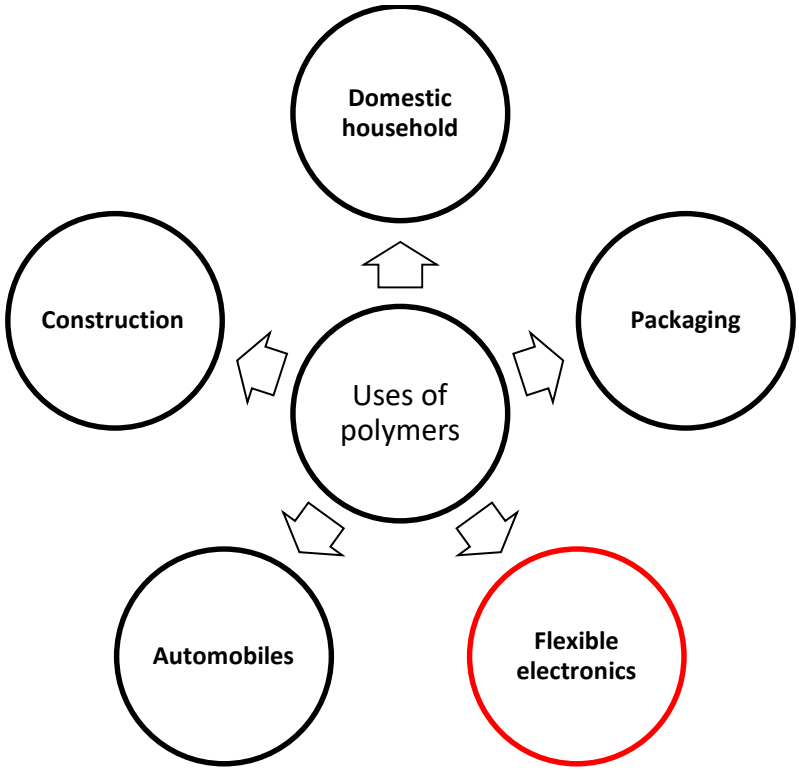

Figure 1.1: Various applications of polymers

Nowadays, electronics have become an inevitable part of human life. The modern technologies are mainly focusing on developing flexible electronics, for the easy and fastest usage of the electronic devices. Recently, polymeric materials find potential applications in flexible electronics owing to their light weight and flexible nature. Flexible displays, batteries, electronic circuits, electronic solar cell arrays, antenna arrays and electronic monitoring devices used in heart patients are some flexible electronic devices in which polymeric materials are widely using for many of the functions. Hence much research work is focused on developing flexible polymer films with excellent

conductivity, considerable thermal and mechanical stability and thus may find applications in various electronics.

1.2 Composites

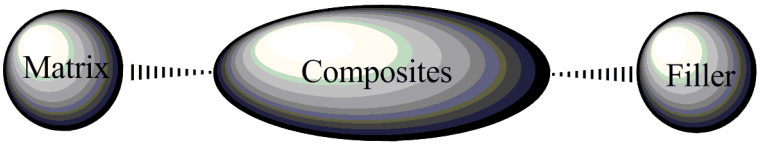

Researchers are trying to improve the inherent properties of polymers and hence extend their applications to various fields. Numerous studies were going on for developing polymeric materials with irreplaceable properties by the addition of different types of fillers and are known as polymer composites [1-4]. Simply, composites are the combination of two or more different constituent materials, exhibiting superior properties than the individual components [5]. Composites bear salient properties like significant thermal strength, high mechanical and better electrical properties than conventional engineering materials. The synergetic interaction between the components present in the composites leads to the superior properties of composite materials than the individual components present in it. Hence composite materials are used in place of conventional engineering materials which possesing inferior properties. Now a day's composite materials are widely used in automobile, space, house hold utensils and in many engineering applications.

Basically, composites consist of two phases, continuous phase (matrix) and discontinuous phase (filler). Depending on the nature of

continuous phase, the composites are categorized into three types and were discussed below [6].

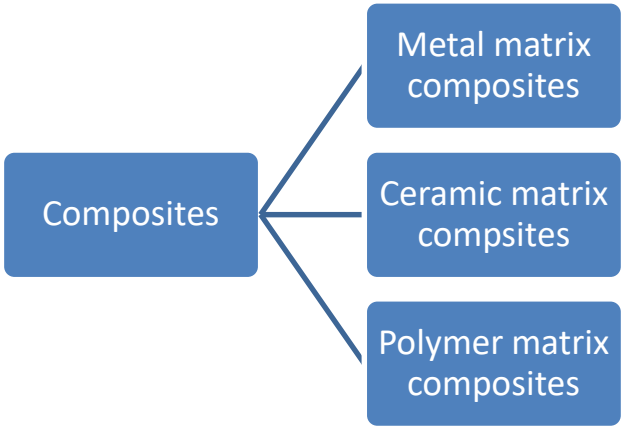

1.2.1 Metal Matrix Composites (MMC): Metal matrix composites consist of metal or alloy matrix reinforced with nano materials. This type of composites exhibits combined properties of metal and ceramic such as ductility, toughness, high strength and modulus etc. Therefore metal matrix composites are mainly used for the production of materials with high sheer strength as well as better processing temperature capabilities. Thus they found immense applications in aerospace and automotive fields. Major examples for metal matrix composites with significant properties are Al/Al_2O_3, Al/SiC, Fe-Cr/Al_2O_3, Ni/Al_2O_3, Co/Cr, Fe/MgO, Al/CNT, Mg/CNT etc.

1.2.2 Ceramic Matrix Composites (CMC): In this type of composites the matrix part is covered by ceramic compounds such as metal oxides, nitrides or borides, whereas the filler part is wrapped usually by metals. Both the components are finely

dispersed to each other to have better compatibility between them and thus exhibit the specific hybrid properties. CMC can be widely used in engineering and industrial applications by utilizing their outstanding optical, mechanical, magnetic and electrical properties arising from microstructures. Al_2O_3/SiO_2, Al_2O_3/TiO_2, Al_2O_3/SiC, Al_2O_3/CNT etc. are some reported examples for ceramic matrix composites.

1.2.3 Polymer Matrix Composites (PMC): Polymer matrix reinforced with filler particles belongs to this category. Polymer matrix composites exhibit versatile properties which are far behind that of the individual polymer matrix and the filler. Here, the interfacial interaction between the added filler and the polymer matrix results in better performance of hybrid polymer composites. The outstanding electrical, optical, thermal and mechanical properties of polymer composites are attributed to their immense applications in various fields. The polymer matrix composites may include thermoplastic or thermosetting polymer matrix and layered silicates, metal oxides, carbon nanotubes (CNT), layered double hydroxides, cellulose, fibres etc as the filler. Moreover, amidst the various types of composites discussed above, polymer matrix composites got pivot attention due to their flexible and light weight nature coupled with easy processability and affordable fabrication conditions.

The composites are also classified based on the nature of filler added to it and are particulate, fibrous, laminate, hybrid and nano composites.

Since, the properties of composites were designed by the amount, dispersion mode, geometry, orientation as well as the interfacial interaction of the reinforced filler particle, the nanocomposites are most dominated than other conventional composites.

1.3 Matrix

The continuous phase present in the composites in which the reinforcing filler particles get incorporated are called the matrix. Matrix provides the binding sites for the filler particles or it hold together the fillers and also act as a medium for filler to filler as well as filler to matrix interactions. Matrix determines the structural and functional properties of composite materials to greater extent. So selection of matrix is a major factor to develop composite materials exhibiting desirable properties. Among various matrix which we discussed elsewhere, polymers are the best known matrix due to its flexible, light weight and the easy processability. The polymer matrix can be either a thermosetting or thermoplastic polymer. However, thermoplastic polymers get pivot attention than thermosetting owing to their significant mechanical properties, higher toughness and better impact resistance etc. Further, thermoplastic polymers have long shelf life and also they are easy to process, need only short processing time. So, researchers are more interested with the thermoplastic polymers [7]. Some of the frequently studied thermoplastic polymers are discussed below

1.3.1 Polyamides (PA)

The polyamides have superior thermal, mechanical properties and are of low cost, thus are widely used in many fields [8]. Particularly polyamides are widely used in textile industries by exploiting their excellent wearing durability. Polyamides with high methylene to amide ratio (eg: PA 12) are more promising because of their low moister sensitivity as well as low melting points. Among various polyamides, PA66 possess better mechanical stability and thus it is used tire, air bag, bullet proof etc [9]. The properties and hence the applications of polyamides can be greatly improved by incorporating different types of fillers. For example, Fredi et al. reported that the polyamide composites reinforced with glass fibres possess significant thermal energy storage and release capabilities [7]. Yesildag et al. observed that graphene oxide has a noticeable impact on thermal as well as mechanical stability of polyamides [10].

1.3.2 Polyethylene (PE)

Polyethylene is an important insulation material used in many devices especially in cables owing to its low permittivity and high electrical break down strength. However, due to the requirement of low operating temperature and the requirement of antioxidants, the application of polyethylene is limited. Nowadays, polyethylene nanocomposites got significant attention, since they overcome the disadvantages of plane polyethylene. Mohagheghian et al. were noted that the energy absorbing capability of linear low density polyethylene (LLDPE) was greatly improved by the addition of carbon black fillers

[11]. Park et al. investigated the effect of graphene oxide on polyethylene and observed that the nanoparticle insertion not only improved the tensile properties but also it affect the electrical resistance of polyethylene matrix [12]. Chaudhry and Mittal reported that the chlorination of polyethylene matrix increase the interaction with the graphene oxide fillers [13]. Thus chlorinated polyethylene-graphene oxide composites exhibited better tensile properties than the un-chlorinated polyethylene composites.

1.3.3 Polystyrene (PS)

Polystyrene is transparent thermoplastic polymer with excellent optical properties. Therefore, polystyrene being widely used as host matrix for developing composites with better optical properties. PS/ZnO nanocomposites shows better UV shielding properties and thus find applications in many antireflection coatings, UV protective sheets and films etc. Moreover, polystyrene is greatly used in manufacturing of plastic models, CD and DVD cases, cutlery etc. Polystyrene nanocomposites got immense attention in many other fields due to the good processability and significant enhancement in mechanical, electrical and thermal properties by the insertion of nanofillers particularly multi-walled carbon nanotubes [14]. Here, the size and morphology of polystyrene composites can be tuned by adjusting the addition of nanoparticles. For example, Zhang et al. were reported that the addition of silica nanoparticles modified with different amount of sodium laurylsulfate surfactant into polystyrene matrix produce composites with different size and morphology [15]. Han et al. investigated that the glass transition temperature (Tg) of PS was

decreased with the addition of filler, and more interestingly the storage modulus was greatly improved by addition of filler [16].

1.3.4 Polyvinylchloride (PVC)

Polyvinylchloride exhibits excellent forming properties by the presence of chlorine and so they are widely used in thermoforming applications. Further, it has better chemical resistance, UV stability, impact resistance and weather resistance. Amidst other thermoplastic materials PVC is the most strong and rigid polymer with high tensile strength and elastic modulus [17]. Thus PVC has been used in electric cables, clothing, membrane separation etc [18]. The major drawback of PVC matrix is its low thermal stability. So, in order to improve the properties certain additives, stabilizers, modifiers and sometimes nanofillers are adding to PVC matrix. Pagacz et al. reported that the thermal stability of PVC can be greatly enhanced by the addition of sodium montmorillonite (Na-MMT) and organically modified MMT (O-MMT) nanoparticles [19]. Taha observed that the addition of Pb_3O_4 nanoparticles also significantly enhanced thermal stability of PVC matrix [20]. It was reported that the inherent mechanical, optical as well as thermal properties of PVC can be greatly improved by the addition of ZrO_2 nanoparticles [18].

1.3.5 Polyacrylates

Polyacrylates, are developed by the polymerization of acrylic esters [21, 22]. Owing to the ease of processing, cheep cost coupled with excellent mechanical, thermal and electrical properties, polyacrylates are widely used in many fields, from utensils to space shuttles. Further,

transparent nature, lower drying time, high mechanical and chemical stability polyacrylates are widely used in paintings and surface coatings [23].

Acrylic acid and acrylic esters are popular from the middle of nineteenth century with the first report published in 1901 by Pechmann and Röhm [24]. Commercially acrylic resins were started to use as paint medium after the Second World War, as an alternative to alkyd resins and drying oils. The dispersion of ethylacrylate and methylmethacrylate copolymer developed by Rohm in 1901 was the acrylic resin initially used. The acrylic resin made by the copolymerization of ethyl acrylate and methyl methacrylate ester was commercialized as a consolidant for fancy stones, masonry and as a adhesives for paintings [25-27]. After this large scale production of polyacrylates was evolved, finally in 1928 the mass production of has poly (methylmethacrylate) (PMMA) was made possible by Bauer due its great demand during the time of 2^{nd} world war [28-30]. Beside this acrylic polymers were introduced as a commercial product under the trade name "Corialgrund" for the surface finishing of leather [31]. Following this initial breakthrough, the applicability of acrylic resins were get more popular in various fields by exploiting their outstanding properties such as flexibility, transparency as well as easy processability [32].

Polyacrylates has the general formula

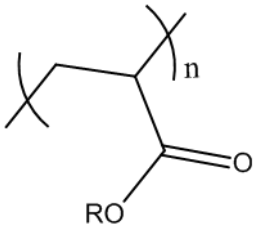

Where ‘R’ means a alkyl group such as methyl, butyl, ethyl, hexyl etc. If the R=-CH_3 it is poly (methylmethacrylate) and if R=-$CH_3CH_2CH_2CH$ it is poly (butylmethacrylate).

1.3.5.1 Poly (butylmethacrylate) (PBMA)

PBMA was chosen as the polymer matrix for this study because of its flexible and transparent nature. Also the easy processability for incorporating nanofillers into PBMA matrix has widely studied. While applications of PBMA are limited due to their low conducting property, glass transition temperature and mechanical property. So in order to improve their thermal, electrical and mechanical properties various fillers were added to PBMA, and nowadays PBMA composites are widely used in many fields [33, 34]. Further, PBMA matrix is a better host for the fillers and it is inert in nature and so PBMA composites are easy to process.

Further, poly (butylmethacrylate) is one of the most studied polymers from polyacrylates family due to various attractive properties such as considerable strength, better weatherability, excellent optical property as well as dimensional stability. Due to the presence of bulky butyl group in PBMA, the ordered arrangement of molecule is less and hence they are flexible, semi-rigid in nature. Further, PBMA has been

widely used as a polymer matrix for developing polymer composites with immense applications. Reports showed that the PBMA nanocomposites offer potential for optical properties, reduced gas permeability and better heat resistance.

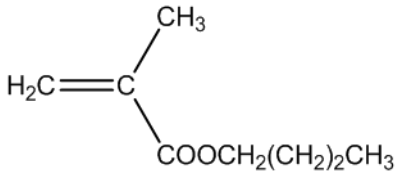

Butylmethacryalte

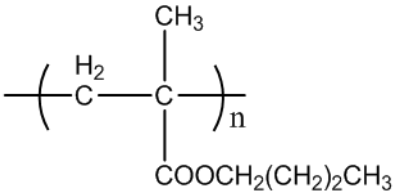

Poly (butylmethacryalte)

1.4 Fillers

The solid additives adding to improve the innate properties of polymeric materials are called fillers [35]. Fillers impart its own physical and chemical properties as well as provide better durability and processability to the polymer matrix. However, the extent of reinforcement provided by the added fillers was greatly depends on their size, shape, surface properties, aggregation state as well as quantity [36].

Conventional micro-sized fillers such as carbon black, calcium carbonate and fibers requires high loading for having a significant improvement in properties and which leads to composites with heavy weight. Moreover, due to high viscosity of these fillers the processing conditions are too tedious. So that the interface between the micro-sized fillers and polymer matrix are too low and which result in composites with poor properties. However, fillers with fine particle

size provide better compatibility with the polymer matrix and there by imparting excellent properties to the resulting polymer composites. So, majority of the studies regarding polymer composites are done by using nanofillers. Most commonly exploiting nanofillers are metal oxide nanoparticles of transition as well as lanthanide ions.

1.4.1 Classification of Nanofillers

Nanofillers are classified into three categories based on their dimensions i) One dimensional nanofillers ii) Two dimensional nanofillers and iii) Three dimensional nanofillers

1.4.1.1 One Dimensional Nanofillers [1D]: Nanofillers consisting one of their dimensions less than 100 nm belongs to this group [37]. This type of nanofillers is generally in the form of sheets having thickness of one to few nanometers and length from 100 to 1000 nm. Nanosheets, nanowalls, nanographene platelets, ZnO nanodiscs, carbon nanowalls and Fe_3O_4 nanodiscs are the common examples [38-42]. 1D nanofillers possess novel electrical, magnetic and optical properties hence are widely used in many nanodevices like microelectronics, biosensors, sensors, biomedical, and coatings [43].

1.4.1.2 Two-Dimensional Nanofillers [2D]: Nanofillers of which two dimensions are less than 100 nm belongs to this group [37]. Nanotubes, nanofibers, nanofilaments are 2D nanofillers. Nanofillers including Carbon nanotubes (CNTs), boron nitride (BN) tubes, gold or silver nanotubes, clay nanotubes, Zinc oxide, titanium oxide, graphene oxide, cerium oxide are some

common examples [44-47]. Due to their unique dimensions, 2D nanofillers exhibit excellent optical and electrical properties and so they commonly used as fillers for developing polymer composites with outstanding optical and electrical properties. Also they are widely used in optoeletronic devices, photocatalysis, sensors, energy storage devices etc [48-49].

1.4.1.3 Three-Dimensional Nanofillers [3D]: In this all the three dimensions are less than 100 nm scale. So 3D nanofillers possesses spherical and cubical shape [50]. Therefore, 3D nanofillers commonly known as nanospheres, nanogranules, and nanocrystals. Nanosilicates, aluminates, nanotitanium dioxides, carbon black etc are some common examples. Nano TiO_2, SiO_2, Fe_3O_4, and ZnO exhibit better thermal stability, good optical transparency, considerable refractive index and high photocatalytic activity [43,51-52]. Polymer nanocomposites developed by using 3D nanofillers are much superior in their properties than that of 1D and 2D nanofillers. They found many applications in coatings, purification process, biomedical fields etc [53-55].

Some of the most studied nanofillers are discussed below:

1.4.2 Carbon Black

Carbon black is excellent reinforcing filler for various polymer matrix, since it enhances the mechanical properties as well as solvent resistance of the polymers. Carbon black present in agglomerated form

are mainly obtained from natural gas, crude oil and aromatic hydrocarbons during their combustion or degradation process.

1.4.3 Silicates

Silicates are non-black reinforcing fillers used in various polymer composites. There are different types of silicates such as sodium aluminium silicates, calcium silicate, aluminium potassium silicates (mica), magnesium silicate (talc) etc. Sodium aluminium silicates have better reinforcing properties and are derived from kaolin. Aluminium potassium silicates exhibit potential insulating properties, thermal stability, water and electrical resistance. Magnesium silicates impart significant barrier properties to the composites. Further it improves the mechanical as well as thermal stability of the host polymer matrix.

1.4.4 Clay

Clay, layered silicates of aluminium and magnesium joined through Van der Waals forces are excellent reinforcing particles for polymer composites. Owing to the hydrophilic nature of the clay particles, they are better fillers for hydrophilic polymers. Hence they are unapt as reinforcing particles for thermoplastic polymers.

1.4.5 Carbon Nanotubes

Carbon nanotubes are cylindrical in shape, classified as single walled and multi-walled carbon nanotubes. Carbon nanotubes are much difficult to disperse in polymer matrix owing to their poor compatibility with the polymer matrix.

1.4.6 Metal Oxide Nanoparticles

Among various fillers, inorganic metal oxide nanoparticles got immense attention from research as well as technological perspectives owing to their unique features. Compared to micro-sized fillers, the nano-sized fillers shows outstanding hybrid properties arising from their suitable size. The unique characteristics of metal oxides make them applicable in various optical, electrical, photo electronic and catalytic devices. Though the metal oxide nanoparticles exhibit excellent properties due to their structural features, there are many limitations too. Due to the nano-size and hence the large surface area the metal oxide nanoparticles have higher tendency to get self agglomerated by the presence of Van der Waals interactions. It reduces their self stability, selectivity and mechanical stability. So, for overcoming these limitations metal oxide nanoparticles are embedded in polymer matrices.

Recently, metal oxide nanoparticle encapsulated polymer composites got greater attention from academic as well as industrial world because of their outstanding properties which are not exhibited by the individual nanoparticle itself. The metal oxide nanoparticles possess unique properties, which when combined with the polymer matrix impart its characteristic properties to the polymer by the effective interaction between them, result to the production of a new hybrid material with interesting properties (thermal, optical, electrical, mechanical etc). However, the properties of nanoparticles are greatly size and morphology dependent. The nanoparticles possess special features such as small particle size, fine particles size distribution,

wide surface area and most of them contain enough number of hydroxyl groups on their surface which helps for having better interaction with the polymer matrix.

Transition metal oxides and rare earth metal oxides are the most exploited metal oxide as fillers for developing polymer nanocomposites. TiO_2, NiO, ZnO, AgO, Fe_2O_3, SiO_2 etc are the most commonly used metal oxides [56-59]. In addition to this, rare earth metal oxides such as CeO_2, Nd_2O_3, ZrO_2, Sm_2O_3, Nb_2O etc were also used for preparing nanocomposites exhibiting superior properties [60-61]. The presence of 4f electrons could be attributed to the attractive optical and electrical properties of rare earth metal oxides [62].

1.4.6.1 Zinc Oxide (ZnO) Nanoparticles

Zinc oxide is a potential material with salient optical properties and thus finds wide applications in optical devices. There are many ZnO based materials like ZnO polycrystalline film, microlasers, hybrids, powders developed for different purposes. Typically, ZnO is n-type semiconductor with a band gap of 3.4 eV, exhibiting excellent UV absorbability and better chemical stability. Further, ZnO is eco-friendly and non-toxic material with cheap rate and so widely used in many low cost materials like conductive glass, white paint and sunscreens. ZnO suits for several applications such as in UV-shielding materials, polymer coatings, solar cells, gas sensors, cosmetics etc as they possess outstanding electrical, magnetic, chemical and optical properties [63]. Vaishnav and Goyal reported an enhanced in thermal and dielectric properties of poly (aryletherketon) by the addition of

ZnO nanoparticles [64]. ZnO nanoparticles are easy to disperse in solvents and polymer matrix. It was reported that polymer/ZnO nanocomposites are excellent materials with better moisture resistance, antibacterial and fungal properties. ZnO based polymer composites are also an excellent anticorrosion additives. Polypyrrole/ ZnO nanocomposites, polyaniline/ZnO, polyethylene glycol/ZnO and polyvinylpyrrolidone/ZnO are some reported examples for anticorrosion inhibiters [65].

1.4.6.2 Nickel Oxide (NiO) Nanoparticles

NiO nanoparticles, a p-type semiconductor with band gap= 3.51 eV are promising materials for electrochemical and gas sensing applications. They are well known for its outstanding catalytic properties such as hydrocracking reactions, hydrocarbon reforming, methane production etc [66]. Further, NiO nanoparticles exhibit ferromagnetic properties, which is size dependent. Karthik et al. were studied the size dependent magnetic properties of NiO nanoparticles [67]. They reported that owing to the excellent magnetic properties, NiO incorporated polymer composites got immense applications in many magnetic devices, gas sensors, light emitting diodes and electrical devices etc. Shambharkar and Umare showed the improved conductivity of polyaniline by the addition of NiO nanoparticles [68]. Soleimani and Niavarzi reported the significant thermal properties of PMMA/NiO nanocomposites [69].

1.4.6.3 Aluminum Oxide (Al_2O_3) Nanoparticles

Al_2O_3 nanoparticles consist high specific strength, considerable electrical and thermal conductivity with low density and low melting

point. Therefore Al_2O_3 nanoparticles are commonly used as reinforcing agent for developing light weighted composites with better conductivity properties. The enhancement in conductivity by the incorporation of Al_2O_3 nanoparticles are reported by Lim et al. [70]. Further, polymer/Al_2O_3 composites showed excellent mechanical properties. The combined effect of enhanced mechanical properties and light weight of the Al_2O_3 composites can be exploited in developing automotive, aircraft and aerospace devices [71]. Glass fibre composites reinforced with SiC/Al_2O_3 nanoparticles exhibiting excellent mechanical properties was developed by Rajesh et al. [72]. Ash et al. reported the improved mechanical properties of PMMA composites by the addition of Al_2O_3 nanoparticles [73].

1.4.6.4 Iron Oxide (Fe_2O_3) Nanoparticles

Fe_2O_3 are naturally abundant, low cost, non-toxic materials and thus got considerable attention in many fields. However, the poor conductivity, lower specific area and lesser cyclic stability limited the application of Fe_2O_3. So in order to overcome the limitations of Fe_2O_3, they are combined with various polymers matrix. Chen et al. reported that Fe_2O_3/GO composites are promising materials for super capacitors [74]. Zhang et al. developed Fe_2O_3 composites using carbon as the core shell possessing excellent dielectric properties [75].

1.4.6.5 Titanium Dioxide (TiO_2) Nanoparticles

Among various transition metal oxides known today, TiO_2 is the most investigated metal oxide nanoparticles due to its better properties and wide applications coupled with the inexpensive and nontoxic nature.

TiO_2 possess excellent optical and electrical properties and so the combination of TiO_2 with the polymer matrix results in polymer composites exhibiting better optical and electrical properties. Therefore, the potential application of polymer/TiO_2 nanocomposites lies in the development of opto-electronic devices. Praveen et al. were reported the improved thermal stabilities of polyaniline by the incorporation of TiO_2 nanoparticles [76]. Another interesting factor towards TiO_2 as a filler is that it enhance the refractive index of glassy materials especially like PMMA and so they posses immense attention in plastic industry [77]. Many research works are carried out on the polyacrylates/TiO_2 nanocomposites and which find applications in various fields. It was reported that the incorporation of TiO_2 nanoparticles resulted in the better electrical conductivity of PMMA by the synergetic interaction between the PMMA matrix and TiO_2 nanoparticles. Further, the encapsulation of TiO_2 nanocrystals in polymer resulted in the development of modified polymer with significant optical properties as well as better thermal and mechanical stability [78]. Haroun and Youssef were observed that the addition of TiO_2 nanowires resulted in better thermal stability as well as high conductivity of PMMA composites [79]. The chemical interaction between PMMA and TiO_2 nanowires facilitate homogenous dispersion of filler in the matrix and which results in higher thermal stability and electrical conductivity for PMMA composites.

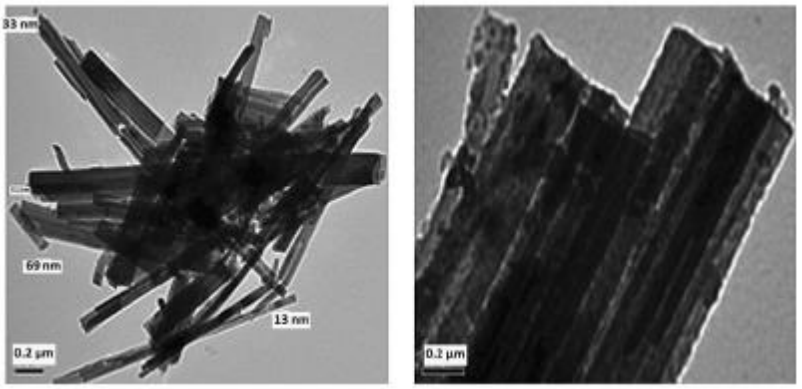

Figure 1.2: TEM images of PMMA/TiO_2 nanocomposites [79]

1.4.6.6 Cerium Dioxide (CeO_2) Nanoparticles

CeO_2 nanoparticles are the most dominated one among the various rare earth metal oxides owing to its immense applications. They are widely used as electrolytes in electrochemical devices, catalysts in automobile systems, abrasives in chemical systems, UV absorbents in sunscreens etc due to the unique optical and electrical properties coupled with better thermal stability and diffusivity [80]. Typically, CeO_2 is a ceramic material with fluorite structure and semiconducting nature with wide band gap of ~3.2 eV, found applications in many areas like solar cells, gas sensors, fuel cells, catalysts etc [81-83]. Though they have wide band gap energy, their uses in photoelectrochemical applications are very limited. Nowadays researchers try to modify the surface properties and to extend their applications into vast areas particularly to photoelectrochemical applications [84]. It was reported that the addition of CeO_2 nanoparticles modified with acidic treatment were enhanced the UV-Vis absorption capacity of polyacrylate polymer without any disturbance to the transparency of polymer

matrix, see **figure 1.3** [85]. They also pointed that the CeO_2 addition greatly improved the thermal stability of polyacrylate matrix by the interaction of CeO_2 nanoparticles with the polymer matrix.

Figure 1.3: Films of polyacrylic nanocomposites with different concentrations of CeO_2 nanoparticles [85]

Parvatikar and Prasad observed that the loading of CeO_2 nanoparticles significantly enhanced the dielectric and conductivity properties of polyaniline [86]. The embedded CeO_2 nanoparticle leads to increase in number of polarons and that result in higher conductivity. PMMA/CeO_2 nanocomposites were used as dye absorbents by exploiting their optical properties. More specifically, the CeO_2 nanoparticles are the active centre for the absorption process and the PMMA matrix act as supporting material for the nanoparticles [87].

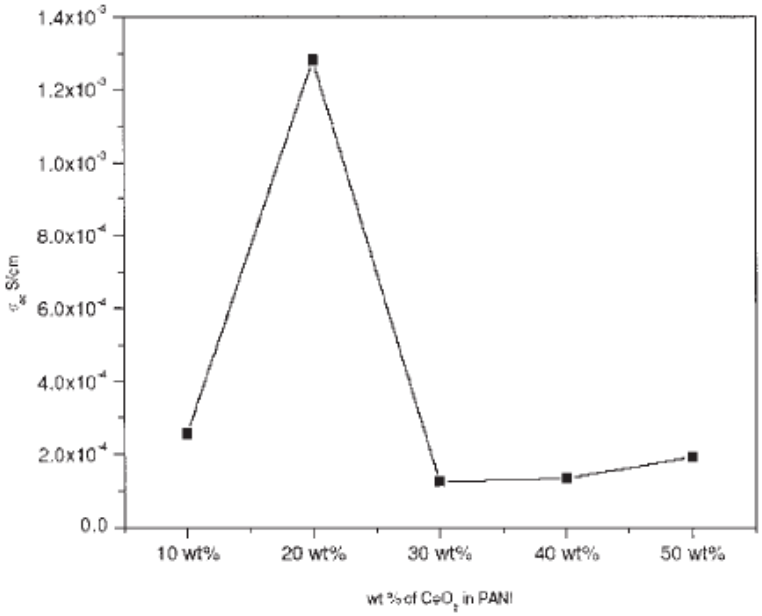

Figure 1.4: The conductivity of PANI/CeO_2 nanocomposites at different loading of CeO_2 nanoparticles [86].

1.4.6.7 Neodymium Dioxide (Nd_2O_3) Nanoparticles

Nd_2O_3 nanoparticles has been used in optical and electrical applications, Luminescence, protective coatings etc. Goel and Arorab reported that there exists a significant enhancement in luminescent properties of ferroelectric liquid crystal nanocomposites encapsulated with Nd_2O_3 nanoparticles [88]. The considerable band gap energy as well as the presence of 4f orbital attributed to this enhancement.

As discussed above there are plenty of works related to polymer nanocomposites based on polyacrylates/metal oxide nanoparticles. However, studies related to metal oxide nanoparticles particularly TiO_2, CeO_2 and Nd_2O_3 for thermal, mechanical and electrical applications are very limited. In our study PBMA is the polymer

matrix. PBMA belongs to important class of hydrophobic plastic type polymers, got significant attention in plastic industry due to their versatile optical property, flexibility and transparency. However the applications of PBMA are very limited in electronic applications due to their poor thermal stability, mechanical strength and conductivity properties. These drawbacks can be replenished by encapsulation of filler particles particularly metal oxide nanoparticles and can extend their applications into many other areas. So, in this work, we try to study the effect of these nanoparticles in the thermal, mechanical and conductivity properties of poly (butylmethacrylate) polymer, and hence examine the applications of these hybrid composites in thermal-mechanical-electrical applications.

1.5 Polymer Nanocomposites: Properties and Applications

Polymer nanocomposites are new type of hybrid materials containing a component in nanometer scale. The encapsulated nano-sized component, ie, the nanofiller improves the thermal, mechanical, optical and electrical properties of polymer matrix without altering the physical and chemical properties. Generally, the fillers such as transition metal oxides, rare earth metal oxides, nanoclays, nanosilicates etc are used in polymer composites. The distinctive properties of added fillers, which contribute to the improved performance of composites, attract the attention of researchers even after decades of study. Any types of polymer matrix, thermoplastics, thermosets or even elastomers are used for developing polymer composites exhibiting desired properties.

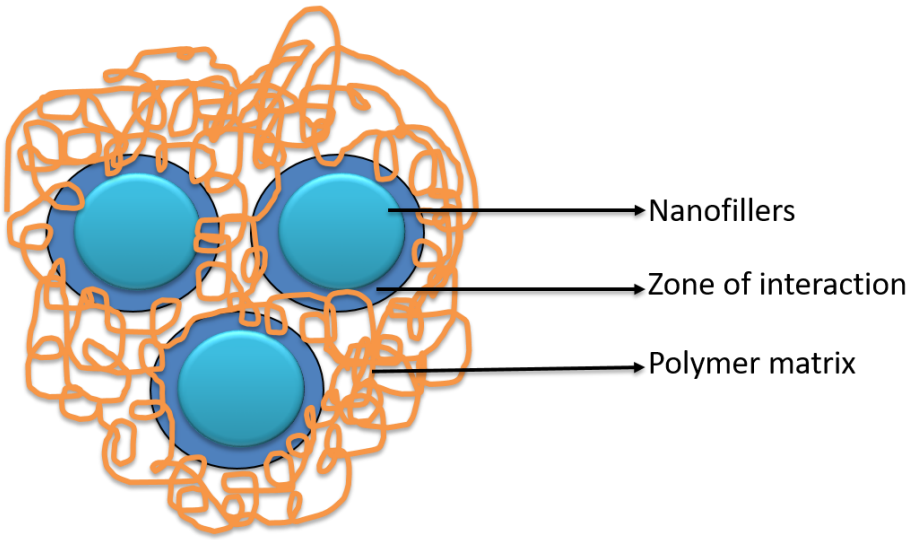

Figure 1.5: Schematic representation of polymer nanocomposites

The polymer nanocomposites integrate the properties of polymer matrix and the nanofiller, which are much superior to that of individual components. As we know, the bare polymers are better in performance with excellent optical and mechanical properties but have poor dielectric properties. On the other hand nanoparticles are superior in their dielectric properties but possess poor mechanical properties. So, by combining the polymer matrix with nanoparticles one can develop polymer nanocomposites possessing superior dielectric as well as mechanical strength. The applicability of any materials in various fields was determined by their property, processability, cost etc. It was established that the properties of polymer materials can be greatly improved by embedding suitable fillers into it. The outstanding properties of polymer composites due to the presence of filler, causes their potential applications in automobile industry, electronics, optical devices, consumer goods etc. Nowadays polymer nanocomposites are

widely used in flexible electronics and nanoelectronic materials owing to their flexibility, homogeneity and easy processability [89]. Therefore, polymer composites with interesting conducting properties are more demanding in research and industrial fields. A conductive composite can be easily made by embedding nanofiller with excellent conducting properties in a polymer matrix provided the amount of nanofiller should be enough to form a conductive network. The better compatibility between the added nanofiller and polymer matrix accelerates the formation of conductive network. Further, the filler and matrix should be chemically inert for having better electrical conductivity. So the selection of nanofiller as well as polymer matrix plays a major role in developing polymer composites with desired conducting properties.

1.5.1 Synthetic Strategies of Polymer Nanocomposites

The properties of polymer nanocomposites also greatly depend on the synthetic method. There exists numerous synthetic strategies for developing polymer nanocomposites, each has its own merits and demerits. For developing polymer composites with high performance, a thorough cross checking towards the material selection (both polymer matrix and filler) as well as the fabrication procedure is needed. The compatibility between the polymer matrix and the filler, adhesion tendency of filler particles, the mode of dispersion of filler in polymer matrix are also to be considered. The major challenge existing during the development of polymer nanocomposites is the uniform dispersion of nanoparticles throughout the matrix. The nanoparticles are hesitant to homogenous dispersion than the conventional micro-

scale fillers, because the nanoparticles are indistinguishable to each other and thus the inter-particle distance is much less. Therefore, there are greater Van der Waals interactions between the nanoparticles than the micro scale particles which are much discernable to each other. Thus the inherent tendency of nanoparticles to get self agglomerated is a big issue. To avoid the agglomeration of nanofillers for ensuring the uniform dispersion, researchers are searching for new methods.

Polymer nanocomposites can be developed either by in situ addition of nanoparticles during the polymerization or by in situ development of nanoparticles in a polymer matrix. The appropriate selection of synthetic strategies is critical to develop nanocomposite materials with desirable properties [90-91]. Mainly two approaches are used, bottom up approach or top down approach [**figure 1.6&1.7**]. In bottom up, the constituent components are allowed to combine each other and grow in nanometric level. While in top down method, the already developed bulk components are break down into smaller. Sol-gel process, template synthesis, chemical vapor deposition method, In-situ polymerization are some examples for bottom up approach. Solution mixing and melt mixing methods belongs to top down approach.

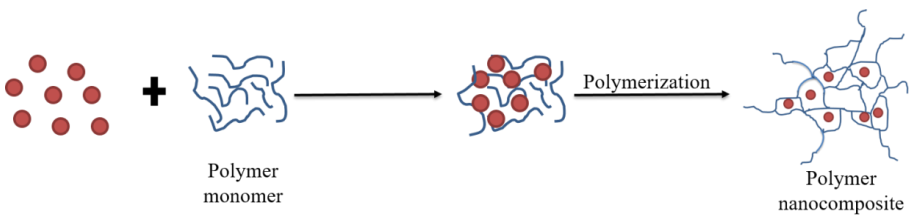

Figure 1.6: Bottom up approach

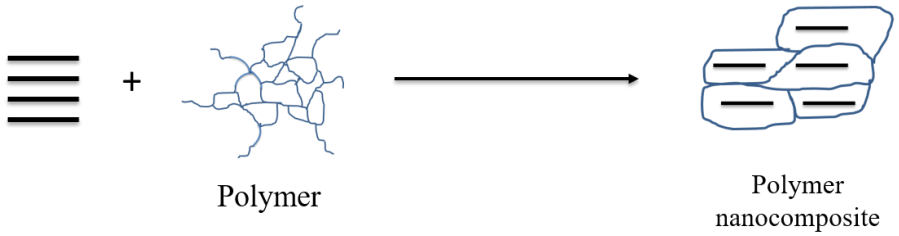

Figure 1.7: Top down approach

Some of the commonly used methods for synthesizing polymer nanocomposites are discussed below.

1.5.1.1 Ultrasonication-Assisted Solution Mixing:

Solution mixing is a simple and direct method for developing polymer nanocomposites. In this, nanofiller dispersions in suitable solvents are mixed with polymer solutions with the help of ultrasonication. After the process of dispersion, the solvents are removed by simple evaporation. The ultrasonication process helps to avoid the agglomeration of nanoparticles within the matrix and thus results polymer composites with proper dispersion of fillers. However, the ultrasonication is useful only for low viscous solutions moreover the removal of solvents is a tedious task.

1.5.1.2 Ball Milling :

Ball milling is a traditional technique in which small rigid balls produce high shear forces which are employed for dispersing nanoparticles within the polymer matrix. Different types of fillers such as silica, graphene, CNTs etc have been embedded in various polymer matrixes by means of ball milling. The exfoliation is much effective by this method especially for graphene sheets process. However,

specific chemicals are required to exfoliate the sheets by reducing the interlayer bond between the sheets. Ball milling is possible with both dry and wet conditions of polymers and thus thermoplastic polymers also can be made into composites very effectively.

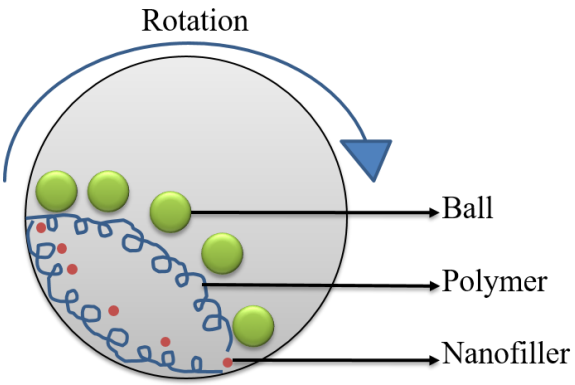

Figure 1.8: Illustration of ball milling process

1.5.1.3 Double Screw Extrusion:

Double screw extrusion is a green process as it is a solvent less technique. In this method, solid thermoplastic polymers are mixed with nanofillers at high temperatures by means of high shear forces. CNTs and nanosilica are successfully dispersed by this method. However, large amount of nanofillers are desired for developing composites with optimum properties using this method. Also, various parameters such as amount of filler, processing conditions, speed of rotation are critical in desiring the properties of developed composites.

1.5.1.4 Sol-gel Process:

Sol-gel method is one of the traditional and easiest methods for developing advanced materials with unique properties. In polymer

composites, the sol gel process is more important due to the better compatibility of nanoparticles with the polymers or during polymerization process, which permits the in situ development of nanoparticles in the presence of polymer matrix [92]. Wu and Liao prepared the hybrid polymer nanocomposites of polyethylene/octene elastomer with SiO_2 nanoparticles via sol gel process [93]. They observed that the in situ incorporation of SiO_2 to the elastomer matrix significantly improved the thermal stability of polyethylene/octene elastomer. Bahloul et al. were prepared polypropylene/TiO_2 nanocomposites by sol gel process under molten conditions [94-95]. The comparative study of nanocomposites prepared via sol gel process and in situ method revealed that the composite fabricated through in situ exhibits better visco elastic properties.

1.5.1.5 In situ Intercalative Polymerization :

In situ intercalative polymerization is useful in the case of polymer nanocomposites with layered silicate nanoparticles. In this method, the monomer in solution is allowed to polymerize between the layers and so the clay particles are expanding and dispersing within the polymer matrix [96]. The tethering effect, linking of clay particles with surface active group with the polymer matrix during polymerization is a great advantage of in situ intercalative process. However, in situ intercalative process mainly produces exfoliated nanocomposites only and so researchers seek other methods for developing polymer composites.

1.5.1.6 Emulsion Polymerization:

Emulsion polymerization is predominantly used in industrial polymerization process of synthetic polymers especially, high impact polymers latex paints and also for developing polymer composites of vinyl as well as acrylate polymers [97]. Emulsion polymerizations offers lot of advantages than bulk and solution polymerization such as low viscosity, high control on reaction rate, considerable molecular weight etc. Thus, efforts are taken to synthesise polymer composites via emulsion polymerization [98]. For example, Hu et al. prepared polystyrene/graphene oxide nanocomposites via emulsion polymerization method [99]. The above mentioned nanocomposites exhibited higher electrical conductivity and thermal stability than the plane polystyrene matrix. Similar results were also reported by Hassan et al. [100]. In this case the stabilising agents like SDS promotes the cross linking between the graphene oxide and the polymer matrix, results in higher properties of polymer composites prepared via emulsion polymerization. Moreover, emulsion polymerization method was also used for preparation of polyacrylate nanocomposites. Sedla´kova´ et al. were developed stable poly (butylmethacrylate) nanocomposite latex containing clay nanoparticles [101].

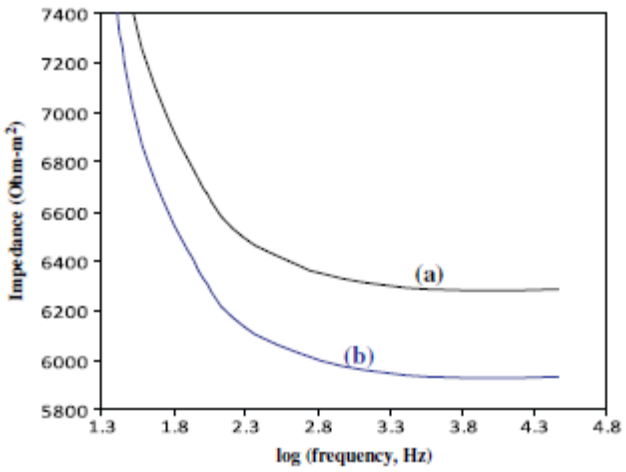

Figure 1.9: Electrical Impedance of polymer-graphene oxide nanocomposites prepared via emulsion polymerization [99].

Even though the emulsion polymerizations produce composites with excellent properties, the necessity of large amount of solvents, the emulsifying and stabilizing agents are the major drawback of emulsion polymerization method.

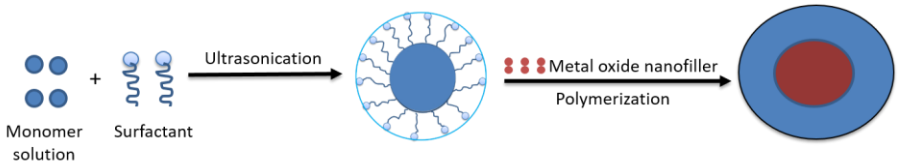

Figure 1.10: Illustration of emulsion polymerization method

1.5.1.7 Blending:

Blending is a well known ex-situ method for developing polymer composites. Blending can be possible in two ways either melt blending or solution blending. The major limitations of blending is the difficulty in producing homogenous composites, because here the possibility for nanoparticle agglomeration is much high. However, the direct mixing of nanoparticles with the polymer matrix is effective through blending. In melt blending, without any requirement of solvents, mixing of nanoparticles with polymers are possible simply with the aid of extruders. Many studies were reported on the fabrication of polymer nanocomposites via melt blending. For example, Hong et al. were developed polyethylene/ZnO nanocomposites with considerable dielectric properties by melt blending [102] and similar observations are also made by Dang et al. [103]. Wong et al. were prepared PMMA/ZnO composites with significant thermal stability via melt blending [104]. But, the requirement of high temperature, which leads to degradation of polymer matrix, limits the applicability of blending method in case of various polymers.

1.5.1.8 Melt Mixing:

Melt mixing method is most promising because there is no need of solvents. This method is useful in preparing bulk amount of composites. The processing devices as well as the processing conditions have a key role in determining the properties of composites. Polymers possessing considerable molecular weight enhance the rate of dispersion of nanoparticles since they can transfer the shear stress to

the particles very effectively. Melt mixing is suitable for fabrication of composites of thermoplastic polymers with strong polar groups such as polyamide, polystyrene where emulsion or in situ polymerization method are not suitable [105]. Melt mixing is not good in the case of poly (butylmethacrylate), since it has very low glass transition temperature, it will make into pasty form even at low temperature and thus the processability became too difficult.

Figure 1.11: Illustration of melt mixing method

1.5.1.9 In situ Polymerization:

Among the various methods for developing polymer nanocomposites, in situ polymerization method has got pivot attention in research field because it ensure the homogenous dispersion of nanoparticles in the polymer matrix [106]. The in situ incorporation of nanoparticles during the process of polymerization attributes to the homogeneity of nanoparticles throughout the matrix. The development of polymer composites containing nanosized particles even at molecular level can be easily achieved through the process of in situ polymerization [107]. In addition, reports revealed that the composites developed through the in-situ method exhibits outstanding thermal, electrical and mechanical properties which are far better than those prepared through other conventional methods like melt mixing, emulsion polymerization etc. The uniform dispersion of nanoparticles helps to have large contact

area with the polymer matrix. Further, here the polymerization is carried out in presence of nanoparticles and so there is a better interfacial interaction between the incorporated nanoparticles and the growing polymer chain, which is attributed to the significant improvement in the properties of composites prepared through in situ method.

Anzlovar et al. were showed that the PMMA/ZnO nanocomposites developed through in situ polymerization exhibited excellent thermal properties [108], Wu et al. reported the higher tensile and electrical properties of polyimide/MWCNT composites fabricated through the same process [109]. Similarly, the significant optical properties of poly (p-phenylenebenzobisoxazole)/MWCNT composites was reported by Zhou et al. [110] and better mechanical stability of polypropylene/clay composites were reported by Baniasadi et al. etc [111].

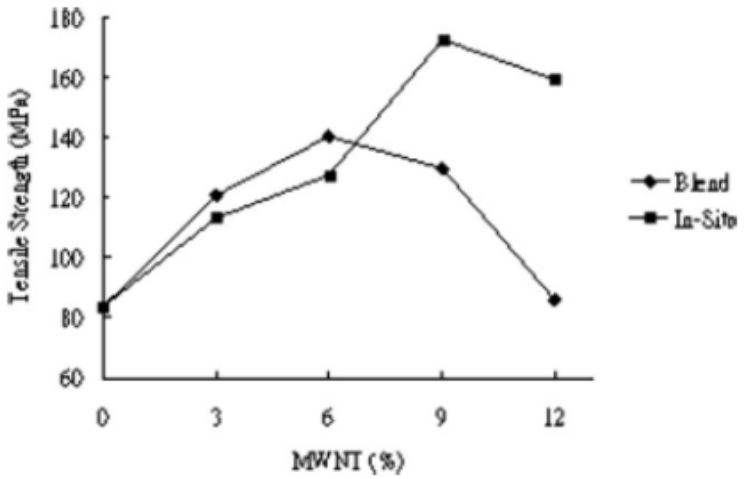

Figure 1.12: Tensile strength of polyimide/MWCNT composites

All these studies revealed that the in situ polymerization is the simple and easiest method for preparing homogenous hybrid polymer nanocomposites. Reviewing these backgrounds, in the present work, we followed in situ polymerization method for preparing PBMA composites containing different nanoparticles.

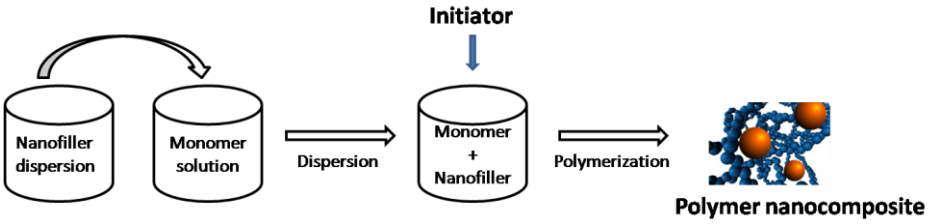

Figure 1.13: Illustration of in situ polymerization method

1.6 Motivation

In recent years, efforts have been carried out by scientist and technologists to develop flexible electronic devices using polymer nanocomposites. The polymer nanocomposites developed by thin, transparent and flexible polymer matrix incorporated with conducting fillers have been identified as promising materials for developing flexible electronic devices. Further, polymer nanocomposites are more attracting because of their excellent mechanical properties from the polymer part and electrical properties from the filler part.

Recently, metal oxide nanoparticles has got pivot attention as reinforcing material for polymer composites owing to their superior physical properties such as high electrical conductivity, mechanical property and high aspect ratio. The better surface properties of metal oxide nanoparticles provide better compatibility with the polymer

matrix and thus stabilize the morphology of polymer composites. This study aimed to develop thin, transparent, flexible polymer nanocomposites possessing significant mechanical and electrical properties using poly (butylmethacrylate) polymer and different types of metal oxide nanoparticles. The substantial properties of the developed PBMA nanocomposites open many applications in the field of flexible electronics.

1.7 Objective of the Work

The main objective of this work is to develop thin, flexible, transparent polymer nanocomposites possessing excellent mechanical and electrical properties which can found various applications in flexible electronic devices. For that PBMA nanocomposite with different types of metal oxide nanoparticles has been developed via in situ polymerization method. The objectives of present work are listed below.

- Preparation of CeO_2, Nd_2O_3, TiO_2, Ce doped TiO_2 and Nd doped TiO_2 nanoparticles
- Characterization of the synthesized nanoparticles by various analytical techniques
- Development of PBMA/CeO_2, PBMA/Nd_2O_3 , PBMA/TiO_2, PBMA/Ce-TiO_2 and PBMA/Nd-TiO_2 nanocomposites using prepared metal oxide nanoparticles
- Analyse the morphology of polymer nanocomposites using FT-IR, UV-Visible, XRD, SEM and TEM analysis

- To study the thermal properties of composites using DSC and TGA
- To study the effect of nanoparticle loading on the mechanical and electrical properties of PBMA polymer
- To investigate the role of various parameters on the mechanical and electrical properties by applying various theoretical modelling.

CHAPTER 2
EXPERIMENTAL AND CHARACTERIZATION

Contents

2.1 Materials

2.1.1 Butylmethacrylate ($C_8H_{14}O_2$)

Butylmethacrylate (Molecular weight = 142.2) was supplied by Himedia. The inhibitor in the butylmethacrylate monomer sample was purified by vacuum distillation.

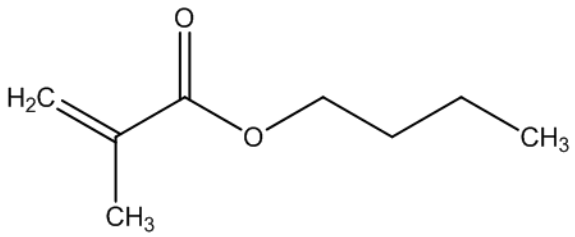

Figure 2.1: Chemical structure of butylmethacrylate

2.1.2 Titanium isopropoxide (Ti (OPr)$_4$)

Titanium isopropoxide (Molecular weight = 284.22) was used as the precursor for preparing TiO_2 nanoparticles and was purchased from Sigma-Aldrich.

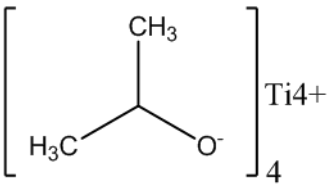

Figure 2.2: Chemical structure of titanium isopropoxide

2.1.3 Cerium (III) nitrate. Haxa hydrate ($Ce(NO_3)_3.6H_2O$)

Cerium nitrate. Haxa hydrate (Molecular weight = 434.22) was used as the precursor for preparing CeO_2 nanoparticles and also it is used as the

metal salt for doping cerium on the TiO_2 nanoparticles. The $Ce(NO_3)_3.6H_2O$ was supplied by Sigma-Aldrich.

2.1.4 Neodymium (III) nitrate. Haxa hydrate ($Nd(NO_3)_3.6H_2O$)

Neodymium nitrate. Haxa hydrate (Molecular weight = 438.35) was used as the precursor for preparing Nd_2O_3 nanoparticles and was supplied by Sigma-Aldrich.

2.1.5 Azobis isobutyro nitrile (AIBN)

Azobis isobutyro nitrile (Molecular weight = 164.21) was used as the initiator for developing PBMA nanocomposites. The AIBN was purchased from Sigma-Aldrich.

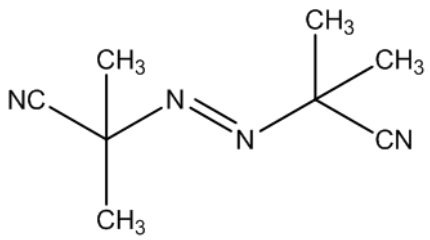

Figure 2.3: Chemical structure of azobis isobutyro nitrile

2.1.6 Cetyl trimethyl ammonium bromide (CTAB)

Cetyl trimethyl ammonium bromide was as the surfactant during the fabrication of PBMA composites. The CTAB was purchased from Merck, India.

2.1.7 Solvents

Toluene, nitric acid, ethanol was procured from Merck, India and was used without further purification.

2.2 Methods

2.2.1 Synthesis of Titanium Dioxide (TiO_2) Nanoparticles

Titanium dioxide nano-powder (TiO_2) was synthesized via sol-gel method [113, 114]. In procedure, 10 ml of ethanol was taken in a beaker and to this required amount of titanium isopropoxide was added slowly with constant stirring. After 30 minutes some drops of water was added and then the sol was allowed to stirring for 12 h. After that the sol was dried in water bath and subjected to calcination at 550°C for 2 h and stored in desiccator.

2.2.2 Synthesis of Cerium Doped Titanium Dioxide (Ce-TiO_2) Nanoparticles

Cerium-doped TiO_2 nanopowder (Ce-TiO_2) was synthesized via sol-gel method [113]. Briefly, titanium isopropoxide was dissolved in ethanol followed by the addition of titanium isopropoxide in drop wise, with constant stirring, to the mixture containing ethanol. To this solution, calculated amount of cerium nitrate with 0.5 mL of nitric acid in ethanol was added slowly with vigorous stirring. After 30 min, few drops of water were added, and the sol was stirred for 12 h. The gel was dried at 60°C to form a solid powder. The powder was calcined at 550°C for 2 h and immediately stored in a desiccator.

2.2.3 Synthesis of Neodymium Doped Titanium Dioxide (Nd-TiO_2) Nanoparticles

The Nd-TiO_2 nanoparticles were prepared through the sol–gel process by using titanium isopropoxide as the precursor and Nd_2O_3 as the

dopant precursor. 1.5 wt% of Nd_2O_3 with HNO_3 was added to ethanol to get the dopant solution. This dopant solution was added to an ethanolic solution of titanium isopropoxide. The solution was constantly stirred for 20 min and mixed with few drops of water. The resulting solution slowly gets converted into a gel. The gel was stirred for 12 h and then dried. The dried powder was calcined at 550°C for 2 h and immediately stored in a desiccator.

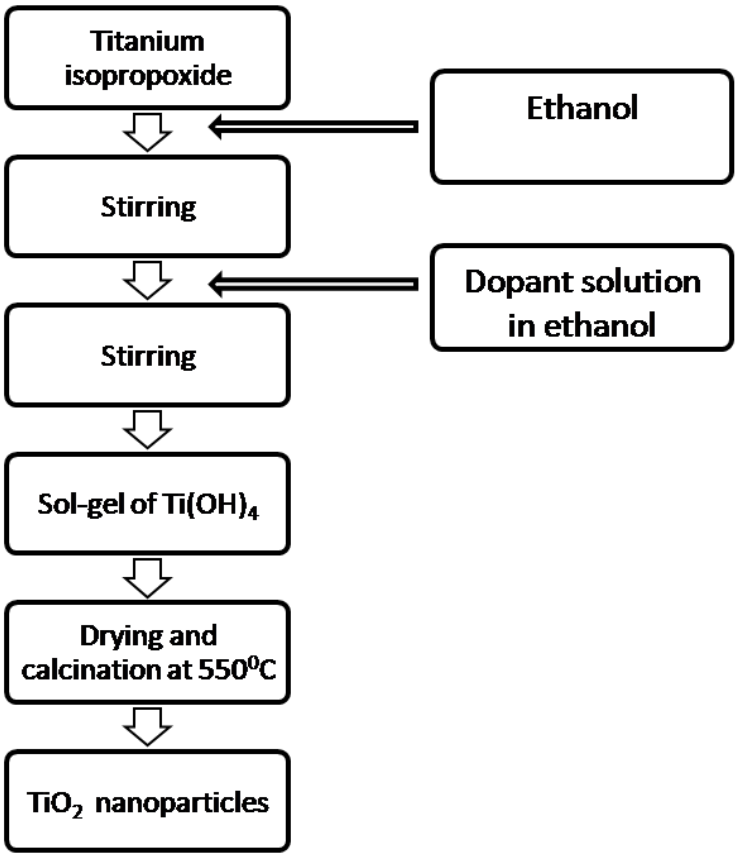

Figure 2.4: Illustration of sol-gel process

2.2.4 Synthesis of Cerium Dioxide (CeO_2) Nanoparticles

The CeO_2 nanoparticles were precipitated out from $Ce(NO_3)_3.6H_2O$ [87, 115]. The required amount of $Ce(NO_3)_3.6H_2O$ was dissolved in ethanol via constant stirring and the solution was subjected to heating to attain a temperature of about 55°C. To this hot solution NH_4OH was added slowly. Immediately, light brown coloured $Ce(OH)_2$ was formed. After sometime, the precipitate was turned into light yellow colour by the formation of CeO_2. Then, the obtained precipitate were centrifuged, washed with ethanol and dried at 100°C to remove the water molecules. Finally, the yellow coloured CeO_2 nanoparticles were obtained after the calcination at 550°C for 2 h.

2.2.5 Synthesis of Neodymium Oxide (Nd_2O_3) Nanoparticles

The Nd_2O_3 nanoparticles were synthesized via precipitation method by using $Nd(NO_3)_3.6H_2O$ as the precursor. The $Nd(NO_3)_3.6H_2O$ was dissolved in ethanol and was heated with constant stirring. To this NH_4OH was added in drop wise. Subsequently light violet coloured $Nd(OH)_3$ were formed, centrifuged, washed with ethanol and dried at 100°C for removing the water molecules. After, the obtained $Nd(OH)_3$ powders were calcined at 550°C for 2 h to give violet coloured Nd_2O_3 nanoparticles.

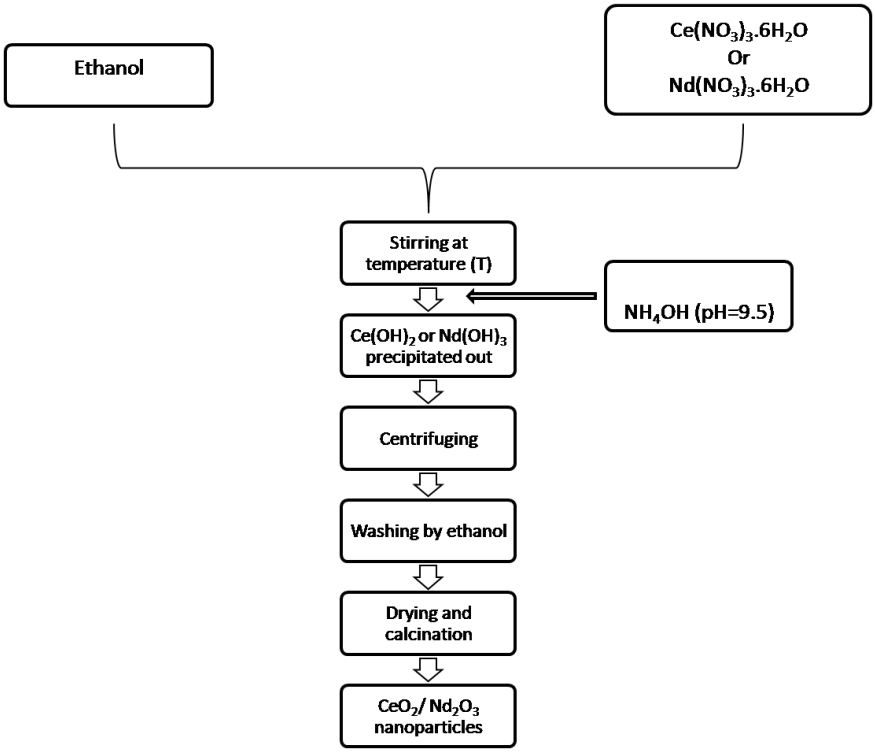

Figure 2.5: Illustration of co-precipitation method

2.2.6 Synthesis of PBMA Nanocomposites using TiO_2 /Ce-TiO_2 /Nd-TiO_2 /CeO_2 /Nd_2O_3 Nanoparticles

Poly (butylmethacrylate) nanocomposites were synthesized via in situ free radical polymerization method. The desired nanoparticles, CeO_2 /Nd_2O_3 /TiO_2 /Ce-TiO_2 /Nd-TiO_2 (0, 3, 5, 7, and 10 weight percentage (wt%)) were dispersed in toluene containing cetyl trimethyl ammonium bromide (CTAB) through ultrasonication method. This solution was then poured into butyl methacrylate monomer under constant stirring. The whole solution was again ultrasonicated for 15 min, and the polymerization was carried out at 85°C for 90 min using

azobis isobutyro nitrile (AIBN) as initiator. After the complete polymerization, the resultant polymer composites formed were separated by precipitation method, and the product washed with water and dried under vacuum for 48 h at 50°C. Finally, the obtained composites were made into a thin film by solution casting method using chloroform as the solvent for further studies. The schematic representation of the formation of nanocomposite is given in **scheme 2.1.**

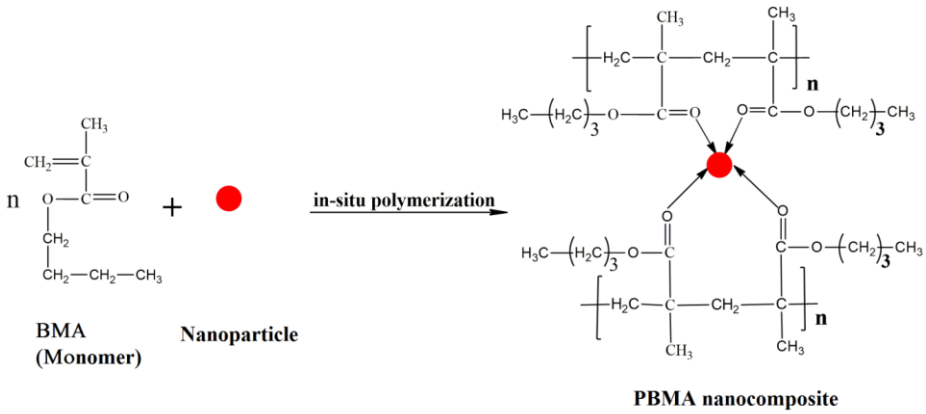

Scheme 2.1: Schematic representation of the formation of PBMA nanocomposites with different nanoparticles

2.3 Characterizations

2.3.1 Fourier-Transform Infrared (FT-IR) Spectroscopy

The FT-IR spectra of PBMA and PBMA nanocomposites were recorded on JASCO (model 4100) Fourier transform infrared spectrophotometer in the region of 4000-400 cm^{-1} by casting thin film of polymer from chloroform solutions between KBR windows of size 25 x 4 mm with 72 scans of 4 cm^{-1} resolution.

2.3.2 Ultraviolet-Visible (UV-Vis) Spectroscopy

The ultraviolet visible (UV-Vis) absorption spectrum of synthesized PBMA and PBMA with different loading of nanoparticles in chloroform was recorded on a Hitachi U-3000 spectrophotometer in the wavelength range of 200-900 nm.

2.3.3 Scanning Electron Microscopy (SEM)

Surface morphology of the fabricated PBMA and PBMA nanocomposites were investigated by a Hitachi S-3000 H scanning electron microscope, after sputter coating of the surface.

2.3.4 Tunnelling Electron Microscopy (TEM)

The TEM images of the PBMA and PBMA/CeO_2 nanocomposites were observed by using the instrument JEM-2100, Japan at an accelerating voltage of 200 kV.

2.3.5 X-Ray Diffraction (XRD) Analysis

The XRD measurements of the synthesized compounds were recorded on a Bruker AXS D X-ray diffractometer using CuKα radiation (k = 1.5406Å) with an accelerating voltage of 30 KV. The diffractograrms were recorded in the range of 2θ = 10 to 80° at a speed rate of 2°/min. XRD is a rapid analytical technique used for phase identification of a crystalline material and can provide information on unit cell dimension. The interaction of the incident rays with the sample produces constructive interference and a diffracted ray when conditions satisfy Bragg's Law. These diffracted X-rays are then

detected, processed and counted. The Bragg's diffraction angle (**2θ**), along with interplanar spacing (**d**), and the relative intensity of the peaks were calculated using Bragg's **equation 2.1**

$$n\lambda = 2\mathrm{d}\sin\theta \qquad (2.1)$$

Where, `**θ**' is one half of the angle read from diffractogram. Scherer's equation was

Used to estimate the particle size & the **equation 2.2** is,

$$\mathrm{D} = 0.9\,\lambda/\beta\cos\theta \qquad (2.2)$$

Where; **D** - Average particle size

λ - Wavelength of radiation of the X-ray beam

β - Width of the peak at half of the maximum intensity (in radian)

θ - Half of the diffraction angle 2θ

2.3.6 Differential Scanning Calorimetry (DSC)

The changes in thermal transition behavior (glass transition temperature) of the composites were noticed using Perkin-Elmer differential scanning calorimetry (DSC) thermal analyzer. For the DSC analysis about 5 mg of the sample was heated from 20°C to 375°C. A heating rate of 10°C/min was used under nitrogen atmosphere and a heat flow of 20 mL/min.

2.3.7 Thermogavimetric Analysis (TGA)

Thermal stability of the prepared composites were examined by Thermogavimetric analyser model Schimadzu TGA-50H from room temperature to 600°C. A heating rate of 10°C/min was used under nitrogen atmosphere at a heat flow rate of 30 mL/min.

2.3.8 Conductivity Studies

The Electrical conductivity of the polymer composite was measured by cutting the samples in a circular shape. The AC resistivity of the samples was measured with a fully automatic Hewlett–Packard LCR Meter at room temperature in a frequency range of 10^2–10^6 Hz. The dielectric constant (ε_r) was calculated by using the relation,

$$\varepsilon_r = \frac{C.d}{\varepsilon_0.A} \qquad (2.3)$$

and the conductivity was calculated by the equation

$$\sigma_{ac} = \varepsilon_0.\varepsilon_r.\omega.tan\,\delta \qquad (2.4)$$

where d is the thickness of the sample, C is the capacitance, A the area of cross section of the sample and ε_0 the permittivity of free space ε_r is the relative permittivity of the material which is a dimensionless quantity. The inherent dielectric loss (tan δ) was also measured directly from the HP LCR meter.

The DC electrical conductivity of all the PBMA nanocomposites was measured by using Keithly 2400 instrument, a fully automatic system.

2.3.9 Mechanical Studies

The tensile strength and elongation at break of polymeric materials were carried out using a Zwick Universal Testing Machine (UTM) at 28°C, according to ASTM D 412 (2016) and at a crosshead speed of 500 mm/min**.** Average of at least of five readings per sample represents each data point.

CHAPTER 3
THERMAL, MECHANICAL AND CONDUCTIVITY STUDIES OF POLY (BUTYLMETHACRYLATE) NANOCOMPOSITES INCORPORATED WITH TiO_2 NANOPARTICLES

Contents

3.2 Introduction

Polymer matrix incorporated with nanofillers got immense attention in research and industrial applications because of their novel properties over that of bare polymer matrix since, it possess the properties of both organic polymer matrix and inorganic filler [116]. The major problem related to the synthesis of polymer nanocomposites are the agglomeration tendency of nanofillers within the matrix [117]. This is a serious issue especially for the thermal, mechanical and electrical conductivity properties because the properties mainly related to the contact between fillers and the polymer matrix [118]. The problem of aggregation of nanoparticle can be overcome by in situ polymerization method [119]. Polymer nanocomposites provide higher mechanical strength, thermal stability, electrical properties, flame retardancy, and resistance towards degradation. The properties depend on the size, shape and nature of the filler particle. In addition to this, the larger surface area along with large interfacial interaction between matrix and filler particles provides higher dielectric properties to polymer nanocomposites [120]. Transparent polymer matrices have been widely studied for their applications towards optical, thermal, mechanical and conductive areas because of their selective absorption towards light, effective inter particle interactions, filler to matrix interaction and obviously due to ease of processing and protection [121]. Acrylate polymer nanocomposites are extrinsive conducting polymers that made by incorporating conducting filler particles. Extrinsive conducting polymers are quite cheaper and very easy to be prepared. Further, the major highlighting factor here is that the

properties as well as the processability of this extrinsive conducting polymers can be tuned according to our interest by changing the shape, nature of the filler particle [122]. During the selection of filler the main objective should be the capability of formation of continues network within the polymer matrix. There have many reports regarding acrylate polymer nanocomposites has led to novel electrical properties with the addition of suitable fillers [123].

Studies reported that polymer nanocomposites made of semiconducting nanoparticles possess higher conductivity at room temperature as well as at higher temperature. TiO_2, NiO and ZnO are the most commonly studied nanofiller particle [124]. TiO_2 possess wide band gap energy and high refractive index suitable for various applications in electronic field. Also the vacant d-orbital on the surface of TiO_2 help in effective dispersion within the polymer matrix and hence efficient conductivity [125, 126]. It was reported that the PBMA matrix encapsulated with TiO_2 exhibit higher optical, thermal, dielectric and electrical properties and made transparent host matrix suitable in electronic appliances [127]. The present work mainly focused on the effect of TiO_2 nanoparticle on thermal, mechanical, AC and DC conductivity of poly (butylmethacrylate)/TiO_2 nanocomposites. Also the present work extended to study the mechanical and conductive nature of the polymer nanocomposites by comparing with different theoretical model studies to understand the applicability of the fabricated hybrid nanocomposites in various fields.

3.4 Results and Discussion

3.4.1 FT-IR Spectra

The successful incorporation of TiO_2 nanoparticles in the PBMA was examined by FT-IR and the obtained FT-IR spectra of TiO_2, PBMA and PBMA/TiO_2 nanocomposites was presented in **figure 3.1.** The FTIR spectra of TiO_2 shows intense and broad band at 3400 cm^{-1} corresponds to the -OH stretching vibrations from the absorbed H_2O molecules. Meanwhile the peak around 400-700 cm^{-1} assigned to the Ti-O vibrations [128]. In the spectra of PBMA and its composites, the peak at 1150 cm^{-1} is assigned to the vibration mode of C-O in the ester group and the peak at 1240 cm^{-1} corresponds to the torsion of CH_2 group. The peak at 1729 cm^{-1} attributed to the C=O stretching band of the ester group. Also, from the spectra of PBMA, the peak at 2873 and 2950 cm^{-1} are attributed to the CH_2 stretching modes, was slightly shifted to 2873 and 2958 cm^{-1} respectively. Shahzada et al. were reported the same observation that the peak at 2900 and 2990 cm^{-1} for CH_2 stretching vibrations in the PMMA was shifted to 2920 and 2951 cm^{-1} respectively, probably due to some interactive role played by TiO_2 on PBMA matrix [129]. Further, in the spectra of PBMA/TiO_2 nanocomposites the appearance of peak corresponds to the Ti-O-Ti vibration (400-700 cm^{-1}) also clearly specify the incorporation of TiO_2 nanoparticles in the PBMA. Moreover the strong and intense peak at 745 cm^{-1} attributes to the Ti-O-Ti stretching vibrations further confirm the successful incorporation of TiO_2 nanoparticles in the PBMA.

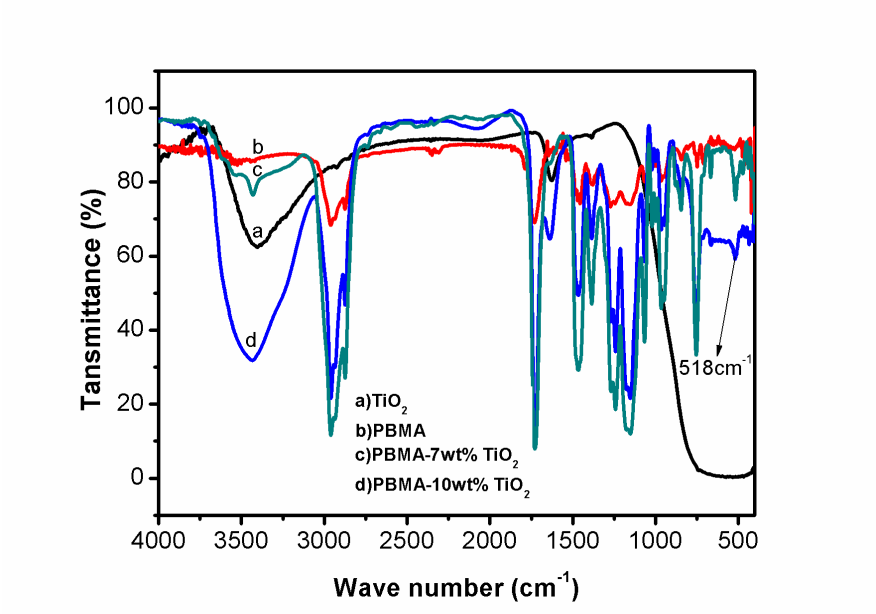

Figure 3.1: FT-IR spectra of TiO_2, PBMA and PBMA/TiO_2 nanocomposites

3.4.2 UV-Visible Spectra

Figure 3.2 represents the UV-Visible spectra of PBMA and PBMA/TiO_2 nanocomposites. As seen from figure, all the samples exhibit a single peak at 245 nm attributes to the n-Π* transitions of -C=O group present in the PBMA backbone [130]. The absence of any peak in the visible region itself reveals the transparent nature of pure PBMA and PBMA/TiO_2 nanocomposites. However, it is interesting that the intensity of absorption is much higher in composites than that of bare PBMA. Moreover, upon addition of TiO_2 nanoparticles the intensity of absorption peak further increasing and here the composite with 7 wt% TiO_2 nanoparticles shows maximum absorption, after this the absorption was slightly decreasing. The absorption edge of

composites was significantly shifted to higher wavelength than bare PBMA indicates the interfacial interaction between the TiO_2 nanoparticles and the PBMA matrix. Here also, the composite with 7 wt% TiO_2 nanoparticles shows higher absorption edge. The results show that the nanoparticles are effectively dispersed in the PBMA matrix with a greater interaction between the matrix and nanoparticle. However, this matrix-filler interaction is lower at higher filler loading (10 wt%) due to greater filler-filler interaction and which ascribed to the lower absorption in the case of PBMA with 10 wt% TiO_2 nanoparticles.

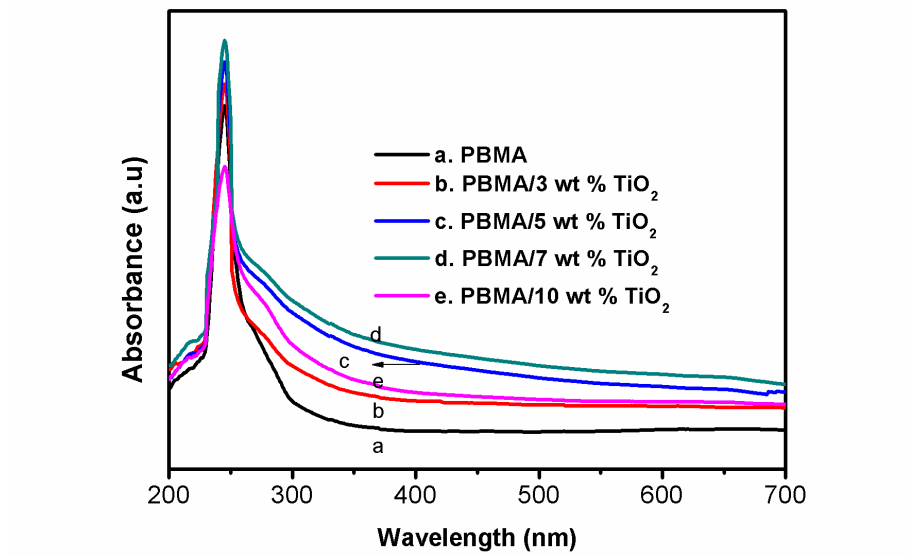

Figure 3.2: UV-Visible spectra of PBMA and PBMA/TiO_2 nanocomposites

3.4.3 XRD Analysis

The X-ray diffraction patterns of TiO_2 nanoparticles, PBMA and PBMA/TiO_2 nanocomposites were displayed in **figure 3.3 (a-b)**. The

XRD of prepared TiO_2 nanoparticle is crystalline in nature with various peaks at $2\theta = 25.32^{\circ}$, 48.15°, 54.5°, 62.76° and 68.78° assigned to reflections from (101), (200), (105), (213) and (116) crystal planes respectively [131]. The average crystalline size of prepared TiO_2 nanoparticle was found to be ~14.99 nm by using Scherrer's formula. The pristine PBMA exhibits a broad diffraction peak at $2\theta = 17.65^{\circ}$, shows its characteristics amorphous nature. However, upon addition of TiO_2 nanoparticles, the composites exhibits extra crystalline peaks corresponds to that of TiO_2 in addition with the amorphous peak, indicate the effective dispersion of nanoparticles in the PBMA matrix. Moreover, the decrease in intensity as well as d-spacing of amorphous peak by the further addition of TiO_2 nanoparticle shows the better dispersion of nanoparticles by interfacial interaction with PBMA backbone.

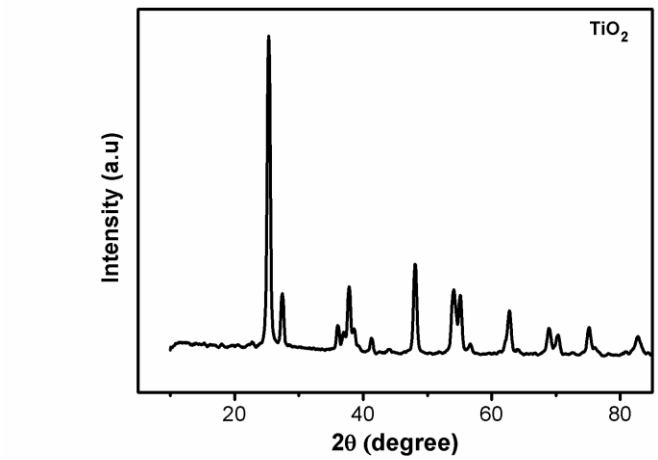

Figure 3.3 (a): XRD pattern of developed TiO_2 nanoparticle

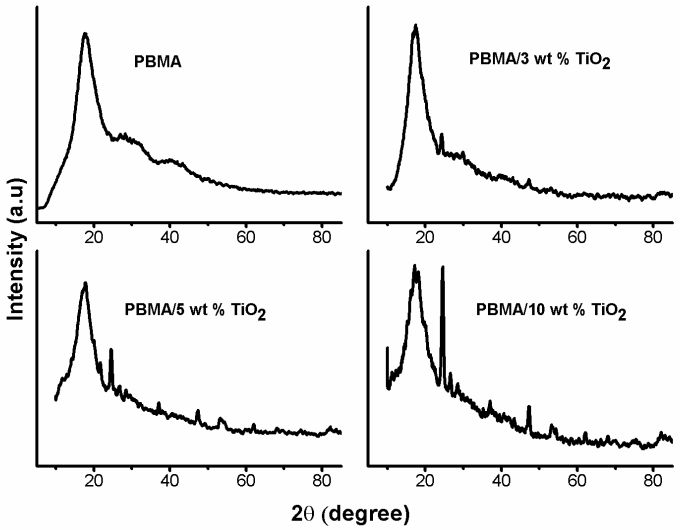

Figure 3.3 (b): XRD pattern of PBMA and PBMA/TiO_2 nanocomposites

3.4.4 FE-SEM Analysis

The surface morphology of TiO_2, PBMA and PBMA with TiO_2 were analysed using FE-SEM and the obtained images are shown in **figure 3.4 (a&b)**. As prepared TiO_2 nanoparticles were spherical in morphology and seemed to be slightly agglomerated with average size of ~12-13 nm. The pure PBMA shows smooth and clean surface morphology with some irregularity in polymer chain, again a distinct characteristics of amorphous phase. However, the presence of nanoparticles was clearly revealed from the SEM images of composites. It shows homogenous morphology with uniform dispersion of nanoparticles up to 7 wt% TiO_2 nanoparticles, might be acquired through better interfacial interaction between the PBMA matrix and TiO_2 nanoparticles. The composite with 10 wt% TiO_2 nanoparticle exhibits irregular morphology with presence of

agglomerated nanoparticles. At higher loading, due to self agglomeration of nanoparticles, the matrix-filler interaction gets disrupted and this leads to improper dispersion of nanoparticles in the polymer matrix.

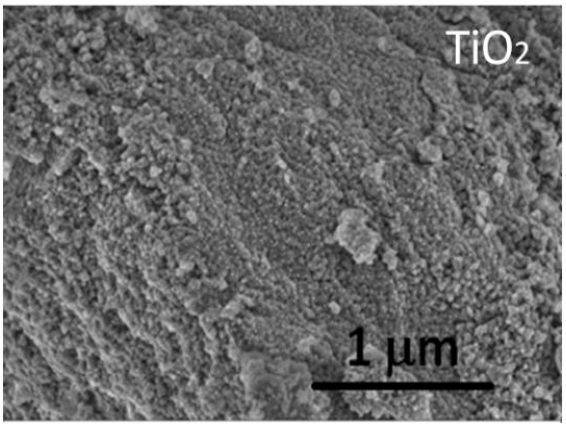

Figure 3.4 (a): FE-SEM image of TiO_2 nanoparticles

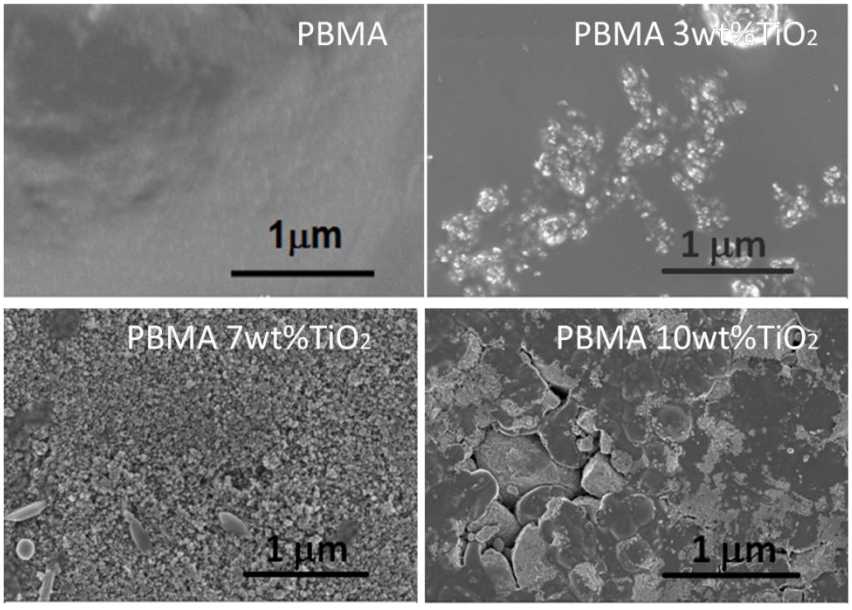

Figure 3.4 (b): FE-SEM images of PBMA and PBMA/TiO_2 nanocomposites

3.4.5 TEM Analysis

The TEM images of prepared TiO_2 nanoparticles, PBMA nanocomposites with 5 and 10 wt% of TiO_2 nanoparticles are shown in **figure 3.5.** The average size of TiO_2 nanoparticles has been found to be ~14 nm, which is much close to that obtained from XRD results. The encapsulation of TiO_2 nanoparticles (dark color) in the PBMA matrix (light color) is clearly evident from the TEM images of nanocomposites. However, the homogenous dispersion of individual nanoparticles is most effective in PBMA nanocomposite with 5 wt% of TiO_2 and in the case of PBMA nanocomposite with 10 wt% of TiO_2 several nanoparticles are get agglomerated, as expected from the SEM images. Further, the uniformly distributed concentric diffraction peaks in the SAED patterns confirmed the homogenous dispersion of TiO_2 nanoparticles in the PBMA matrix.

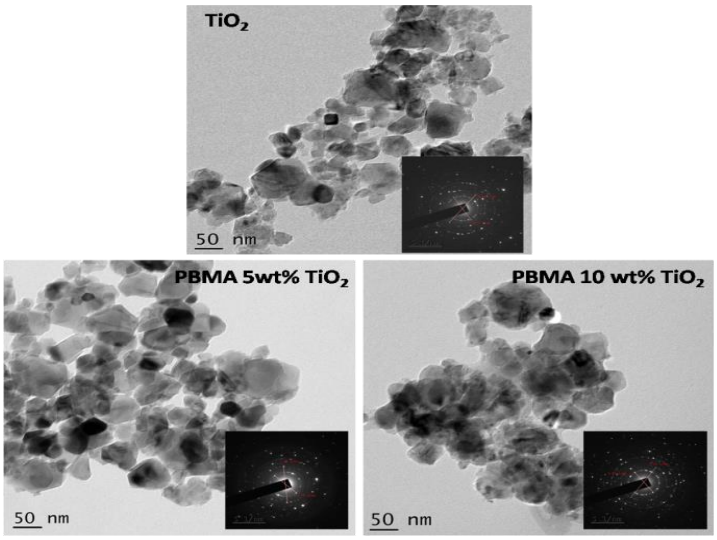

Figure 3.5: TEM images of TiO_2 and PBMA/TiO_2 nanocomposites

3.4.6 Thermal Properties

3.4.6.1 DSC Analysis

Thermal properties of PBMA and PBMA/TiO_2 nanocomposites were examined via DSC analysis and the obtained results are presented in **figure 3.6.** The PBMA and PBMA/TiO_2 nanocomposites exhibits a minor endothermic peak at ~20°C corresponds to the glass transition temperature (Tg) of the sample. The other major two endothermic dip attributes to their melting points (Tm). From the figure, it is clear that the Tg as well as Tm of PBMA was substantially enhanced upon addition of TiO_2 nanoparticles, indicate the improved thermal properties of composites than the plane PBMA matrix. The interfacial interaction of TiO_2 nanoparticles with the PBMA matrix (as revealed from XRD and SEM results) resist the free movement of polymer segments, which results in higher thermal properties of composites than the plane PBMA polymer.

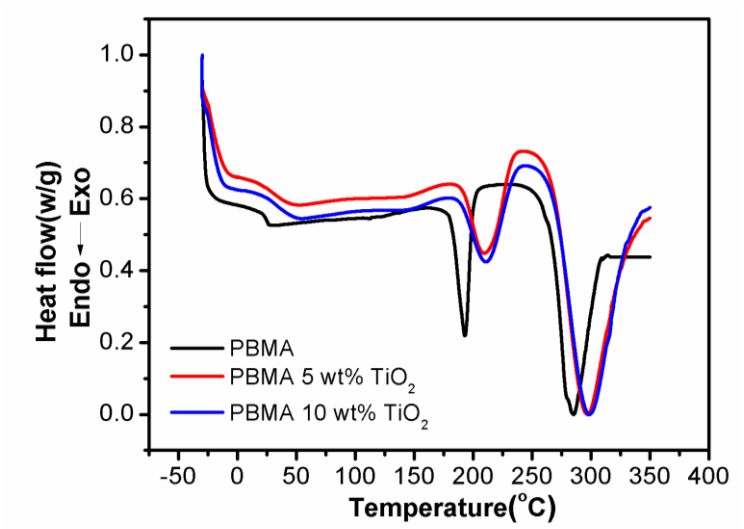

Figure 3.6: DSC curve of PBMA and PBMA/TiO_2 nanocomposites

3.4.6.2 TGA Analysis

Figure 3.7 shows the TGA and corresponding DTG curve of pure PBMA and its nanocomposites with different content of TiO_2 nanoparticles. As seen from figure, all samples exhibit two step of degradation. The initial weight loss around 250°C attributes to the homolytic cleavage of vinyl group present in the PBMA backbone and the second step around 320°C corresponds to the rapid scission of polymeric backbone [132]. The obtained degradation temperature (initial (Ti) and second (Ts)) from TGA and the maximum degradation temperature (Tmax) from DTG are presented in **table 3.1.** It clearly seen from the table that the nanoparticle addition significantly improved the thermal stability of the PBMA. For example, the bare PBMA exhibit the initial weight loss at 256.01°C, while the PBMA with 5 and 10 wt% of TiO_2 nanoparticle shows the initial weight loss at 262.29°C and 266.48°C respectively. Similarly, the Ts and Tmax were substantially enhanced with the addition of TiO_2. The improved thermal stability by the incorporation of nanoparticles is might be due to the better dispersion and interfacial interaction of nanoparticles with the PBMA matrix, support the data obtained from SEM and XRD results.

Table 3.1: The value of Ti, Ts and Tmax obtained from the TGA and corresponding DTG curves for PBMA and PBMA/TiO_2 nanocomposites

	TGA		DTG	
	T_i (°C)	Ts(°C)	T_{max} (°C) Ist stage	T_{max} (°C) IInd stage
PBMA	256.01	330.49	280.29	364.33
PBMA/5 wt% TiO_2	267.12	342.57	282.68	374.98
PBMA/10 wt% TiO_2	271.71	346.14	288.49	377.02

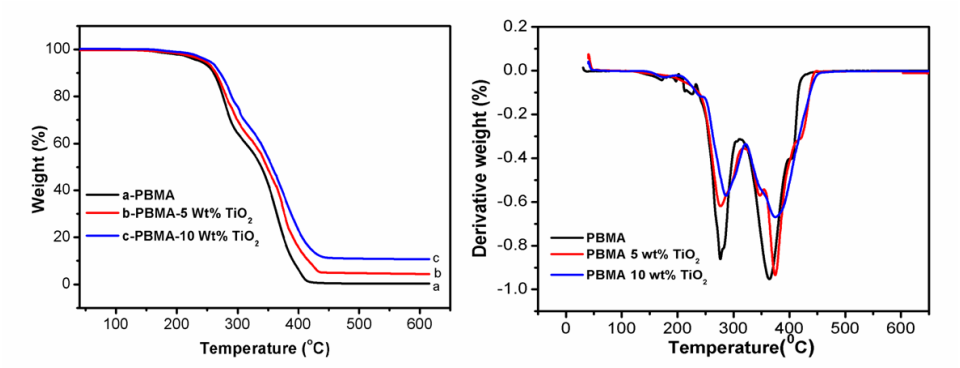

Figure 3.7: TGA and corresponding DTG curve of PBMA and PBMA/TiO_2 nanocomposites

3.4.7 Tensile Strength Studies

The tensile strength and elongation at break of PBMA and PBMA/TiO_2 nanocomposites were investigated and the obtained result is given in **figure 3.8.** It is cleared from the figure that the tensile strength was substantially enhanced with the addition of nanoparticles and reaches its maximum at 7 wt% (40.22 %). The incorporation of nanoparticles creates additional stress concentration sites and this facilitate in effective stress transfer from matrix to the filler [133, 134].

In other words, the interfacial interaction between the TiO_2 nanoparticles and the PBMA matrix helps in imparting the stress created in the matrix surface to the nanoparticles and this leads to the higher tensile strength in the case of nanocomposites than that of plane polymer [135]. The maximum value of 7 wt% sample indicates that the better dispersion and hence effective interfacial interaction is high at 7 wt% and after, there might be some interruptions in the matrix-filler interaction. These interruptions at higher concentrations might be due to the presence of agglomerated nanoparticles (revealed from SEM) which results in poor dispersion and so weak interfacial interaction with the matrix. The elongation at break shows marginal decrease in value with the addition of nanoparticles implies the reinforcing effect of TiO_2 nanoparticles. The homogenous dispersion and the phase interaction of nanoparticles with the matrix increase the stretching resistance and correspondingly decrease the elongation at break.

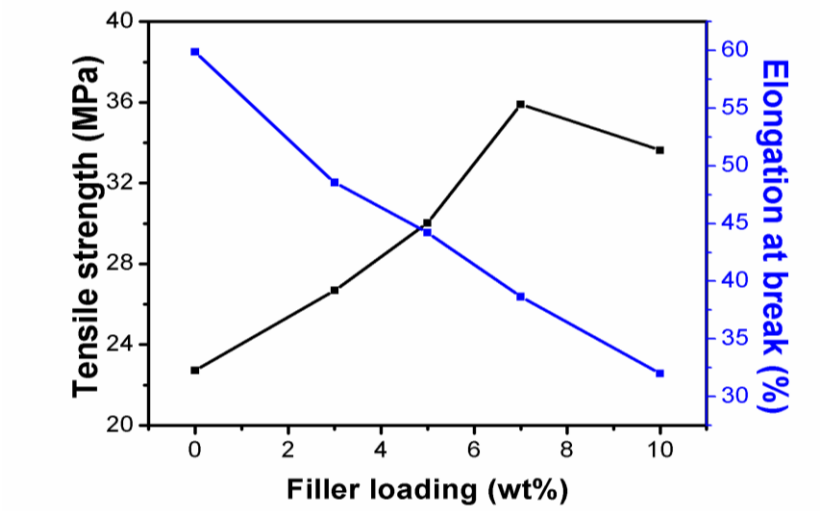

Figure 3.8: Tensile strength and elongation at break of PBMA and PBMA/TiO_2 nanocomposites

3.4.8 Theoretical Modelling to Tensile Strength

The theoretical modeling approaches are much effective in predicting the tensile properties of the polymer systems especially for polymer nanocomposites. Various theoretical models have been introduced to examine the effect of different parameters like filler geometry, arrangement, concentration etc to the tensile property [136-142]. In the present study Einstein, Mooney, Guth and Pukanszky equations have been employed to analyze the tensile properties of PBMA/TiO_2 nanocomposites.

According to Einstein model, the total tensile property of the composites having perfect phase interaction between the polymer matrix and the filler is directly related to the amount of filler present in the matrix [137]. The equation can be written as

$$Mc = Mm(1 + 2.5Vf) \qquad (3.1)$$

Where Mc and Mm represents the tensile property of composites and the plane polymer respectively, Vf implies the filler concentration.

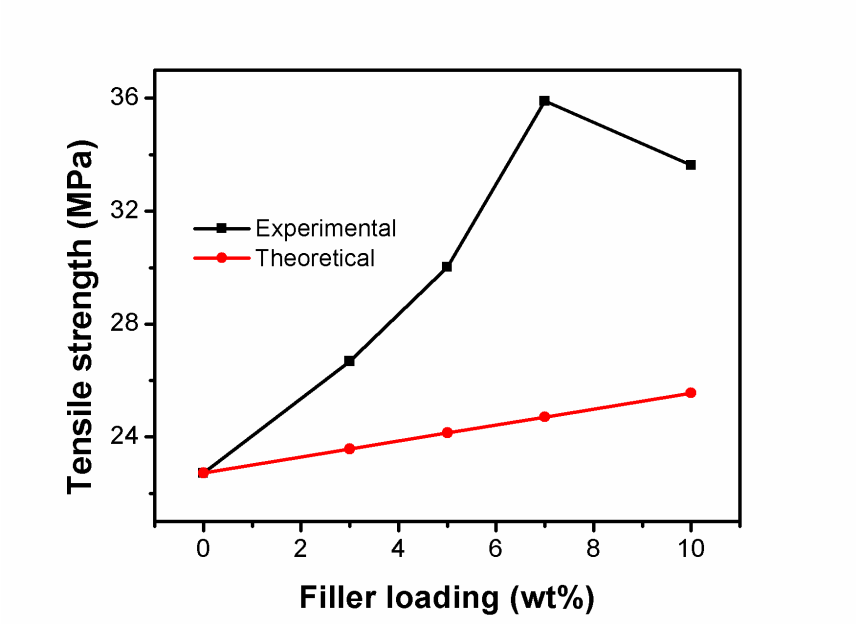

Figure 3.9: Theoretical and experimental tensile strength plots for PBMA and PBMA/TiO_2 nanocomposites based on Einstein model.

Mooney modified the Einstein equation by introducing a new variable 'S' (crowding factor) whose value is 1-1.25 for loosely packed systems and 1.35 for closely packed systems [138]. And the Mooney equation is given as

$$Mc = Mm * exp[\frac{2.5Vf}{1-SVf}] \quad (3.2)$$

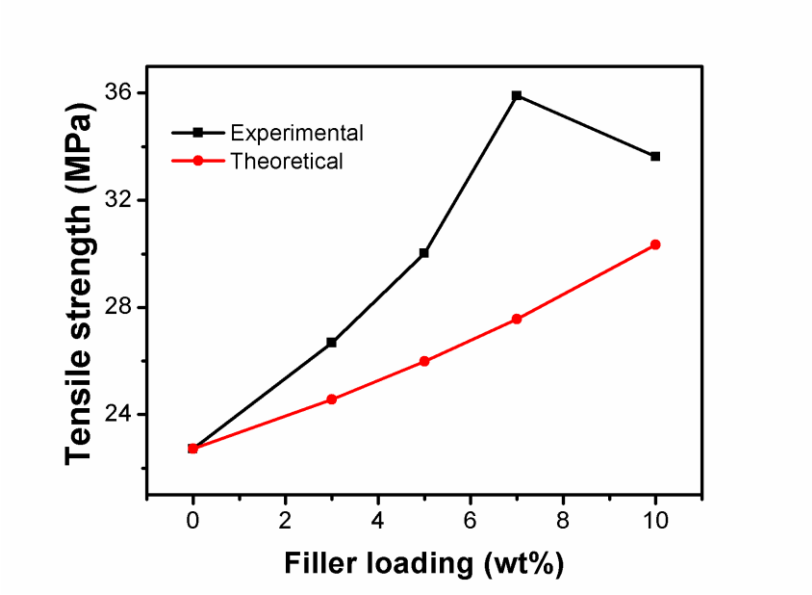

Figure 3.10: Theoretical and experimental tensile strength plots for PBMA and PBMA/TiO_2 nanocomposites based on Mooney model

Guth modified Einstein equation for perfect phase interaction [139] and it is given as

$$Mc = Mm(1 + 2.5Vf) + 14.1\,Vf\text{^}2 \qquad (3.3)$$

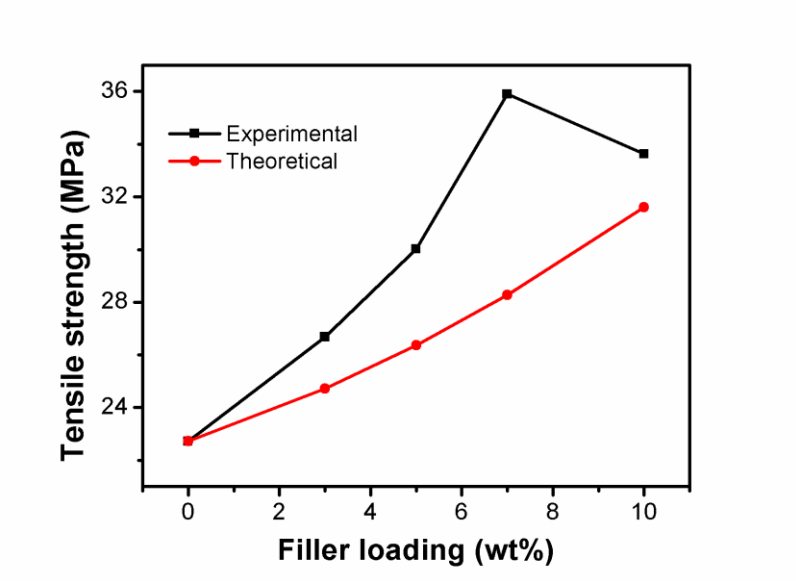

Figure 3.11: Theoretical and experimental tensile strength plots for PBMA and PBMA/TiO_2 nanocomposites based on Guth model

Kerner derived an equation for predicting the tensile property of polymer composites having moderate filler concentration as follows [140]

$$Mc = Mm * 1 + \left[\frac{Vf\ 15(1-Vm)}{(1-Vf)(8-10Vm)}\right] \qquad (3.4)$$

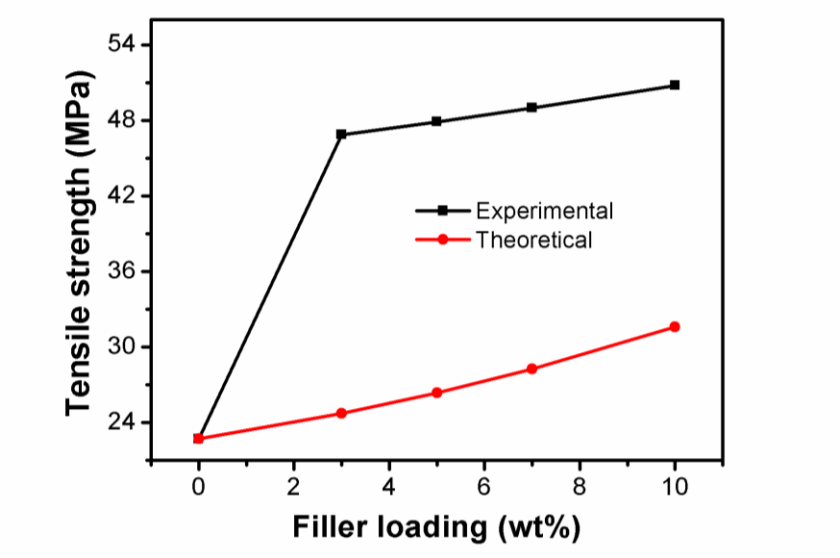

Figure 3.12: Theoretical and experimental tensile strength plots for PBMA and PBMA/TiO_2 nanocomposites based on Kerner model

The tensile strength of PBMA/TiO_2 nanocomposites were calculated by using Einstein, Mooney, Guth and Kerner equations and is given in **figure 3.9, 3.10, 3.11 and 3.12** respectively. As seen from the figures, the Einstein, Mooney and Guth equation used in present case does not show any agreement with that of experimental value. The main assumption of both these equations is that the tensile property is mainly depends on filler concentration only and not consider about the effect of aspect ratio, geometry, extend of interaction with polymer matrix etc of the filler to the tensile property. So most cases these models fail to calculate the actual tensile property of the polymer composites.

Pukanszky Model: Pukanszky developed an equation for calculating tensile property. The model considers that the interfacial interaction of

filler with the matrix strongly influence the final tensile property of the composites along with filler concentration [141, 142]. And the equation can be given as

$$Mc = Mm * \frac{1-Vf}{1+2.5Vf} * exp(Bvf) \qquad (3.5)$$

The parameter B depends on strength of interfacial interaction between the filler and the matrix. The value of B can be obtained by comparing the experimental tensile value with that of Pukanszky model. In the present case Pukanszky equation shows better fit that of experimental value **(figure 3.13)**. That means, the interfacial interaction between the TiO_2 nanoparticles and the PBMA matrix plays a major role in improving the tensile properties of nanocomposites than the plane PBMA.

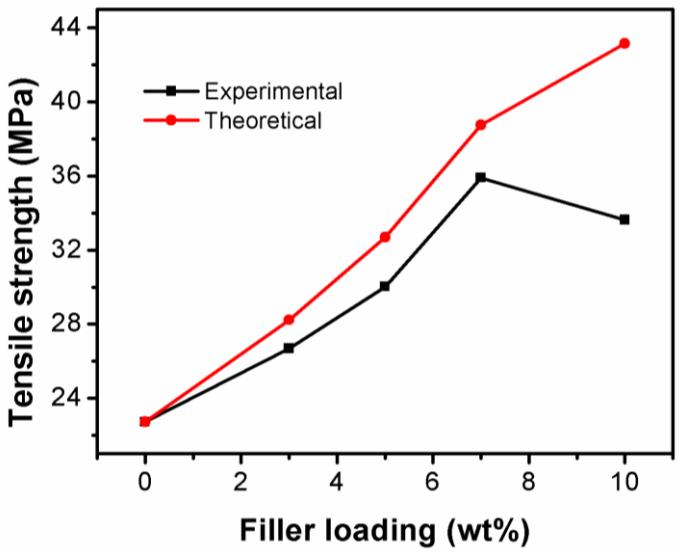

Figure 3.13: Theoretical and experimental tensile strength plots for PBMA and PBMA/TiO_2 nanocomposites based on Pukanszky model

3.4.9 AC Conductivity Studies

The frequency dependence of inherent dielectric loss (tan δ) for PBMA and PBMA/TiO_2 nanocomposites is shown in **figure 3.14.** From figure, we can see that the dielectric loss decreases with frequency up to 10^4 Hz and after it remains constant for all composites. The higher dielectric loss at low frequency arises from the interfacial as well as orientation polarization developed in polymer segments. Further it can be seen that the loss value increases with the loading of TiO_2 nanoparticles up to 7 wt% and after the dielectric loss shows slight decrease. The increase in loss value with addition of nanoparticles shows the better interfacial interaction between the PBMA matrix and the TiO_2 nanoparticles. Further, the nanoparticle addition brought some modifications in the PBMA matrix, which leads to overlapping of relaxation process and results in higher dielectric loss in PBMA composites. The presence of agglomerated particles at higher loading (revealed from SEM) reduces the interfacial interaction between the matrix and filler and this leads to low dielectric loss at higher concentration (at 10 wt% of TiO_2 nanoparticles).

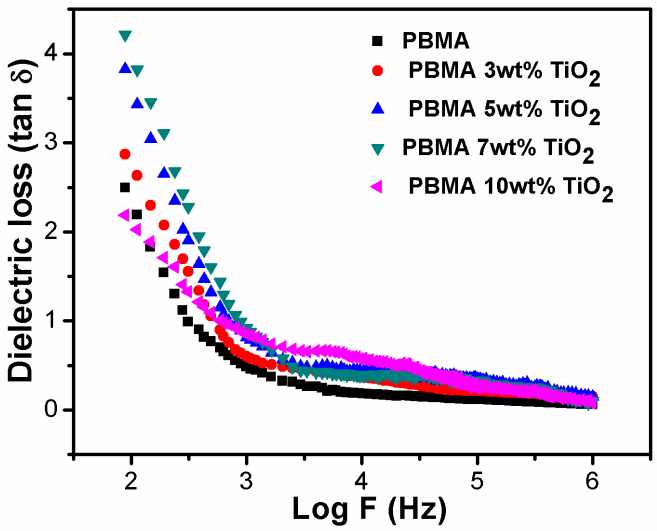

Figure 3.14: Variation of dielectric loss (tan δ) with frequency for PBMA and its composites with different content of TiO_2 nanoparticles.

Figure 3.15 shows the variation of dielectric constant (ε_r) with frequency for PBMA and its composites with different content of TiO_2 nanoparticles. The dielectric constant is decreasing with frequency up to 10^4 Hz and there after it remains independent of frequency. The higher dielectric constant at lower frequency is due to the contributions from space charge polarization at the PBMA/TiO_2 interfaces and also from the polarization effect of PBMA polymer segments and TiO_2 nanoparticles. More over at lower frequency the dipoles can arrange themselves with the applied frequency. However, at higher frequency the dipoles fail to come with same pace as that of the applied frequency and so the dielectric constant remains constant at higher frequencies. It can be seen from figure that the dielectric constant was

substantially enhanced with the addition of nanoparticles. Because during the addition of nanoparticle, there is gradual formation of micro-capacitor network at the interface between insulating polymer matrix and the conducting filler. However, in PBMA/TiO_2 nanocomposites the maximum dielectric constant was shown by 7 wt% nanocomposites and after there is slight decrease in dielectric constant obviously due to the agglomeration of nanoparticles, which result in poor interfacial interaction between the PBMA matrix and the TiO_2 nanoparticles.

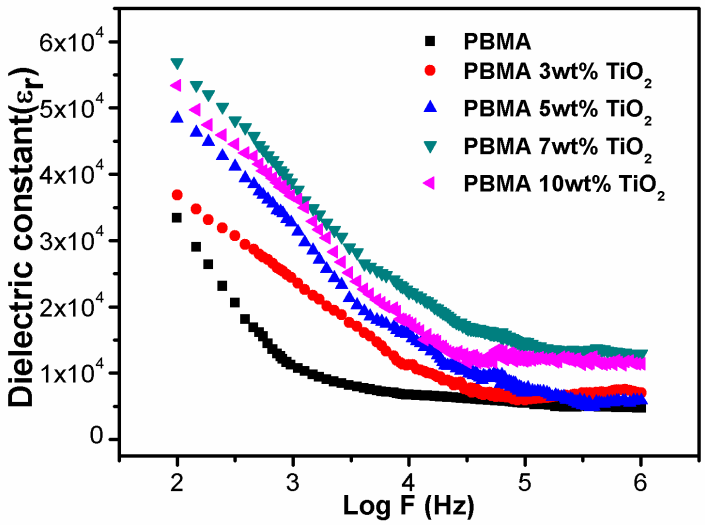

Figure 3.15: Variation of dielectric constant (ε_r) with frequency for PBMA and its composites with different content of TiO_2 nanoparticles.

The room temperature AC conductivity of PBMA and its nanocomposites with various concentrations of TiO_2 were investigated

and shown in **figure 3.16.** From figure it is clear that for all the composites the conductivity increases with increase in frequency, indicates the hopping conduction behaviour present in polymer composite [143]. Also it is interesting to see that all the composites have higher conductivity than that of pure PBMA matrix, which means the incorporation of TiO_2 enhances the conductivity of PBMA matrix. The poor compactness of PBMA matrix (which is well clear from the SEM image) leads to its poor conductivity while the dispersion of nanoparticles leads to have high compactness and hence higher conductivity. The conductivity increases with further addition of nanoparticles up to 7 wt% and there after it shows slight decrease in conductivity. The poor conductivity at higher filler loading (10 wt%) is due to the aggregation of nanoparticles. The aggregation of nanoparticles reduces the possibility of hopping by increasing the distance between adjacent charge carrier centres.

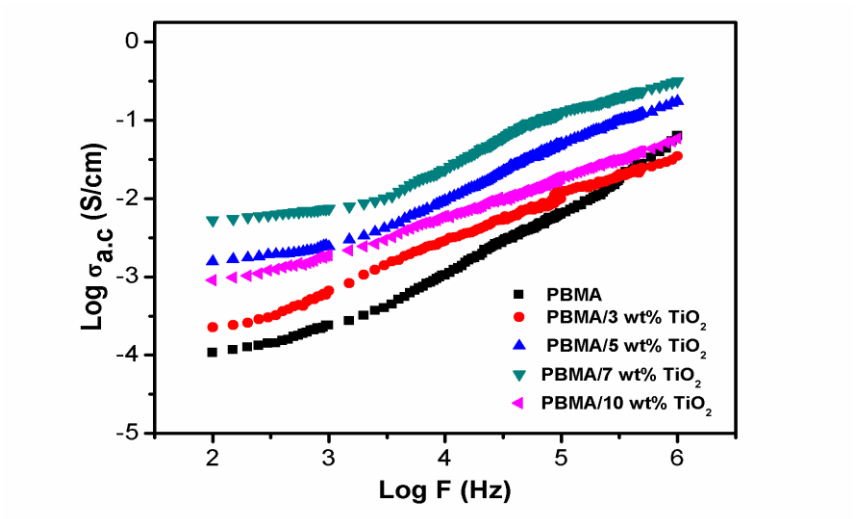

Figure 3.16: Room temperature AC conductivity ($\sigma_{a.c}$) of PBMA and its composites with different content of TiO_2 nanoparticles.

3.2.10 Temperature Dependence Electrical Conductivity of PBMA/TiO_2 Nanocomposites

The frequency dependent AC conductivity ($\sigma_{a.c}$) of PBMA and PBMA/TiO_2 nanocomposites at various temperatures (298K-363K) was presented in **figure 3.17.** For all the composites conductivity is found to be increased with the frequency and temperature as observed in the case of many polymer and semiconducting nanoparticles composite. It is due to the higher hopping of charge carriers on enhancing the temperature [144]. Since, as the temperature increases the charge carriers got more energy for hopping and therefore conductivity increases with temperature. Generally polymer nanocomposites exhibits conductivity due to hopping of charge carries, flow of charge carries through conductive path and polarization. Polarization may occur due to dipole polarization developed in the polar polymer matrix and interfacial polarization. The interfacial polarization is arises from the mismatch between the non conducting polymer matrix and the conducting filler particle [145]. The frequency dependence of AC conductivity is given in the formula [146, 147]

$$\sigma_{a.c} = A\omega^{s} \qquad (3.6)$$

where A(T) is a constant determine the intensity of polarizability, $\sigma_{a.c}$ is the AC conductivity due to the trapped charge carries predominant in higher frequencies, ‘s’ be the frequency exponent with the value ranging from 0 to 1 indicate the degree of interaction between the polymer matrix and mobile charge carries and its value indicate towards the conduction mechanism present in the sample. The value of ‘s’ determined from the slope of the plot $\log(\sigma_{a.c})$ vs. $\log(\omega)$ of all the samples are presented in **table 3.2.** From the table it is clear that as the

temperature increases the s value decreases further confirms the hopping mechanism.

Table 3.2. Frequency exponent 's' at different temperatures from the AC conductivity of PBMA and PBMA with different content of metal oxide nanoparticles

Samples	Temperature(°C)					
	30	40	50	60	70	80
PBMA	0.6018	0.6017	0.6168	0.6159	0.6141	0.6138
PBMA/3 wt% TiO_2	0.6411	0.6401	0.6395	0.6348	0.6342	0.6337
PBMA/5 wt% TiO_2	0.6434	0.6430	0.6425	0.6421	0.6418	0.6413
PBMA/7 wt% TiO_2	0.6570	0.6564	0.6559	0.6552	0.6547	0.6543
PBMA/10 wt% TiO_2	0.6386	0.6383	0.6380	0.6376	0.6372	0.6366

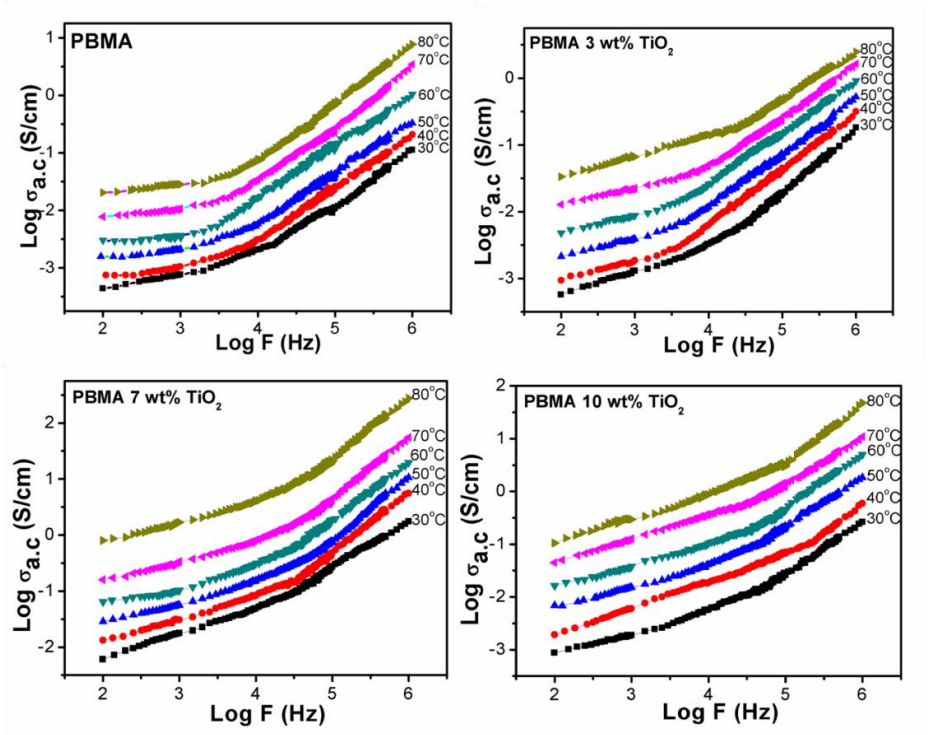

Figure 3.17: Frequency dependent AC conductivity ($\sigma_{a.c}$) of PBMA and PBMA/TiO_2 nanocomposites at various temperatures

3.4.9.1 Activation Energy Calculations

The log($\sigma_{a.c}$) vs. 1000/T for all the nanocomposites were ploted and were shown in the **figure 3.18.** The curves obey the Arrhenius equation and from these Arrhenius plots the activation energies were calculated using the curve fitting method and the obtained values are tabulated in **table 3.3.** It is clear that the activation energy of polymer nanocomposites are lesser than that of pure PBMA matrix might be due to the free hoping of charge carriers from one charge carrier sites to another, as similar in the case of PVCin/NiO polymer nanocomposites reported by Ramesan et al. [148].

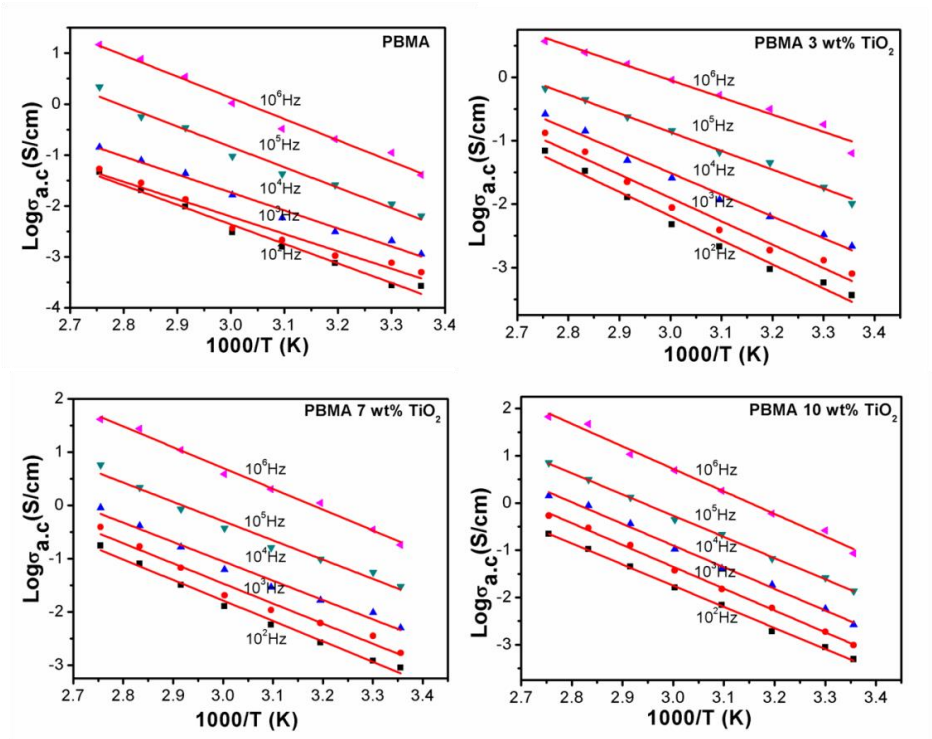

Figure 3.18: Activation energy plot of PBMA and PBMA nanocomposites with different content of TiO_2 nanoparticles

Table 3.3: Frequency dependent activation energy of PBMA and its composites with TiO_2 nanoparticles

Samples	Frequency (Hz)				
	10^2	10^3	10^4	10^5	10^6
PBMA	-3.834	-3.414	-3.531	-4.005	-4.167
PBMA/3 wt% TiO_2	-3.851	-3.856	-3.862	-3.869	-3.874
PBMA/5 wt% TiO_2	-3.881	-3.886	-3.892	- 3.898	-3.902
PBMA/7 wt% TiO_2	-3.941	-3.948	-3.953	-3.959	-3.964
PBMA/10 wt% TiO_2	-3.862	-3.869	-3.875	-3.882	-3.887

3.4.10 DC Conductivity

The DC conductivity of PBMA and its nanocomposites with various loading of TiO_2 at room temperature were measured and the plot is shown in **figure 3.19.** The conductivity strongly depends on the mobility and nature of filler nanoparticles. From the figure it is clear that the conductivity of nanocomposites are higher than that of pure PBMA which further confirm the increase in conductivity of PBMA matrix with the encapsulation of TiO_2 nanoparticles. It is pronounced that with increasing the concentrations of TiO_2 nanoparticles, the conductivity also increases. This phenomenon of increase in conductivity is due to the strong interfacial adhesion between the PBMA matrix and TiO_2 nanoparticles as result of coordination bond between carbonyl group in PBMA and hydroxyl group on the surface of TiO_2. As the amount of filler particle increases the distance between adjacent charge carriers decreases and hence the conductivity increases. The homogenous dispersion of TiO_2 is acquired through in

situ polymerization method which, helps in having uniform conducting charge carriers throughout the matrix. It is concluded that conductivity is highly depends on the loading of TiO_2 and the incorporation of TiO_2 brought interesting electrical properties suitable to use in various electronic devices.

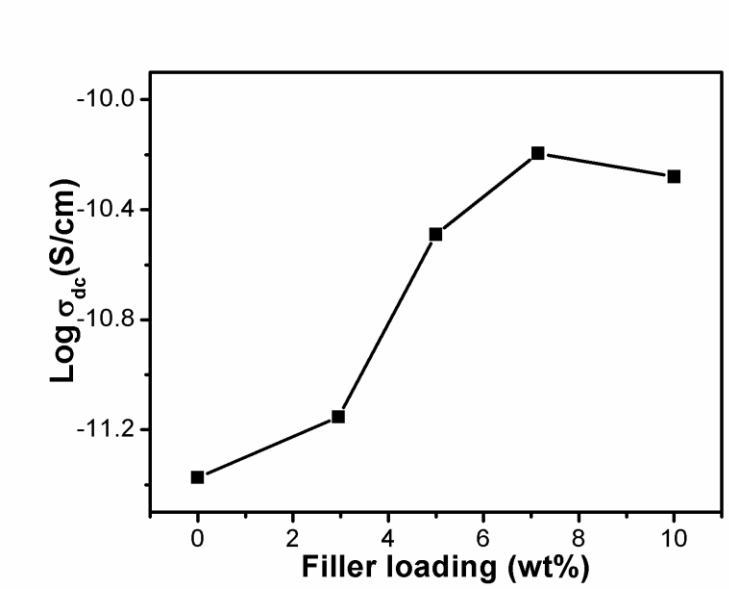

Figure 3.19: DC conductivity of PBMA and its nanocomposites with various concentrations of TiO_2 nanoparticles

3.4.11 Comparison of Experimental Conductivity with Theoretical Conductivity

In order to understand the formation of conductive paths in the polymer matrix upon addition of nanoparticles different theoretical models were proposed [145, 149]. Bueche, McCullough, Scarisbrick and Mamunya are some of the well known models to calculate the theoretical conductivities. In the present study the theoretical

conductivities of PBMA nanocomposites with the various concentrations of TiO_2 were calculated using Bueche, McCullough, Scarisbrick and Mamunya models. The values and plots obtained from these models are compared with that obtained from experimental calculations and the results are presented below.

3.4.11.1 McCullough Model

McCullough proposed a theoretical conductivity model to predict the electrical conductivity of systems having homogeneous combination of two phases based on the use of transport properties of polymer [150]. According to McCullough model, the electrical conductivity of binary systems like polymer composites depends on the conductivity as well as volume fractions of both filler and polymer matrix and the equation is

$$\sigma c = \sigma p.\Phi p + \sigma.\Phi f - \left[\frac{\lambda.\Phi p.\Phi f+(\sigma f-\sigma p)^2}{\nu f.\sigma f+\nu p.\sigma p}\right] \qquad (3.7)$$

Where σc is the conductivity of composite film, σp is the conductivity of pure polymer matrix (4.23×10^{-12} S/cm), σf is the conductivity of filler particle (1×10^{6} S/cm), Φp is the volume fraction of polymer matrix and Φf is the volume fraction of filler particles. νf and νp are defined as,

$$\nu f = (1-\lambda).\Phi f + \Phi p.\lambda \qquad (3.8)$$

$$\nu p = (1-\lambda).\Phi p + \Phi f.\lambda \qquad (3.9)$$

Where λ is the structural factor and its value varies from 0 to 1. The λ value indicates the extent of conductive chain and network formation.

Moreover the λ value depends on the size, shape, aspect ratio and the concentration of nanoparticles. The theoretical conductivity of PBMA having various concentrations of TiO_2 were calculated using McCullough model (**equ: 3.7-3.9**) at λ = 0, 0.1, 0.5, 0.9, 0.9999. The calculated theoretical conductivity along with experimental results is shown in **figure 3.20.** The theoretical conductivity is not in agreement with those obtained from experimental results in entire value of λ = 0 to λ = 0.9999. So the McCullough model is not suitable to predict the conductivity of composite materials.

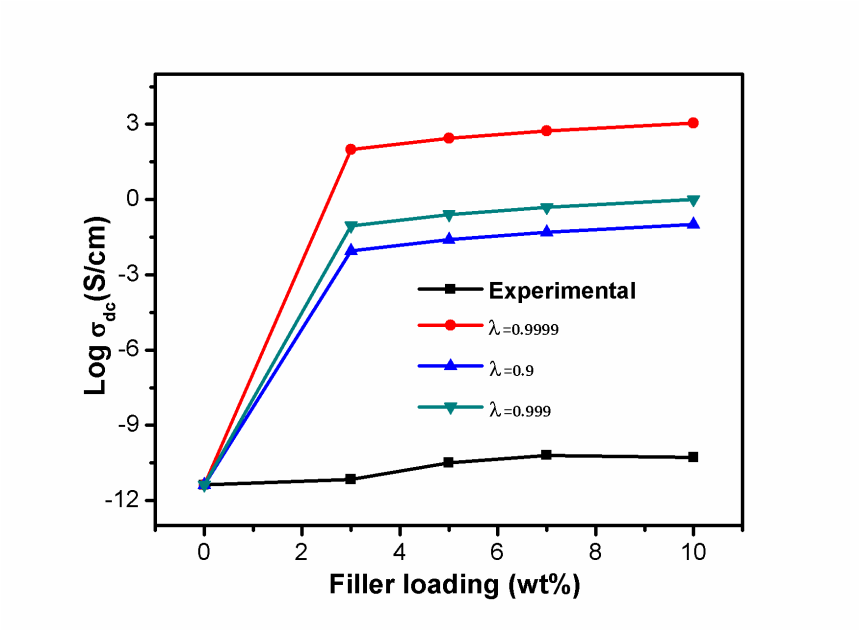

Figure 3.20: Theoretical and experimental plots of electrical conductivity based on the McCullough model

3.4.11.2 Bueche Model

Bueche model considered that the conductivity of composites is due to the contributions from the conducting particle aggregations and from the insulating polymer matrix [151] and the equation is given as

$$\sigma c = \Phi f \sigma f + (1 - \Phi f)\sigma p \qquad (3.10)$$

Where, Φf is the volume fraction of filler particles, σf is the conductivity of filler particle and σp is the conductivity of pure polymer matrix and σc is the conductivity of composite film. The theoretical conductivity using the Bueche model (**equation 3.10)** and experimental conductivity investigated for the composites of PBMA with various concentrations of TiO_2 are given in **figure 3.21.** From the figure it can be seen that the theoretical conductivity obtained using Bueche is not matches with those of experimental and so the Bueche model also fails to predict the conductivity of polymer composites under investigations. According to this model the conductivity is mainly depends on the nature of filler and polymer matrix and so it is suitable for multi component systems in which there is no much difference in conductivity between the components. So the theoretical conductivity obtained using Bueche model is always quiet different from those obtained from experimental study.

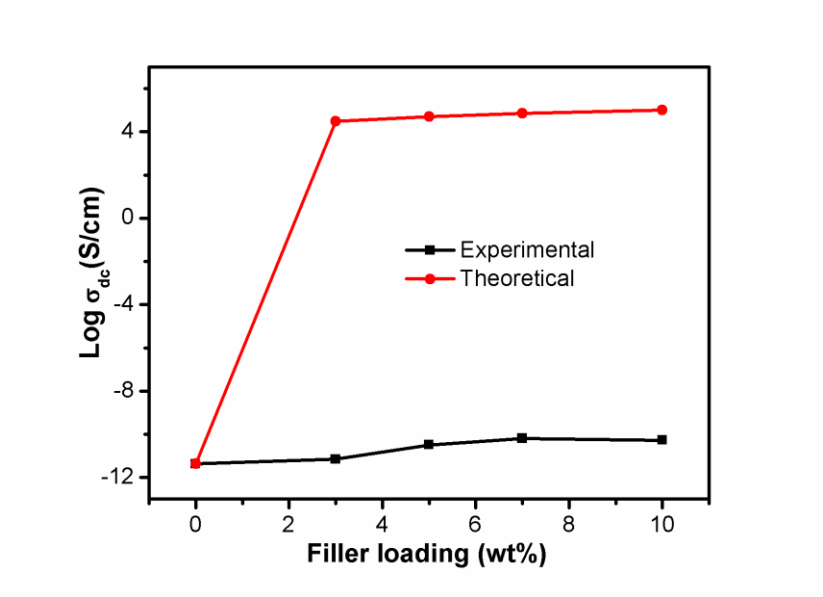

Figure 3.21: Theoretical and experimental plots of electrical conductivity based on the Bueche model

3.4.11.3 Scarisbrick Model

According to Scarisbrick model the conductivity is Ohmic in nature. That means the inter-particle contacts within the polymer matrix is responsible for the formation of conductive path and based on these assumptions he derived an equation to calculate the probability of conductive network formation through the particle-particle contact [152]. By this model the theoretical conductivity is function of volume fraction of filler and can be expressed as

$$\frac{\sigma c}{\sigma f} = C^2.\Phi.\Phi[exp(\Phi^{-\frac{2}{3}})] \qquad (3.11)$$

Where σc is the conductivity of composite film, σf is the conductivity of filler particle, Φ is the volume fraction of the filler in the composite

and C is the geometrical factor depends on the arrangement conductive paths within the polymer matrix. The value of C^2 varies from 1 to 3 x 10^{-3}. Then the equation is expressed as is

$$\frac{\sigma c}{\sigma f} = \Phi.\Phi\left[exp\left(\Phi^{-\frac{2}{3}}\right)\right] (\text{When } C^2 = 1) \qquad (3.12)$$

$$\frac{\sigma c}{\sigma f} = 3\ x\ 10^{-3}.\Phi.\Phi[exp(\Phi^{-\frac{2}{3}})] (\text{When } C^2 = 3\text{x}10^{-3}) (3.13)$$

Using the above equations (**equations: 3.11-3.13**) the theoretical conductivity of PBMA and PBMA/TiO_2 nanocomposites were calculated and the comparative study of experimental conductivity and theoretical conductivity made using Scarisbrick model were shown in **figure 3.22.** The trend of increase in conductivity as increase in concentration of filler particle is more pronounced in theoretical calculation than that of experimental conductivity. Here also, there is large difference between theoretical and experimental conductivity at entire concentration of filler. Therefore, Scarisbrick model is not suitable for predicting the conductivity of PBMA/TiO_2 nanocomposites. Since, in Scarisbrick model contributions from polymer matrix is not considered and also the actual value of C^2 is difficult to calculate and thus there is large deviations between the experimental and theoretical conductivity based on Scarisbrick model in most case of polymer composites.

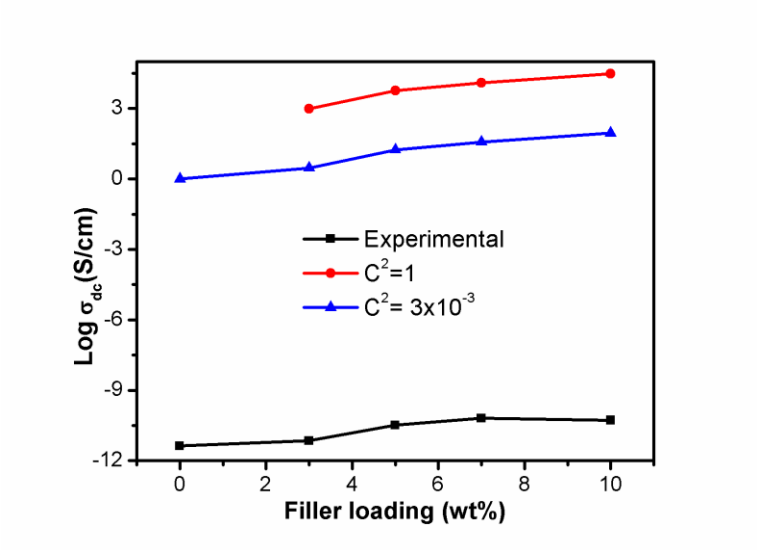

Figure 3.22: Theoretical and experimental plots of electrical conductivity based on the Scarisbrick model

3.4.11.4 Mamunya Model

Mamunya et al. were proposed that the electrical conductivity of polymer composites highly depends on polymer-filler interface at the percolation threshold in addition to the conductivity as well as volume fraction of filler and matrix [153]. However, the extent of polymer-filler interaction depends on the polymer and filler surface energies, aspect ratio, size, shape polymer melt viscosity etc. There for, conductivity of composites can be expressed as

$$\text{Log}\,\sigma \;=\; \log\sigma c \;+ (\log\sigma F - \log\sigma c\,)(\frac{\Phi-\Phi c}{F-\Phi c})k \qquad (3.14)$$

Where, Φ is the filler volume fraction, Φc is the filler volume fraction at the percolation threshold, σc is the electrical conductivity at the percolation threshold, σ_F is the composite electrical conductivity when Φ = F, F is the maximum packing volume fraction, k is an exponent

depends on the filler volume fraction and the relation is shown in **equation 3.15**.

$$k = K\Phi/(\Phi\text{-}\Phi c)^{0.75} \qquad (3.15)$$

K is a coefficient, its value depends on the interfacial interaction between the polymer matrix and filler, can be expressed in **equation 3.16.**

$$K = A - B\,\gamma_{pf} \qquad (3.16)$$

Where, γ_{pf} is the interfacial surface tension; and A and B are constants.

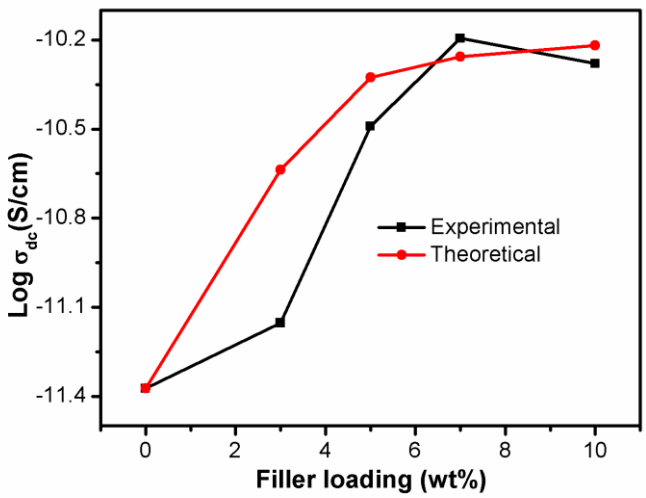

Figure 3.23: Theoretical and experimental plots of electrical conductivity based on the Mamunya model

The theoretical conductivity of PBMA/TiO_2 nanocomposites was calculated by using Mamunya equations **(equations: 3.14-3.16)** and

compared with the experimental conductivity. The results were shown in **figure 3.23.** The experimental and theoretical values shows exact match at entire concentrations of filler, of course slight deviations at low filler concentrations. At low concentrations the conductivity of composites is governed by only that of polymer matrix and after reaching the percolation value the conductivity governed by both filler and matrix. So it can be conclude that, for PBMA/TiO_2 nanocomposites the Mamunya model is the suitable one. That means the conductivity mainly depends on the interfacial interaction between the matrix and filler, which in turn influenced by the surface properties of filler.

3.5 Conclusion

The nanocomposites of PBMA with various loading of TiO_2 were successfully synthesized by in situ polymerization method and the interfacial interaction between the polymer matrix and filler was revealed from FT-IR and UV-Visible analysis. The XRD results showed the ordered arrangement of TiO_2 nanoparticles in the PBMA matrix. The uniform dispersion of nanoparticles was confirmed through FE-SEM and TEM analysis. The incorporation of TiO_2 nanoparticles substantially enhanced the thermal stability of PBMA composites, as revealed from the higher Tg, Tm and thermal degradation temperature of composites. The tensile strength and elongation at break of PBMA/TiO_2 nanocomposites was measured and it shows the improved mechanical properties of composites than the

plane PBMA. The tensile properties of composites were predicted by using different theoretical models such as Einstein, Mooney, Guth and Pukanszky equations and among these Pukanszky model shows close match with the experimental tensile values. The room temperature as well as temperature dependent AC conductivity of composites was measured and the result shows the conductivity increases with increase in temperature, frequency and concentration of filler particles. The maximum AC conductivity was obtained for 7 wt% loading of TiO_2 and above it the conductivity decreased due to the aggregation of nanoparticles at higher filler loading. The dielectric as well as dielectric loss also exhibits significant enhancement with the addition of TiO_2 nanoparticles. The activation energy and exponential values were calculated from the AC conductivity studies and it revealed that the composites exhibit hopping conduction mechanism. The DC conductivity of composites was higher than that of pure PBMA, means the conductivity is strongly depends on the content of TiO_2 nanoparticles. The conductivity of polymer composites were predicted using theoretical models based on Bueche, Scarisbrick, McCullough and Mamunya models. In Bueche, Scarisbrick and McCullough models the theoretical value exceeds than that of experimental values and so these models fail to explain the conductivity of composite material over a wide range of concentration of filler particles. The reason for the large variation between experimental conductivity and theoretical conductivity is the large difference in the conductivity of PBMA matrix and TiO_2 nanoparticles. However, Mamunya model

exhibits better fit that of experimental conductivity. Thus it can be conclude that the conductivity of PBMA/TiO_2 nanocomposites was mainly governed by the interface between PBMA matrix and the filler.

CHAPTER 4
INVESTIGATIONS ON THE STRUCTURAL, MECHANICAL, THERMAL AND ELECTRICAL PROPERTIES OF Ce DOPED TiO_2/POLY (BUTYLMETHACRYLATE) NANOCOMPOSITES

Contents

K. Suhailath, M. T. Ramesan, Effect of nano-Ce-Doped TiO_2 on AC conductivity and DC conductivity modeling studies of poly (n-butylmethacrylate), J. Electron. Mater. 47 (2018) 6487.

K. Suhailath, M. T. Ramesan, Investigations on the structural, mechanical, thermal, and electrical properties of Ce-doped TiO_2/poly (n-butylmethacrylate) nanocomposites, J. Therm. Anal. Calorim. 135 (2019) 2159.

4.1 Introduction

Nanoparticles filled polymer composites are well known for their interesting optical, thermal, mechanical and conductivity properties, resulting from the synergetic interaction of polymer with the nano-fillers [154]. These nanocomposites are widely used in many applications such as dielectric ceramics, electro-chromic devices, biosensors, super capacitors and optoelectronic devices [155]. Especially the dispersion of inorganic nanoparticles in organic polymer results in a hybrid polymer nanocomposite with fabulous properties. The polymer provides its own excellent mechanical properties and the nanoparticles impart immense thermal and electrical properties and hence the hybrid variety made of these two components exhibits the excellent and unpredictable properties [156]. Several works were reported on the electrical as well as mechanical properties of polymer composites and the mechanism behind the enhanced properties. Theoretical modeling studies are the widely accepted method to identify the mechanism of enhanced properties and the role of nanoparticles in polymer composites. So the development and the application of new theoretical modeling studies are more facile to study and predict the nature of mechanical and electrical properties in the polymer nanocomposites.

The properties of polymer nanocomposites depends on the size, shape and nature of nano-filler present in the polymer matrix [157]. Therefore the properties of the polymer nanocomposite can be tuned by selecting appropriate nanoparticles. The improvements in properties of polymer nanocomposites are also due to the large surface area of

nanosized particles which provide high contact area with the polymer matrix [158]. Further the surface to volume ratio of nanosized particles are very high compared to that of micro-sized particles means there have high interaction zone around the nanoparticles with the polymer matrix and hence brought interesting change in the functions of polymer matrix [159]. Depending on the strength of interfacial interactions between the polymer matrix and nanoparticles, the free volume and hence the mobility of nanoparticles may change and so different nanoparticles brought same properties in different dimensions to the same polymer matrix.

TiO_2 nanoparticles have been widely used as nano-filler for many polymer nanocomposites due to its remarkable electrical and optical properties [160]. The surface modification of TiO_2 with different metal ions especially rare earth metal ions result in nanoparticles carrying high functionality. It has been reported that the use of rare-earth-metal doped TiO_2 nanoparticles in polymers could impart excellent thermal, electrical, and sensing properties and anticorrosive properties [161]. Shende et al. showed that the photocatalytic activity of graphene with Ce-doped TiO_2 nanocomposites has higher activity than graphene-TiO_2 nanocomposites [162]. Similarly, the carbon nanotubes with cerium-doped TiO_2 nanocomposites can perform as an excellent tool for the photodegradation process of phenol [163]. However, the conductivity and mechanical properties of poly (butylmethacrylate) containing Ce-TiO_2 nanoparticles still remain unfamiliar. The present study focused on fabrication of poly (butylmethacrylate)/Ce-TiO_2 nanocomposites and their characterizations by FT-IR, UV-Visible, XRD, FE-SEM,

DSC, TG analysis and then study the mechanical, AC and DC conductivity properties of developed composites. This work also concentrates on the theoretical modeling of tensile strength as well as DC conductivity of composites for studying the mechanism behind the enhanced properties of poly (butylmethacrylate)/cerium doped TiO_2 nanocomposites.

4.2 Results and Discussion

4.2.1 FT-IR Spectra

The interaction of Ce-TiO_2 nanoparticles with PBMA was analyzed by FT-IR and is given in **figure 4.1.** The IR spectra of Ce-TiO_2 show the typical peak at 655 cm^{-1} endorses the formation of Ti-O bond [164]. The strong and intensified peaks at 3417 cm^{-1} and 1630 cm^{-1} are the surface adsorbed water molecules of Ce-TiO_2 nanoparticles. The FT-IR spectra of PBMA shows a peak at 1730 cm^{-1} is the C=O absorption of the ester group in PBMA matrix and the peaks at 2690 and 2874 cm^{-1} are the absorption peak of C-H bond vibrations of CH_2 and CH_3 groups respectively. The peak at 1060 cm^{-1} corresponds to the C-O stretching vibration of ester group of PBMA and one at 1261 cm^{-1} attributes C-H wagging vibrations in PBMA. The PBMA with Ce-TiO_2 nanoparticles shows the absorption peak at 661 cm^{-1} is the Ti-O-Ti vibrations, which is absent in pure PBMA confirms the presence of TiO_2 nanoparticles in the PBMA matrix [165]. The Ti-OH band appeared at 3417 cm^{-1} in Ce-TiO_2 is absent in PBMA/Ce-TiO_2 nanocomposites implies the formation of bonding interaction of Ti-OH with the carbonyl group present in PBMA [166]. It can be seen from the figure that, the two absorption peaks of pure PBMA at 745 and 708 cm^{-1} are found to be

shifted to higher wavelength region at 755 cm^{-1} in PBMA/Ce-TiO_2 nanocomposite and this is another evidence for the interaction of Ce-TiO_2 nanoparticles with PBMA matrix.

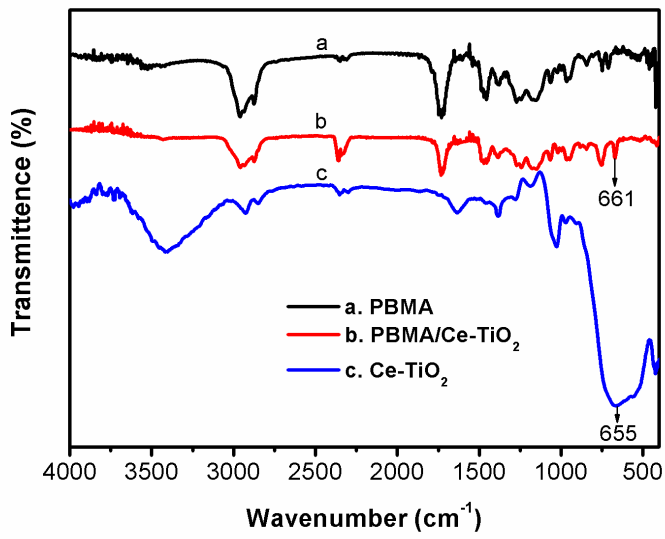

Figure 4.1: FT-IR spectra of Ce doped TiO_2, PBMA and PBMA with Ce doped TiO_2

4.2.2 UV-Visible Spectra

The UV-Visible spectra of PBMA and PBMA with various loading of Ce-TiO_2 nanoparticles are shown in **figure 4.2.** The strong absorption peak around 245 nm attributes to the n-π* transition in the C=O group [167]. It is clear from the figure that all the composites have higher intensity and broadens than pure PBMA. The well dispersed Ce-TiO_2 nanoparticles in the PBMA contribute to the increased UV absorption of composites than the pure PBMA. The broadness and intensity of UV absorption peak is maximum at 7 wt% loading. This means that

the effective dispersion and so the interfacial interaction is maximum at this loading and this is in accordance with the work reported earlier [168]. However, the intensity is found to be decreasing at higher loading of nanoparticles (i.e. at 10 wt%). The agglomerated nanoparticles at higher loading interrupt the effective dispersion, which in turn disturb the interaction with polymer matrix, causes the decrease in absorbance of polymer nanocomposites. Hence it can be concluded that the Ce-TiO_2 nanoparticles are effectively dispersed in the PBMA chain and it plays significant role in the optical properties of PBMA polymer.

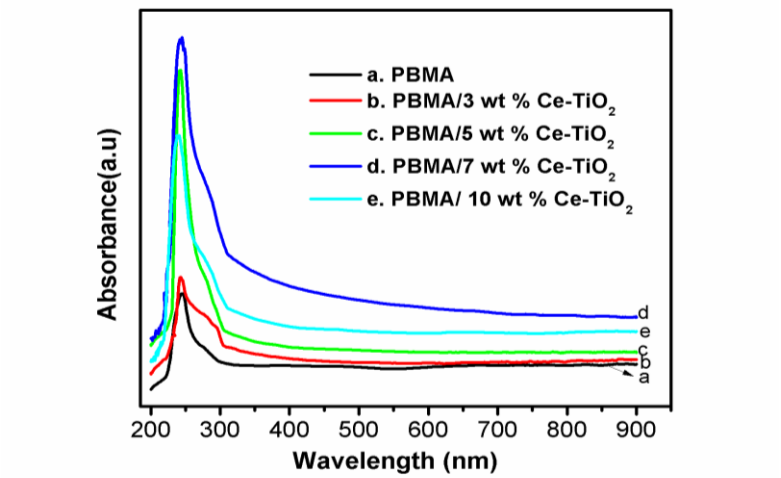

Figure 4.2: UV-Visible spectra of PBMA and PBMA with different contents of Ce doped TiO_2

4.2.3 XRD Analysis

The XRD patterns of Ce-TiO_2 nanoparticles, PBMA and PBMA with different contents of Ce-TiO_2 nanoparticles are presented in **figure 4.3.** The nanoparticles show several diffraction peaks indicating the crystalline nature of synthesized Ce doped TiO_2 [169]. However, the

synthesized PBMA exhibits broad and intense peak at $2\theta = 18.19^{\circ}$ implies the amorphous nature of the polymer. The XRD pattern of nanocomposite shows all the diffraction peaks of Ce-TiO_2 with the broad diffraction curve of PBMA. It can be observed from the figure that the amorphous nature of PBMA phase is decreasing with the addition of Ce-TiO_2 nanoparticles and the amorphous peak of PBMA at $2\theta = 18.19^{\circ}$ is found to be shifting to $2\theta = 17.65^{\circ}$. The shift in diffraction peaks reveals interaction of nanoparticles with the PBMA matrix. Also the intensity of the crystalline peaks was increasing in the composite with increase in concentration of nanoparticles. The percent crystalinity of the composites was calculated by the general formula, percent crystallinity = $I_{crystalline}/(I_{crystalline} + I_{amorphous})$. The percent crystallinity for PBMA with 5 wt% of Ce-TiO_2 is 25 %, while that for PBMA with 10 wt% of Ce-TiO_2 is 67 %.

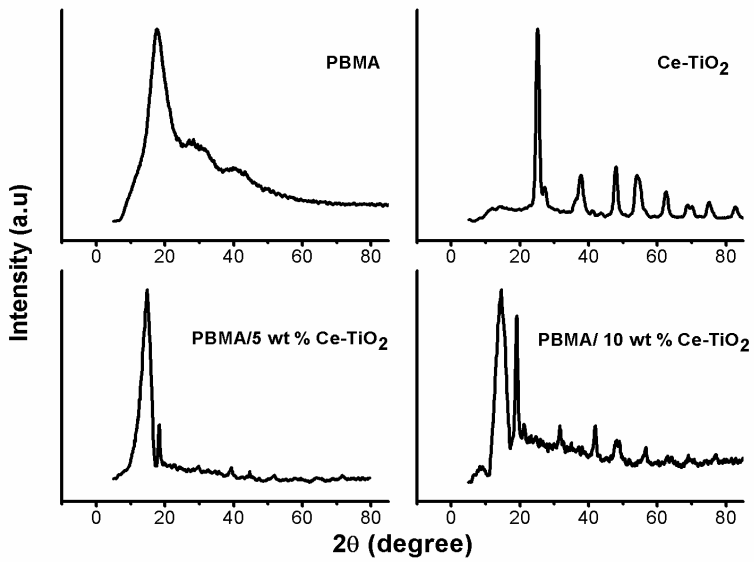

Figure 4.3: XRD patterns of Ce doped TiO_2, PBMA with different contents of Ce doped TiO_2

4.2.4 FE-SEM Morphology

The SEM images of Ce-TiO_2 nanoparicle, PBMA and PBMA/Ce-TiO_2 nanocomposites are given in **figure 4.4.** It can be seen from figure that the Ce-TiO_2 has cluster of hemispherical particles. The pure PBMA **(figure 4.4b)** exhibits smooth and homogenous surface morphology, while the smoothness of polymer disappears gradually with the presence of particles in the composites denotes the dispersion of nanoparticles in the polymer matrix.

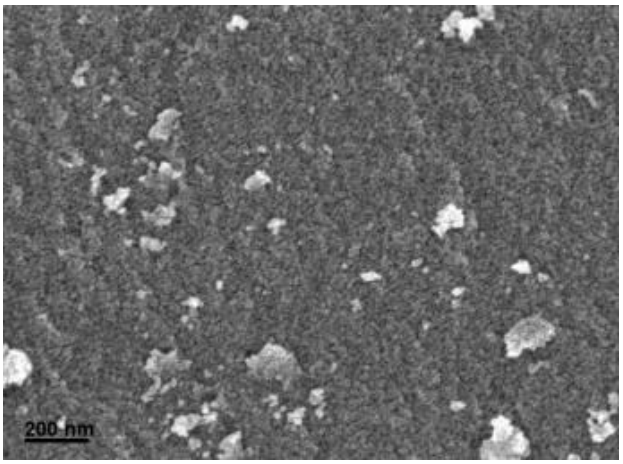

Figure 4.4a: FE-SEM image of Ce-TiO_2 nanoparicle

The PBMA with 3 wt% Ce-TiO_2 shows the homogeneity with irregularly distributed nanoparticles, obviously due to the lack of enough number of nanoparticles. However, PBMA with 7 wt% Ce-TiO_2 exhibits good morphology with several distributed nanoparticles (truly with some agglomeration of Ce-TiO_2 which cannot be ignored) shows the better adhesion of nanoparticles with the PBMA matrix. The interaction of polar carbonyl groups present in the PBMA backbone with Ce-TiO_2 nanoparticles is responsible for the effective dispersion

of nanoparticles within the polymer matrix [170]. However, when the loading of nanoparticles reached to 10 wt%, the uniform adhesion of nanoparticles within the polymer matrix is totally changed with more number of agglomerated nanoparticles. At higher loading, greater stress is developed in the polymer matrix which leads to more agglomeration of nanoparticles, consistent with the UV studies discussed earlier.

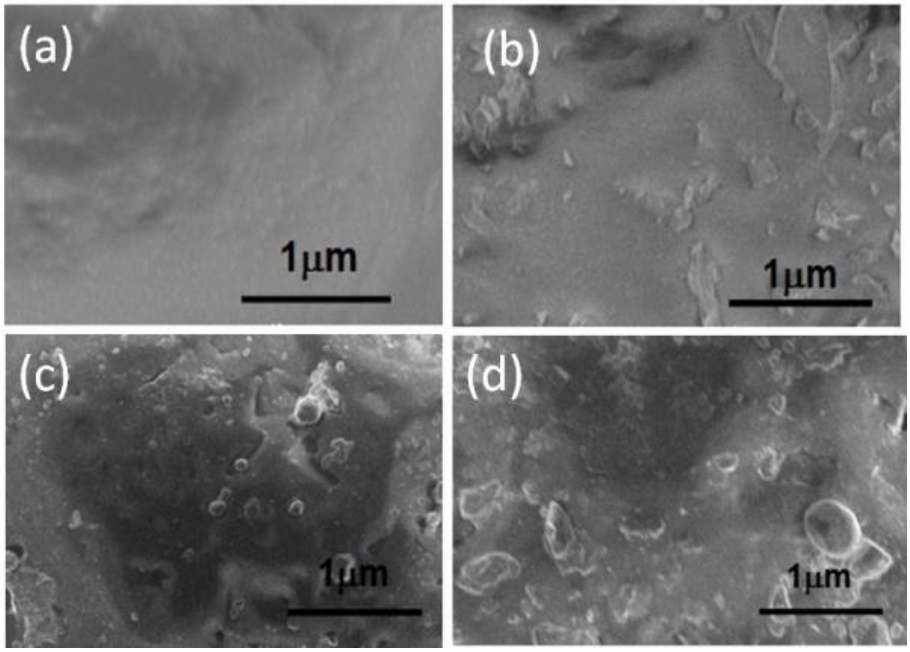

Figure 4.4b: FE-SEM images of (a) PBMA (b) PBMA/3 wt% Ce-TiO_2 (c) PBMA/7 wt% Ce-TiO_2 and (d) PBMA/10 wt% Ce-TiO_2

4.2.5 DSC Analysis

The glass transition temperature (Tg) of PBMA and PBMA with various loading of Ce-TiO_2 nanoparticles are investigated by DSC and is given in **figure 4.5.** It can be observed that the Tg value of

composites are greatly influenced by the addition of nanoparticles and all the composites shows higher Tg than that of PBMA implies the strong interaction of PBMA with Ce-TiO_2 nanoparticles. It is well recognized that the interaction of filler particles with the polymer matrix alter the arrangement and segmental mobility of polymer chain which in turn alter the Tg values [171]. The obtained Tg values of PBMA and PBMA with 5 and 10 wt% Ce-TiO_2 nanoparticles are appears at 21.54°C, 33.74°C and 37.54°C respectively. The increased Tg arises from the loss in segmental mobility of PBMA chain, obviously due to the well dispersion of Ce-TiO_2 nanoparticles. This uniform dispersion was possible through the strong interaction of nanoparticles to the surrounding polymer matrix [172].

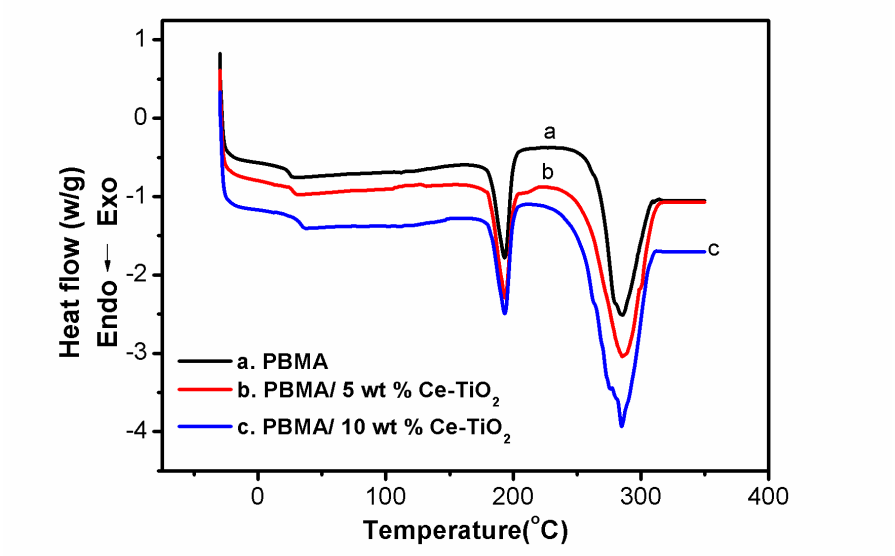

Figure 4.5: DSC profiles of PBMA with different contents of Ce-TiO_2 nanoparticles.

4.2.6 TGA Analysis

The thermal stability of PBMA and its nanocomposite with different loading of Ce-TiO_2 has been examined by thermogravimetric analysis and is given in **figure 4.6.** The corresponding DTG curve was also given. Typically PBMA shows two thermal degradation steps. Firstly, the vinyl end groups present in PBMA begins to degrade at around ~250°C. Subsequently upon further rising of temperatures, rapid random scission of polymer chain leads to complete degradation of PBMA chain structure [173]. Usually the thermal degradation begins with the random scission of polymer chain and the formed radical polymer chain react with unsaturated end groups or with the some weak bonds leads to complete degradation [174]. From the TGA curves, it can be noted that the PBMA and its nanocomposite with Ce-TiO_2 has similar type of degradation behavior. It is also noticed that there is no residue beyond 400°C indicating the depolymerization of PBMA is mainly through random scission process. The obtained initial degradation temperature (Ti) and major decomposition temperature (Tmax) for the plane PBMA and PBMA/Ce-TiO_2 nanocomposites were documented in **table 4.1.** The PBMA has the initial degradation temperature at 256°C while the composites have degradation temperature 257°C and 264°C for 5 wt% and 10 wt% filler ratios respectively. From table, it is clear that all the composites have higher degradation temperature and major decomposition temperature than that of pure PBMA confirming the contribution of metal oxide nanoparticles in the enhanced thermal stability of PBMA composites.

The higher thermal stability of nanocomposite arises from the strong interfacial interaction of Ce-TiO_2 nanoparticles with PBMA matrix.

Table 4.1: The value of Ti and Tmax obtained from the TGA and corresponding DTG curves for PBMA and PBMA/Ce-TiO_2 nanocomposites

	TGA	**DTG**	
	T_i (°C)	**T_{max} (°C) Ist stage**	**T_{max} (°C) IInd stage**
PBMA	256	280.29	364.33
PBMA/5 wt% Ce-TiO_2	257	290.05	368.40
PBMA/10 wt% Ce-TiO_2	264	307.91	376.55

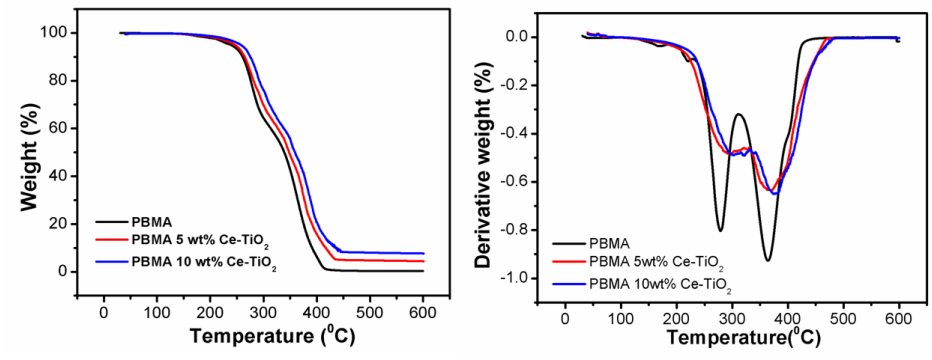

Figure 4.6: TGA and corresponding DTG patterns of PBMA and PBMA with different contents of Ce doped TiO_2

4.2.7 Mechanical Studies

The effect of Ce-TiO_2 nanoparticles on the tensile strength and elongation at break of PBMA matrix has been investigated. The tensile strength (**figure 4.7**) of PBMA is greatly enhanced with the dispersion of Ce-TiO_2 nanoparticles. The tensile strength is increased to 26.7 % for 3 wt% addition of Ce-TiO_2 nanoparticles as compared to pure

PBMA. The maximum tensile strength is observed for 7 wt% of Ce-TiO_2 loading (61.79%). The better reinforcing of metal oxide nanoparticles along with the interfacial interaction between the nano-filler and polymer matrix is responsible for the enhanced tensile strength of polymer composites [175]. The elongation @ break of PBMA and PBMA with different contents of Ce-TiO_2 nanoparticles is also given in **figure 4.7.** It can be seen that the value of elongation at break is found to be decreasing with the addition of Ce-TiO_2 nanoparticles. Due to the presence of metal oxide nanoparticles, the mobility of molecular chains is partially suppressed in nanocomposites which in turn reduce the deformability of polymer chains. In other words, the addition of nanoparticles increases the stiffness of the polymer matrix and therefore the elongation at break decreases. So it is clear that the inclusion of metal oxide nanoparticles greatly enhanced the mechanical strength of PBMA matrix.

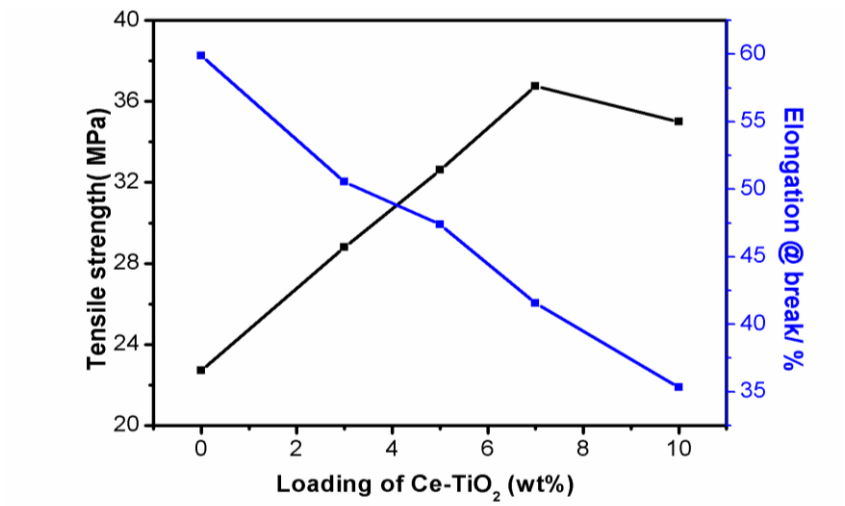

Figure 4.7: Tensile strength and elongation @ break of PBMA and PBMA with differentcontents of Ce doped TiO_2

4.2.8 Theoretical Studies of Tensile Strength

Different theoretical approaches of mechanical properties for studying the effect of parameters like interfacial properties, filler concentration, thickness etc. on the mechanical properties of composites. Though experimental studies are most effective, they are limited due to the difficult in manipulation of nano-scale interaction. The role of various parameters for the reinforcing nature of PBMA/Ce-TiO_2 nanocomposite is analyzed with various theoretical modeling such as Einstein, Mooney and Pukanszky equations.

4.2.8.1 Einstein Model

Einstein derived a theoretical equation for tensile strength of two phase composites in which the tensile strength of composites is linearly related to filler volume fraction [136, 176] and the equation is

$$Mc = Mm(1 + 2.5Vf) \qquad (4.1)$$

where Mc is the tensile strength of the composite, Mm is the tensile strength of bare polymer and Vf is the filler volume fraction. Using the Einstein model (**equation 4.1**), tensile strength of PBMA/Ce-TiO_2 nanocomposite are evaluated and shown in **figure 4.8**. It is clear from the figure that the theoretical values show large deviation from the experimental values. Since the Einstein model does not consider the parameters like aspect ratio, interaction parameter, thickness etc, it only useful in low concentrations of filler. In the present study, the Einstein model fails in predicting the reinforcing nature of PBMA/Ce-TiO_2 nanocomposites.

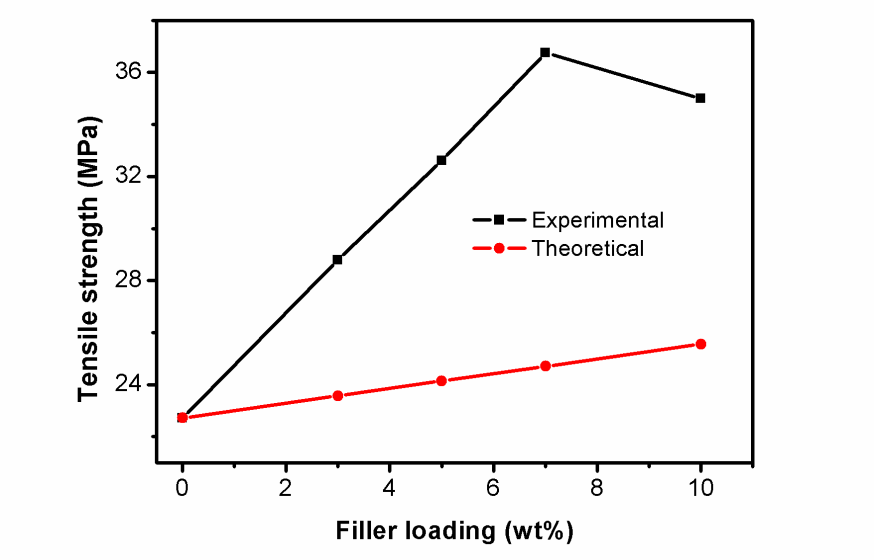

Figure 4.8: Theoretical and experimental curve of tensile strength based on Einstein model

4.2.8.2 Mooney Model

Mooney brought few modifications to the Einstein equation by introducing another parameter 'S' called crowding factor [137, 177] and the equation is

$$Mc = Mm * exp[\frac{2.5Vf}{1-SVf}] \quad (4.2)$$

where the Mc and Mm are the tensile strength of composite and bare polymer respectively and Vf is the volume fraction of nanoparticles. The parameter S represents the strain field in the interphase between the polymer matrix and the nanoparticles. The value of S has been suggested by various studies and it is equal to 1.35 for closely packed systems or it is for loosely packed systems. Mooney model (**equation 4.2**) is used to calculate the tensile strength of PBMA/Ce-TiO_2

nanocomposites and the obtained results is shown in **figure 4.9** along with the experimental results. The theoretical model does not match with the experimental results in entire filler loadings. Since the Mooney model does not consider the effect of interfacial properties on the tensile strength, the theoretical values shows greater deviation from that of experimental one. The Mooney model also fails in the case of PBMA/Ce-TiO_2 nanocomposites.

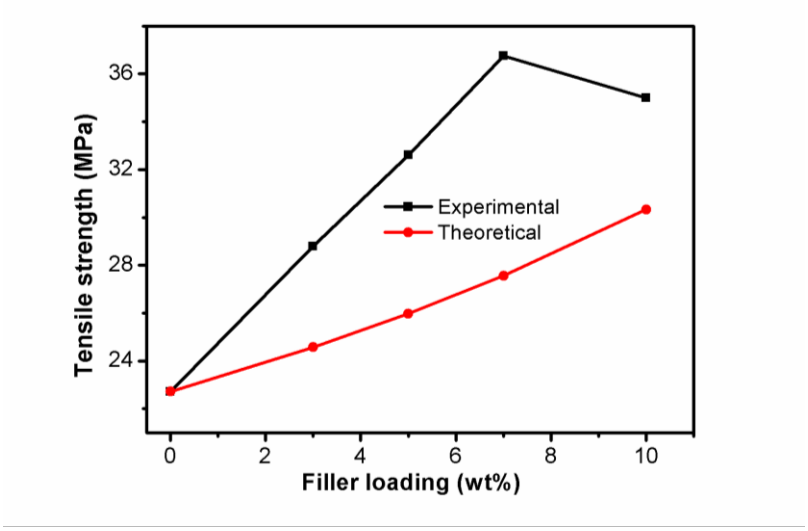

Figure 4.9: Theoretical and experimental curve of tensile strength based on Mooney model

4.2.8.3 Pukanszky Model

Pukanszky proposed a theoretical model for tensile strength of two phase nanocomposite systems [135, 141]. According to this approach the tensile strength is related to filler volume fraction and polymer-filler interfacial parameter and can be expressed as

$$Mc = Mm * \frac{1-Vf}{1+2.5Vf} * exp(BVf) \qquad (4.3)$$

Where Mc and Mm are the tensile strength of composites and polymer matrix respectively, Vf is the filler volume fraction and B is the interfacial parameter can determine from the experimental data. The parameter B determine the interfacial properties of polymer matrix with the filler, means the capacity of stress transfer from the matrix to filler. The values of B calculated by using the experimental tensile strength values and put it into the equation of Pukanszky model **(equation 4.3)** for the theoretical evaluation of tensile strength of PBMA and its nanocomposites with Ce-TiO_2 nanoparticles. The theoretical and experimental results are exhibited in **figure 4.10**. From the figure it is clear that data obtained using Pukanszky model shows close match with that of experimental one. The theoretical data shows slight positive deviation at higher volume fraction of nanoparticles. The more the reinforcing effect of filler into the polymer matrix, more will be the stress transfer capacity [178].

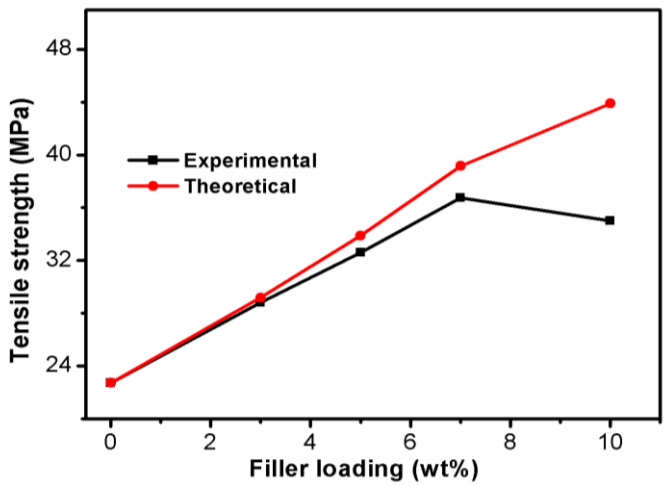

Figure 4.10: Theoretical and experimental curve of tensile strength based on Pukanszky model

4.2.9 Conductivity Studies

4.2.9.1 AC Conductivity

The addition of conducting nanoparticles can change the conductivity properties of polymer matrix. The variation of AC electrical conductivity with frequency at room temperature is measured for PBMA/Ce-TiO_2 nanocomposite and given in **figure 4.11.** It can be seen that the conductivity is found to be increasing in entire frequency range for all composites demonstrates the hopping conduction mechanism present in the PBMA matrix. The enhancement in conductivity of composites is attributed to the interfacial polarization between the PBMA matrix and Ce-TiO_2 nanoparticles. The increased conductivity at higher frequency range is not only due to the contribution from interfacial polarization but also from the electronic polarization [179]. All the PBMA/Ce-TiO_2 nanocomposites have high electrical conductivity than pristine PBMA and the maximum conductivity is noticed up to 7 wt% loading, which might be due to the large number of charge carriers. Moreover the availability of more number of charge carriers at the interface causes more interfacial polarization also contributes towards the conductivity at this concentration. The poor conductivity beyond 7 wt% is due to the agglomeration of nanoparticles and the agglomerated particles have less interaction zone with the polymer matrix causes decrease in the interfacial polarization between the filler and polymer matrix.

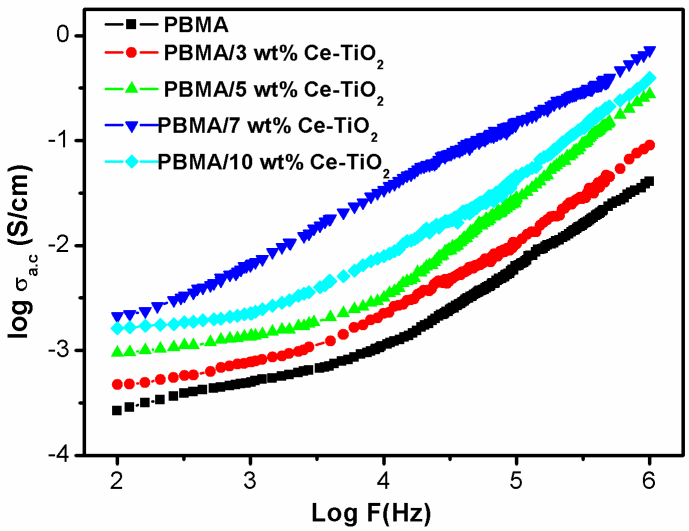

Figure 4.11: AC conductivity of PBMA with various loading of Ce doped TiO_2

4.2.9.2 Dielectric Constant

The nanoparticles can act as a tunnel for conduction between electrodes and hence increase the dielectric constant of the polymer composites than that of bare polymer. The variation of dielectric constant of PBMA and its nanocomposite with Ce-TiO_2 nanoparticles is given in **figure 4.12.** The dielectric constant of all the samples decreases with the increase in frequency. The free polar functional groups present in the PBMA chain arrange themselves in lower frequency attributed to the higher dielectric constant at lower frequency region. Moreover, the space charge distribution which in turn depends on the interfacial interaction of polymer with the filler particle plays a significant role in the higher dielectric constant of polymer composites at lower frequency. While upon increasing the

frequencies, the larger polar groups fail to orient themselves in the same pace of applied frequency results in the continuous decrease in the dielectric constant [180]. The dielectric constant of PBMA/Ce-TiO_2 nanocomposites is higher than the pure PBMA; determine the contribution of metal oxide nanoparticles in the storage capacity of polymer nanocomposites. The PBMA with 10 wt% Ce-TiO_2 composite shows lower dielectric constant than PBMA with 7 wt% Ce-TiO_2 samples. This is due to the fact that the nanoparticles have higher tendency for agglomeration at higher loading. The agglomeration of nanoparticles reduces the interfacial interaction of nanoparticles with the polymer and it also disturbs the orientation of polar groups and results in the lower dielectric constant.

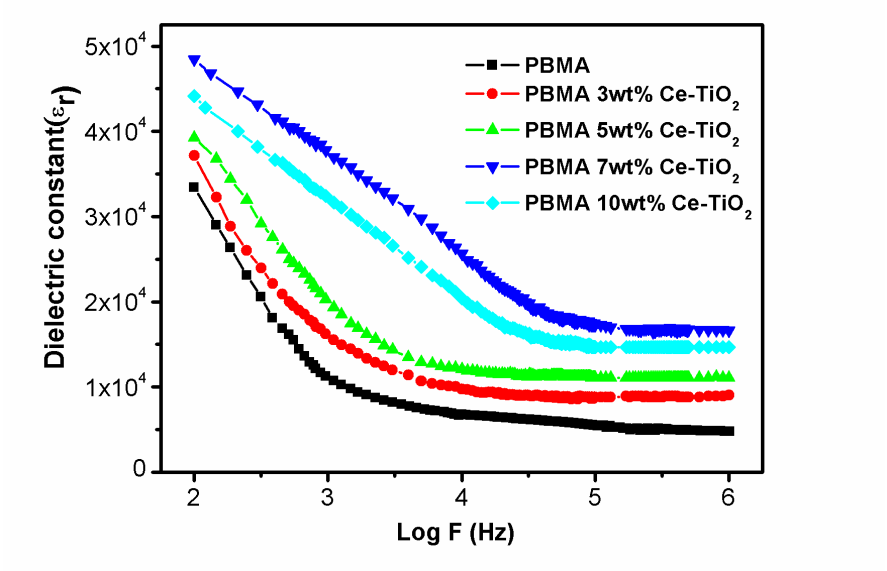

Figure 4.12: Dielectric constant of PBMA with different loading of Ce doped TiO_2

4.2.9.3 Dielectric Loss Tangent (Tan δ)

The variation of dielectric loss tangent of PBMA/Ce-TiO_2 nanocomposites as a function of frequency is presented in **figure 4.13.** The tan δ value is higher at lower frequencies and it continuously decreasing upon increasing the frequency, shows some structural changes in the polymer backbone after the addition of nanoparticles. The higher tan δ at lower frequency arises from the strong interfacial interaction and the space charge polarization at the interfaces. The tan δ shows an oscillatory behaviour which arises from the relaxation process occur in the heterogeneous interfaces between PBMA and Ce-TiO_2. The continuous decrease in dielectric loss with frequency can be explained as the interaction of viscous polymer matrix surrounding the dipoles resist the rotation of dipoles. The dipoles (charge carrier) use some part of energy absorbed from the applied field to overcome the resistance offered from the polymer matrix. This affects the transition of charge carriers between the interfaces which in turn decreases the tan δ with increasing frequency [181]. The PBMA/Ce-TiO_2 nanocomposites show higher tan δ than PBMA and the tan δ increases with the weight fraction of Ce-TiO_2 nanoparticles up to 7 wt%. This suggests that the better interfacial interaction is higher at a loading of 7 wt%. These interactions lead to an ordered arrangement of metal oxide nanoparticles in the polymer causes high space charge polarization at the interfaces. The decrease in tan δ after 7 wt% loading is the poor interfacial interaction of metal oxide nanoparticles with the polymer matrix.

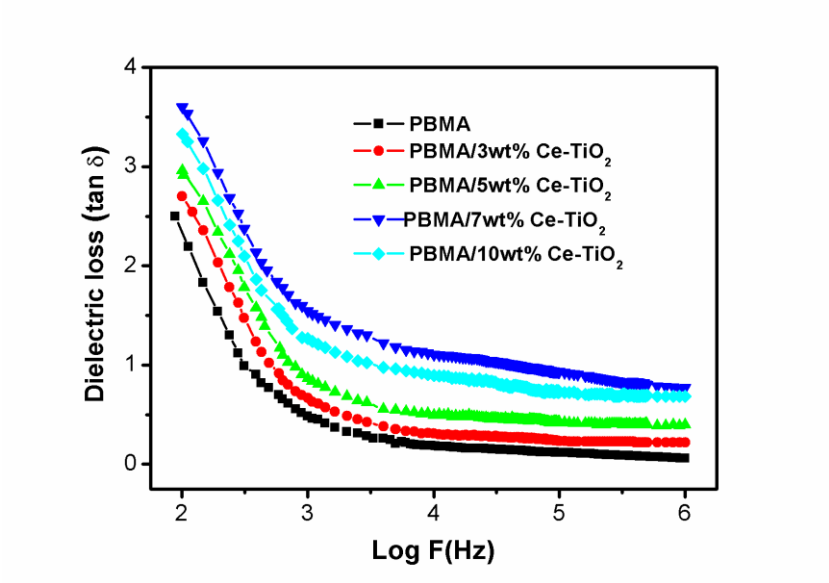

Figure 4.13: Dielectric loss tangent versus frequency plots for PBMA with Ce doped TiO_2

4.2.10 Temperature Dependent AC Conductivity Studies

Figure 4.14 represents the frequency dependent AC electrical conductivity of PBMA and PBMA with different contents of Ce-TiO_2 nanoparticles at various temperatures. All the samples show the typical dielectric behavior of an insulating polymer. In all cases, the conductivity increases linearly with increase in frequency from 10^2 to 10^6 Hz. The conductivity of all the composites is greater than pristine PBMA. The higher conductivity of the composites is due to the formation of excess charge carriers developed in the polymer composite. At lower loading of fillers, the distance between the conducting particles are high and hence the chance for the conductivity arising through the hopping of charge carriers is less, this result in lesser conductivity. However, as the loading of Ce-TiO_2 in PBMA

increases to 7 wt% the inter particle distance decreases. This favours the hopping phenomena and results in higher conductivity values at 7 wt% loading. In other words, the increase in conductivity with the filler loading suggests the formation of an effective conducting path within the polymer matrix. But, a slight decrease in conductivity at 10 wt% of Ce-TiO_2 is possibly due to the formation of aggregated nanoparticles in the polymer matrix. This is because the particle to particle distance is too short at higher loading of fillers, which leads to the poor interfacial interactions between polymer and nanoparticles and thereby resist the hopping of charge carriers. This in turn causes the decrease in conductivity. It is also clear from the figure 4.14 that the conductivity of all the samples increases with the temperature. This behavior is typical for semi-conducting matrix such as PBMA. The increase in conductivity with the temperature is attributed to the higher hopping of charge carriers within the polymer matrix. Further the formation of dipoles and greater interfacial polarization at higher temperature results in enhanced conductivity. The enhanced conductivity in the composites has been explained by the polaron hopping theory, in which two types of polarons, small polaron or the large polaron model conduction is developed in the composites [182]. According to large polaron theory, a band type mechanism occurs which results in a decrease in conductivity with frequency at all temperatures. According to small polaron theory, the developed conductivity increases with frequency. So it can be suggested that in PBMA/Ce-TiO_2 nanocomposites, small polaron theory is applicable at all temperatures.

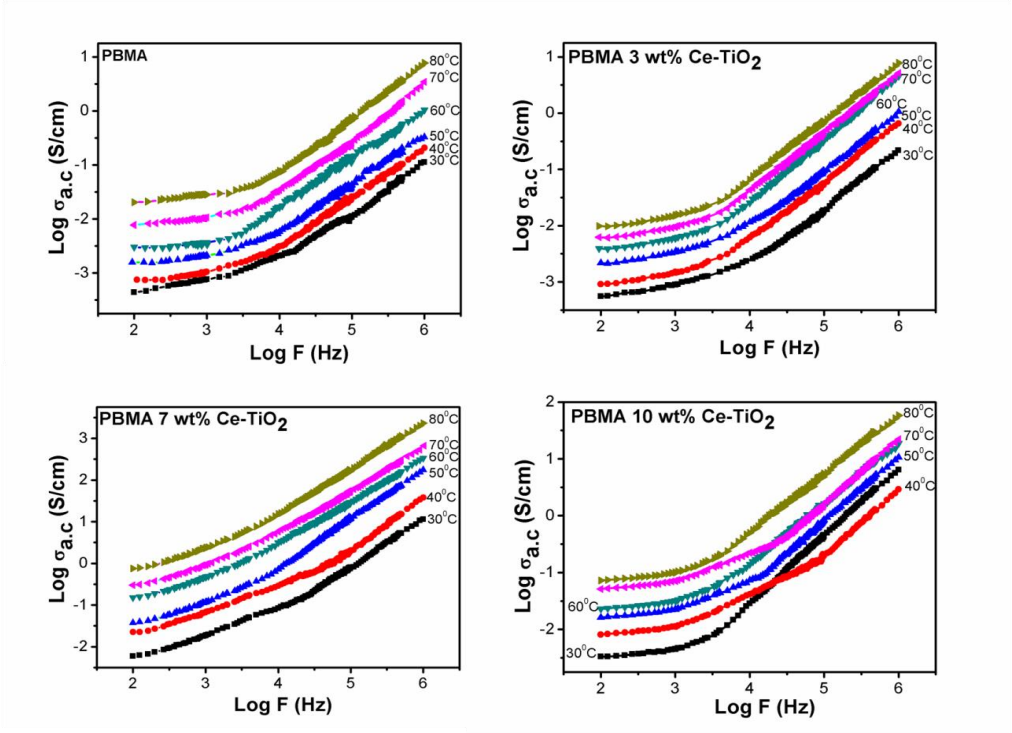

Figure 4.14: Variation of $\sigma_{a.c}$ with frequency for PBMA/Ce doped TiO_2 nanocomposites at different temperatures

The variation of activation energy in the conductivity process with the frequency at various temperatures (303K to 453K) has been investigated for PBMA/Ce-TiO_2 nanocomposite films and the results are given in **table 4.2.** The activation energy obtained from the slope of the Arrhenius plot, $\log(\sigma_{a.c})$ vs 1000/T and is given in **figure 4.15.** The activation energy is the minimum energy required to overcome the conductivity potential barrier in the polymer. So, larger the activation energy values, the smaller conductivity of the composites and vice versa. The activation energy is decreasing with frequency (i.e., the conductivity increases with frequency) for all the composites. The smaller conductivity at the lower frequency is due to the low mobility

of hopping charge carriers. The mobility of carriers enhances with a rise in frequency and hence conductivity is higher at larger frequencies. Further, the activation energy values decrease with temperature indicates the enhanced conductivity at higher temperatures. From table 4.2 it can be noticed that the activation energy of the composites is lesser than that of pure PBMA. The enhanced conductivity of PBMA is due to the incorporation of metal oxide nanoparticles. The activation energy is found to be decreased with the addition of nanoparticles up to 7 wt% and after that, it shows a slight increase. This confirms the enhanced conductivity with the incorporation of nanoparticles up to a certain concentration. The increase in activation energy at higher concentration of Ce-TiO_2 is arising from the disturbance in the conducting network. This might be due to the self-aggregation of nanoparticles at higher concentrations.

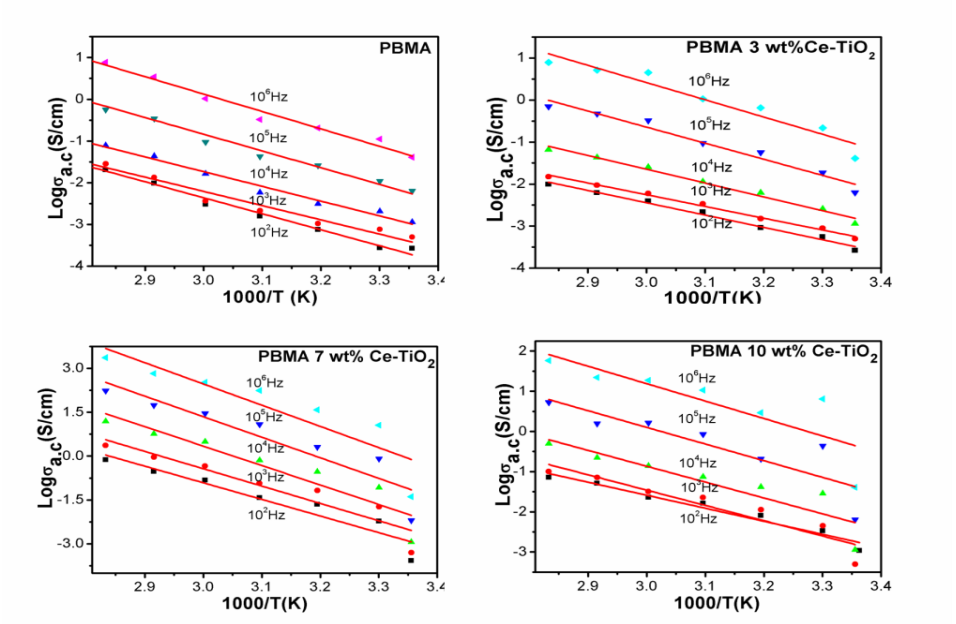

Figure 4.15: Activation energy plots for PBMA and PBMA/Ce doped TiO_2 nanocomposites

Table 4.2: Frequency dependent activation energy of PBMA with Ce doped TiO_2 nanoparticles.

Samples	Frequency (Hz)				
	10^2	10^3	10^4	10^5	10^6
PBMA	-3.834	-3.414	-3.531	-4.005	-4.167
PBMA/3 wt% Ce-TiO_2	-3.965	-3.994	-4.002	-4.123	-4.488
PBMA/5 wt% Ce-TiO_2	-4.068	-4.085	-4.147	-4.326	-4.670
PBMA/7 wt% Ce-TiO_2	-5.680	-5.930	-6.651	-7.025	-7.258
PBMA/10 wt% Ce- TiO_2	-3.840	-3.870	-3.949	-4.146	-4.337

The dependence of conductivity on frequency is given by the equation $\sigma_{a.c}\,(\omega) = A\ \omega^s$ where the 's' is an exponent and its value denote the type of conductivity mechanism present in the composites. The value of '*s*' calculated from the slope of the plot of $\log(\sigma_{a.c})$ vs $\log(\omega)$ is tabulated in **table 4.3.** From the table, it is clear that the value of 's' decreases with temperature, further confirms the hopping conduction mechanism present in the PBMA/Ce-TiO_2 nanocomposites [146].

Table 4.3: Frequency exponent‘s’ from the AC conductivity of PBMA and PBMA with different contents of Ce doped TiO_2 nanoparticles

Samples	Temperature (°C)					
	30	40	50	60	70	80
PBMA	0.6018	0.6017	0.6168	0.6159	0.6141	0.6138
PBMA/3 wt% Ce-TiO_2	0.7601	0. 7533	0.7494	0.7203	0.7202	0.7121
PBMA/5 wt% Ce-TiO_2	0.7856	0.7832	0.7810	0.7788	0.7745	0.7643
PBMA/7 wt% Ce-TiO_2	0.8461	0.8363	0.8296	0.8281	0.8181	0.8012
PBMA/10 wt% Ce-TiO_2	0.8380	0.8351	0.8345	0.8330	0.8061	0.8001

4.2.11 DC Conductivity

Figure 4.16 represents the variation of DC electrical conductivity of the PBMA nanocomposite films with the Ce-TiO_2 filler loading. As depicted in the figure, the conductivity increases slowly at the initial loading of filler loading and at particular filler loading the conductivity shows a sudden increase. This is followed by a slow increase again at 10 wt% of Ce-TiO_2. At lower filler loading, the conducting metal oxide particles are isolated from each other and therefore the conductivity is less. As the loading of Ce-TiO_2 increases, the conducting particles become closer and the conductivity gradually increases. However, at particular loading of filler, there is high enough number of conducting particles form a continuous conducting path which presents an abrupt change in conductivity. The loading of filler

at which the conductive network formation completes is called the percolation threshold [183, 184]. In other words, at the percolation threshold, the insulating polymer matrix converts into conducting polymer matrix. In the case of PBMA/Ce-TiO_2 nanocomposite films, the percolation threshold is 3 wt%.

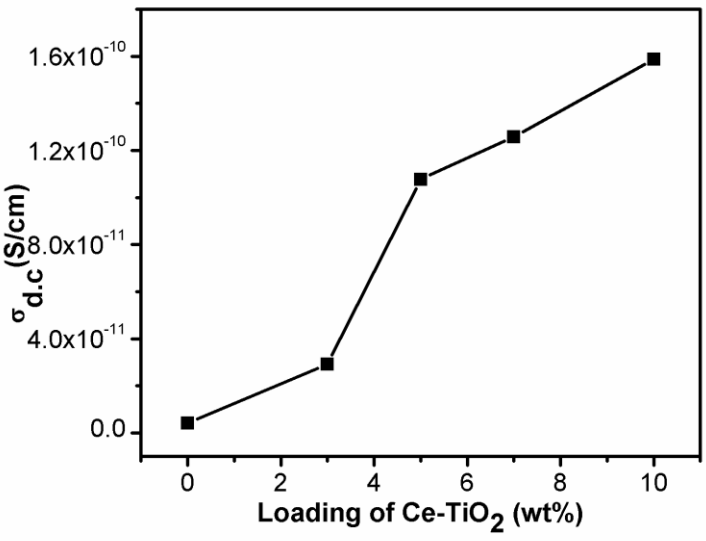

Figure 4.16: Variation of DC electrical conductivity of PBMA with nanoparticles loading

4.2.12 Theoretical Approaches to the DC Conductivity

Various theoretical models were proposed in order to predict the nature of electrical conductivity in the polymer composites [145, 149]. Basically, the modeling studies help to evaluate the influence of different parameters like filler volume fraction, percolation threshold, shape, aspect ratio, surface energy, filler orientation etc. in the conductivity of composites. Each model considers the effect of these

parameters to the electrical conductivity in distinct ways. In the present study the Scarisbrick, McCullough, Bueche and Mamunya models are applied in order to predict the nature of electrical conductivity.

4.2.12.1 Scarisbrick Model

In Scarisbrick model, it is assumed that the inter-particle contact between the conducting filler particle in the insulating polymer matrix is ohmic nature [152]. This ohmic conduction is responsible for the conductivity of the two-phase systems like inorganic-organic hybrid polymer nanocomposites as the present case of PBMA/Ce-TiO_2. So, the total conductivity of the composite system is higher when there is good contact among the conducting particles. Based on these assumptions he derived an expression for calculating conductivity as

$$\frac{\sigma c}{\sigma f} = C^2.\Psi.\Psi[exp(\Psi^{-\frac{2}{3}})] \qquad (4.4)$$

Where, σc depicts the conductivity of composites, σf the conductivity of filler particle (1.39×10^6 S/cm) and Ψ the volume fraction of the filler in the composite. C is the geometrical factor which depends on the arrangement conductive paths within the polymer matrix. The value of C^2 varies from 1 to 3×10^{-3}. Then the equation is expressed as

$$\frac{\sigma c}{\sigma f} = \Psi.\Psi[exp(\Psi^{-\frac{2}{3}})] \text{(When } C^2 = 1\text{)} \qquad (4.5)$$

$$\frac{\sigma c}{\sigma f} = 3\ x\ 10^{-3}.\Psi.\Psi[exp(\Psi^{-\frac{2}{3}})] \text{ (When } C^2 = 3x10^{-3}\text{)} \quad (4.6)$$

The conductivity of the PBMA/Ce-TiO_2 composites calculated using the **equation: 4.4 - 4.6.** This is compared with that of experimentally determined conductivity in **figure 4.17.** The theoretically calculated conductivity is very much higher than that of experimental one at all concentrations. In Scarisbrick model, the contribution from polymer matrix is not considered and therefore there is large difference between the conductivity theoretically calculated and experimentally determined. So Scarisbrick model fails to predict the conductivity of the PBMA/Ce-TiO_2 composites.

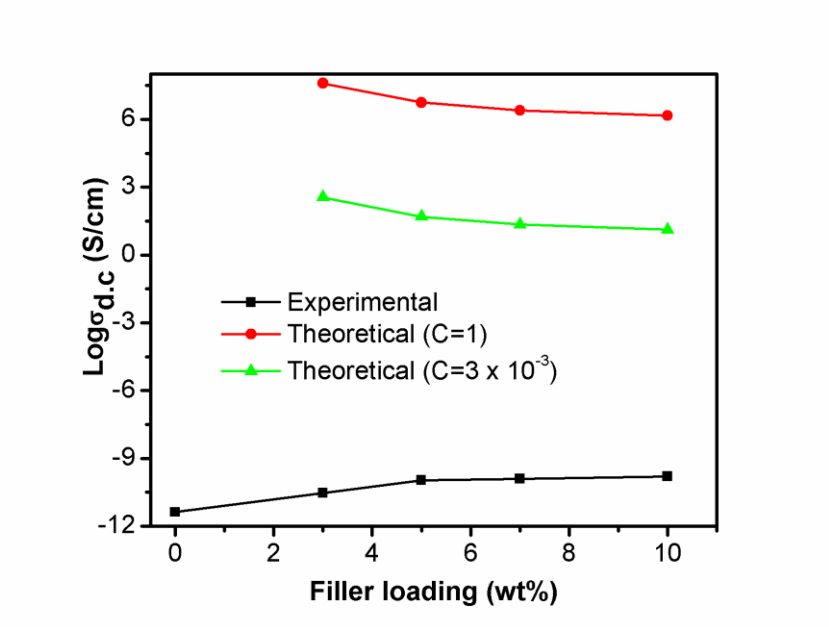

Figure 4.17: Theoretical and experimental variations of $\sigma_{d.c}$ based on Scarisbrick model.

4.2.12.2 McCullough Model

McCullough proposed a model for predicting the conductivity of binary systems like polymer composites consists of an insulating polymer matrix and conducting nanofillers [150]. The equation is,

$$\sigma c = \sigma p.\Psi p + \sigma f.\Psi f - \left[\frac{\lambda.\Psi p.\Psi f+(\sigma f-\sigma p)^2}{vf.\sigma f+vp.\sigma p}\right] \qquad (4.7)$$

where, σc is the conductivity of composite film, σp is the conductivity of pure polymer matrix (4.23×10^{-12} S/cm), σf is the conductivity of filler particles, Ψp is the volume fraction of the polymer matrix and Ψf is the volume fraction of filler particles. Vf and Vp are defined as,

$$vf = (1-\lambda).\Psi f + \Psi p.\lambda \qquad (4.8)$$

$$vp = (1-\lambda).\Psi p + \Psi f.\lambda \qquad (4.9)$$

Where λ is the structural factor that gives an idea about the extent of network formation and its value varies from 0 to 1.

Based on the McCullough model, the conductivity of PBMA/Ce-TiO_2 composites is calculated using **equation: 4.7 to 4.9** at various values of λ and the obtained theoretical and experimental conductivity is given in **figure 4.18.** The increasing trend of theoretical and experimental conductivity with filler loading is same, but the difference between them is too large. The λ value depends on the concentration, size and aspect ratio of filler. So the actual value of λ is difficult to calculate. Therefore McCullough model is also fails to predict the exact conductivity of composites.

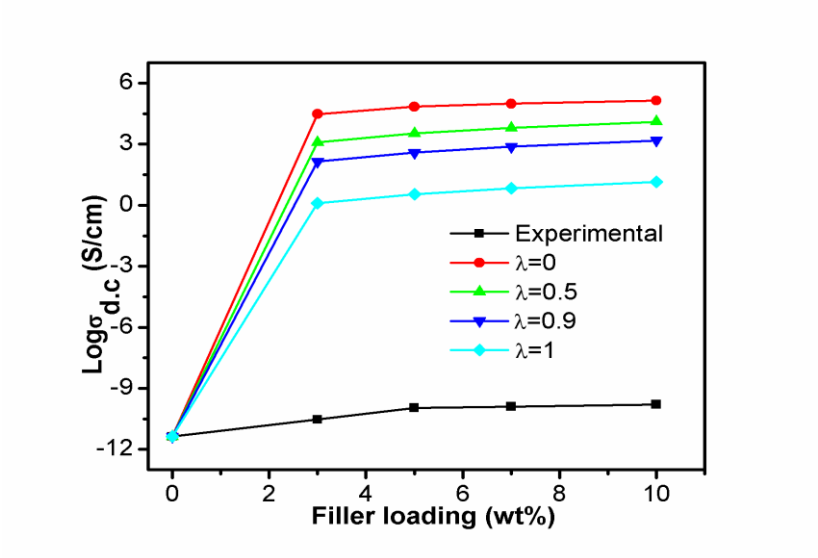

Figure 4.18: Theoretical and experimental variations of $\sigma_{d.c}$ based on McCullough model.

4.2.12.3 Bueche Model

According to Bueche model, the interaction of conducting particle with insulating polymer matrix plays a crucial role in the conductivity of polymer composites [151]. The aggregate of conducting particles can form a continuous conducting path in the insulating polymer matrix during the polymerization. Hence the conductivity has a contribution from both filler and polymer. So the conductivity of two phase systems like polymer composites can be expressed as

$$\sigma c = \sigma f . \Psi f + \sigma p(1 - \Psi f) \qquad (4.10)$$

Where Ψf is the volume fraction of filler particles, σf is the conductivity of filler particles, σp is the conductivity of pure polymer matrix and σc is the conductivity of the composite film.

The conductivity of PBMA/Ce-TiO_2 composites is calculated from the **equation: 4.10** and the variation of conductivity with the volume fraction of filler is given in **figure 4.19.** From the theoretical and experimental plots, the change in conductivity is more pronounced with filler concentrations. The Bueche model is based on an additive rule. If the conductivities of the two components, polymer matrix and inorganic filler have large difference then the resultant conductivity of the composites will be similar to that of conducting phase. In the case of composites, the theoretically calculated conductivity using Bueche model is always higher than that of the experimental one. So Bueche model also fails to predict the conductivity of PBMA/Ce-TiO_2 composites in which there is a large difference in conductivities of PBMA matrix and Ce-TiO_2 nanofillers.

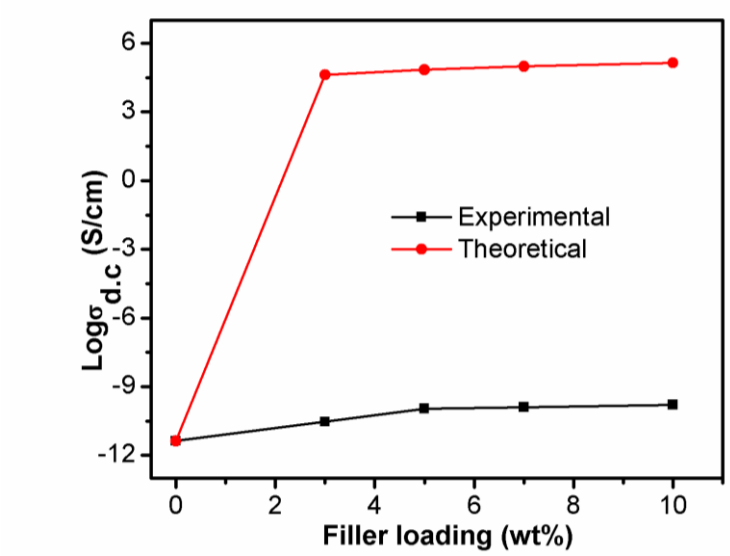

Figure 4.19: Theoretical and experimental variations of $\sigma_{d.c}$ based on Bueche model.

4.2.13 Mamunya Model

According to Mamunya model the polymer-filler interfacial interaction plays a major role in the conductivity of the polymer nanocomposites [153, 185]. He pointed out that the conductivity of composites not only depends on the individual conductivity of polymer and filler but also on the factors like aspect ratio, surface properties and percolation threshold of the filler etc. which in turn depends on the polymer-filler interfacial interactions. By considering the contribution from these various factors towards the conductivity Mamunya proposed a thermodynamic theoretical model and can be expressed

$$Log\ \sigma = \ log\ \sigma c\ + (log\ \sigma F - log\ \sigma c\ )(\frac{\Phi-\Phi c}{F-\Phi c})k \quad (4.11)$$

where, Φ signify the filler volume fraction, Φc the filler volume fraction at the percolation threshold, σc the electrical conductivity at the percolation threshold and σ_F the electrical conductivity at maximum packing volume fraction. k is an exponent depends on Φ as shown in **equation: 4.12 & 4.13.**

$$k = K\Phi/(\Phi\text{-}\Phi c)^{0.75} \quad (4.12)$$

$$K = A - B\ \gamma_{pf} \quad (4.13)$$

where, A and B are the constants and its value is 0.28 and 0.036 respectively. γ_{pf} symbolize the polymer and filler interfacial surface tension and is given by the equation

$$pf = \Upsilon p + \Upsilon f - 2(\Upsilon p \Upsilon f)^{0.5} \quad (4.14)$$

where, ϒp and ϒf attributes to the surface energies of polymer (43.5 mJ/m^2) and filler (55 mJ/m^2) respectively [153, 186].

The conductivity of PBMA/Ce-TiO_2 nanocomposites is calculated using the **equation: 4.11 to 4.14** and the obtained plots for the conductivity is given in **figure 4.20.** It is distinct that the experimental conductivity is matching with the theoretical one at higher filler volume fraction but shows some deviation at lower filler volume fraction. The polymer- filler interfacial interaction is effective at higher filler loading due to uniform dispersion. Hence, it can conclude that among the various model tried, the Mamunya model is suitable to predict the conductivity of PBMA/Ce-TiO_2 nanocomposites which have better polymer-filler interfacial interactions.

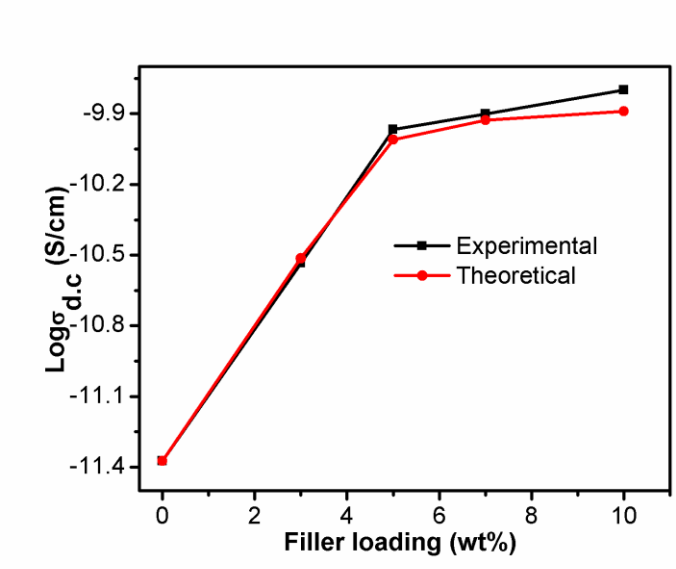

Figure 4.20: Theoretical and experimental variations of $\sigma_{d.c}$ based on Mamunya model.

4.3 Conclusion

The PBMA/Ce-TiO_2 nanocomposites were successfully prepared via in situ polymerization technique. The FT-IR spectra revealed the presence of Ce-TiO_2 in the PBMA matrix. The UV visible spectra exhibits red shift in absorption edge of PBMA upon addition of Ce-TiO_2 nanoparticles confirmed the presence and the interaction of metal oxide nanoparticles with the polymer matrix. The XRD studies showed a decrease in amorphous structure of PBMA with addition of Ce-TiO_2 nanoparticles. The DSC results showed an increase in glass transition temperature with increase in loading of metal oxide nanoparticles. TGA analysis showed the enhanced thermal stability of PBMA matrix with the addition of metal oxide nanoparticles. The nanocomposite shows excellent tensile strength than pure PBMA and the composite with 7 wt% sample shows the maximum tensile strength. The reinforcing nature of Ce-TiO_2 nanoparticles in PBMA was also carried with different theoretical modeling such as Einstein, Mooney and Pukanszky equations. Among these models, Pukanszky model showed better agreement in PBMA/Ce-TiO_2 nanocomposites. The AC conductivity, dielectric properties of the PBMA/Ce-TiO_2 nanocomposites was significantly higher than pure PBMA and these properties increases with filler loading up to 7 wt% and after that it decreases. Further, the AC conductivity of PBMA and all PBMA/Ce-TiO_2 nanocomposites showed direct dependence on the temperature as well as frequency. The activation energy of all the composites decreased with temperature. The DC conductivity of all the nanocomposites was higher than pure PBMA and the conductivity

increased regularly with the loading of nanoparticles. Various theoretical models were studied based on Scarisbrick, McCullough, Bueche and Mamunya equations to predict the DC conductivity nature of PBMA/Ce-TiO_2 nanocomposites. The conductivity calculated using the thermodynamic model introduced by Mamunya showed the best agreement with that of the experimental data. However, the statistical approaches given by Scarisbrick, McCullough and Bueche models fail to predict the conductivity of PBMA/Ce-TiO_2 nanocomposites.

CHAPTER 5

EFFECT OF NEODYMIUM DOPED TITANIUM DIOXIDE NANOPARTICLES ON THE STRUCTURAL, MECHANICAL AND ELECTRICAL PROPERTIES OF POLY (BUTYLMETHACRYLATE) NANOCOMPOSITES

Contents

K. Suhailath, M. T. Ramesan, Effect of neodymium-doped titanium dioxide nanoparticles on the structural, mechanical, and electrical properties of poly (butylmethacrylate) nanocomposites, J. Vinyl Addit. Techn. 25 (2019) 9.

K. Suhailath, M. T. Ramesan, Theoretical and experimental studies on DC conductivity and temperature dependent AC conductivity of poly (butylmethacrylate)/Nd-TiO_2 nanocomposites, J. Thermoplast. Compos. Mater. 33 (2019) 1061.

5.1 Introduction

Recent years have witnessed an explosive growth in research in the field of polymer nanocomposites. The most thrilling aspect in this field is the unique in properties of the resulting nanocomposites coupled with the high performance to weight ratio [187]. The development of novel polymers, chemically modified polymers and novel nanoparticles catalyzed the industrial and academic in this field. Many of their outstanding properties, revealed by research, paved way for their explorations in novel and diverse applications [188]. Acrylate polymers are amorphous thermoplastic materials with transparency, good processability, protection against ultraviolet radiation, good weather stability, high strength, and dimensional stability [189, 190]. Moreover, it has good resistance to chemicals and finds applications in coatings, lubrication, bio-microsystems, organic light emitting diodes etc [191]. However, acrylate polymers have poor thermal stability, flame resistance, electrical conductivity and mechanical-dynamical properties at high temperatures. The performance of acrylate polymers has been reported to be greatly improved by the addition of nanoparticles such as clays, silica and carbon nanotubes [192]. However, the nanocomposites based on these nano-fillers often exhibit poor mechanical properties, thermal stability and dielectric constant and this is mainly due to the absence of efficient interfacial interactions between nano-fillers and the polymer. The material properties of acrylate polymers can be enhanced by mixing it with metal oxide nanoparticles. The addition of nanoparticles brought significant changes in the molecular dynamics of the polymer matrix which

results in good interfacial interaction leading to excellent and novel mechanical properties in the resultant polymer nanocomposites.

Various types of nanoparticles are used for the fabrication of polymer nanocomposites including alumina (Al_2O_3), silica (SiO_2), titania (TiO_2), clay etc. [193-195]. Owing to excellent optical and electrical properties, TiO_2 nanoparticles are of great interest in the production of polymer nanocomposites [196]. Further, the electron-rich TiO_2 nanoparticles can effectively coordinate or interact with polymer matrix having carbonyl groups such as polyacrylates. The TiO_2 nanoparticles imparting excellent UV shielding properties in poly acrylates were reported by Man et al. [197]. Moreover, the enhancement in the thermal properties of PMMA with the addition of methacrylic acid modified TiO_2 was studied by Khaled et al. [198]. The surface modification of nanoparticles through the doping of various metal ions, especially the rare earth metals, can further improve their surface properties and hence the interaction with polymer matrix [199]. Neodymium is one of the important dopants due to its ability to interact with functional –OH groups. The interaction occurs through their f orbital's and this result in their effective doping on to TiO_2 surfaces [200].

The present work focused on the reinforcement of poly (butylmethacrylate) with neodymium-doped titanium dioxide nanoparticles through a simple in situ polymerization technique. The effect of Nd-doped TiO_2 nanoparticles on the structural and material properties of PBMA/Nd-TiO_2 composites were studied by using FT-IR, UV spectroscopy, XRD, FE-SEM, DSC and TGA analysis. The

change in tensile strength of the PBMA composites by the addition of Nd-TiO_2 nanoparticles was correlated with various theoretical modelling for studying the reinforcing mechanism of the resulting PBMA nanocomposites. The AC conductivity and dielectric properties of PBMA/Nd-TiO_2 nanocomposites were investigated with respect to frequency and volume fractions of nanoparticles. Further, the present work emphasized on the effect of Nd-TiO_2 nanoparticles on the temperature dependent AC and the DC conductivity of poly (butylmethacrylate) matrix. Also, the role of Nd-TiO_2 nanoparticles in the DC conductivity of PBMA matrix has been correlated with different theoretical models for studying the applicability of modeling in various fields.

5.2 Results and Discussion

5.2.1 FT-IR Spectra

The molecular structure of Nd-TiO_2 and PBMA/Nd-TiO_2 nanocomposites were investigated by FT-IR spectroscopy and the spectrum is given in **figure 5.1.** The FT-IR spectra of Nd-TiO_2 nanoparticle exhibits an intense broad absorption peak around 3400 cm^{-1} corresponds to the stretching vibrations of -OH or water molecules in the surface of nanoparticles [201]. The intense peak around 1630 cm^{-1} is due to the -OH bending vibrations of chemisorbed water molecules. The absorption band in the region of 900-400 cm^{-1} is due to the Ti-O-Ti, Ti-O, and Nd-O stretching vibrations [202]. The absorption peaks at 2951 and 2873 cm^{-1} are assigned to C-H stretching vibrations of CH_3 and CH_2 groups respectively in the PBMA

backbone. The characteristics peaks at 1729 cm^{-1} and 1459 cm^{-1} corresponds to C=O and C-O vibration bands respectively, of the ester part present in the PBMA backbone [203]. The bands at 1461 cm^{-1} are associated with C-O-C stretching vibrations. The FT-IR spectra of composites show all the characteristic peaks of PBMA with the presence of Nd-doped TiO_2 at 665 cm^{-1}, indicating the presence of Nd-TiO_2 nanoparticles in the PBMA matrix.

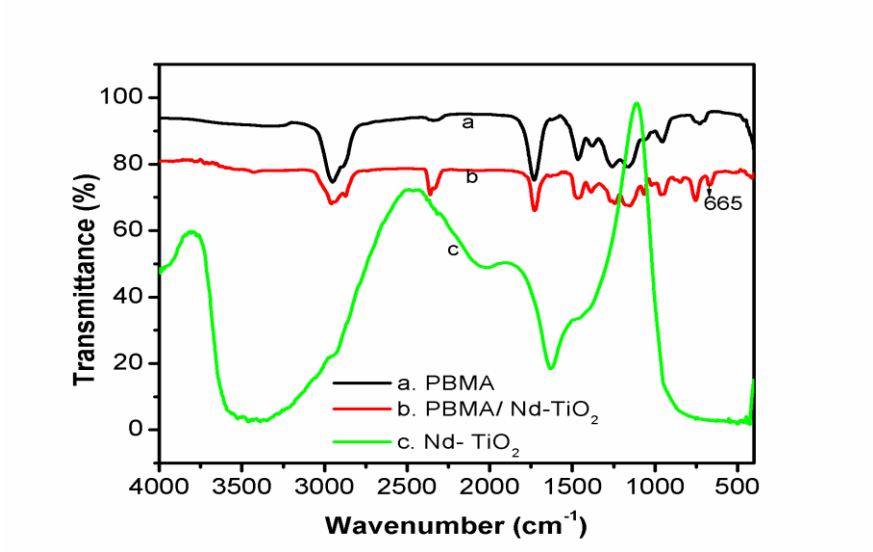

Figure 5.1: FTIR spectra of Nd doped TiO_2, PBMA and PBMA with Nd-doped TiO_2

5.2.2 UV-Visible Absorption Spectra

Figure 5.2 represents the UV-Visible absorption spectra of PBMA and PBMA with different concentrations of Nd-TiO_2 nanoparticles. All the nanocomposites exhibit an intense peak at 245 nm and a weak broad peak around 275 nm corresponds to the π-π* and n-π* transitions respectively in the carbonyl group of ester group present in the PBMA

backbone. There is no absorption peaks in the visible region shows the transparent nature of PBMA/Nd-TiO_2 composites. All the composites show higher absorption than the bare PBMA indicates the influence of nanoparticles in the enhancement of optical properties of PBMA matrix. It is clear from the figure that the absorption edge of PBMA/Nd-TiO_2 nanocomposites is higher than that of the pure PBMA indicating the strong interaction of Nd-TiO_2 nanoparticles with the PBMA matrix. The absorption edge of the composite increases with the addition of Nd-TiO_2 nanoparticles up to 7 wt% and beyond this loading the absorption edge is found to be decreasing. This means that the interfacial interaction is higher at 7 wt% loading. The agglomeration of nanoparticles at higher loading (10 wt%) reduces the interaction of nanoparticles with PBMA matrix causes a decrease in absorption.

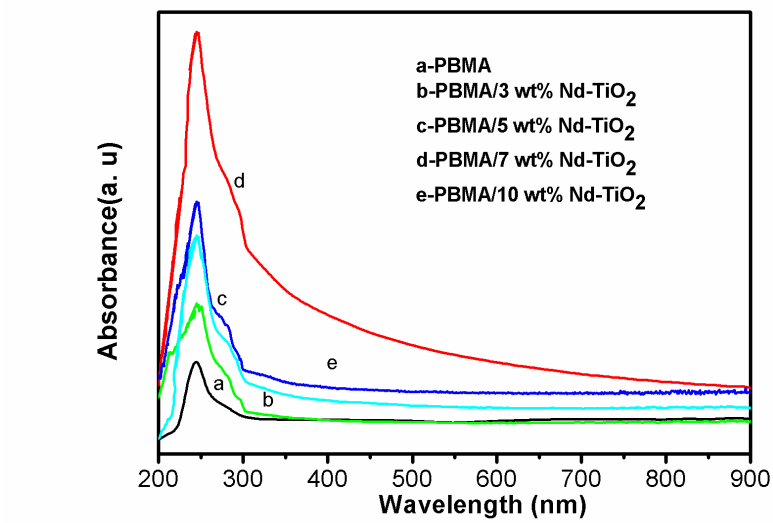

Figure 5.2: UV-Visible spectra of PBMA and PBMA with different contents of Nd-doped TiO_2

5.2.3 XRD Analysis

Figure 5.3 represents the XRD patterns of Nd-TiO_2 nanoparticles, PBMA and PBMA/Nd-TiO_2 nanocomposites. The XRD curve of synthesized Nd-TiO_2 nanoparticles shows the crystalline peaks at 2θ = 25.3°, 37.8°, 47.6°, 54.2°, 62.4°, 69.3° and 76.1° which are assigned to the (101), (004), (200), (211), (204), (220), and (215) crystal reflection planes respectively [204]. The broad and diffused peak observed at 2θ = 18.8° is the amorphous phase of conventional PBMA. However, the addition of Nd-TiO_2 nanoparticles into the PBMA decreases the amorphous phase of PBMA with a shift of 2θ value from 18.8° to18.1°. The decrease in amorphous nature with the addition of nanoparticles indicates the effective interfacial interaction between the Nd-TiO_2 nanoparticles and PBMA segments.

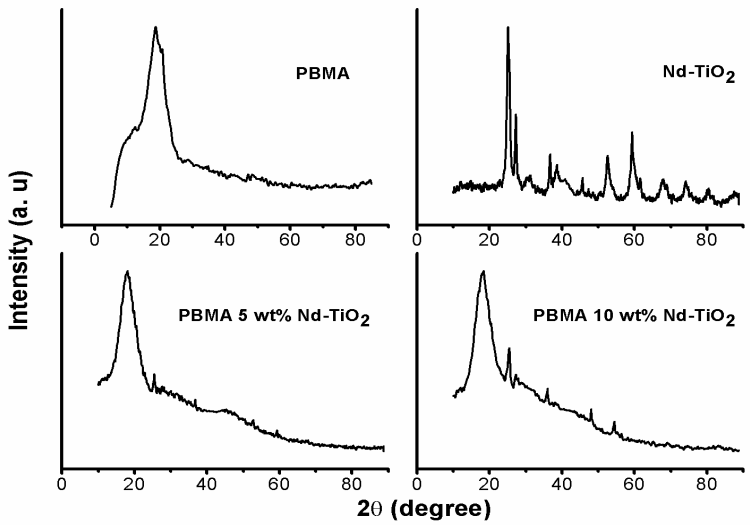

Figure 5.3: XRD patterns of Nd-doped TiO_2, PBMA with different contents of Nd-doped TiO_2

5.2.4 FE-SEM Analysis

Figure 5.4 illustrates the FE-SEM micrographs of Nd-TiO_2, pure PBMA and PBMA/Nd-TiO_2 nanocomposites. The Nd-TiO_2 nanoparticles are in finely powdered form with spherical shape (Fig.5.4a). The pure PBMA (Fig.5.4b) exhibits smooth and homogenous surface morphology. The SEM images of all the composites show the dispersion of nanoparticles in the PBMA matrix. The uniform dispersion of nanoparticles is more visible in the composite with 7 wt% Nd-TiO_2 (Fig.5.4c) indicating the maximum interfacial interaction of nanoparticles with the PBMA matrix. However, the uniform adhesion of nanoparticles in the polymer decreases at higher loading of nanoparticles (Fig. 5.4d). The particles to particles distance are too short at higher loading and therefore they undergo agglomeration with each other.

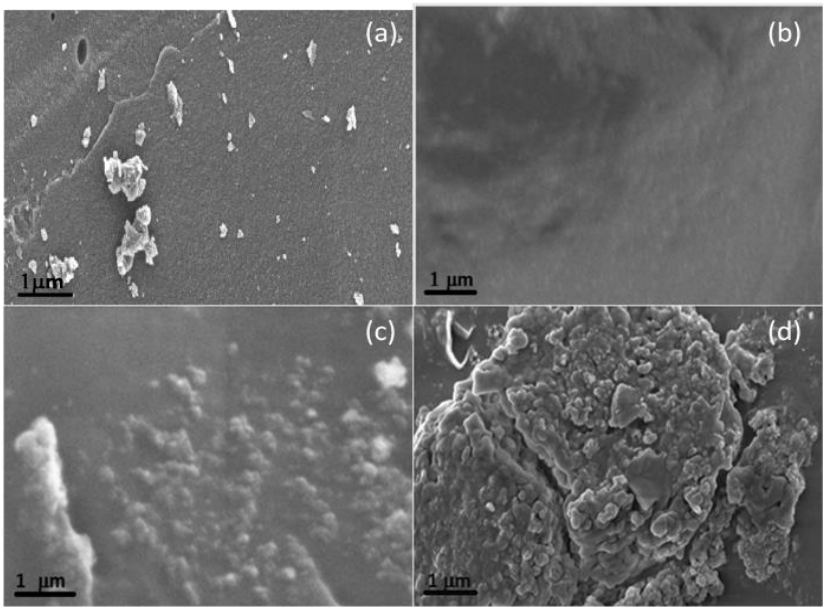

Figure 5.4: FE-SEM images of (a) Nd-TiO_2 (b) PBMA (c) PBMA/7 wt% Nd-TiO_2 and (d) PBMA/10 wt% Nd-TiO_2

5.2.5 Thermal Properties

5.2.5.1 DSC Analysis

The glass transition temperature (T_g) of PBMA/Nd-TiO_2 nanocomposites is analyzed by DSC and is presented in **figure 5.5.** It can be seen that all the samples show three endothermic peaks. The weak endothermic peak at lower temperature is the glass transition temperature of the polymer. The major endothermic peak represents the primary crystallization temperature while the middle one is the secondary crystallization temperature of polymers [205, 206]. PBMA showed T_g at 21.54°C, whereas the Nd-TiO_2 incorporated PBMA showed the T_g at 26.12 and 34.03°C for 5 and 10 wt% nanoparticles respectively. The increase in T_g of polymer with the addition of nanoparticles is due to the strong interfacial interaction of nanoparticles with the PBMA matrix. It can be seen from the figure that the primary and secondary crystallization melting of all the composites are higher than pure PBMA and the melting of the composite slight increases with increasing the loading of nanoparticles.

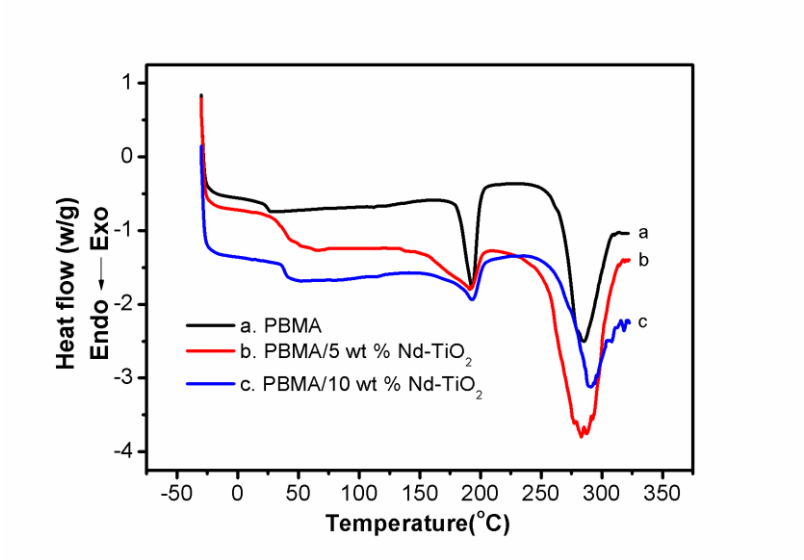

Figure 5.5: DSC profiles of PBMA with different contents of Nd-TiO_2 nanoparticles.

5.2.5.2 TGA Analysis

Table 5.1: The value of Ti and Tmax obtained from the TGA and corresponding DTG curves for PBMA and PBMA/Nd-TiO_2 nanocomposites

	TGA	**DTG**	
	T_i (°C)	**T_{max} (°C) I^{st} stage**	**T_{max} (°C) II^{nd} stage**
PBMA	256	280.29	364.33
PBMA/5 wt% Nd-TiO_2	258	294.05	370.22
PBMA/10 wt% Nd-TiO_2	265	304.03	390.28

The thermal resistance of PBMA and PBMA/Nd-TiO_2 nanocomposites are given in **figure 5.6** along with the DTG curve. Typically the

PBMA thermally degrades in two steps [207]. Initially, the weaker vinyl end groups are unzipped and form small polymer segments through chain transfer process, around 250°C. And in the second stage, these polymer segments further undergo degradation through random chain scission into simple molecules or monomers around 300°C. In the case of PBMA/Nd-TiO_2 nanocomposites, there is no residual material after ~400°C. This indicates the completion of degradation through random chain scission process [208]. The obtained degradation temperature (initial (Ti) from TGA and the maximum degradation temperature (Tmax) from DTG are presented in **table 5.1.** It is clear from the table that the thermal stability of the composites is higher than that of pure PBMA. The PBMA shows the initial degradation temperature at 256°C while the composite with 5 and 10 wt% samples show the decomposition temperature at 258°C and 265°C respectively. Similarly the maximum decomposition temperature of composites is higher than that of plane PBMA. The increase in thermal stability of PBMA by the addition of Nd-TiO_2 nanoparticles arises from the effective interfacial interaction between Nd-TiO_2 and the PBMA matrix. Also, the free radicals generated during the thermal degradation can transfer the electrons to the Nd-TiO_2 nanoparticles and this type of quenching of free radicals results in resistance to thermal degradation at higher concentration of Nd-TiO_2 nanoparticles. Further, the increase in char residue with an increase in nanoparticles content shows the reduced tendency for the decomposition of the composite compared to that of pure PBMA. This arises from the hindered segmental mobility of the polymer by the interaction with nanoparticles.

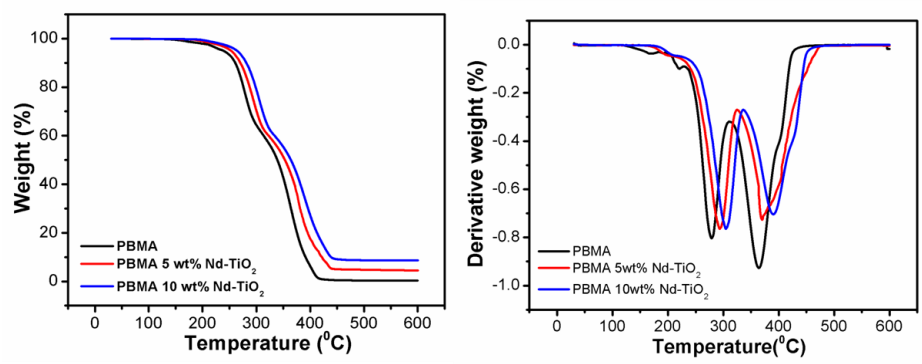

Figure 5.6: TGA and corresponding DTG curve of PBMA and PBMA with different contents of Nd-doped TiO_2

5.2.6 Mechanical Studies

The mechanical properties such as tensile strength and elongation at break of PBMA and PBMA/Nd-TiO_2 nanocomposites are displayed in **figure 5.7.** The tensile strength of PBMA increases with the incorporation of Nd-TiO_2 nanoparticles up to 7 wt% loading. The results indicate the effective stress transfer from the PBMA matrix to the Nd-TiO_2 nanoparticles is occurs in PBMA/Nd-TiO_2 composite which is responsible for the improved tensile property of the composites than the PBMA. Moreover, the interaction of Nd-TiO_2 nanoparticles with the PBMA matrix restricts the free movement of polymer segments leads to higher tensile strength [136]. The slight decrease in tensile strength at higher concentration (at 10 wt%) of nanocomposite arises from the greater agglomeration of nanoparticles (as revealed from SEM results). As expected, with the improvement in interfacial adhesion, the elongation at break decreases with the addition of nanoparticles. The better reinforcement of the Nd-TiO_2 nanoparticles in PBMA matrix leads to an increase in stiffness of composite materials and thereby leads to a decrease in elongation at break with increasing concentrations of Nd-TiO_2.

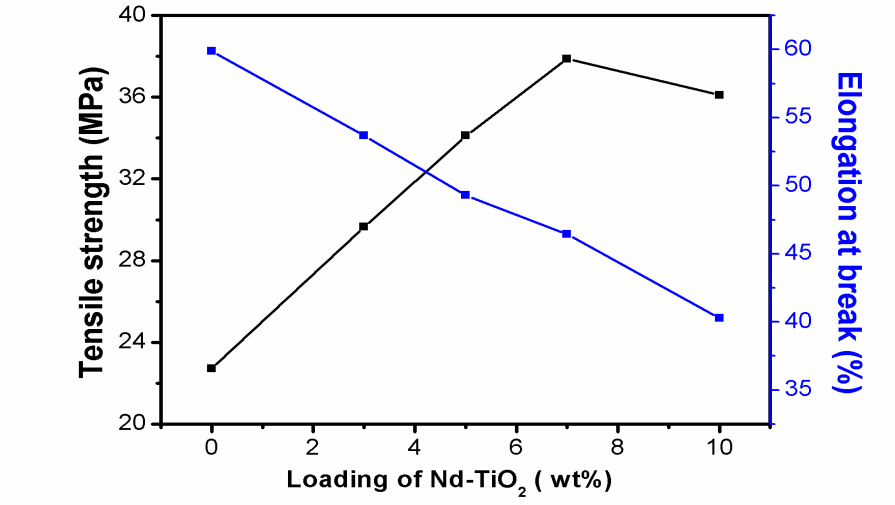

Figure 5.7: Tensile strength and elongation at break of PBMA and PBMA with different contents of Nd-doped TiO_2

5.2.7 Tensile Modeling

Several theoretical models have been used to predict the mechanism of reinforcement of nanoparticles in the polymer matrix. These models are based on various assumptions. The comparative studies of experimental plot with that of theoretical plot can give a clear picture of the role of filler-matrix interactions in the mechanical properties. In the present study, various theoretical tensile modeling such as Einstein, Mooney and Pukanszky equations are employed to study the mechanism of the improved tensile strength of PBMA/Nd-TiO_2 nanocomposites.

5.2.7.1 Einstein Model

Einstein assumed that the tensile property of binary systems possess better filler-matrix interaction which depends on the volume fraction of the filler can be expressed as following [137, 176].

$$Mc = Mm(1 + 1.25Vf) \qquad (5.1)$$

Where Mc and Mm represent the tensile strength of the composite and bare polymer respectively and Vf represents the volume fraction of filler. The theoretical tensile strength of nanocomposites calculated from Einstein model along with the experimental values are given in **figure 5.8.** It can be seen that the experimental plots show a large deviation from the theoretical values. This is because the Einstein model considers only the effect of filler volume fraction and neglects the influence of interaction parameter, aspect ratio, strain field around the filler and matrix. This model is applicable to very low concentration of filler and fail in most of the cases for predicting the tensile mechanism of polymer composites.

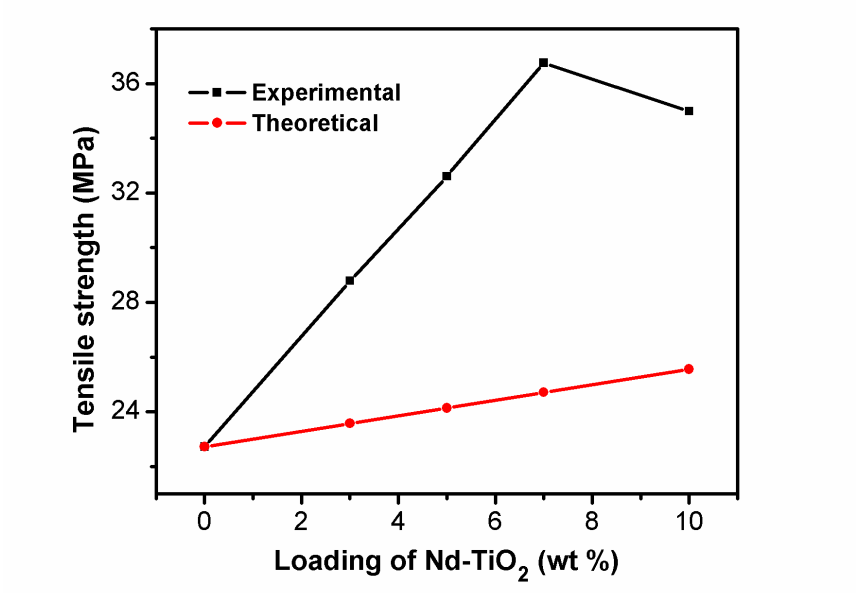

Figure 5.8: Theoretical and experimental curve of tensile strength based on Einstein model

5.2.7.2 Mooney Model

Mooney modified the theoretical equation of Einstein equation by introducing a new parameter 'S', denotes the crowding factor or the strain field around the two phases, the matrix and filler [138, 177] and the modified equation is given as follows

$$Mc = Mm * exp[\frac{2.5Vf}{1-SVf}] \quad (5.2)$$

The tensile strength of PBMA/Nd-TiO_2 nanocomposites is calculated from Mooney model and is presented in **figure 5.9.** The theoretical and experimental plots are not coinciding in any of the loadings and therefore the Mooney model also fails to predict the tensile mechanism of PBMA/Nd-TiO_2 nanocomposites. One of the advantages of the Mooney model is the crowding factor of the nano-filler. Therefore this model is applicable to higher filler concentrations. Also, the model does not consider the influence of parameters like interaction parameter and it has a greater role in the tensile properties of composites.

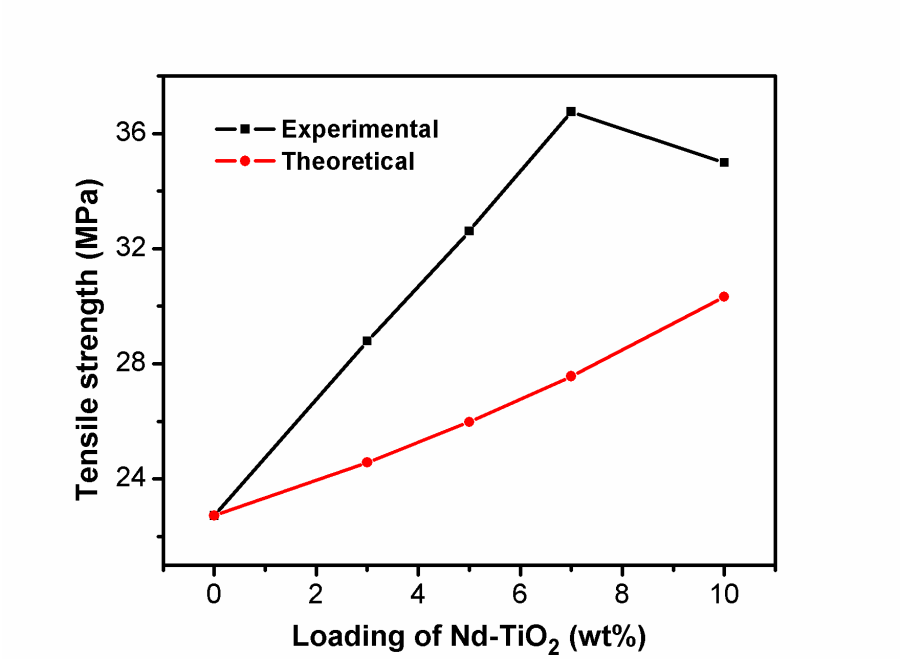

Figure 5.9: Theoretical and experimental curve of tensile strength based on Mooney model

5.2.7.3 Pukanszky Model

Pukanszky proposed that the interfacial interaction between the polymer matrix and filler plays a key role in improving the tensile strength of polymer composites [141, 178]. In other words, the major reason for the enhanced tensile strength of composites is due to the stress transfer from filler to the polymer matrix through the interphase region, which creates a greater interfacial interaction. Based on these observations, Pukanszky derived an equation for the tensile strength of composites and the equation can be expressed as

$$Mc = Mm * \frac{1-Vf}{1+2.5Vf} * exp(BVf) \qquad (5.3)$$

where B is the interaction parameter and other parameters have their usual meanings. **Figure 5.10** shows the theoretical plot from Pukanszky model and experimental tensile strength of PBMA/Nd-TiO_2 nanocomposites. The Pukanszky model shows better agreement with the experimental tensile value of PBMA/Nd-TiO_2 nanocomposites especially at lower loading of nano-filler. In fact the deviation is higher at higher loadings. The good agreement of experimental tensile strength with theoretical values indicates the role of interfacial interaction between the polymer matrix and filler in controlling the tensile strength of the resulting nancomposites. So it can be concluded that Pukanszky model is comparatively more successful in predicting the tensile strength of PBMA/Nd-TiO_2 at loading ranging from 3 to 10 wt %.

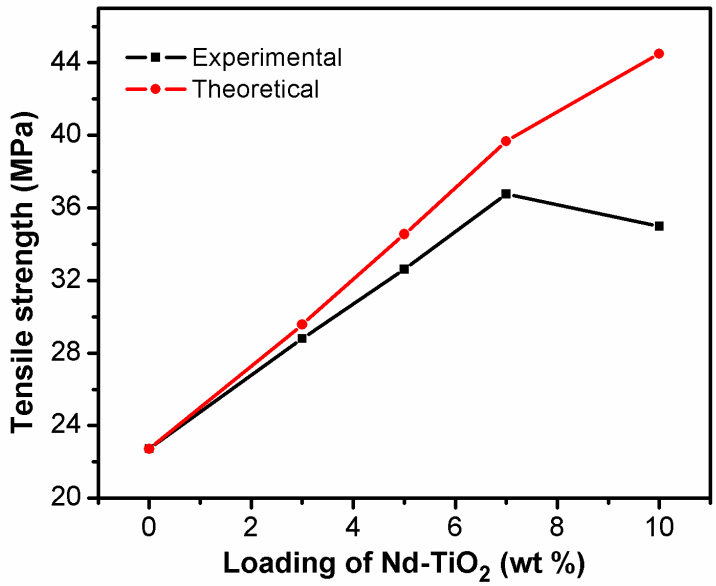

Figure 5.10: Theoretical and experimental curve of tensile strength based on Pukanszky model

5.2.8 Electrical Properties

5.2.8.1 AC Conductivity

Figure 5.11 shows the room temperature AC electrical conductivity of PBMA and PBMA/Nd-TiO_2 nanocomposites. The increasing trend of conductivity with frequency for all the samples in the entire frequency range is attributed to the hopping conduction mechanism. It is evident that the conductivity of PBMA is greatly improved by the addition of Nd-TiO_2 nanoparticles and the conductivity showed the higher value at 7 wt% loading. The increase in conductivity with the addition of nanoparticles is originating from the increase in the number of charge carriers and also from the formation of conducting path through the particle network [209]. Further, the conducting route developed by the particle network enhances the hopping of charge carriers which results in higher electrical conductivity of PBMA/Nd-TiO_2 nanocomposites. In the case of 10 wt% loading of nanoparticles, the conductivity falls to lower values. This is due to the agglomeration of nanoparticles in PBMA matrix at higher loading.

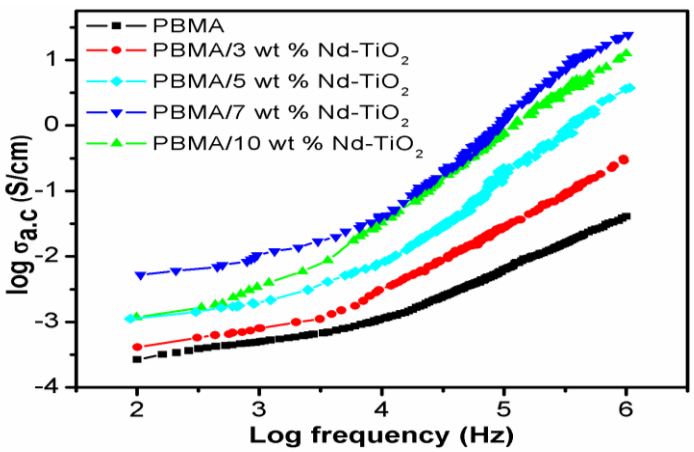

Figure 5.11: AC conductivity of PBMA with various concentrations of Nd-doped TiO_2

5.2.8.2 Dielectric Constant

Figure 5.12 shows the variation of dielectric constant with the frequency for PBMA and PBMA/Nd-TiO_2 nanocomposites, recorded at room temperature. The dielectric constant of the entire composite is higher than PBMA and the magnitude of dielectric property increases with the loading of nanoparticles. The higher dielectric constant of composites at lower frequency indicates the role of space charge polarization along with interfacial polarization between the PBMA matrix and Nd-TiO_2 [143, 210]. It can be seen that the dielectric constant decreases with increase in frequency for all the samples. The low dielectric constant at higher frequency shows the decreased contribution from space charge polarization. The dipolar groups present in the PBMA matrix fail to arrange themselves with the applied frequency results in a lower dielectric constant at higher frequencies. Among the nanocomposites, 7 wt% sample shows the maximum dielectric property and the PBMA with 10 wt% Nd-TiO_2 composite shows lower dielectric constant. The nanoparticles undergo agglomeration at higher loading and hence the interfacial interaction between the nanoparticles and the polymer is poor. The poor interfacial interaction also disturbs the orientation of polar groups leading to a poor dielectric constant at highest loading (10 wt%) of nanoparticles.

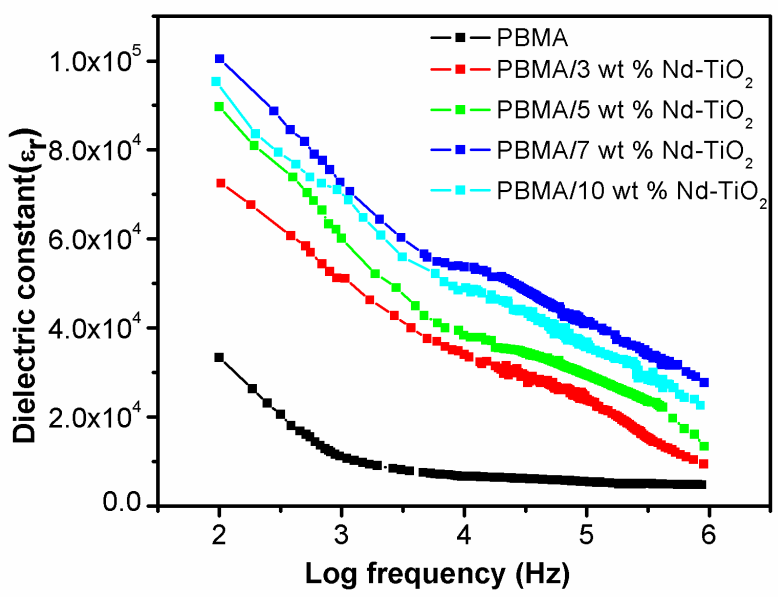

Figure 5.12: Dielectric constant of PBMA with different concentrations of Nd-doped TiO_2

5.2.8.3 Dielectric Loss (Tan δ)

The room temperature dielectric loss of PBMA and PBMA/Nd-TiO_2 nanocomposites at different frequencies is shown in **figure 5.13.** It can be seen that the dielectric loss of PBMA increased by the dispersion of Nd-TiO_2 nanoparticles. The addition of Nd-TiO_2 nanoparticles brought changes in the molecular dynamics of the PBMA matrix. This is the reason for the higher dielectric loss of PBMA/Nd-TiO_2 nanocomposite than the PBMA [211]. The dielectric loss is decreasing with the frequency for all the samples. At lower frequency, the dielectric loss is higher, which might be due to the interfacial polarization. The decrease in dielectric loss at higher frequency is due to the electrical relaxation process. The dipolar groups absorb more energy from the applied electric field to overcome the external resistances from the viscous

matrix. This causes a decrease in the transition of charge carriers between the capacitor and the dipoles. Also, the dipoles need higher energy to get into relaxation causes decrease in the dielectric loss with an increase in frequencies. The PBMA with 10 wt% of Nd-TiO_2 sample shows a lower dielectric loss than 7 wt% loading of nanoparticles. This is due to the poor interfacial interaction of nanoparticles with the polymer matrix which leads to the agglomeration of nanoparticles at higher loading (10 wt%).

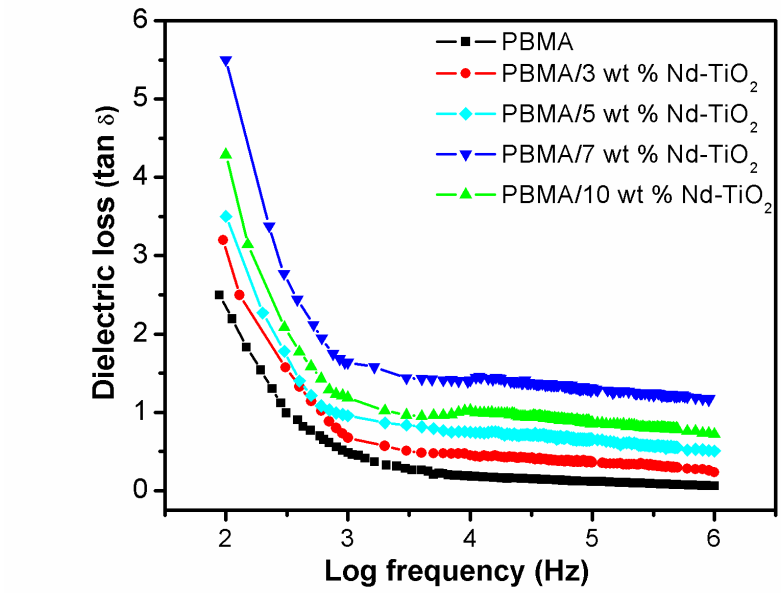

Figure 5.13: Dielectric loss tangent versus frequency plots for PBMA with Nd-doped TiO_2

5.2.9 Temperature Dependent AC Conductivity

Figure 5.14 shows the AC conductivity plots of PBMA/Nd-TiO_2 nanocomposites at different temperatures (298 K to 353 K). The linear nature of the plot log(F) vs log($\sigma_{a.c}$) clearly indicates the typical

semiconducting behavior of PBMA/Nd-TiO_2 nanocomposites. It is clear from the figure that the conductivity increases with increase in temperature which might be due to increase in mobility of charge carriers. The increase in conductivity with frequency can be explained by the hopping conduction mechanism present in the PBMA/Nd-TiO_2 nanocomposites, and the higher conductivity at higher frequency indicates the contribution from polarization effect along with hopping of charge carriers [212]. The results also showed that the conductivity of PBMA is greatly enhanced by the addition of Nd-TiO_2 nanoparticles and the maximum conductivity is obtained for 7 wt% of Nd-TiO_2 composite.

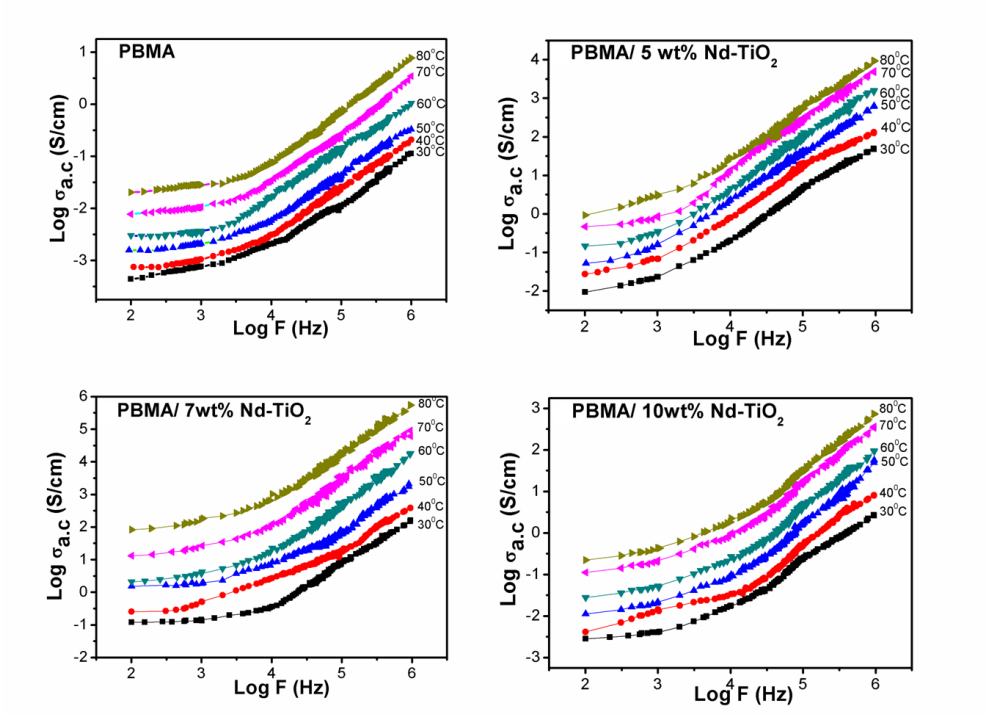

Figure 5.14: The temperature dependent AC conductivity of PBMA with various contents of Nd-doped TiO_2

The improvement in conductivity with the addition of nanoparticles is due to the increase in the number of charge carriers which increases the interfacial polarization and thereby an increase in the hopping of charge carriers. As the concentration of nanoparticles increases, the distance between charge carriers decreases and hence hopping of charge carriers also increases. The unexpected decrease in conductivity of 10 wt% sample might be due to the presence of agglomerated nanoparticles, which results large separation between conducting particles leads to lesser hopping of charge carries.

Figure 5.15 shows the activation energy of PBMA/Nd-TiO_2 nanocomposites. The activation energy obtained from the slope of the plots is tabulated in **table 5.2.** The lower values of activation energy indicate that the hopping conduction mechanism present in the PBMA/Nd-TiO_2 nanocomposites is due to electronic conduction rather than ions [165]. The dependence of AC conductivity with angular frequency can be expressed as $\sigma_{a.c} = A\omega^s$ where 's' is an exponent whose value lies between 0 and 1 [146]. The value of 's' indicates the extent of interaction of charge carriers in the lattice and also the type of conduction mechanism present in the composites.

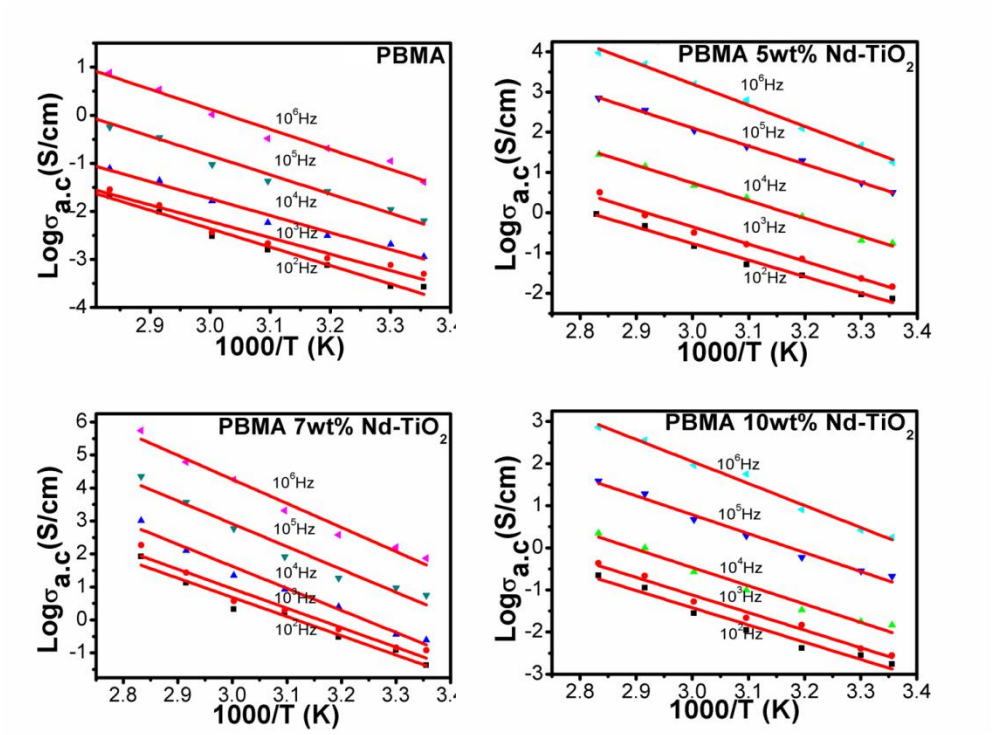

Figure 5.15: The activation energy of PBMA with different contents of Nd-TiO_2 nanoparticles

Table 5.3 represents the value of 's' obtained from the slope of the plot $\log(\sigma_{a.c})$ vs $\log(\omega)$. The nature of conducting mechanism in polymer nanocomposite is explained on the basis of small polaron and large polaron assisted tunneling. In small polaron models, the 's' value decreases with temperature while in large polaron the 's' value increases with temperature [213]. In the present study, the value of 's' decreases with temperature and hence this system follows small polaron assisted tunneling or hopping mechanism.

Table 5.2: Activation energy of PBMA and its composites with Nd doped TiO_2 nanoparticles.

Samples	Frequency (Hz)				
	10^2	10^3	10^4	10^5	10^6
PBMA	-3.834	-3.414	-3.531	-4.005	-4.167
PBMA/3 wt% Nd- TiO_2	-3.922	-4.001	-4.326	-4.456	-5.143
PBMA/5 wt% Nd-TiO_2	-4.179	-4.183	-4.426	-4.506	-5.253
PBMA/7 wt% Nd-TiO_2	-5.842	-5.964	-6.681	-6.953	-7.278
PBMA/10 wt% Nd-TiO_2	-4.023	-4.156	-4.304	-4.486	-5.213

Table 5.3: Frequency exponent‘s’ at different temperatures from the AC conductivity of PBMA and its nanocomposites

Samples	Temperature (^oC)					
	30	40	50	60	70	80
PBMA	0.6018	0.6017	0.6168	0.6159	0.6141	0.6138
PBMA/3 wt% Nd-TiO_2	0.9095	0.8955	0.8637	0.8521	0.8356	0.8195
PBMA/5 wt% Nd-TiO_2	0.9747	0.9691	0.9539	0.9309	0.9201	0.9138
PBMA/7 wt% Nd-TiO_2	0.9829	0.9787	0.9682	0.9410	0.9296	0.9051
PBMA/10 wt% Nd-TiO_2	0.9115	0.9042	0.8732	0.8481	0.8435	0.8038

5.2.10 DC Conductivity

The variation in DC electrical conductivity of PBMA/Nd-TiO_2 nanocomposites is given in **figure 5.16.** As depicted in the figure, the addition of nanoparticles enhances the DC electrical conductivity of PBMA matrix almost two orders by the addition of 10 wt% nanoparticles. Since, the PBMA/Nd-TiO_2 nanocomposites follows hopping or tunneling charge carrier mechanism (revealed from AC conductivity results) the conductivity increases with filler concentration due to increase in the number of charge carriers [204,

214]. Further, as the amount of nanoparticles increases the interfacial interaction between PBMA and Nd-TiO_2 nanoparticles increases and therefore the contribution from polarization effect is also added to the conductivity along with hopping effect. As seen from figure, the DC curve shows a percolation threshold at 3 wt%. Above the percolation threshold, there is a marginal increase in conductivity up to 7 wt%. Below the percolation threshold, the conducting particles are separated with interruptions in the conducting path and it shows a slight increase in conductivity with the addition of nanoparticles [215]. The percolation threshold attained is an indication of the improved conductivity of the system which arises from the greater hopping of charge carriers through the conducting path.

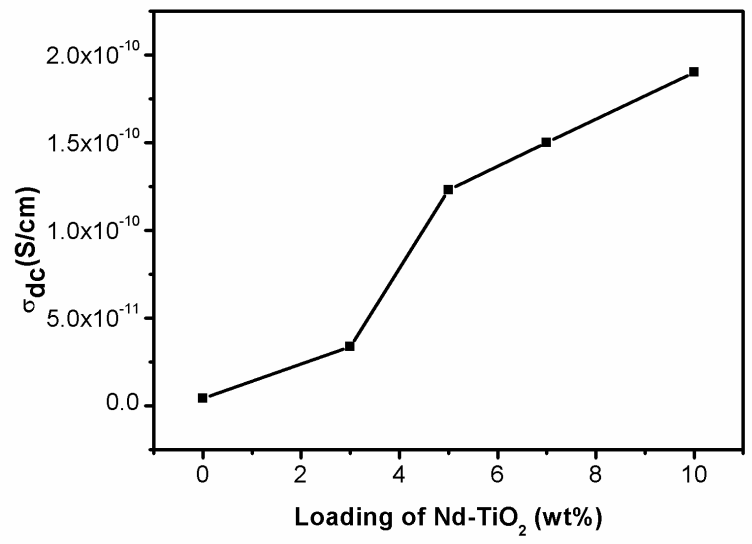

Figure 5.16: Variation in DC electrical conductivity of PBMA with nanoparticles loading

5.2.11 Theoretical Modeling to DC Conductivity

Theoretical modeling is used to study the conducting mechanism present in the polymer composites. The DC electrical conductivity of metal oxide nanoparticles filled polymer is discrete in nature and therefore at a particular concentration, the conductivity shows an abrupt increase called percolation threshold. Further, the conductivity of composites depends on various factors such as percolation threshold; surface energy, aspect ratio, filler volume fraction etc. Many theoretical modeling has been reported based on these factors for predicting the conductivity studies of polymer composites [145, 149]. Various theoretical modeling such as McCullough, Bueche, Scarisbrick and Mamunya equations are used to study the DC electrical conductivity of PBMA/Nd-TiO_2 nanocomposites.

5.2.11.1 McCullough Model

McCullough model predicts the DC conductivity of composites by the relation given in **equation 5.4**. In this model, the conductivity of composites depends on a parameter λ which indicate the extent of interaction between the filler and polymer matrix which in turn relates to the size, shape, aspect ratio and volume fraction of filler [150].

$$\sigma c = \sigma p.\Phi p + \sigma.\Phi f - \left[\frac{\lambda.\Phi p.\Phi f+(\sigma f-\sigma p)^2}{vf.\sigma f+vp.\sigma p}\right] \qquad (5.4)$$

where σc is the conductivity of composite, σp and Φp are the conductivity and volume fraction of polymer matrix respectively and σf and Φf are the conductivity and volume fraction of filler respectively. The νf and νp are defined as

$$vf = (1 - \lambda).\Phi f + \Phi p.\lambda \quad (5.5)$$

$$vp = (1 - \lambda).\Phi p + \Phi f.\lambda \quad (5.6)$$

λ is the structural factor which determines the extent of conducting network formation in the polymer matrix and its value varies from 0 to 1. **Figure 5.17** represents the conductivity of PBMA/Nd-TiO_2 nanocomposites based on experimental and theoretical modeling. It can be seen that the conductivity obtained from McCullough model shows a large deviation from the experimental conductivity in the entire volume fraction of fillers. So McCullough model is not applicable to study the conductivity of PBMA/Nd-TiO_2 nanocomposite.

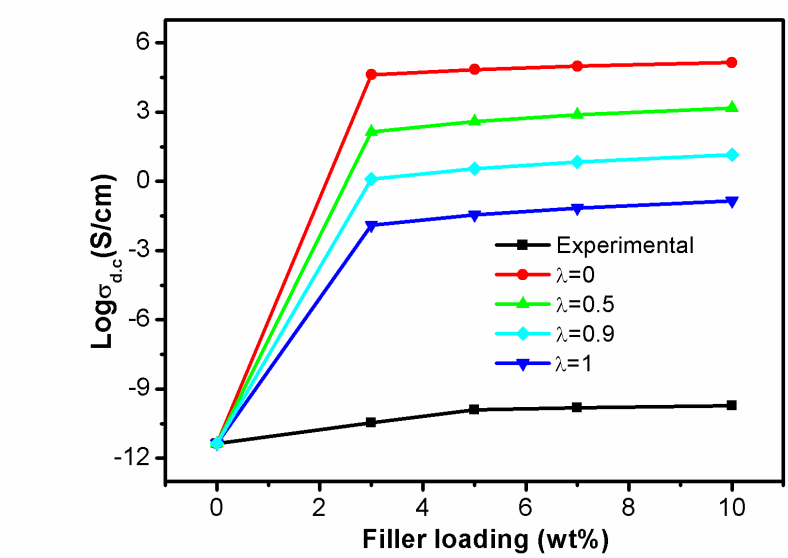

Figure 5.17: Theoretical and experimental conductivity based on McCullough model.

5.2.11.2 Bueche Model

Bueche proposed a theoretical equation for the DC electrical conductivity of binary system containing conducting the filler particles dispersed in an insulating polymer matrix [151]. The conductivity of polymer composites is calculated using the **equation 5.7**

$$\sigma c = \Phi f \sigma f + (1 - \Phi f)\sigma p \qquad (5.7)$$

where σc denotes the conductivity of composite, σf and Φf denotes the conductivity and volume fraction of filler respectively. The experimental conductivity and theoretical conductivity (Bueche model) of PBMA/Nd-TiO_2 nanocomposites is presented in **figure 5.18.** The theoretical conductivity obtained from Bueche model shows a large deviation from the experimental one. Since the Bueche model is simply additive in which the total conductivity is sum of the conductivity of filler and the polymer matrix. Therefore Bueche model applied for polymer composites where the individual components in the composites have almost the same electrical conductivity. In the present study the difference in conductivity is due to the higher conductivity of the metal nanoparticles than the polymer.

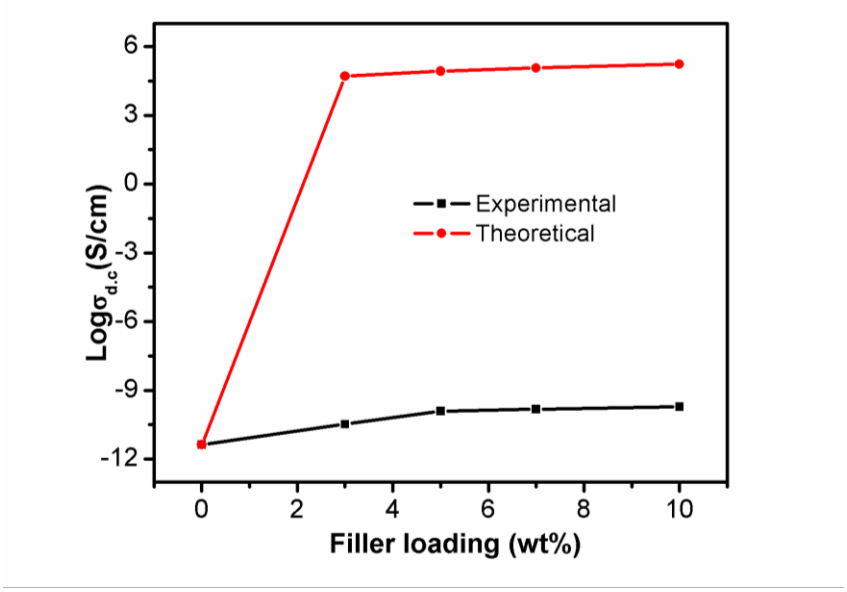

Figure 5.18: Theoretical and experimental conductivity based on Bueche model.

5.2.11.3 Scarisbrick Model

Scarisbrick suggested a statistical model for the DC electrical conductivity of binary composites using the following equations. Scarisbrick model suggests that the conducting filler particles are oriented in a regular manner within the insulating polymer and hence there is an effective particle to particle contact within the polymer matrix [152]. Here the conductivity mainly depends on the arrangement of filler in the polymer and the concentration of filler particles.

$$\frac{\sigma c}{\sigma f} = C^2.\Phi.\Phi[exp(\Phi^{-\frac{2}{3}})] \qquad (5.8)$$

where σc and σf are the conductivity of the composite and conducting filler particle respectively, Φ is the filler concentration and C is the geometrical factor, depends on the arrangement and interfacial interaction of nanoparticle with the polymer matrix and its value varies from 1 to 3x 10^{-3}.

$$\frac{\sigma c}{\sigma f} = \Phi.\Phi\left[exp\left(\Phi^{-\frac{2}{3}}\right)\right](\text{When } C^2 = 1) \quad (5.9)$$

$$\frac{\sigma c}{\sigma f} = 3\ x\ 10^{-3}.\Phi.\Phi[exp(\Phi^{-\frac{2}{3}})](\text{When } C^2 = 3\text{x}10^{-3}) \quad (5.10)$$

The plots for the conductivity of PBMA/Nd-TiO_2 nanocomposites by using Scarisbrick model along with experimental conductivity is given in **figure 5.19.** Scarisbrick model shows greater deviation from the experimental conductivity in the entire range of filler loading. So this model is not useful for predicting the conductivity of polymer composites like PBMA/Nd-TiO_2 nanocomposites.

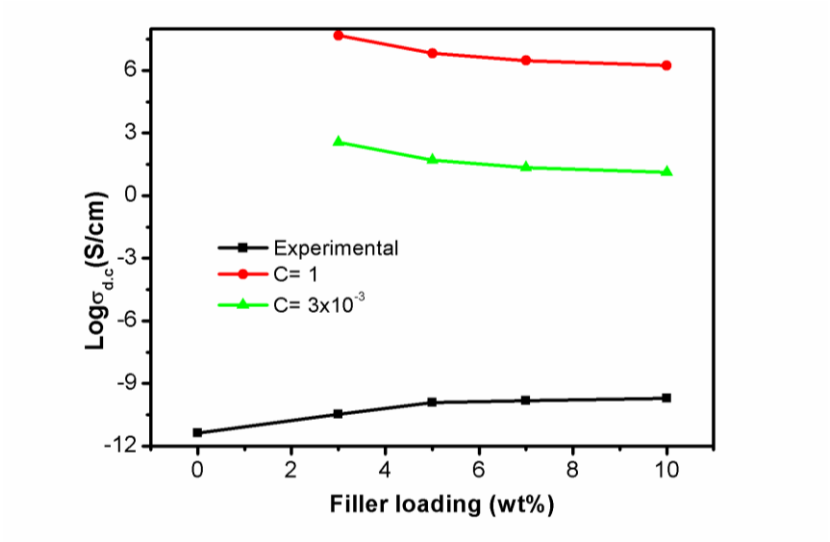

Figure 5.19: Theoretical and experimental plots of electrical conductivity based on Scarisbrick model.

5.2.11.4 Mamunya Model

Mamunya derived a theoretical equation for calculating the electrical conductivity of polymer composites by considering various factors such as volume fraction of filler, aspect ratio, percolation threshold of filler, the surface energy of filler, interfacial interaction as well as the distribution of filler within the polymer matrix etc [153, 216]. The percolation threshold mainly depends on the interaction of filler with the matrix as well as the size and amount of filler. The equation is

$$\text{Log}\,\sigma = \log\sigma c + (\log\sigma F - \log\sigma c)\left(\frac{\Phi-\Phi c}{F-\Phi c}\right)\text{^k} \qquad (5.11)$$

where σ is the conductivity of the composite, σc is the conductivity of the composite at percolation threshold, σF is the conductivity at maximum volume fraction of filler (F), φ is the volume fraction of filler, φc is the volume fraction of filler at percolation threshold, the exponent 'k' can be defined as in **equation 5.12**

$$k = K\Phi/(\Phi\text{-}\Phi c)^{0.75} \qquad (5.12)$$

$$K = A - B\,\gamma_{pf} \qquad (5.13)$$

Here, K is a constant whose value depends on the extent of interaction of filler with the polymer matrix, A and B are constants and γ_{pf} is the surface tension at the interface of polymer matrix and filler. Mamunya et al. were assumed this model was true in all cases they studied and reported the acceptable values for A, B and ϒpf for various polymer systems. In the present study we used the reported values of A, B and ϒpf for calculating the conductivity of PBMA/Nd-TiO_2

nanocomposites using the **equations 5.11-5.13**, and the obtained theoretical conductivity along the experimental was presented in **figure 5.20.** The conductivity shows close relations to that of experimental one in all concentrations. So it can be concluded that the conductivity of PBMA/Nd-TiO_2 nanocomposites is governed by the conductivity at percolation threshold as well as the degree of interaction of filler with the polymer matrix. Further the result indicates that the better interfacial interaction between the PBMA matrix and filler was contributing to the improved conducting property of PBMA/Nd-TiO_2 nanocomposites. The mismatch at low concentration is obviously due to the unavailability of conducting particles to form the continuous conducting path.

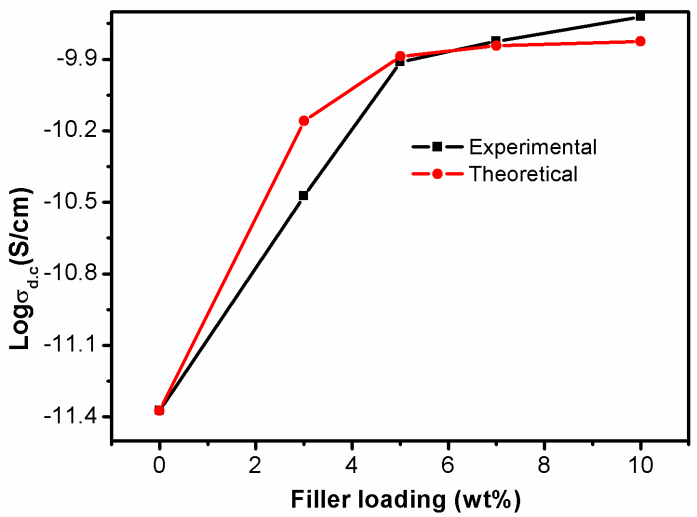

Figure 5.20: Theoretical and experimental conductivity based on Mamunya model

5.3 Conclusion

The PBMA/Nd-TiO_2 nanocomposites were prepared by an in situ polymerization method. The presence of Ti-O vibration peak in the FT-IR spectra of composite confirmed the presence of Nd-TiO_2 nanoparticles in the PBMA matrix. The UV-Visible spectra exhibited a shift in absorption edge with the addition of Nd-TiO_2 nanoparticles up to 7 wt%. This indicated the enhancement in optical properties of PBMA by the addition of Nd-TiO_2 nanoparticles. The SEM study revealed the homogenous distribution of nanoparticles in the polymer matrix. XRD showed the appearance of crystalline peaks of Nd-TiO_2 in PBMA. The glass transition temperature (Tg) from DSC and the degradation temperature of nanocomposites from TGA were shifted to higher temperatures and this indicated the enhanced thermal stability of PBMA with the addition of Nd-TiO_2 nanoparticles. The tensile strength of PBMA/Nd-TiO_2 nanocomposite also increased with the addition of nanoparticles whereas the elongation at break was found to be decreasing. The reinforcing nature of nano-filler in PBMA was studied with various theoretical models based on Einstein, Mooney and Pukanszky. Among the models, Pukanszky showed the best agreement with the experimental tensile plots. The AC conductivity, dielectric constant and dielectric loss of PBMA nanocomposites increased with the addition of Nd-TiO_2 nanoparticles. The AC conductivity of hybrid nanocomposites was increased with increase in the addition of nanoparticles as well as with temperature and frequencies. The parameters such as activation energy and the exponent values were determined and the variations in their value denoted the hopping

conduction mechanism present in the PBMA/Nd-TiO_2 nanocomposites. Among the nanocomposites, the 7 wt% sample shows the maximum AC conductivity. The DC conductivity of nanocomposites was higher than the pure PBMA and the conductivity increases with the loading of nanoparticles. The formation of conducting network increases the chance for the hopping that results in an increase in the DC conductivity. The applicability of DC conductivity was investigated by various theoretical models like McCullough, Bueche, Scarisbrick and Mamunya models. The theoretical conductivity obtained from Mamunya model was more suitable for the experimental conductivity of PBMA/Nd-TiO_2 nanocomposites, suggest that in the case of PBMA/Nd-TiO_2 nanocomposites, there have an effective interfacial interaction between both the components and it was responsible for the improved conducting properties of PBMA nanocomposites than the plane PBMA.

CHAPTER 6

EFFECT OF CERIUM DIOXIDE NANOPARTICLES ON THERMAL, MECHANICAL AND ELECTRICAL PROPERTIES OF POLY (BUTYLMETHACRYLATE) AND APPLICABILITY OF DIFFERENT MODELLING STUDIES

Contents

K. Suhailath, M. T. Ramesan, Effect of ceria nanoparticles on mechanical properties,thermal and dielectric properties of poly (butylmethacrylate) nanocomposites, Polym. Compos. 41 (2020) 2244.

K. Suhailath, Meenu Thomas, M. T. Ramesan, Effect of temperature on ac conductivity of poly (butylmethacrylate)/cerium dioxide nanocomposites and applicability of different conductivity modeling studies, Res. Chem. Intermed. (2020) DOI: 10.1007/s 11164-020-04107-w

6.1 Introduction

Polymer composites became an inevitable material in our day to day life, obviously due to their interesting optical, thermal, mechanical and electrical properties [217]. In particular organic polymer-inorganic nanocomposites got greater attention because they integrate the properties of both polymer matrix and the nanofiller [218]. The fabulous interfacial chemistry existing between the polymer matrix and the filled nanoparticles attributed to the outstanding properties of the polymer nanocomposites than the parent polymer [219]. Recently, the polymer nanocomposite materials are widely used in thin-film devices, owing to their attractive electrical properties [220]. In electronic devices, the polymer composite materials are used as capacitors due to their dielectric properties, here the space charge polarization between the polymer matrix and the filler particles enable them to act as a working capacitor [221]. Owing to the greater need for thin polymer-based materials in electrostatic charge dissipation and electromagnetic shielding applications, fabrication of new polymer nanocomposites with higher conductivity properties is still going on [222]. Several approaches were developed for the fabrication of polymer nanocomposites such as solution casting, emulsion polymerization, sol-gel technique, and in situ polymerization method [223, 224]. Amidst them in situ polymerization method is the best one, because the agglomeration of nanoparticles inside the polymer can be controlled to a greater extent and thereby ensure the uniform dispersion of nanoparticles in the polymer matrix [225].

Poly (butylmethacrylate) belongs to methacrylic polymers are well known for their excellent properties and wide applications in optical and electrical devices. The transparent nature, better flexibility, higher dimension stability and excellent strength of the PBMA polymer further make them suitable to these devices. Significant efforts were taken by researchers to improve the properties and hence the application of methacrylic polymers in electrical applications [226]. Compared to the micro fillers, nanofillers can impart excellent properties aroused from their nano-size [227]. Also, the nanofillers possess better dispersion ability than that of micro fillers. Another interesting fact regarding nanofiller addition is that even a small amount of particle can bring unexpected change in the bulk properties of parent polymer [228]. CeO_2 is a promising rare earth metal-oxide, which has been used as filler in polymeric materials due to its immense optical and electrical properties [229]. Several studies were reported regarding the applications of polymer/CeO_2 based nanocomposites. Aguirre et al. was reported about acrylic/CeO_2 nanocomposites having excellent UV-Visible absorption capacity [230], PMMA/CeO_2 nanocomposites possessing better photo-catalytic activity as outlined by Latha et al. [87].

In the present work, CeO_2 nanoparticles were incorporated into the poly (butylmethacrylate) matrix and the effect of nanoparticles on the thermal, mechanical and electrical properties of PBMA matrix were studied well. As we know, the properties of the polymer matrix dramatically change with the addition of small amount of fillers, the chemistry behind this change is still a controversial subject. It has

been proposed that the variables like volume fraction, size, shape and geometry of fillers greatly influence the tensile properties of composites. In order to explain the actual role of these variables in improving the mechanical and electrical properties, many theoretical models were suggested. In this study, some of the theoretical models were used to predict the tensile and electrical properties of PBMA/CeO_2 nanocomposites.

6.2 Results and Discussion

6.2.1 FT-IR Spectra

The incorporation of CeO_2 nanoparticles in the PBMA matrix is well established through FT-IR spectroscopy. The FT-IR spectra of CeO_2 nanoparticles, pure PBMA and PBMA/CeO_2 nanocomposite is given in **figure 6.1.** The FT-IR spectra of CeO_2 exhibits strong and broad absorption band at 527cm^{-1} is the Ce-O vibration [231]. The band at 3500 cm^{-1} and 1623 cm^{-1} are assigned to the stretching and bending vibrations of -OH group on the surface of CeO_2 particles. The characteristics peaks of PBMA matrix are found to be at 2948 and 1380 cm^{-1}(-C-H stretching vibrations), 1731 cm^{-1} (-C=O stretching vibrations) and 1256 cm^{-1} (-C-O stretching vibrations). However, the PBMA/CeO_2 composites exhibit a new peak at 521 cm^{-1} indicating the presence of nanoparticles in the polymer chain. In addition to this, there is a slight shift in the absorption band of PBMA by the incorporation of CeO_2 particles. The notable shift in the peaks corresponds to C=O (from 1731 to 1727 cm^{-1}) and C-O (from 1256 to 1250 cm^{-1}) bonds in PBMA/CeO_2 composites clearly indicate the effective incorporation of nanoparticles, through the interaction of

carbonyl group of PBMA with CeO_2 nanoparticles. The formation of polymer nanocomposite and schematic representation of the interaction of PBMA with CeO_2 is given in **scheme 6.1.**

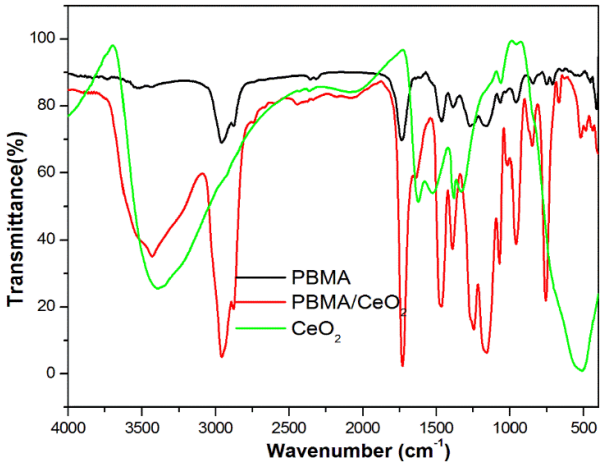

Figure 6.1: The FT-IR spectra of bare PBMA, PBMA/CeO_2 nanocomposite and CeO_2 nanoparticle

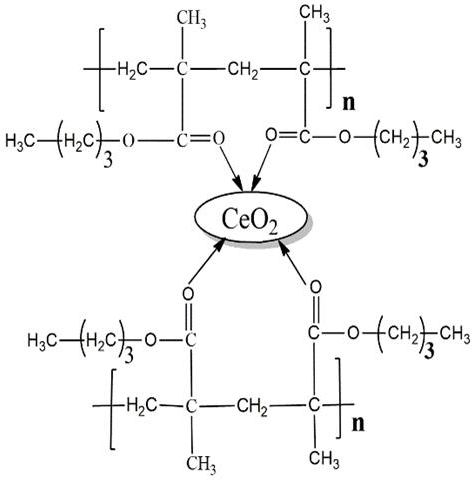

PBMA/CeO_2 nanocomposite

Scheme 6.1. Interaction of CeO_2 nanoparticles with PBMA

6.2.2 UV-Visible Spectra

The UV-Visible spectra of PBMA and PBMA/CeO_2 nanocomposites are illustrated in **figure 6.2.** The absence of peaks in the visible region shows the highly transparent nature of all the samples. The pure PBMA exhibits low absorption intensity, however by the addition of CeO_2 nanoparticles the absorption is gradually increasing up to 7 wt% loading of nanoparticles. The PBMA with 10 wt% CeO_2 nanoparticles exhibit lower absorption than the 7 wt% sample. The increase in absorption with the addition of nanoparticles attributes to the increase in surface area by the presence of nanosized CeO_2 nanoparticles, and hence the absorption becomes more pronounced at higher loading of nanofillers [232]. The better interfacial interaction between the CeO_2 nanoparticles and the PBMA chain enhances the absorption of light by the addition of nanoparticles. The slight decrease in intensity of UV peak at 10 wt% loading is due to the poor polymer-filler interactions and that leads to the agglomeration of nanoparticles.

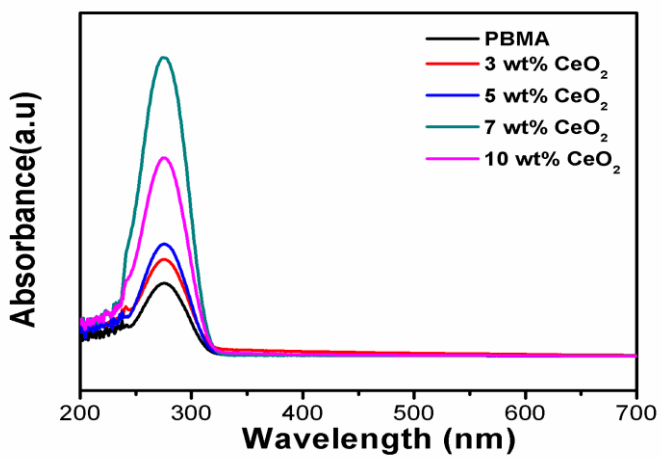

Figure 6.2: UV-Visible spectra of PBMA and PBMA/CeO_2 nanocomposites

6.2.3 XRD Analysis

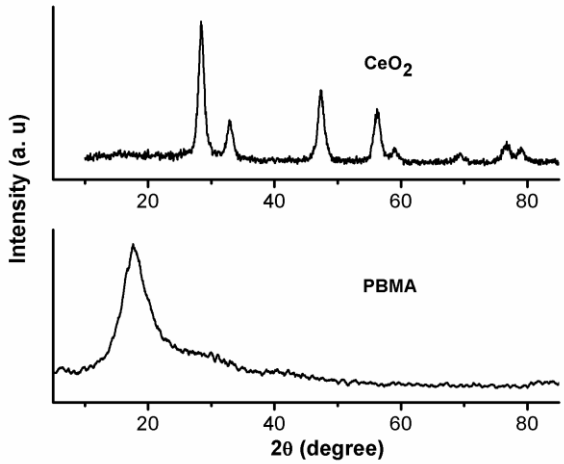

Figure 6.3a: XRD patterns of bare PBMA and CeO_2 nanoparticle

The structural information of the synthesized CeO_2 nanoparticles, PBMA and the PBMA/CeO_2 nanocomposites are assigned from their XRD analysis and the obtained patterns are shown in **figure 6.3.** The synthesized CeO_2 nanoparticle shows several crystalline peaks at 2θ = 28.37°, 32.9°, 47.17° and 56.33° corresponds to the (111), (200), (220) and (311) plane of the CeO_2 crystal respectively. All the peaks in the patterns are corresponding to the phase of pure CeO_2 [233]. The average crystallite size of CeO_2 powder has been determined fromcorresponding XRD data using Scherrer formula and the size is 7.2 nm. The pure PBMA shows a strong XRD peak centered at 2θ = 17.65° indicating the amorphous nature of the polymer. It is evident from the figure that the presence of crystalline peaks of nanoparticles along with the amorphous peak of PBMA specifies the appearance of some crystalline regions by the reinforcement of CeO_2 nanoparticles. It might be attributed due to the uniform distribution of CeO_2 nanoparticles with effective interfacial interaction with the PBMA

matrix. Similar observations were also reported by Latha et al. [87]. Further, a decrease in intensity of amorphous peak (at $2\theta = 17.65^{\circ}$) is observed with the addition of CeO_2 nanoparticles clearly indicate the interfacial interaction between the PBMA matrix and the nanoparticles. The percentage of crystallinity induced by the addition of nanoparticles is 58.7 % for PBMA with 5 wt% CeO_2, 71.5 % for PBMA with 7 wt% CeO_2 and 63.2 % for PBMA with 10 wt% CeO_2 nanoparticles. As cleared from the values, the percentage crystallinity is increased upon the addition of nanoparticles. However, the maximum value of percentage crystallinity is showed in the case of PBMA with 7 wt% of CeO_2 nanoparticles and beyond this loading the percentage crystallinity is slightly decreased. This means that at higher loading of fillers (10 wt%) there are some interruptions in the interfacial interaction between the PBMA matrix and the CeO_2 nanoparticles which may be due to the presence of agglomerated nanoparticles.

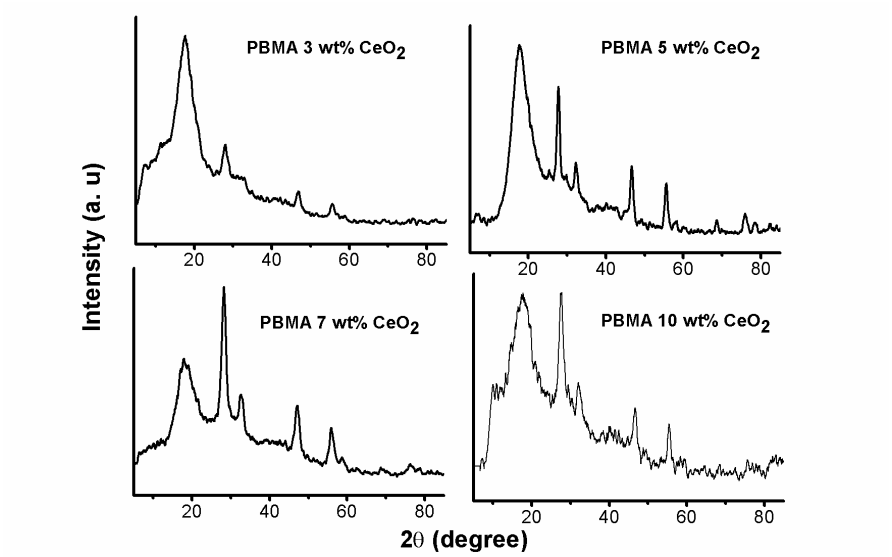

Figure 6.3b: XRD patterns of PBMA/CeO_2 nanocomposites

6.2.4 FE-SEM Analysis

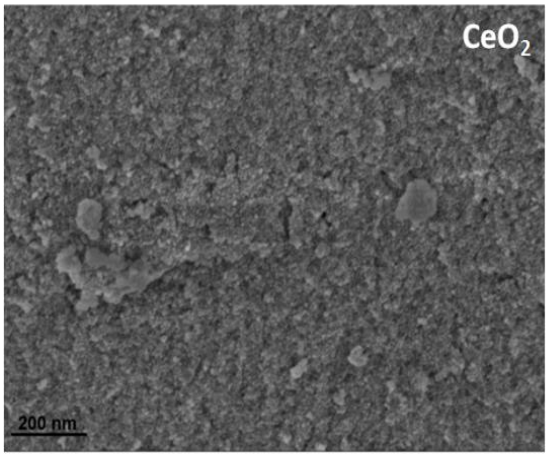

Figure 6.4a: FE-SEM image of CeO_2 nanocomposites

The surface morphology as well as the dispersion mode of the CeO_2 nanoparticle in the PBMA matrix was analyzed using FE-SEM and the obtained images were given in **figure 6a and 6b.** The FE-SEM image of CeO_2 suggests the formation of finely powdered nanoparticles. The pure PBMA exhibits the smooth and plane surface morphology indicating the homogeneous morphology of the synthesized polymer. However, the uniform morphology of the polymer is changed into a rough morphology with the presence nanoparticles in PBMA/CeO_2 composites. Among the nanocomposites, 7 wt% CeO_2 nanoparticles filled PBMA showed the good dispersion of filler with spherically shaped particles. When the loading of nanoparticles in the polymer reached to 10 wt% CeO_2, the uniform dispersion of filler is not visible in the composite. This means that a higher loading, the nanoparticles have a tendency to undergo self-agglomeration which results in poor compatibility between polymer and nanoparticles.

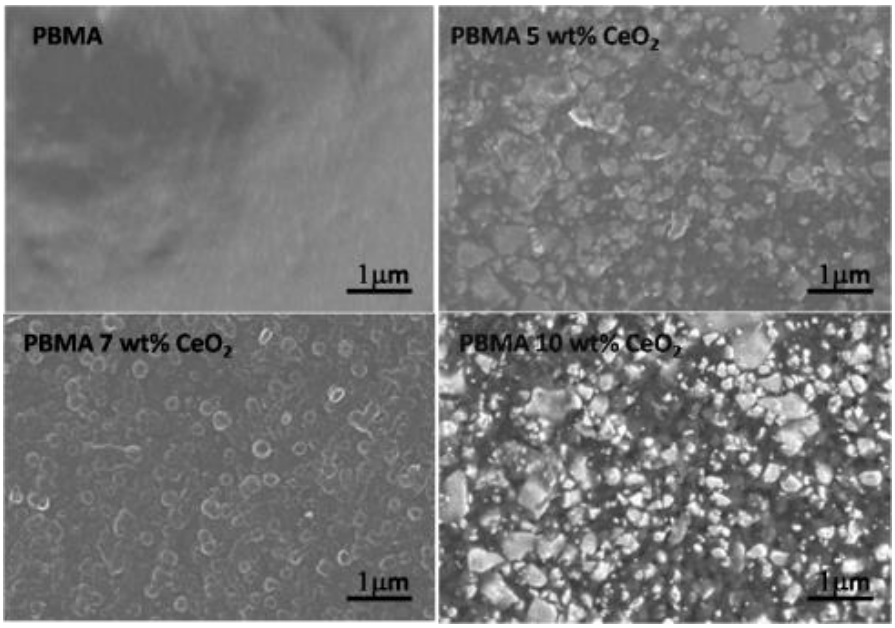

Figure 6.4b: FE-SEM images of bare PBMA and PBMA/CeO_2 nanocomposites

6.2.5 TEM Analysis

TEM measurements are important in the polymer nanocomposite studies which give a direct evidence for the dispersion of fillers in the polymer and also more detailed information regarding the arrangement of PBMA and CeO_2 during the composite formation. The TEM images given in **figure 6.5** clearly indicate the better incorporation of CeO_2 nanoparticles into the PBMA matrix. For CeO_2 nanoparticles, the average particle size has been found to be ~8.8 nm. The TEM image of PBMA with 5 wt% of composite reveals that CeO_2 has been homogenously distribute on macromolecular chain of polymer (with average size of 9.21 nm) giving maximum surface area with intimate and close interaction between the host and guest components. The SAED pattern with bright spots in figure denotes the crystalline

character of PBMA/CeO_2 composites as evidenced by bright spots with uniform diffusive circles. The TEM image of PBMA with 10 wt% CeO_2 sample shows the randomly oriented polymeric nanostructures with few layer of nano CeO_2 flakes in the PBMA network. Also, the size of the nanoparticles is slightly increased at higher loading of nano-fillers and the diameter of polymer composite appears to be in the nano-regime confirming the formation of nanocomposites.

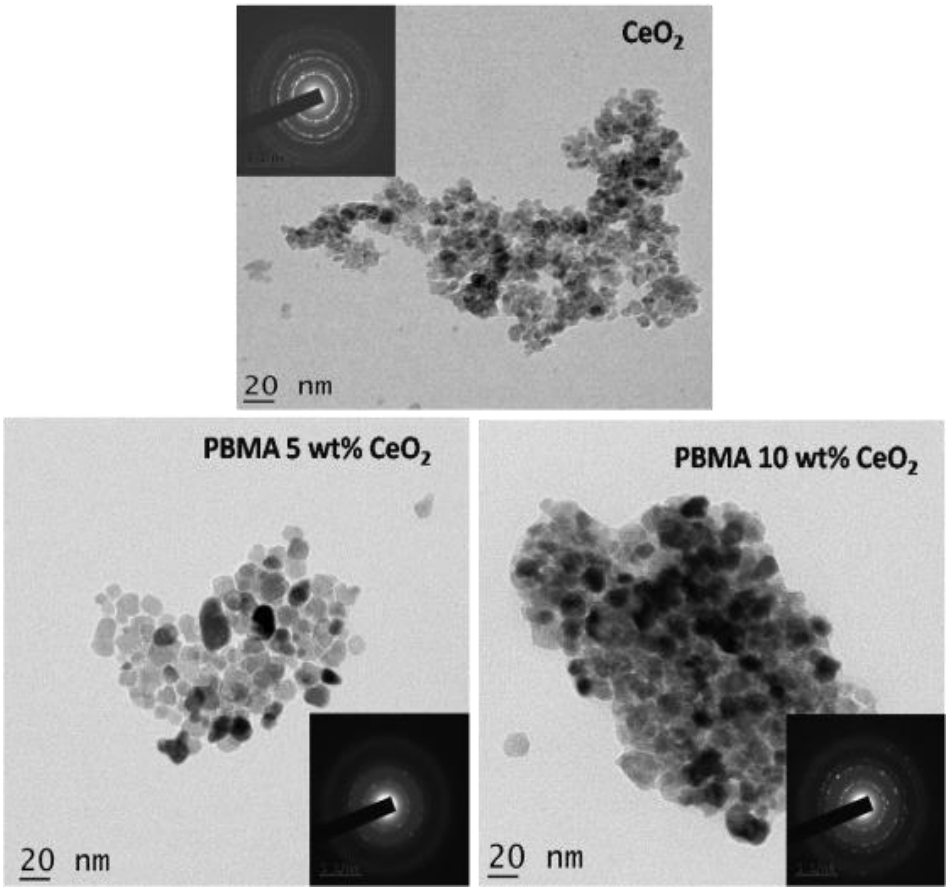

Figure 6.5: TEM images of CeO_2 and PBMA/CeO_2 nanocomposites

6.2.6 Thermal Properties

6.2.6.1 TG Analysis

Table 6.1: The different degradation temperature obtained from TGA and DTG of PBMA/CeO_2 nanocomposites

	TGA	DTG	
	T_i(°C)	T_{max} (°C) Ist stage	T_{max} (°C) IInd stage
PBMA	256	279	365
PBMA/5 wt% CeO_2	271	296	375
PBMA/10 wt% CeO_2	280	305	379

The thermal stability of bare PBMA and its composites with different contents of CeO_2 nanoparticles is measured by TG analysis and the corresponding TGA and DTG curves are presented in **figure 6.6.** The initial degradation temperature (T_i) and major decomposition temperature (T_{max}) for the pure PBMA and PBMA/CeO_2 nanocomposites are documented in **table 6.1.** The PBMA/CeO_2 nanocomposite exhibits better thermal stability than pure PBMA. The PBMA started to loss its weight at ~279°C upon heating with a weight loss of 6 % due to the unzipping of the vinyl group. From the DTG curve, it can be seen that PBMA with 5 wt% CeO_2 starts its first weight loss at ~296°C and the PBMA with 10 wt% CeO_2 starts its first weight loss at ~305°C. All the sample shows another major weight loss around ~300°C, attributes to the degradation of the polymer backbone chain. The major weight loss begins at ~365°C for bare PBMA, at ~375°C for PBMA with 5 wt% CeO_2 and at ~379°C for PBMA with 10 wt% CeO_2. These observations suggest the enhanced thermal stability of PBMA

by the incorporation of CeO_2 nanoparticles and it arises from the better interfacial interaction between the PBMA matrix and CeO_2 nanoparticles. Meanwhile, the major decomposition peak (T_{max}) from the DTG (Table 6.1) curve also increased correspondingly with an increase in the loading of CeO_2 nanoparticles.

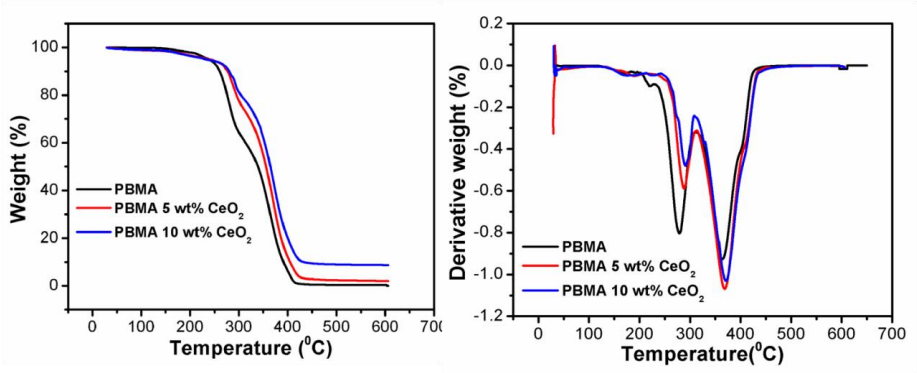

Figure 6.6: TGA and corresponding DTG curve of PBMA and PBMA/CeO_2 nanocomposites

6.2.6.2 DSC Analysis

Figure 6.7 illustrates the DSC thermograms of PBMA and PBMA/CeO_2 nanocomposites. All the samples exhibit two endothermic peaks, of which the first small dip corresponds to the glass transition (T_g) and the second major dip attributes to the flow point (T_f) or melting point (Tm). It is noticed that the T_g of PBMA has substantially increased by the incorporation of CeO_2 nanoparticles. The PBMA has T_g at 21.54°C while the PBMA with 5 wt% CeO_2 shows T_g at 25.66°C and PBMA with 10 wt% CeO_2 shows T_g at 30.96°C. This clearly implies the interfacial interaction of CeO_2 nanoparticles with the PBMA matrix. The better interaction between the matrix and the filler restricts the mobility of chain segments of PBMA, leads to an

increase in T_g of the composites. With an increase in the loading of CeO_2 nanoparticles, the T_m of PBMA is also increasing. This observation shows that by the incorporation of nanoparticles, some crystalline regions are created by the ordered arrangements of polymer segments obviously through the interfacial interaction between the polymer backbone and the filler [234].

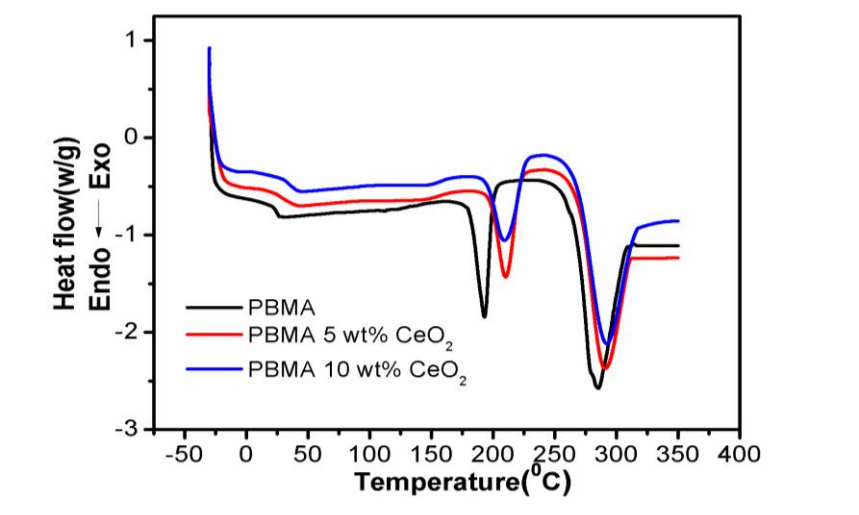

Figure 6.7: DSC curve of PBMA and PBMA/CeO_2 nanocomposites

6.2.7 Mechanical Properties

The mechanical properties such as tensile strength and elongation at break of PBMA with different contents of CeO_2 nanoparticles are measured and the obtained result is presented in **figure 6.8.** The tensile strength of all the composites is higher than the pure PBMA. The uniform dispersion and the interfacial interaction of nanoparticles with the PBMA matrix attribute to the higher tensile properties of the composites. Here, the nanoparticles act as stress concentration sites for accompanying the extra stress transferred from the PBMA matrix and thus results in enhancing the tensile properties of composites. The

improvement in tensile properties is becoming more pronounced on the addition of nanoparticles and the composite with 7 wt% shows the maximum property. The pure PBMA exhibits the tensile strength of 22.72 MPa and the PBMA with 7 wt% of CeO_2 nanoparticles show the tensile strength around 38.14 MPa (i.e., 67.86 % increases). Beyond 7 wt% loading of composite, the composites exhibit a slight decrease in tensile strength (36.01 MPa). As revealed from UV results, the 7 wt% exhibits the maximum dispersion limit and after the homogenous dispersion has been interrupted. At higher loading of fillers, there are defects in the composites due to poor matrix-filler interactions by the presence of agglomerated nanoparticles and this lead to the poor tensile property. The elongation at break is found to be decreasing with the incorporation of CeO_2 nanoparticles shows the reinforcing effect of CeO_2 nanoparticles. The addition of nanoparticles increases the stiffness of the composites and which in turn results in a decrease in elongation at break [235].

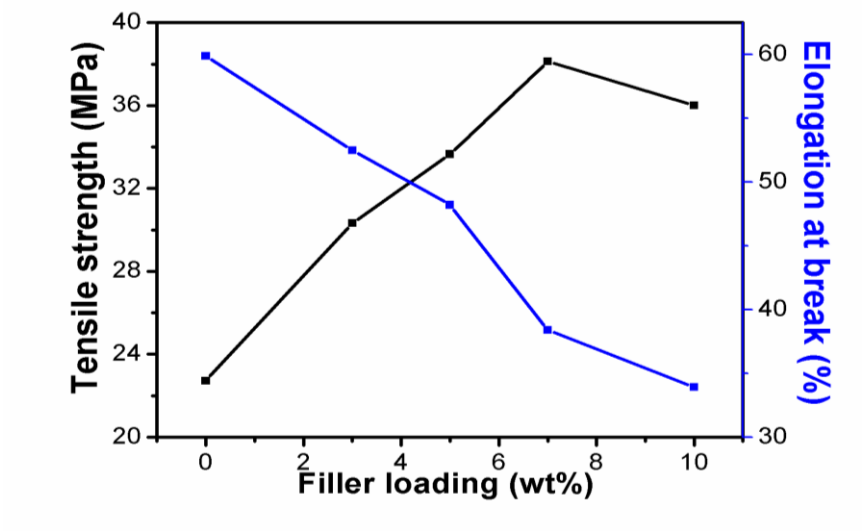

Figure 6.8: Variation of tensile strength and elongation at break with filler concentration for PBMA/CeO_2 nanocomposites

6.2.8 Tensile Modeling

The tensile property of the polymer composites depend on various factors such as size, shape, geometry and the extent of dispersion of fillers and the stiffness of the polymer matrix. The theoretical modeling approaches help to give an idea about the role of different parameters responsible for the increased tensile properties of polymer composites [136]. So in this study, various theoretical assumptions made by Einstein, Mooney, Guth, Kerner and Pukanszky models are employed to analyze the different parameters affecting the tensile property and to predict the mechanism of the increase in tensile strength of the PBMA/CeO_2 nanocomposites.

6.2.8.1 Einstein Model

Einstein derived an equation for the prediction of the tensile property of polymer composite systems containing rigid filler particle in the non-rigid polymer matrix as follows [137]

$$Mc = Mm(1 + 2.5Vf) \qquad (6.1)$$

Where Mc and Mm are the tensile strength of composite and polymer matrix respectively, and Vf represents the filler volume fraction. The experimental tensile data obtained for PBMA/CeO_2 nanocomposites is applied to the Einstein model and the results are given in **figure 6.9.** As evident from the figure, the experimental values are more deviated from that of the theoretical values. Einstein equation is mainly employed for the polymeric systems containing rigid spherical particles at a very lower concentration of fillers. So in most cases, the

Einstein equation fails to predict the tensile property of polymer composite systems.

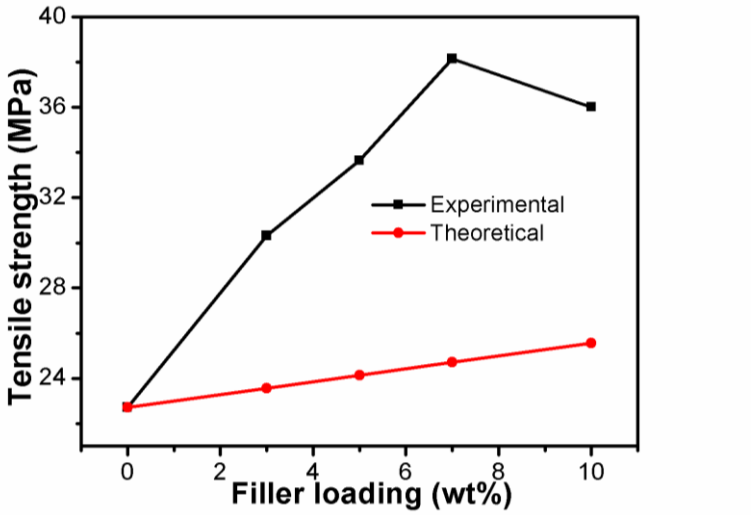

Figure 6.9: Experimental and theoretical tensile strength of PBMA/CeO_2 nanocomposites based on Einstein model

6.2.8.2 Mooney Model

The major drawback of the Einstein model has been overcome by the Mooney model by introducing a new parameter using the following equation [138].

$$Mc = Mm * exp[\frac{2.5Vf}{1-SVf}] \qquad (6.2)$$

Where 'S' denotes the crowding factor whose value lies between 1 to 1.35. The 'S' factor considers the strain field around the filler and the polymer matrix. The experimental tensile strength of PBMA/CeO_2 nanocomposites is compared with the theoretical tensile strength obtained from the Mooney model and the results are given in **figure**

6.10. It can be observed that the theoretical tensile strength values are higher as compared to that of experimental values. This means that the Mooney model also fails to explain the reinforcing nature of CeO_2 nanofiller into the PBMA matrix. The Mooney equations are based on the assumptions that the tensile values of filler are much higher than the polymer matrix, hence the applicability of Mooney equations is limited.

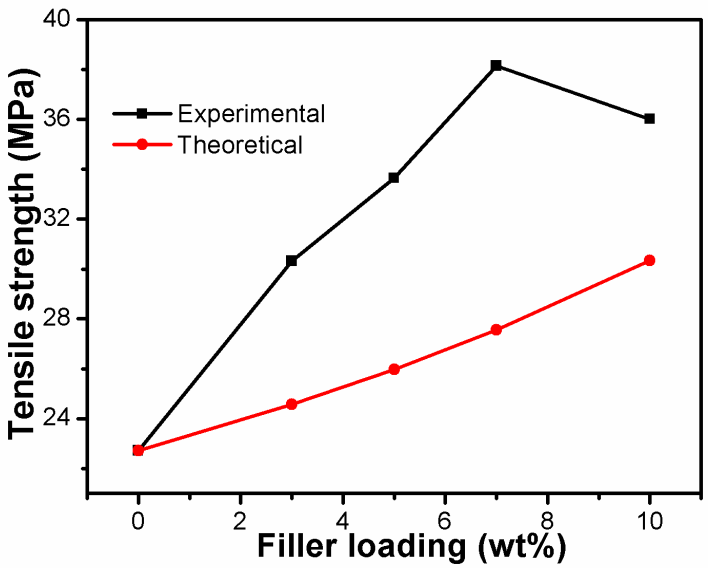

Figure 6.10: Experimental and theoretical tensile strength of PBMA/CeO_2 nanocomposites based on Mooney model

6.2.8.3 Guth Model

Guth modified the Einstein equation by adding a new term, based on the assumption that there is a phase interaction between the particles and polymer which enhances the tensile property of the polymer composites [139]. The Guth equation is given as

$$Mc = Mm(1 + 2.5Vf) + 14.1\,Vf\text{^}2 \qquad (6.3)$$

The comparative tensile strength of PBMA/CeO_2 nanocomposites from the experimental results and the theoretical values from the Guth equation are given in **figure 6.11.** Here also, the theoretical model does not match with the experimental results in entire filler loadings. The Guth model is based on spheres embedded in a continuous polymer matrix. So in the present study, Guth model fails to predict the reinforcing nature of the polymer composites.

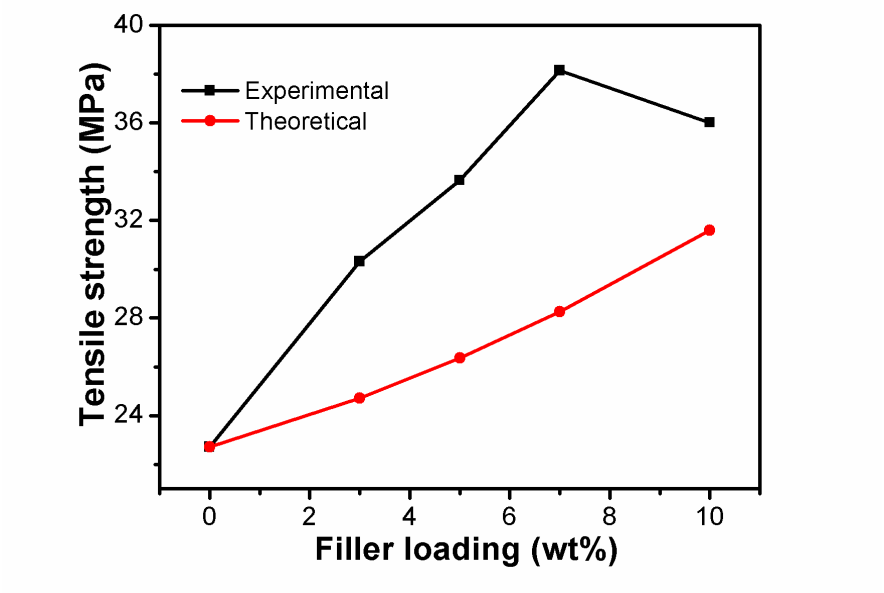

Figure 6.11: Experimental and theoretical tensile strength of PBMA/CeO_2 nanocomposites based on Guth model

6.2.8.4 Kerner Model

Kerner derived an equation for predicting the tensile property of polymer composites having moderate filler concentration as follows [140].

$$Mc = Mm * 1 + \left[\frac{Vf\ 15(1-Vm)}{(1-Vf)(8-10Vm)}\right] \quad (6.4)$$

Figure 6.12 shows the tensile strength of PBMA/CeO_2 nanocomposites measured by using Kerner model along with the experimental tensile value. It is evident from the figure that the theoretical tensile values largely deviate from the experimental values. This model is applicable to the reinforcement of spherically shaped particles in which there should not be any interaction between particles to particles or matrix to particles. The increase in tensile strength of nanocomposite in the present study is mainly due to the interaction between nanoparticles and polymer matrix, hence the experimental tensile does not agree with the experimental results.

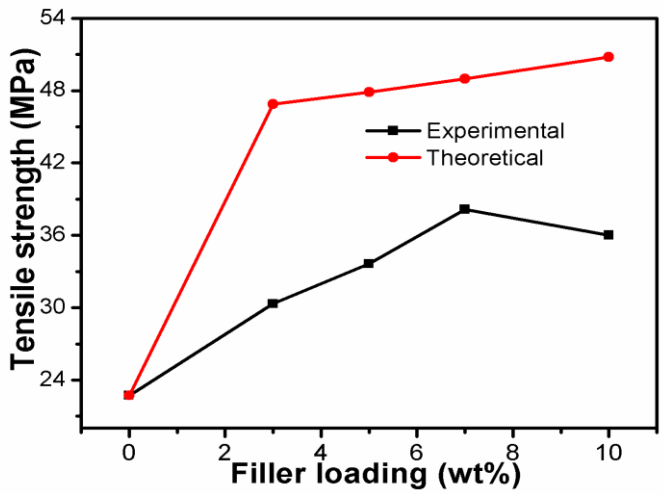

Figure 6.12: Experimental and theoretical tensile strength of PBMA/CeO_2 nanocomposites based on Kerner model

6.2.8.4 Pukanszky Model

In all the models explained above, the basic assumption is that the tensile property of the polymer composite systems mainly depends on the number of filler particles as well as the particle interactions. They negotiated the influence of matrix-filler interactions since it is the major factor responsible for the improved tensile property of polymer composites. Pukanszky considers the effect of interfacial interaction between the matrix and filler to explain the tensile property of polymer composite systems and suggested an equation as follows [141]

$$Mc = Mm * \frac{1-Vf}{1+2.5Vf} * exp(Bvf) \qquad (6.5)$$

where the parameter 'B' denotes the extent of polymer-filler interaction as well as the yield stress around the matrix. The experimental tensile values are applied to the Pukanszky equation and the resultant theoretical values with the experimental tensile values are given in **figure 6.13.** It is clear from the figure that the theoretical values are in good agreement with the experimental values in the entire loading of fillers. So it can be concluded that the matrix-filler interfacial interaction plays a major role in improving the tensile property of PBMA/CeO_2 nanocomposites and this result is in good agreement with the electrical properties and UV studies.

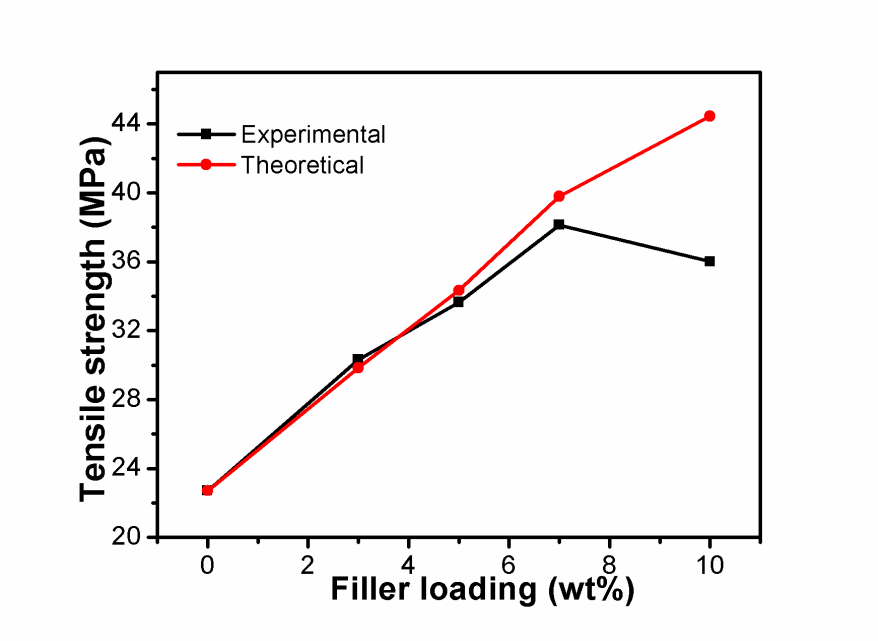

Figure 6.13: Experimental and theoretical tensile strength of PBMA/CeO_2 nanocomposites based on Pukanszky model

6.2.9 Dielectric Properties and AC Conductivity Studies

The variation of dielectric constant (εr) with the frequency for PBMA and PBMA/CeO_2 nanocomposites is given in **figure 6.14.** It can be observed that the dielectric constant of the entire sample is decreasing with frequency up to 10^4 Hz and after it remain almost the same. The higher dielectric value at lower frequency might be due to the proper orientation of the dipolar segments with the applied frequency. As the frequency increases the polar groups fail to arrange themselves with the applied frequency and there by the dielectric constant decreases. But, it is noted that the dielectric constant increases appreciably in the region of 10^2 Hz to 10^4 Hz with the addition of CeO_2 nanoparticles and after it remains almost independent of frequency. Among the

nanocomposites, PBMA with 7 wt% CeO_2 shows maximum value and after the dielectric constant decreases. The increase in the dielectric constant of composites is due to the additional contribution from the space charge polarization that exists between the PBMA matrix and the CeO_2 nanoparticles [143]. However, at higher loading of the nanoparticles, due to the self-agglomeration of nanoparticles, the effective interfacial interaction between the PBMA and the CeO_2 nanoparticles gets interrupted and result in a decrease in the dielectric value.

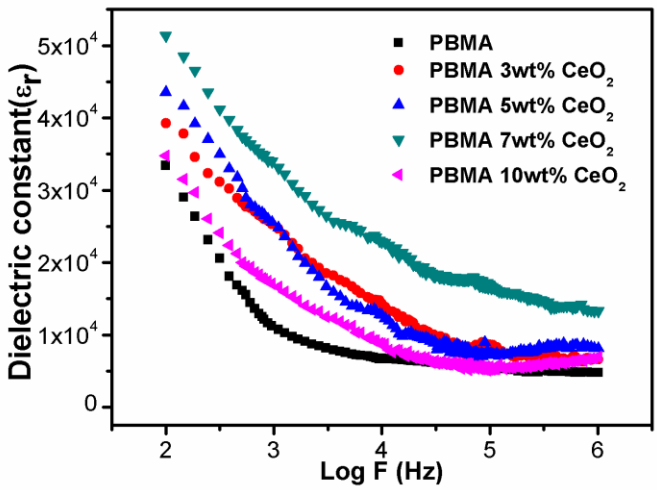

Figure 6.14: The variation of dielectric constant with frequency of PBMA/CeO_2 nanocomposites

The dielectric loss of PBMA and PBMA/CeO_2 nanocomposites with various frequencies is given in **figure 6.15.** The dielectric loss decreases with frequency up to 10^3 Hz and then it remains almost constant for all the composites under study. The higher dielectric loss

at lower frequency is attributed to the interfacial polarization effect [236]. Interestingly, the PBMA/CeO_2 nanocomposites show higher dielectric loss value than pure PBMA and the dielectric loss value further increased with the addition of CeO_2 nanoparticles. The dielectric loss value @ 100 Hz for pure PBMA is 2.49 and it has increased to 4.34 in the case of PBMA with 7 wt% CeO_2 loading. This means the nanoparticle addition brought some modifications in the PBMA matrix, which leads to overlapping of relaxation process and results in higher dielectric loss in PBMA composites.

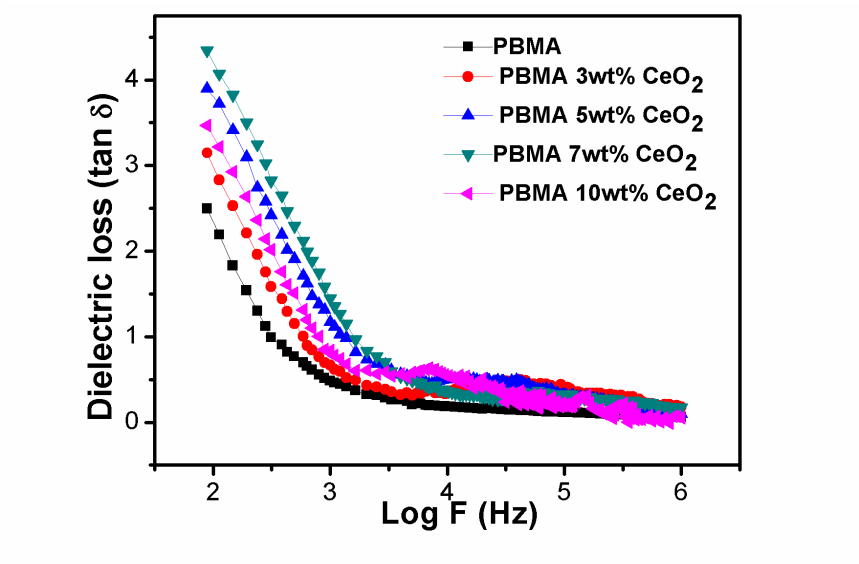

Figure 6.15: The variation of dielectric loss with frequency for PBMA/CeO_2 nanocomposites

The AC conductivity ($\sigma_{a.c}$) of PBMA and its composites with CeO_2 nanoparticles are given in **figure 6.16.** The conductivity is found to be increased with the frequency in all cases in a not perfect linear manner. The increase in AC conductivity at lower frequency region is might be due to interfacial polarization effect and as the frequency increases the

electronic polarization also comes to act. The conductivity is significantly improved by the addition of CeO_2 nanoparticles up to 7 wt% loading, which specifies the role of CeO_2 nanoparticles in improving the conductivity properties of pure PBMA. It can be explained as upon incorporation of nanoparticles, the number of charge carriers increases and also there is a gradual development of conducting network in the PBMA matrix which facilitates the transfer of charge carriers in the polymer backbone [237]. The space charge defects created by the CeO_2 nanoparticles in the PBMA backbone also contributes to the enhanced conductivity. The slight decrease in the conductivity at higher concentration (10 wt%) might be due to a decrease in conducting networks by the presence of agglomerated nanoparticles.

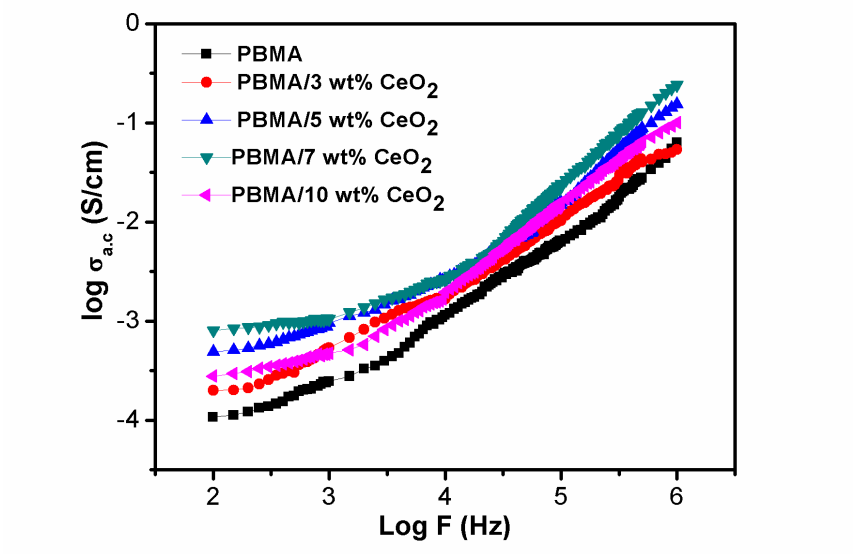

Figure 6.16: The AC conductivity of PBMA/CeO_2 nanocomposites at different frequencies

6.2.10 Effect of Temperature on AC Conductivity

The variation of AC conductivity with the temperature for PBMA and PBMA with different contents of CeO_2 nanoparticles is presented in **figure 6.17.** The AC conductivity was increasing with temperature in all cases. Since, in the polymer composites the conductivity is due to the availability of charge carriers. As the temperature increases, the available charge carriers get extra energy and therefore conductivity enhances by an increase in the mobility of charge carriers [238]. Besides, more vacant sites are created by the thermal excitation of charge carriers, further facilitate the movement of charge carriers.

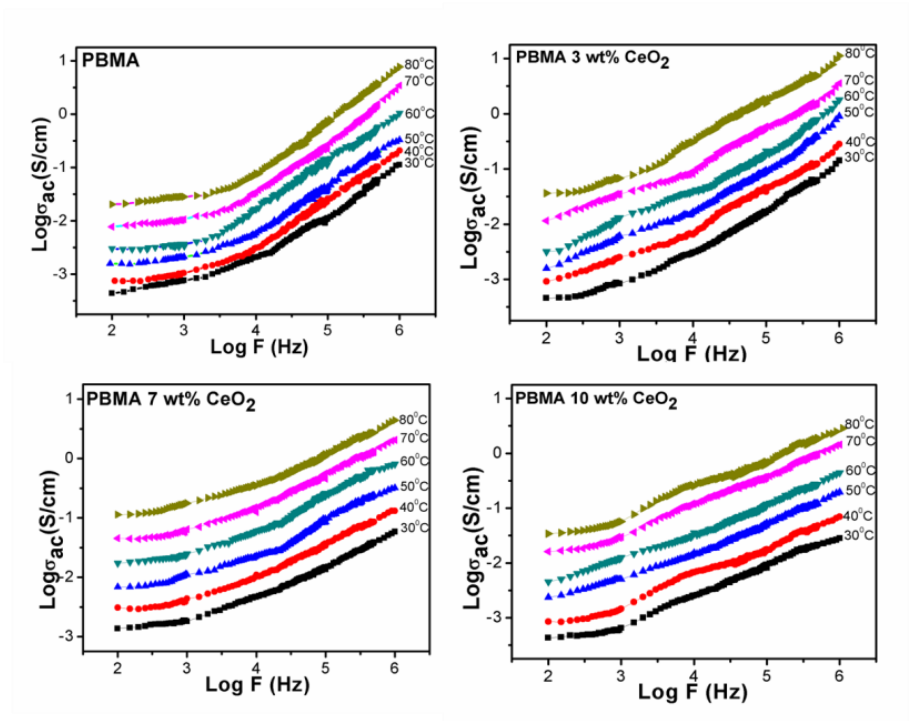

Figure 6.17: The temperature dependent- AC conductivity of PBMA and PBMA/CeO_2 nanocomposites

The dependence of conductivity on temperature can be explained by two mechanisms large polaron theory and small polaron theory [239, 240]. According to large polaron theory, the conductivity decrease with temperature, while in the case of small polaron theory conductivity increases with temperature which means the system follows the hopping conduction mechanism. In the present case, the conductivity increases with temperature and therefore the PBMA/CeO_2 nanocomposites follow the small polaron model. Further, it indicates that the increase in hopping of charge carriers is responsible for the enhanced conductivity with temperature in the present composite systems.

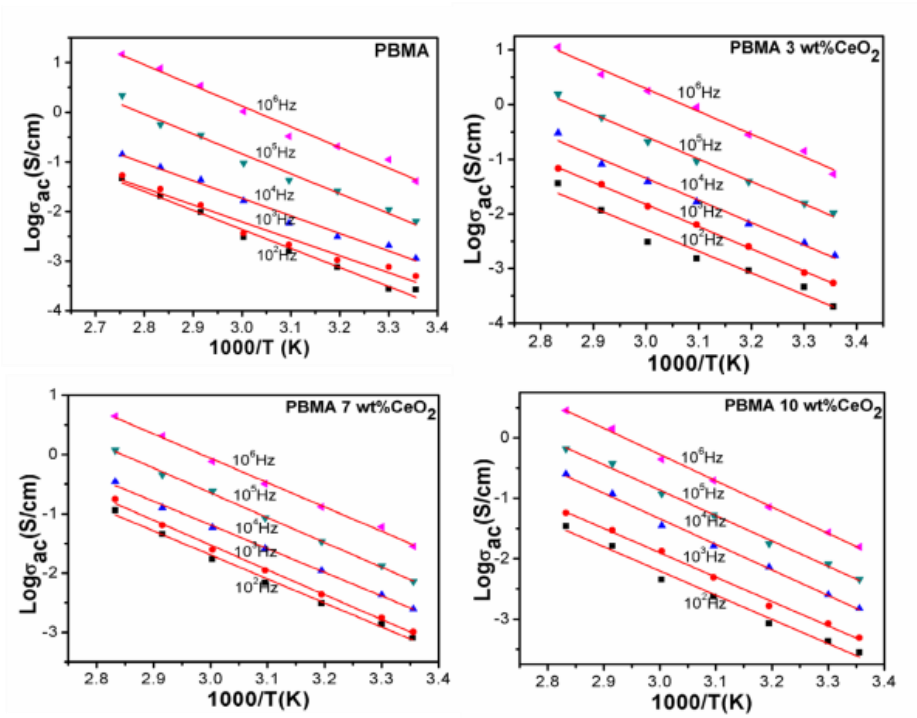

Figure 6.18: Log($\sigma_{a.c}$) vs 1/T plot for PBMA and PBMA/CeO_2 nanocomposites at different frequencies

The activation energy of PBMA/CeO_2 nanocomposites is measured from the plot of $\log(\sigma_{a.c})$ vs 1/T at different frequencies and the plots are given in **figure 6.18.** The linear nature of the graph in the entire temperature region shows the thermally activated conduction in the composites [238]. The obtained activation energy values in various frequencies are documented in **table 6.2.** The decrease in activation energy value with frequency specifies the hopping conduction in the PBMA/CeO_2 nanocomposites. Moreover, the activation energy values are higher for pure PBMA as compared to that of composites, shows the significantly improved conductivity by the incorporation of CeO_2 nanoparticles in the PBMA matrix.

TABLE 6.2. The activation energy values at different frequencies for PBMA and PBMA/CeO_2 nanocomposites.

Samples	**Frequency (Hz)**				
	10^2	**10^3**	**10^4**	**10^5**	**10^6**
PBMA	-3.834	-3.414	-3.531	-4.005	-4.167
PBMA/3 wt% CeO_2	-3.965	-4.065	-4.091	-4.117	-4.157
PBMA/5 wt% CeO_2	-3.998	-4.010	-4.096	-4.121	-4.169
PBMA/7 wt% CeO_2	-4.048	-4.182	-4.189	-4.201	-4.209
PBMA/10 wt% CeO_2	-4.006	-4.033	-4.232	-4.200	-4.352

The dependence of AC conductivity on frequency can be explained by the equation $\sigma_{a.c} = A\omega^s$**,** where A is the frequency factor and 's' implies the exponential factor. The value's' indicates the mechanism of conductivity in the given system and it can be obtained by plotting $\log(\sigma_{a.c})$ vs $\log(\omega)$. If the value of $s<1$, the conductivity is from the hopping conduction and if $s>1$ the conduction is from the localised sites [241]. The 's' value obtained for PBMA/CeO_2 nanocomposites in

the various temperatures is given in **table 6.3.** As it cleared from the table, the 's' value is decreases with temperature for all the composites. It is also noted that, the value of 's' is less than 1, indicates the hopping conduction present in the PBMA/CeO_2 nanocomposites.

TABLE 6.3. The 's' value at different temperatures for PBMA and PBMA/CeO_2 nanocomposites.

Samples	Temperature (°C)					
	30	40	50	60	70	80
PBMA	0.6018	0.6017	0.6168	0.6159	0.6141	0.6138
PBMA/3 wt% CeO_2	0.6286	0.6194	0.6120	0.6093	0.5998	0.5962
PBMA/5 wt% CeO_2	0.6444	0.6401	0.6372	0.6300	0.6294	0.6273
PBMA/7 wt% CeO_2	0.6606	0.6536	0.6423	0.6405	0.6385	0.6379
PBMA/10 wt% CeO_2	0.6302	0.6285	0.6271	0.6254	0.6223	0.6113

6.2.11 DC Conductivity Studies

Figure 6.19 represents the variation of DC conductivity (log $\sigma_{d.c}$) of PBMA with different loading of CeO_2 nanoparticles. It appears that the conductivity increases with the addition of CeO_2 nanoparticles. The addition of nanoparticle increases the number of charge carriers and it leads to the enhanced conductivity for the PBMA/CeO_2 nanocomposites than the pure PBMA. Further, with an increase in the amount of nanoparticles, the distance between the active centers gets reduced and this facilitates the easy transfer of charge carriers throughout the polymer surface. It can be seen that the $\sigma_{d.c}$ of composite shows a significant increase in value at an initial loading from ~10^{-12} S/cm (pure PBMA) to 10^{-11} S/cm (PBMA with 3 wt%

CeO_2). Beyond this loading, there is only a slight increase in value with a further addition of filler particles and the maximum conductivity is observed by PBMA with 7 wt% CeO_2 nanoparticles. So, it can be explained that in the case of PBMA/CeO_2 nanocomposite, a better conductive network is formed in the initial stage as well by the proper arrangement of filler particles in the PBMA backbone [145].

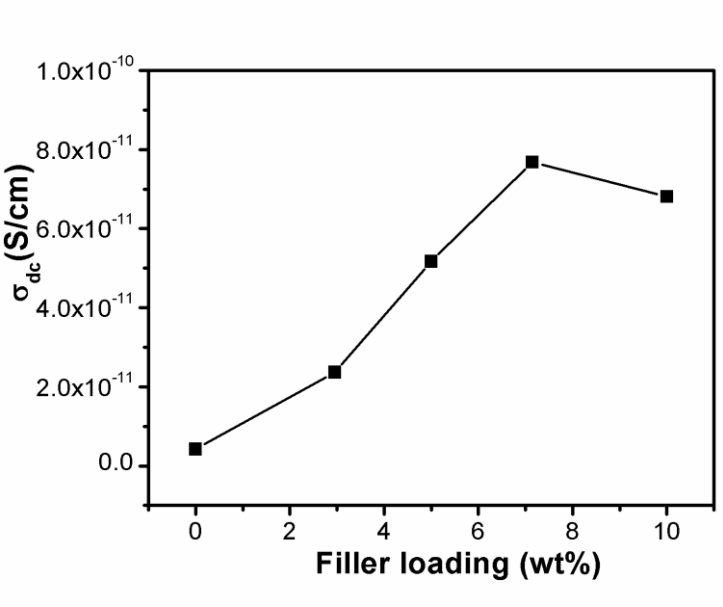

Figure 6.19: The variation of DC conductivity with filler concentrations for PBMA/CeO_2 nanocomposites

6.2.12 Applicability of Theoretical Modeling to the DC Conductivity

Various theoretical models are applicable to filler reinforced polymeric systems for predicting the conductivity mechanism of the prepared polymer nanocomposites. The assumptions behind each of the models that the conductivity mainly depends on the inter-particle contact as

well as the interaction of filler with the polymer matrix, which in turn depends on the size, shape, aspect ratio, volume fraction and the arrangement of filler in the polymer matrix. In the present study, the experimental result obtained for PBMA/CeO_2 nancomposites is compared with various theoretical assumptions such as Bueche, McCullough and Scarisbrick models. But these models fail in our case. So we introduced a new model and was explained below.

6.2.12.1 Bueche Model

The main theory behind Bueche model is that the conducting particles are segregated in the insulating polymer matrix in such a way that it forms a complete conductive network [151]. So that the total conductivity of the two-phase polymer composite system is the sum of the conductivities of two individual components and can be given as

$$\sigma c = \Phi f \sigma f + (1 - \Phi f)\sigma p \qquad (6.6)$$

Where σc, σf and σp denotes the conductivities of composite, filler (0.044 S/cm) and polymer matrix (4.23 x 10^{-12} S/cm) respectively and Φf denotes the volume fraction of filler.

The $\sigma_{d.c}$ of PBMA/CeO_2 nanocomposites at different filler loading is theoretically calculated by the Bueche model. The theoretical and experimental conductivity of the composites is given in **figure 6.20.** The theoretically calculated conductivity shows large deviations from that of experimental values in the entire loading of fillers, indicate that the Bueche model is not applicable to the conductivity study of PBMA/CeO_2 nanocomposites**.** The Bueche model is working on the

additive rule and so it is most suitable for multi-component systems in which the conductivity of components present in the polymer composite has no much difference. In the present case, the conductivity of PBMA matrix is widely different from that of CeO_2 nanoparticles. So, the Bueche model fails in the present study.

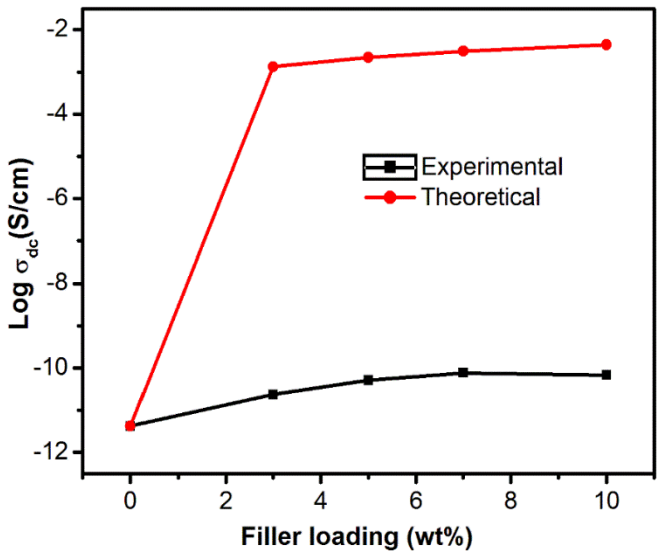

Figure 6.20: Theoretical conductivity using Bueche model and experimental conductivity of PBMA/ CeO_2 nanocomposites

6.2.12.2 Scarisbrick Model

Based on Scarisbrick model the conductivity is governed by inter-particle contact and thus the conductivity is ohmic in nature [152]. He suggested that the conducting particles are randomly distributed in the polymer matrix and there should be an electrical contact between the particles. The equation is given as follows

$$\frac{\sigma c}{\sigma f} = C^2.\Phi.\Phi[exp(\Phi^{-\frac{2}{3}})] \quad (6.7)$$

$$\frac{\sigma c}{\sigma f} = \Phi.\Phi\left[ex\,p\left(\Phi^{-\frac{2}{3}}\right)\right] \text{(When } C^2 = 1\text{)} \quad (6.8)$$

$$\frac{\sigma c}{\sigma f} = 3\ x\ 10^{-3}.\Phi.\Phi[exp(\Phi^{-\frac{2}{3}})] \text{(When } C^2 = 3x10^{-3}\text{)} \quad (6.9)$$

Where C^2 is a geometrical element that determines the arrangements as well as the extent of inter-particle contact in the polymer matrix (value lies between 1 and $3x10^{-3}$) and other parameters have their usual meanings. The experimental conductivity and conductivity measured from the Scarisbrick model (**equations: 6.7-6.9**) of PBMA/CeO_2 nanocomposites are given in **figure 6.21.** The theoretical conductivity shows a large difference with the experimental conductivity at entire loading of CeO_2 for both ranges of C^2. The mismatch in the case of PBMA/CeO_2 composites might be due to the formation of conducting networks even at low concentrations, as revealed from the DC conductivity study. Further, in the case of Scarisbrick model the contribution from the polymer matrix does not consider. So in most cases, the theoretical conductivity using the Scarisbrick model shows a large deviation from the experimental conductivity especially at lower concentrations of filler in the polymer.

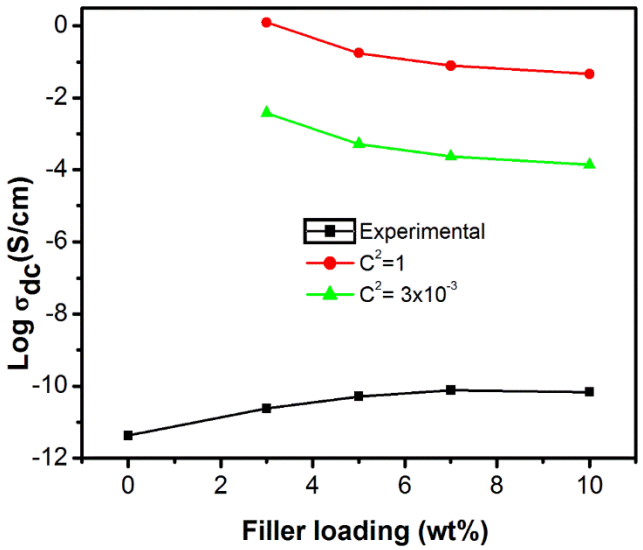

Figure 6.21: Theoretical conductivity using Scarisbrick model and experimental conductivity of PBMA/CeO_2 nanocomposites

6.2.12.3 McCullough Model

According to McCullough model, the conductivity of binary composites not only depends on the amount of filler but also on the extent of conductive networks formed by the filler particles [150] and can be expressed as

$$\sigma c = \sigma p.\Phi p + \sigma f.\Phi f - \left[\frac{\lambda.\Phi p.\Phi f+(\sigma f-\sigma p)^2}{vf.\sigma f+vp.\sigma p}\right] \qquad (6.10)$$

Where λ is the structural factor, indicate the extent of conductive network formation in the polymer matrix and its value differ from 0 to 1, vf and vp are given as

$$vf = (1-\lambda).\Phi f + \Phi p.\lambda \qquad (6.11)$$

$$vp = (1-\lambda).\Phi p + \Phi f.\lambda \qquad (6.12)$$

The $\sigma_{d.c}$ of PBMA/CeO_2 nanocomposites are theoretically calculated by the McCullough model (**equations: 6.10-6.12**). The experimental and theoretical conductivity of the polymer composite is presented in **figure 6.22.** In the McCullough model, the conductivity value is determined by the parameter λ, whose exact value is difficult to measure. So that in most cases the McCullough model fails to predicts the exact conductivity of the composites. So, in order to validate the McCullough model the conductivity is measured for different values of λ. However, in the case of PBMA/CeO_2 nanocomposites, theoretical conductivity values not at all agree with the experimental conductivity for all λ values. The theoretical conductivity largely deviates from experimental conductivity in all cases. So McCullough model also fails in the case of PBMA/CeO_2 nanocomposites.

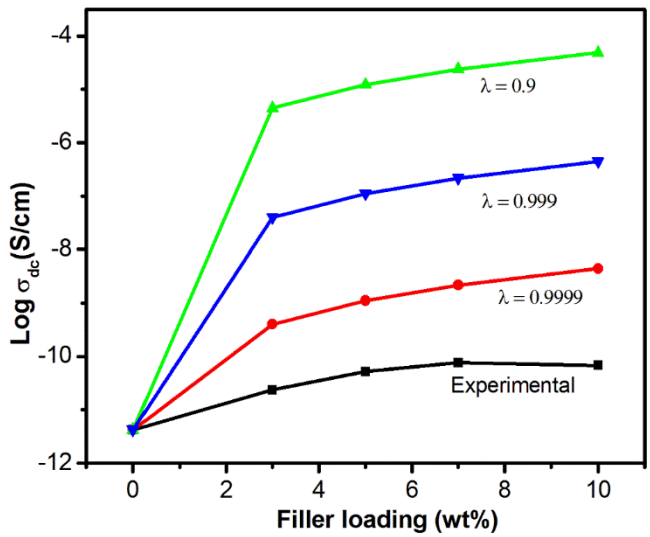

Figure 6.22: Theoretical conductivity using McCullough model and experimental conductivity of PBMA/CeO_2 nanocomposites

6.2.12.4. Proposed Model for PBMA/CeO_2 Nanocomposites

The conductivity of binary composites depends on the shape, geometry, aspect ratio and surface to volume ratio of the filler. However, these factors are not considered in the above discussed models (Bueche, McCullough and Scarisbrick models) and this might be the reason to the large deviations between the experimental and theoretical values. So we have proposed a new model by considering the shape factor (S) of the polymer composite and the proposed equation is

$$log\sigma c = \frac{\Phi p.\log \sigma p + \Phi f.S.log\sigma f}{\Phi p.e^{\Phi f} + \Phi f.S.e^{\Phi p}} \qquad (6.13)$$

The theoretical conductivity of the samples estimated from above model along with the experimental values are presented in **figure 6.23.** The theoretical and experimental plots coincide with the loading of nanoparticles and, therefore, the proposed model used to predict the conductive mechanism of PBMA/CeO_2 nanocomposites. This finding has been considered encouraging for developing new and innovative thermoplastic materials for fabricating or improving the properties of nanoelectronic devices.

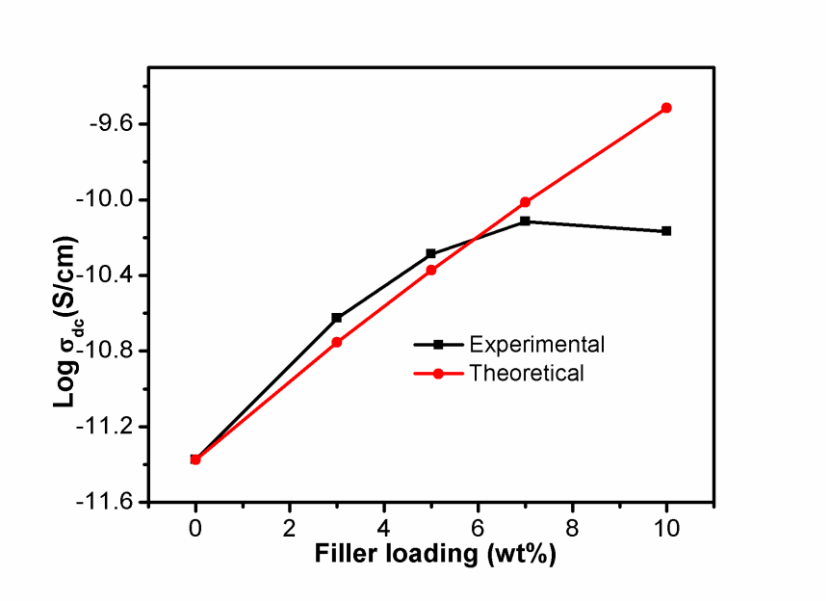

Figure 6.23: Theoretical conductivity using proposed model and experimental conductivity of PBMA/CeO_2 nanocomposites

6.3 Conclusion

PBMA nanocomposites with enhanced electrical conductivity were prepared by incorporating various amounts of CeO_2 nanoparticles via in situ polymerization method. The FT-IR spectra revealed that the CeO_2 nanoparticles were effectively incorporated in the PBMA matrix through the interactions of nanoparticles with the carbonyl group in the PBMA matrix. The UV-Visible absorption spectra exhibits an increase in intensity with the addition of nanoparticles, indicates the better dispersion of CeO_2 nanoparticles by effective interfacial interaction with the PBMA matrix. The appearance of crystalline peaks in PBMA/CeO_2 nanocomposites obtained from the XRD profile showed the more ordered dispersion of nanoparticles in the polymer matrix. The FE-SEM images showed a better dispersion of nanoparticles in the

PBMA matrix. The TEM results showed the successful incorporation of CeO_2 nanoparticles with particle clustering in the 9.21 nm scale. The glass transition temperature of composites also gradually increased with the amount of CeO_2 particles. The thermal stability of PBMA composites was found to be increased with the addition of CeO_2 nanoparticles. PBMA/CeO_2 nanocomposite exhibited higher tensile strength than pure PBMA and it denotes that nanoparticles act as stress-relieving sites by the effective interaction with the PBMA matrix. The decrease in elongation at break with the loading of CeO_2 nanoparticles shows the higher compatibility between the filler and polymer. The comparison of experimental tensile strength with theoretical models like Einstein, Mooney, Guth, Kerner and Pukanszky equation was carried out and the results shows the Pukanszky model was more applicable in the case of PBMA/CeO_2 nanocomposites.The effect of loading of CeO_2 on AC conductivity and activation energy of PBMA nanocomposites was studied at different temperatures and various frequencies. The AC conductivity was substantially enhanced with an increase in temperature as well as with the frequencies. The activation energy shows a drastic reduction in values upon the addition of CeO_2 nanoparticles further implies the improved conductivity of composites. The value of exponential parameter indicates that the PBMA/CeO_2 nanocomposites follow hopping conduction. Increased DC conductivity of composites was observed with the addition of CeO_2 nanoparticles. The changes in DC conductivity of PBMA/CeO_2 nanocomposites were correlated with theoretical models like Bueche, Scarisbrick and McCullough models. The Bueche, Scarisbrick and McCullough model fails to explain the conductivity of polymer

composite in the entire loading of fillers. So we proposed a new model for theoretical conductivity, which is in good agreement with the experimentally observed conductivity and therefore this proposed model can be applied to thermoplastic polymers nanocomposite system.

CHAPTER 7

PREPARATION, CHARACTERIZATION, THERMAL, MECHANICAL AND CONDUCTIVITY STUDIES OF POLY (BUTYLMETHACRYLATE)/NEODYMIUM OXIDE NANOCOMPOSITES

Contents

K. Suhailath, Meenu Thomas, M. T. Ramesan, Studies on mechanical properties, dielectric behavior and DC conductivity of neodymium oxide/poly (butylmethacrylate) nanocomposites. Polym. Polym. Compos. (2020) doi: 10.1177/0967391120960658.

K. Suhailath, B. K. Bahuleyan, M. T. Ramesan, Synthesis, characterization, thermal properties and temperature-dependent AC conductivity studies of poly (butylmethacrylate)/neodymium oxide nanocomposites. J. Inorg. Polym. Mater. (2020) doi: 10.1007/s10904-020-01665-9.

7.1 Introduction

Composite materials are becoming an inevitable product in our daily life due to the advantage of having low weight, better heat and chemical resistance, remarkable thermal and electrical properties [242, 243]. Amidst, polymer nanocomposites got greater importance owing to outstanding properties. The interest of polymeric nanocomposite materials is mainly arising from their ease of processing and flexible nature [244]. Moreover, polymer nanocomposites can exhibit the properties of both the polymer and nanoparticle components and so finds numerous applications in various areas. Therefore, in some cases, the polymer composites may replace other materials exhibiting similar properties [245]. For example, ceramic materials have considerable dielectric properties, but due to the brittle nature and requirement of high temperature for the fabrication, their use is very limited [246].

Recently, there is greater importance in the development of polymer nanocomposites with convenient weight, appropriate thermal, mechanical and conductivity properties due to their immense applications in various fields [247]. However, the properties of polymer nanocomposite greatly depend on the nano-component present in the polymer matrix and the nature of the polymer itself. So that judicial selection of components is an important thing for the fabrication of polymer nanocomposites with desirable properties. Poly (butylmethacrylate) (PBMA) is one of the transparent material with light-weight, flexible and can be made to thin films very easily. Further their innate properties can be improved by incorporating nanofillers

and thus can be applied in various fields. The reinforcement of nanofillers with PBMA was reported recently [123, 127].

The importance of nanoparticle is the availability of adequate surface area for interactions with the polymer matrix. Therefore, even a small amount of nanoparticles brought unexpected modifications to the polymer properties and the changes are reflected in the improved thermal, electrical, mechanical and optical properties [248]. Metal oxide nanoparticles with outstanding properties are widely used as fillers for the development of polymer composites with remarkable properties [249]. Amidst, rare earth metal oxides especially the Nd_2O_3, got greater attention owing to their immense optical and electrical properties [250]. The Nd_2O_3 nanoparticles have been widely used in various electronic applications [251]. Compared to conventional Nd_2O_3 particles, the nano Nd_2O_3 nanoparticles are most interesting due to its potential applications arises from the well-defined surface morphology.

Based on this, the present study focused on fabrication of PBMA/Nd_2O_3 nanocomposite by simple in situ polymerization method and their characterization by FT-IR, UV, XRD, FE-SEM and TEM analysis. The effect of Nd_2O_3 nanoparticles on the thermal properties of PBMA was analyzed by DSC and TGA analysis. Further, the influence of Nd_2O_3 nanoparticles on the tensile strength, AC and DC conductivity of the PBMA matrix are studied in detail with respect to different loading of nanoparticles. The mechanism behind the enhanced tensile properties and DC conductivity were studied by correlating the experimental data with various theoretical modeling.

7.2 Results and Discussion

7.2.1 FT-IR Spectra

The FT-IR spectra of Nd_2O_3 nanoparticles, PBMA and the PBMA/Nd_2O_3 nanocomposite are given in **figure 7.1.** The peaks at 411 and 533 cm^{-1} correspond to the characteristics Nd-O vibrations of Nd_2O_3 nanoparticles [252]. From the FT-IR spectra of PBMA, the strong peak at 1731 cm^{-1} attributes to the C=O stretching vibrations and the peaks appears at 1149 cm^{-1} and 1242 cm^{-1} are ascribed to the C-O-C stretching vibrations of ester group present in PBMA backbone. Another peak at 1060 cm^{-1} and 1262 cm^{-1} correspond to the C-O stretching and C-H wagging vibrations respectively [253]. The FT-IR spectra of PBMA/Nd_2O_3 nanocomposite show the characteristic peaks of PBMA with the characteristic stretching of Nd_2O_3 at 522 cm^{-1}. It is interesting to observe that the C=O group (1731 cm^{-1}) of PBMA is found to be shifted to a lower wave number at 1726 cm^{-1} by the insertion of Nd_2O_3 clearly indicated the attachment of nanoparticles in the macromolecular chain of PBMA.

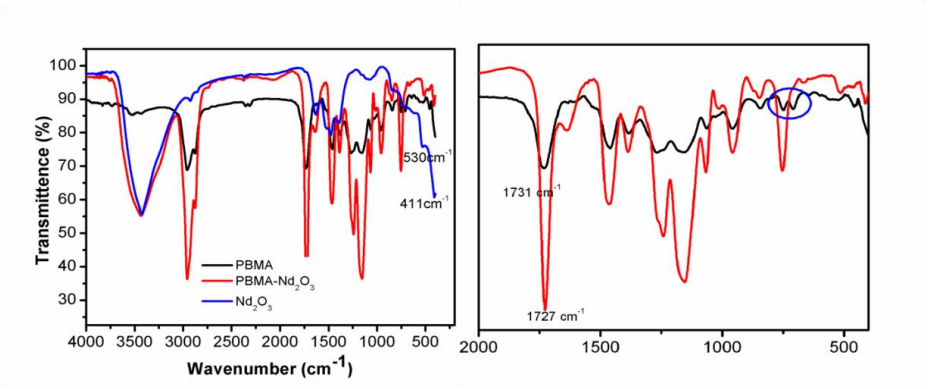

Figure 7.1: The FT-IR spectra of PBMA and PBMA/Nd_2O_3 nanocomposites

7.2.2 Optical Properties

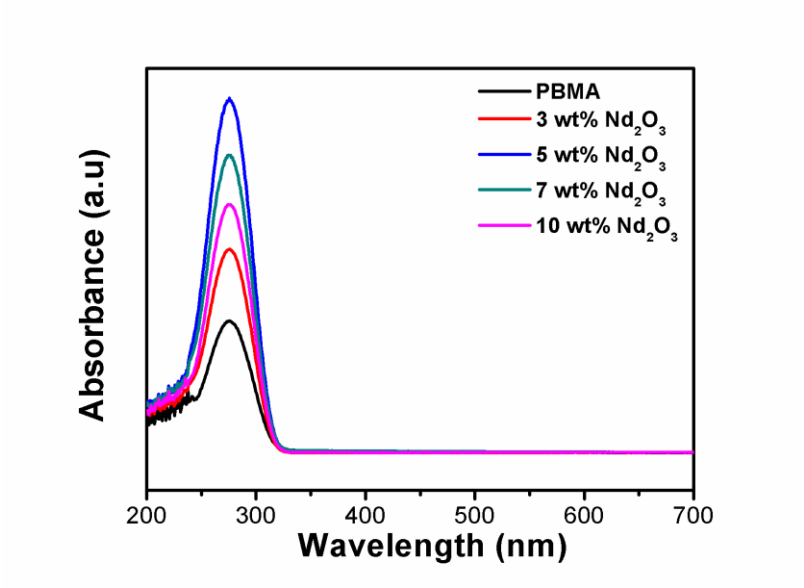

Figure 7.2: The UV-Visible spectra of PBMA and PBMA/Nd_2O_3 nanocomposites

The optical property of PBMA and synthesized PBMA/Nd_2O_3 nanocomposites are analyzed through UV-Visible spectra and the result is presented in **figure 7.2.** There are no absorption peaks in the visible region (400 to 800 nm) in all cases shows the transparent nature of the PBMA and the developed PBMA/Nd_2O_3 nanocomposites. Also, in the case of composites, the better polymer-filler interface attributes to the absence of peaks in the visible region. The PBMA and PBMA composites exhibit similar types of absorption spectra with a strong intense peak at 246 nm attributes to the n- π^* transitions in C=O group present in the PBMA matrix. It can be seen from the figure that the absorption intensity increases with the loading of Nd_2O_3 nanoparticles up to a certain limit (5 wt%), shows the influence of nanoparticles in

enhancing the UV absorption of PBMA. The increase in intensity of UV peak might be arises from the interaction of nanoparticles with the PBMA matrix. Further, due to the nano-size of Nd_2O_3 provides high surface area for the interaction zone and so large absorption is produced. The decrease in absorption at higher loading of filler (after 10 wt%) might be due to poor polymer-filler interface by the presence of agglomerated nanoparticles.

7.2.3 XRD Analysis

Structural information of the prepared PBMA and PBMA/Nd_2O_3 nanocomposites are analysed by XRD and the results are presented in **figure 7.3.** As seen in the figure, the synthesised PBMA exhibits an amorphous peak at $2\theta=17.65^{\circ}$. However, the XRD patterns of the composites are distinct from that of plane PBMA. The composite exhibits the characteristic crystalline peaks of Nd_2O_3 nanoparticles along with the amorphous peak of pure PBMA which implies the better compatibility between the polymer matrix and nanoparticles. It can be seen from the figure that the intensity of the Nd_2O_3 peaks increases with the loading of nanoparticles in the polymer composite. The increase in the crystalline nature of composites signified the better reinforcement of Nd_2O_3 nanoparticles into the PBMA.

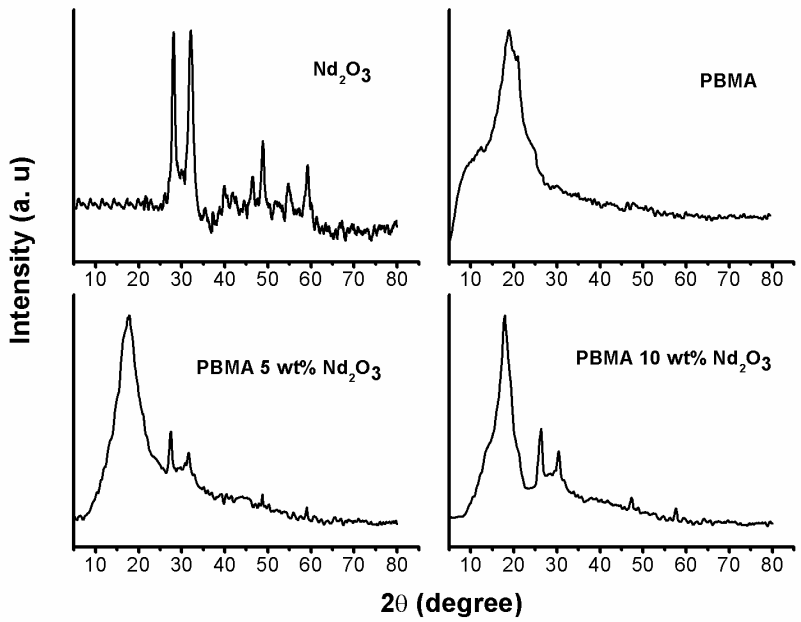

Figure 7.3: XRD pattern of Nd_2O_3, PBMA and PBMA/Nd_2O_3 nanocomposites

7.2.4 FE-SEM Analysis

Surface morphological assessments of Nd_2O_3 nanoparticle, PBMA and PBMA with different contents of Nd_2O_3 nanoparticles are presented in **figure 7.4.** The as prepared nanoparticles are seemed to be agglomerated and the bare PBMA exhibited a smooth surface. However, the smooth morphology of PBMA is changed by the insertion of nanoparticles into PBMA matrix and the presence of nanoparticles is clearly visible in the images of composites. The better dispersion of nanoparticles in the PBMA phase is observed at 5 wt% Nd_2O_3 loading which indicated the better adhesion between the polymer and the nanoparticles. However, the uniform dispersion of

filler in the polymer is slightly changed into an agglomerated structure at higher loading of Nd_2O_3 particles (at 10 wt% loading). The coupling of adjacent nanoparticles creates more stress in the polymer composite which ultimately results in the clustering of nanoparticles at higher loading.

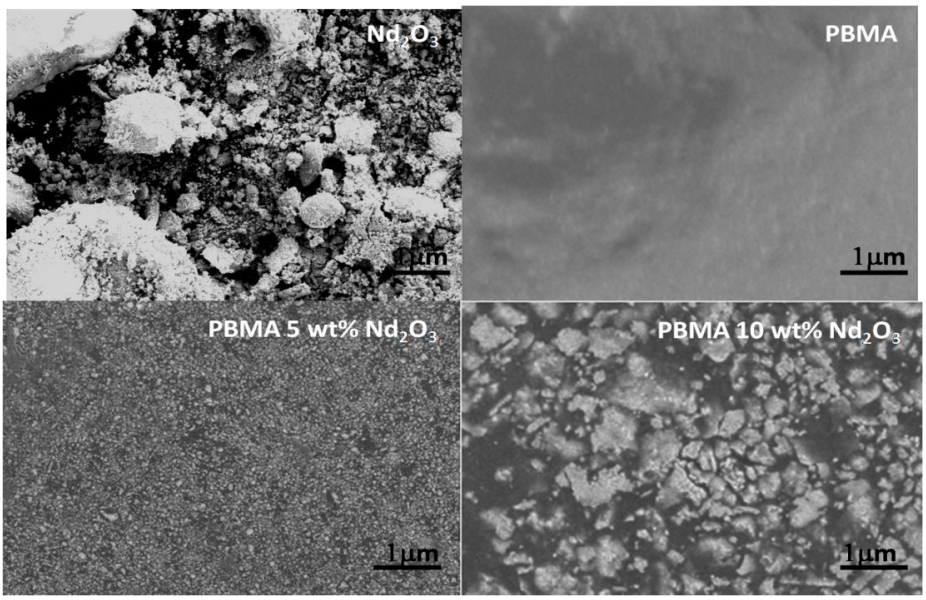

Figure 7.4: FE-SEM images of Nd_2O_3, PBMA and PBMA/Nd_2O_3 nanocomposites

7.2.5. TEM Analysis

TEM measurements of PBMA/Nd_2O_3 composite reveals more detailed information regarding the arrangement of nanoparticles in PBMA during composite formation and it also provides additional supporting information that will aid in the interpretation of other results. TEM images of Nd_2O_3 nanoparticle and different contents of Nd_2O_3 incorporated PBMA samples are given in **figure 7.5.** The Nd_2O_3

nanoparticle has elongated structure with average size of 27.30 nm. The images of PBMA composites hinted that the nanoparticles are well dispersed in the PBMA matrix with maximum surface area of contact and close interaction between the host and guest components. From the selected are diffraction pattern, the PBMA/Nd_2O_3 composite is crystalline in nature as evidenced by bright spots with concentric ring. The particle size of PBMA with 5 wt% Nd_2O_3 sample is ~28.36 nm whereas the size of the nanoparticle increased to ~30.72 nm for 10 wt% Nd_2O_3 sample. It can be seen that Nd_2O_3 nanoparticles are evenly dispersed inside the PBMA matrix at 10 wt% loading with few agglomeration of nanoparticles and this result is in good agreement with the SEM result.

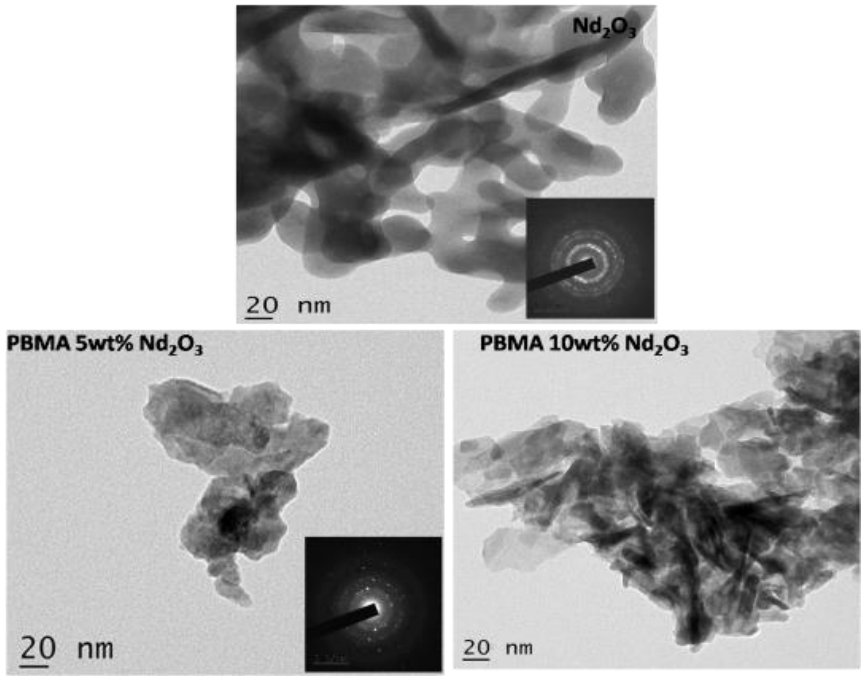

Figure 7.5: TEM images of Nd_2O_3 nanoparticle and PBMA/Nd_2O_3 nanocomposites

7.2.6 Thermal Studies

7.2.6.1 TG Analysis

The effect of nanoparticles on the thermal stability of PBMA has been observed by TGA and the corresponding DTG curves are presented in **figure 7.6.** Generally, the PBMA degrades in two steps, the first begins with cleavage of the head to head linkages by unzipping of vinyl groups (~250°C) and followed by cleavage of end chain through random scission of backbone (~300-400°C) [33, 254]. The pure PBMA and PBMA/Nd_2O_3 nanocomposites exhibit two step degradation processes. As clear from the figure, the Nd_2O_3 nanoparticles significantly improve the initial degradation temperature (Tonset) and major decomposition temperature (Tmax) of the pure PBMA, obviously due to the better interfacial interaction and compatibility of Nd_2O_3 nanoparticles with the PBMA matrix. In PBMA, the T onset is at ~256°C, but for PBMA with 5 wt% Nd_2O_3 the T onset is at ~264°C and for PBMA with 10 wt% Nd_2O_3 the T onset is at ~268°C. Similarly, the T max from DTA for PBMA is about 280°C. However, the PBMA with 5 wt% Nd_2O_3 shows Tmax around 292°C and PBMA with 10 wt% Nd_2O_3 shows Tmax around 300°C. These results clearly indicate the role of Nd_2O_3 nanoparticles in improving the thermal stability of PBMA. The nanoparticles hinder or resist the diffusion of volatile components from the polymer backbone through better interaction with the polymer matrix. The residue after complete degradation is expected to be zero, but in the present case, it is observed that the pure PBMA has 2% residue at 400°C and has 4% and

7% residues for PBMA with 5 wt% Nd_2O_3 and PBMA with 10 wt% Nd_2O_3 respectively.

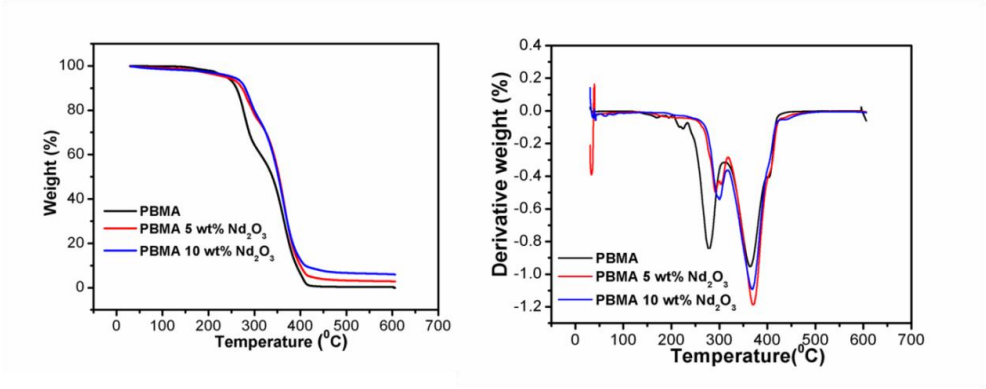

Figure 7.6: TGA and corresponding DTG curve of PBMA and PBMA/Nd_2O_3 nanocomposites

7.2.6.2 DSC Analysis

The effect of Nd_2O_3 nanoparticles on the glass transition temperature (T_g) of PBMA is also investigated through DSC analysis and the thermogram is given in **figure 7.7.** It is known that the better interaction of nanofillers restricts the molecular mobility of polymer segments by the addition of nanoparticles and it reflects in the higher T_g value of composites than the plane polymer matrix [255]. It can be seen from the figure that the T_g value of PBMA/Nd_2O_3 nanocomposites are higher than the pure PBMA revealed the better interaction between the PBMA and Nd_2O_3 nanoparticles. The T_g of neat PBMA is 21.54°C while that of PBMA with 5 wt% Nd_2O_3 and PBMA with 10 wt% Nd_2O_3 is 35.16°C and 41.75°C respectively. The significant enhancement in T_g value shows that the Nd_2O_3 nanoparticles has a major role in increasing the thermal behavior and this might be

attributed to the restricted movement of molecular segments of polymer backbone at the polymer-filler interface [256]. The melting point of the PBMA and PBMA/Nd_2O_3 nanocomposites are also evaluated from the DSC study. The second sharp endothermic dip corresponds to the melting point (T_m) and it is at 285°C for pure PBMA. Further, on the addition of Nd_2O_3 nanoparticles the T_m is also shifted to higher values, shows the ordered arrangement of Nd_2O_3 nanoparticles in the PBMA matrix obviously through better polymer-filler interaction.

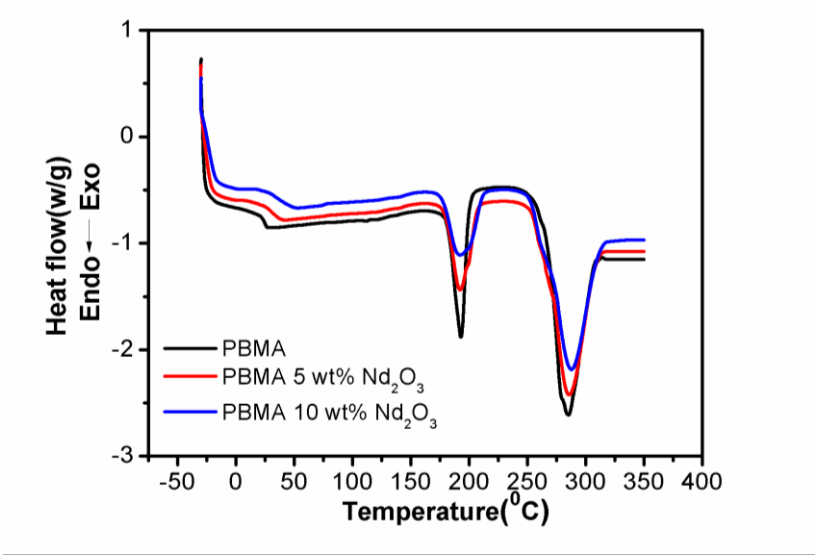

Figure 7.7: The DSC curve of PBMA and PBMA/Nd_2O_3 nanocomposites

7.2.7 Mechanical Studies

Mechanical properties of polymer composites have a major role in the application of polymer products in many fields. In the present study, the tensile strength and elongation at break of the pure PBMA as well as PBMA/Nd_2O_3 nanocomposites are analysed and the results are

given in **table 7.1.** The interfacial interaction and the extent of stress transfer play a key role in improving the tensile properties of composites. The tensile strength of nanocomposite increases with the loading of nanoparticles up to 5 wt% loading. The incorporation of nanoparticles creates additional stress-bearing sites and therefore an effective stress transfer from the polymer matrix to the nanoparticles through the better interface between them [257]. So, the increase in tensile strength for PBMA/Nd_2O_3 nanocomposites attributed to the better reinforcement effect of Nd_2O_3 nanoparticles in the PBMA matrix. However, the maximum tensile strength of the composite decreased slightly beyond 5 wt% loading. The decrease in tensile strength at higher loading arises from the incomplete interface between the matrix and nanoparticles due to the presence of agglomerated particles, as revealed from SEM images. The elongation at break of the composite is found to decrease with the addition of Nd_2O_3 nanoparticles is due to the presence of brittle nanoparticles in the polymeric chain.

Table 7.1: Tensile strength and elongation at break of PBMA and PBMA/Nd_2O_3 nanocomposites

	Tensile strength (MPa)	**Elongation at break (%)**
PBMA	22.72	59.87
PBMA/3 wt% Nd_2O_3	24.32	45.55
PBMA/5 wt% Nd_2O_3	27.59	44.62
PBMA/7 wt% Nd_2O_3	26.45	42.14
PBMA/10wt% Nd_2O_3	25.92	40.32

7.2.7 Tensile Modeling Studies

Many theoretical equations are used to predict the effect of various factors (size, shape, aspect ratio, filler concentration, the extent of interfacial interaction between filler and polymer matrix) towards the improved tensile properties of polymer nanocomposites [135, 136]. In the present work theoretical models suggested by Einstein, Mooney, Guth, Kerner and Pukanszky equations are employed to predict the tensile properties of PBMA/Nd_2O_3 nanocomposites. The experimental value obtained from the tensile analysis is compared with the theoretical tensile strength to predict the reinforcing factors behind the enhanced mechanical properties of polymers.

7.2.7.1 Einstein Model

Einstein suggested the following equation to predict the tensile properties of polymer composites [137].

$$Mc = Mm(1 + 2.5Vf) \qquad (7.1)$$

where Mc and Mm denote the tensile properties of composite and polymer matrix respectively and Vf denotes the filler volume fraction. The tensile strength of composites is applied to the Einstein equation and the theoretical tensile values are compared with experimental values and the results are given in **figure 7.8.** It shows that the theoretical values based on the Einstein model is much lower than the experimental tensile values. This is because the Einstein model is applies to polymer composite with a very low concentration of fillers

(>1) and hence this model fails in most cases to predict the tensile mechanism of polymer composites.

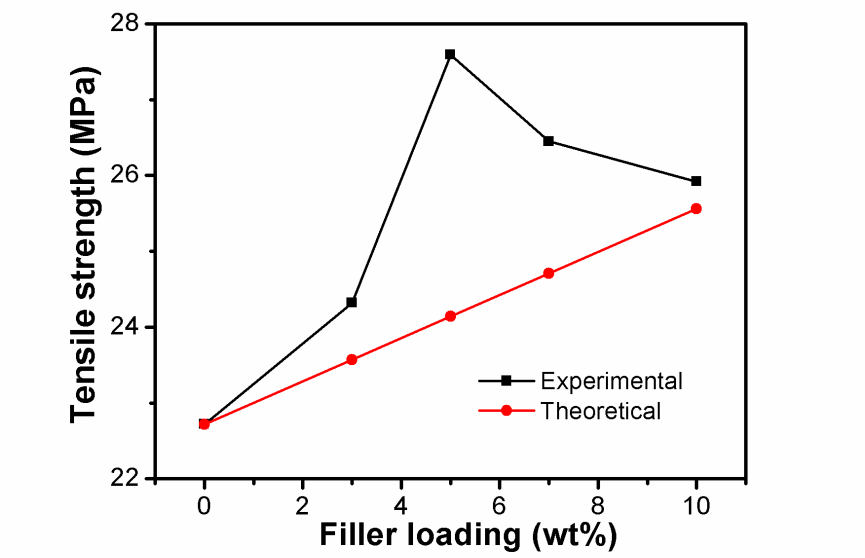

Figure 7.8: Theoretical and experimental curve of tensile strength based on Einstein model

7.2.7.2 Mooney Model

Mooney modified the Einstein equation by introducing a parameter 'S' to make it suitable in all concentrations [138]. The value of 'S' signifies the strain field around the polymer matrix and the filler. For filler particles the S = 1.35. The Mooney equation can be expressed as

$$Mc = Mm * exp\left[\frac{2.5Vf}{1-SVf}\right] \qquad (7.2)$$

where, the parameters have their usual meanings as explained above. The tensile strength of PBMA/Nd_2O_3 nanocomposites is calculated using the Mooney equation and the results obtained are given in **figure 7.9** along with the experimental tensile value. The theoretical value

using the Mooney equation and the experimental value shows a close match at lower filler concentrations, but the theoretical tensile values lie far away from that of experimental values at higher filler loading. The Mooney model assumes that the filler and polymer matrix have comparable tensile values and so it fails in predicting the tensile properties especially in systems with large differences in tensile properties of components like PBMA/Nd_2O_3 nanocomposites.

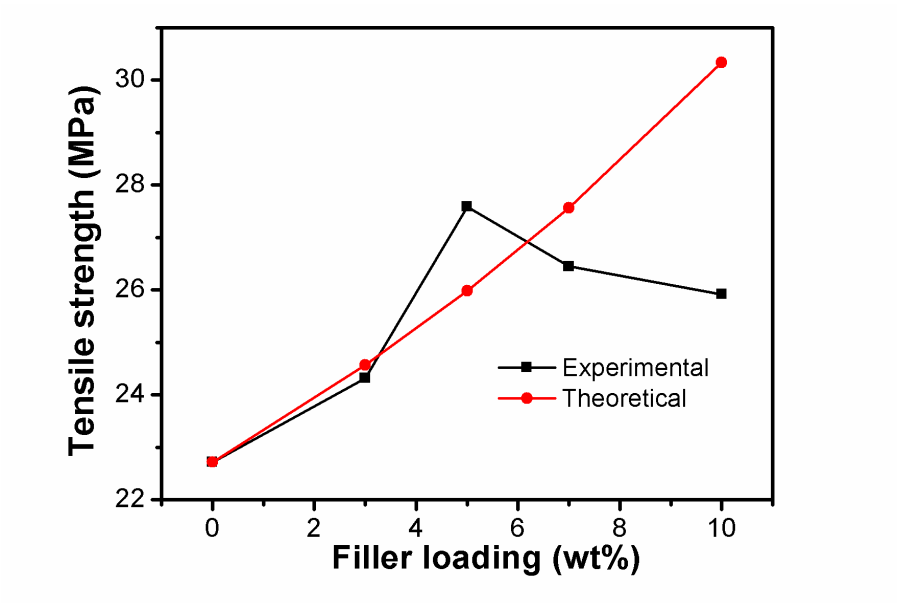

Figure 7.9: Theoretical and experimental curve of tensile strength based on Mooney model

7.2.7.3 Guth Model

Guth considered the role of inter-particle interactions along with the amount of filler to the tensile strength and then he modified the Einstein equation by adding a term as follows [139]

$$Mc = Mm(1 + 2.5Vf) + 14.1\,Vf\text{^}2 \qquad (7.3)$$

The Guth equation is generally used to calculate the tensile strength of polymer nanocomposites and the obtained theoretical tensile values along with the experimental values obtained for PBMA/Nd_2O_3 nanocomposites are presented in **figure 7.10.** It can be seen that the tensile value using the Guth model is close to experimental values at lower filler concentrations but it is much higher than the experimental tensile values at higher concentrations. Similarly with Mooney model, the trend of increase in the tensile strength using Guth model is not comparable with that of experimental values. So the Guth model also fails to explain the tensile strength of PBMA/Nd_2O_3 nanocomposites.

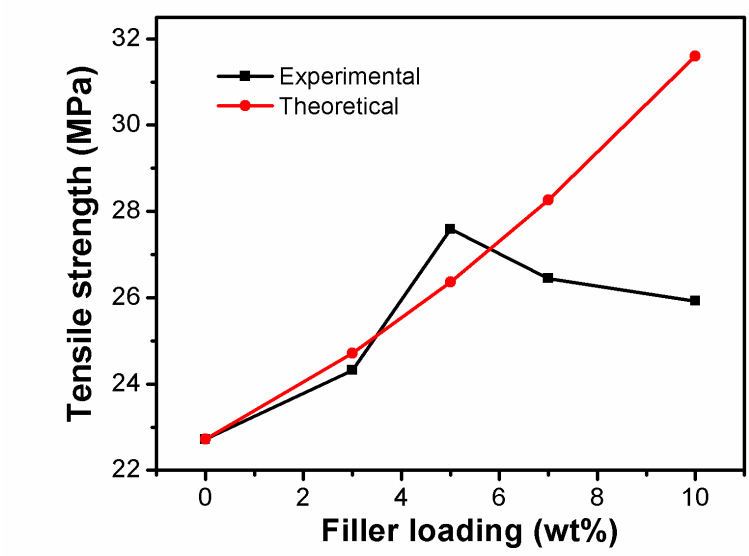

Figure 7.10: Theoretical and experimental curve of tensile strength based on Guth model

7.2.7.4 Kerner Model

Kerner proposed another theoretical model for predicting the tensile strength up to moderate concentrations as follows [140]

$$Mc = Mm * 1 + \left[\frac{Vf\ 15(1-Vm)}{(1-Vf)(8-10Vm)}\right] \quad (7.4)$$

Where Vm represents the poisons ratio and other parameters have their usual meanings. The value of Vm = 0.35. The tensile strength of composite from the Kerner model and the experimental tensile values are of PBMA/Nd_2O_3 nanocomposites is given in **figure 7.11.** It can be seen that theoretical tensile values show large deviations from that of experimental values. This is because the Kerner model is applicable to study the reinforcement of spherically shaped particles incorporated polymer composite and also there is no interaction between particles to particles or matrix to particles. The increase in tensile strength of PBMA/Nd_2O_3 composite in the present study is mainly due to the interaction between nanoparticles and polymer matrix, hence the experimental tensile values do not agree with the experimental results.

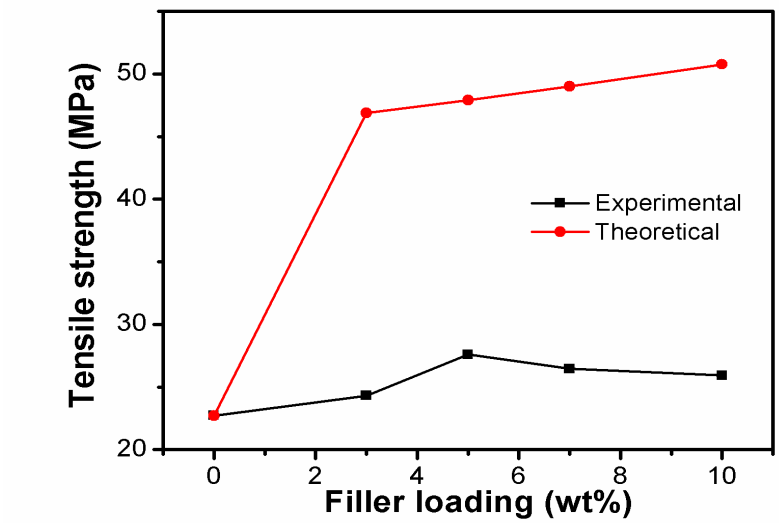

Figure 7.11: Theoretical and experimental curve of tensile strength based on Kerner model

7.2.7.4 Pukanszky Model

Pukanszky put forward a theoretical model for the polymer composite in which the interfacial interaction between the polymer matrix and filler major role in the enhancement of tensile strength by the following equation.

$$Mc = Mm * \frac{1-Vf}{1+2.5Vf} * exp(Bvf) \quad (7.5)$$

where the parameter 'B' determines the level of interfacial interaction between the polymer matrix and the filled nanoparticles. The value of B depends on the size and loading of filler as well as on the thickness and extent of interphase [141]. The correlating graph of experimental tensile value with that of theoretical value obtained using the Pukanszky model is shown in **figure 7.12.** As clear from the figure, the Pukanszky model exhibits better fit in the case of PBMA/Nd_2O_3 nanocomposites. Both the theoretical tensile values using the Pukanszky equation and experimental values show a close match at entire filler loading. So it can be concluded that the effective loading of filler in the polymer depends on the interfacial interaction between the PBMA and Nd_2O_3 nanoparticles and these interactions lead to the improved tensile properties of PBMA/Nd_2O_3 nanocomposites.

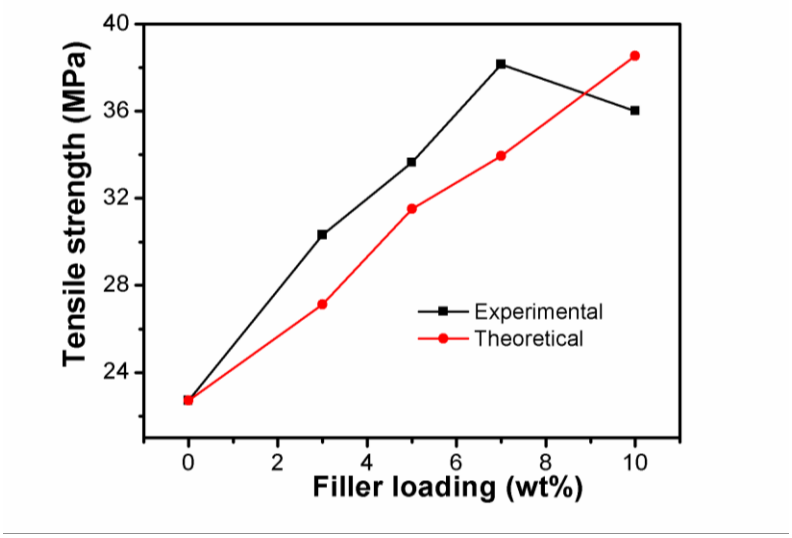

Figure 7.12: Theoretical and experimental curve of tensile strength based on Pukanszky model

7.2.8 Electrical Properties

The change in electrical properties such as dielectric loss and dielectric constant of PBMA by the addition of Nd_2O_3 nanoparticles are measured at different frequencies 10^2 to 10^6 Hz. **Figure 7.13** shows the variation of dielectric loss (tanδ) value with frequency for the PBMA and PBMA/Nd_2O_3 nanocomposites. As seen from the figure, the dielectric loss value of all the composites decreases with frequency up to 10^3 Hz and then it remains constant. However, the introduction of Nd_2O_3 nanoparticles increases the dielectric loss value indicate that the nanoparticles brought some modifications in the PBMA matrix obviously by the better interface between them [258, 259]. But, in the present case, though the dielectric loss value increases with the addition of nanoparticles, the composites with 7 and 10 wt% Nd_2O_3 nanoparticles exhibit lower dielectric loss value than the PBMA with 5 wt% Nd_2O_3 nanoparticles. This might be due to poor polymer-filler

interface by the presence of agglomerated nanoparticles at higher concentrations, as revealed from SEM images.

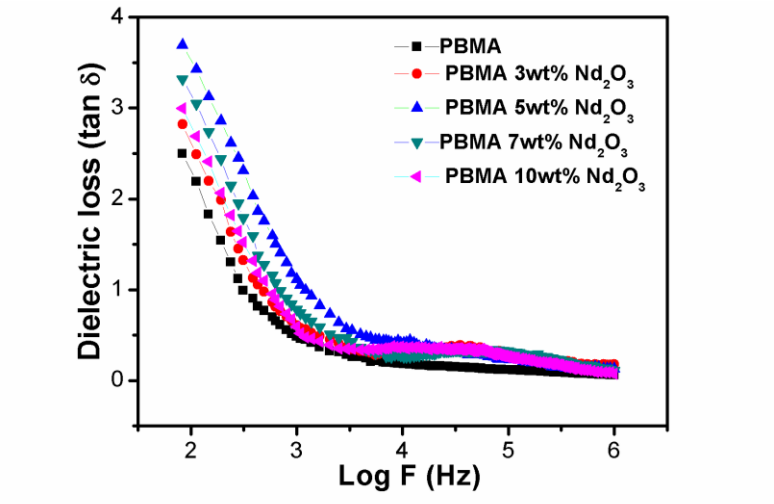

Figure 7.13: Variation of dielectric loss (tanδ) of PBMA and PBMA/Nd_2O_3 nanocomposites at different frequencies

The variation in dielectric constant (ε_r) with frequency for PBMA and PBMA/Nd_2O_3 nanocomposites is shown in **figure 7.14.** The dielectric constant decreases with frequency in all cases up to 10^4 Hz and after it remains independent of frequency. The higher value of dielectric constant at lower frequency attributes to the proper alignment of polymer dipoles with the applied frequency. As the frequency increases the dipoles fail to arrange themselves with the applied frequency and so the dielectric constant remains independent of frequency at higher frequency [260]. But, interestingly the dielectric constant increases with the addition of Nd_2O_3 nanoparticles up to 5 wt% and after it shows a slight decrease in value. The contribution from space charge polarization arises from better interfacial interaction between the polymer and filler results in higher dielectric constant for polymer composites. The slight decrease in dielectric constant at

higher loading of nanoparticles (7 and 10 wt%) might be due to poor interface between the PBMA and Nd_2O_3 nanoparticles by the presence of aggregated nanoparticles.

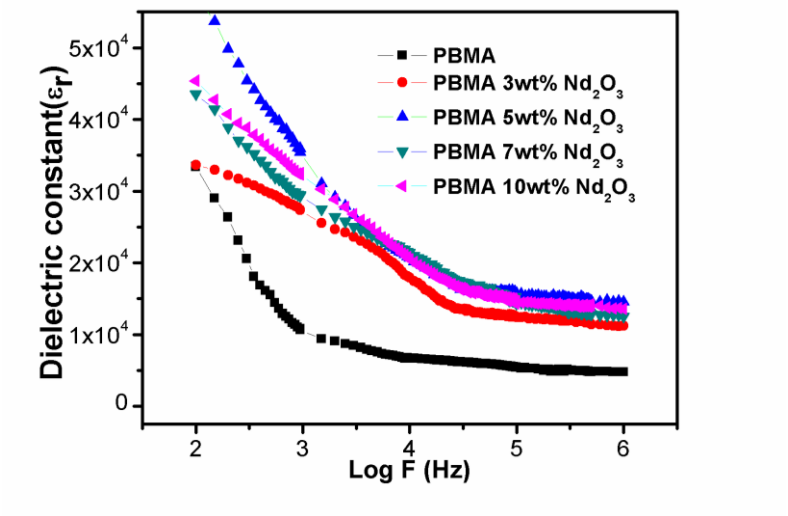

Figure 7.14: Variation of dielectric constant (ε_r) of PBMA and PBMA/Nd_2O_3 nanocomposites at different frequencies

Figure 7.15 shows the variation of AC conductivity ($\sigma_{a.c}$) with frequency for PBMA and PBMA/Nd_2O_3 nanocomposites. It can be seen that the conductivity increases with applied frequency in all cases in a non-perfect linear manner, which implies the composites follows non-ohmic type conduction. Further, the $\sigma_{a.c}$ of bare PBMA is significantly improved by the addition of Nd_2O_3 nanoparticles up to 5 wt% loading and then a slight decrease is observed. However, the increase in $\sigma_{a.c}$ with the addition of nanoparticles is more pronounced at a lower frequency and at the higher frequency, it remains almost the same for all the composites. By the addition of nanoparticles, there is number of charge carriers as well as there is a gradual development of the conductive network. Moreover, the contribution from interfacial polarization by the better polymer-filler interface along with the

electronic polarization also added to higher conductivity with the addition of nanoparticles [214]. The decrease in conductivity at higher concentration might be due to poor polymer-filler interface by the presence of agglomerated nanoparticles.

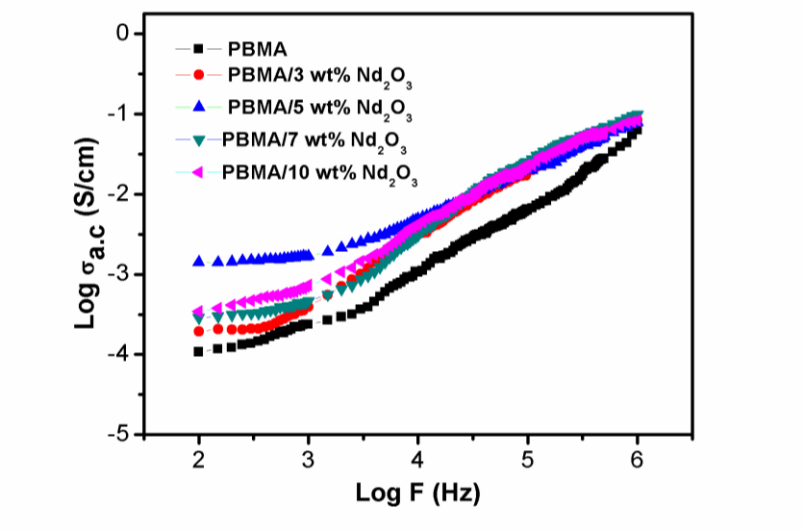

Figure 7.15: Variation of AC conductivity ($\sigma_{a.c}$) with frequency for the PBMA and PBMA/Nd_2O_3 nanocomposites

The dependence of conductivity on temperature has been explained by two models, small polaron and large polaron model [261]. Based on the small polaron model, the conductivity arises from the thermally activated hopping of charge carries and so here the conductivity increases with the temperature. But, in large polaron model, the conductivity decreases with temperature. For PBMA/Nd_2O_3 nanocomposites, the conductivity measurements are carried out at different temperatures (from 303 to 353 K) and the plot showing the variation of $\sigma_{a.c}$ with frequency at different temperatures are given in **figure 7.16.** As seen from the plot, the conductivity increases with temperature in all cases, which means that the PBMA/Nd_2O_3

composites follow hopping conduction model. The reason for the increase in conductivity can be explained as, with a rise in temperature the polymer segment gets extra mobility and thus creates the free volume which facilitates more hoping of charge carriers [262]. In addition to this, the charge carriers also get activated by the extra thermal energy and thus increase the rate of hopping and exhibit more conductivity. Further, the thermally activated charge carriers may create space charge centers by the accumulation of charge carriers and at still high temperature, there is the formation of more space charge sites and creates more polarization, which also added to enhanced conductivity at high temperatures [263].

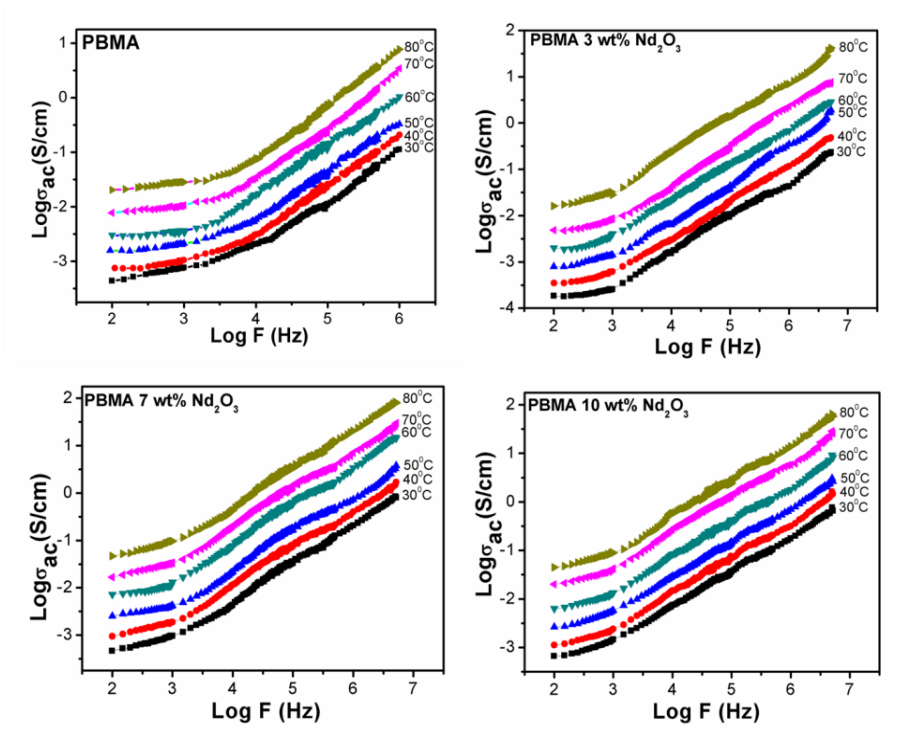

Figure 7.16: Temperature dependent AC conductivity of PBMA and PBMA/Nd_2O_3 nanocomposites

The activation energy values of PBMA and PBMA/Nd_2O_3 nanocomposites are measured from the plot of log($\sigma_{a.c}$) vs 1000/T at different frequencies. The plot is presented in **figure 7.17** and the obtained activation energy values are given in **table 7.2.** The linear nature of the plots in all cases implies the thermally activated hopping conduction in the PBMA/Nd_2O_3 nanocomposites, as explained above. As clear from the table, the activation energy values are decreasing with frequency also shows the hopping conduction in PBMA/Nd_2O_3 nanocomposites. Further, the activation energy values are decreasing with the addition of Nd_2O_3 nanoparticles indicates the significantly improved conductivity of PBMA/Nd_2O_3 nanocomposites than the pure PBMA.

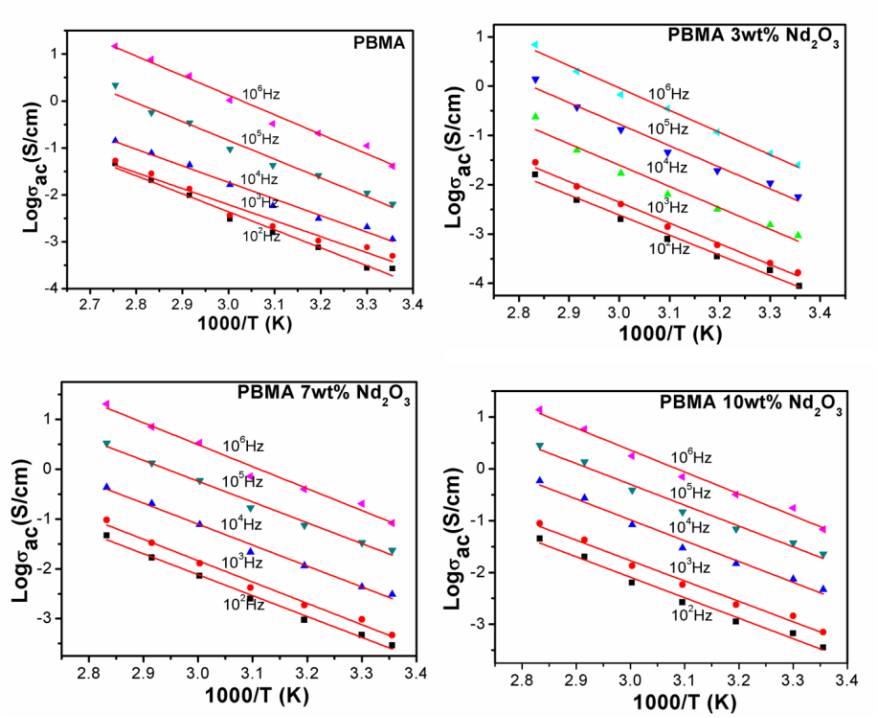

Figure 7.17: Log($\sigma_{a.c}$) versus 1000/T plot for PBMA and PBMA/Nd_2O_3 nanocomposites at different frequencies

Table 7.2: The activation energy values of PBMA and PBMA/Nd_2O_3 nanocomposites

Samples	Frequency (Hz)				
	10^2	10^3	10^4	10^5	10^6
PBMA	-3.834	-3.414	-3.531	-4.005	-4.167
PBMA/3 wt% Nd_2O_3	-4.078	-4.205	-4.331	-4.369	-4.513
PBMA/5 wt% Nd_2O_3	-4.329	-4.598	-4.736	-4.762	-4.801
PBMA/7 wt% Nd_2O_3	-4.198	-4.203	-4.282	-4.303	-4.324
PBMA/10 wt% Nd_2O_3	-3.906	-3.933	-4.018	-4.208	-4.221

The dependence of conductivity on frequency at different temperatures is given as $\sigma_{a.c} = A\omega^s$, where A is the pre-exponential factor, constant at a particular temperature and 's' is the exponential factor, its value determines the degree of interaction of charge carriers with the surroundings [146]. Generally, the value of s lies between 0 and 1. Further, if the 's' value decreases with temperature the system follows hopping conduction and if the 's' value increases with temperature the system possess localized sites for conduction. The 's' value is measured from the plot of $\log(\sigma_{a.c})$ vs $\log(\omega)$. In the case of PBMA/Nd_2O_3 nanocomposites the 's' value is calculated at different temperatures and the obtained values are documented in **table 7.3.** It is clear from the table that the 's' value is less than one in all the cases and further the 's' value decreases with temperature which further confirms the hopping conduction in PBMA/Nd_2O_3 composites. Moreover, the dependence of 's' value on temperature indicates that a thermally activated polaron hopping conduction takes place in the case of PBMA/Nd_2O_3 nanocomposites.

Table 7.3: Frequency exponential factor 's' at different temperatures for PBMA and PBMA/Nd_2O_3 nanocomposites.

Samples	Temperature(°C)					
	30	**40**	**50**	**60**	**70**	**80**
PBMA	0.6018	0.6017	0.6168	0.6159	0.6141	0.6138
PBMA/3 wt% Nd_2O_3	0.7454	0.7432	0.7426	0.7422	0.7419	0.7415
PBMA/5 wt% Nd_2O_3	0.7544	0.7540	0.7536	0.7533	0.7529	0.7525
PBMA/7 wt% Nd_2O_3	0.7481	0.7476	0.7470	0.7463	0.7460	0.7458
PBMA/10 wt% Nd_2O_3	0.7352	0.7348	0.7345	0.7341	0.7334	0.7330

7.2.9 DC Conductivity Studies

Metal oxide nanoparticles, especially Nd_2O_3 nanoparticles having considerable semiconducting properties can impart good electrical properties to the insulating polymer matrix. The variation in DC conductivity ($\sigma_{d.c}$) of PBMA with different loading of Nd_2O_3 nanoparticles is presented in **figure 7.18.** It is clear that the $\sigma_{d.c}$ of PBMA is substantially improved by the addition of Nd_2O_3 nanoparticles. Further, the $\sigma_{d.c}$ value is increasing with the loading of Nd_2O_3 nanoparticles. However, from 0 to 3 wt% the composites exhibit a drastic change in the $\sigma_{d.c}$ (from 4.23 $x10^{-12}$ to 4.3$x10^{-9}$ S/cm) and after that, there is not much variation in the values especially after 5 wt% loading. The $\sigma_{d.c}$ of the 3 wt% composite is obtained at 4.3$x10^{-9}$ S/cm, while that of 5, 7 and 10 wt% composites are measured at 5.9$x10^{-9,}$ 4.6$x10^{-9,}$ 4.4$x10^{-9}$ S/cm respectively. The conductivity of PBMA arises from the restricted movement of bipolaron charge centers under the applied voltage [150]. But in the case of composites there is a gradual formation of conducting network within the polymer matrix by the insertion of Nd_2O_3 nanoparticles, which results in higher

conductivity of composites than the bare PBMA. Also, the interfacial polarization at the interface between the nanoparticles and PBMA matrix further contributes to the enhanced conductivity of PBMA/Nd_2O_3 nanocomposites [264]. The maximum conductivity is obtained for PBMA with 5 wt% Nd_2O_3 and beyond the 5 wt% loading the conductivity is slightly decreasing which might be due to the presence of agglomerated nanoparticles in the PBMA matrix at higher concentrations.

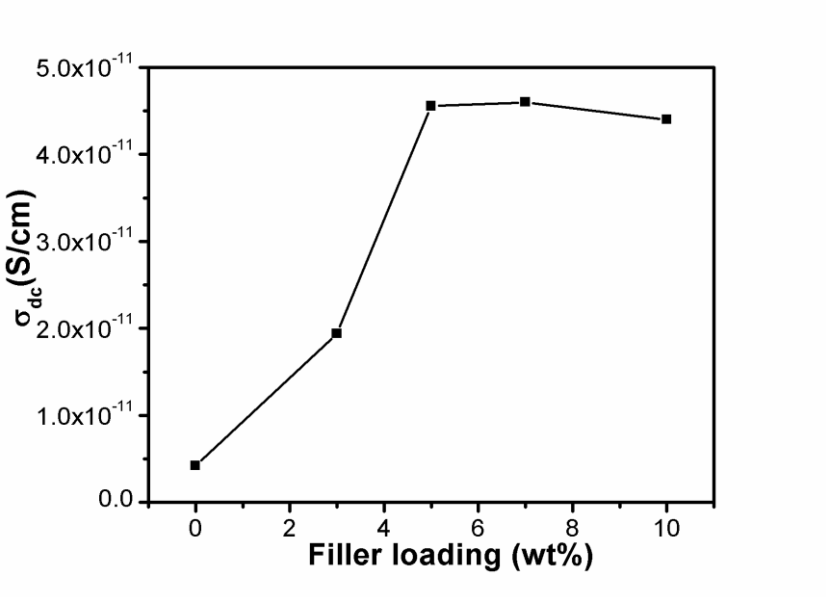

Figure 7.18: The variation of DC conductivity of PBMA/Nd_2O_3 nanocomposites as a function of filler loading

7.2.10. Theoretical Modeling to DC Conductivity

Several theoretical models have been used to investigate the role of fillers in the conductive mechanism in a polymer matrix. These models have been formulated on the basis of various assumptions. The main

focus of these models is to explain how the conducting network is formed in the polymer composite and also to explain the effect of other parameters like the interaction of filler and polymer, nature of fillers, the arrangement and concentration of fillers for enhancing the conductivity properties of the composite materials. In the present work different theoretical models like Bueche, Scarisbrick and McCullough models are employed to predict the conductivity of PBMA nanocomposites containing different loading of Nd_2O_3 nanoparticles.

7.2.10.1 Bueche Model

Bueche model describes that the conductivity of binary systems like polymer nanocomposites consisting of conducting nanoparticles dispersed in an insulating polymer matrix is a parallel connection of individual conductivity of these two phases [151]. The basic assumption in this model is that the conductivity in composites occurs through the conducting network formed by the particle aggregation and therefore, the conductivity of polymer composites can be expressed as:

$$\sigma c = \Phi f \sigma f + (1 - \Phi f)\sigma p \qquad (7.6)$$

where σc, σp and σf represent the DC conductivity ($\sigma_{d.c}$) of the composite, polymer matrix and the filler respectively and Φf represents the filler volume fraction. The measured value of $\sigma_{d.c}$ for PBMA (σp) is 4.23 $x10^{-12}$ S/cm and for Nd_2O_3 nanoparticles (σf) is 7.96x 10^{-7}S/cm. Using the Bueche model, the theoretical $\sigma_{d.c}$ of PBMA/Nd_2O_3 nanocomposites at different loading of nanoparticles are calculated and a comparative graph of theoretically calculated conductivity and experimental conductivity is presented in **figure 7.19.** As seen, though

the trend in increasing the $\sigma_{d.c}$ with nanoparticle loadings is the same in both cases, the theoretically calculated conductivity using Bueche equations shows much deviation from the experimental conductivity. So Bueche model is not a suitable one to predict the conductivity of PBMA/Nd_2O_3 nanocomposites. Since the Bueche model is based on the additive rule and it is suitable to binary systems in which there is not much difference in the conductivity values of individual components.

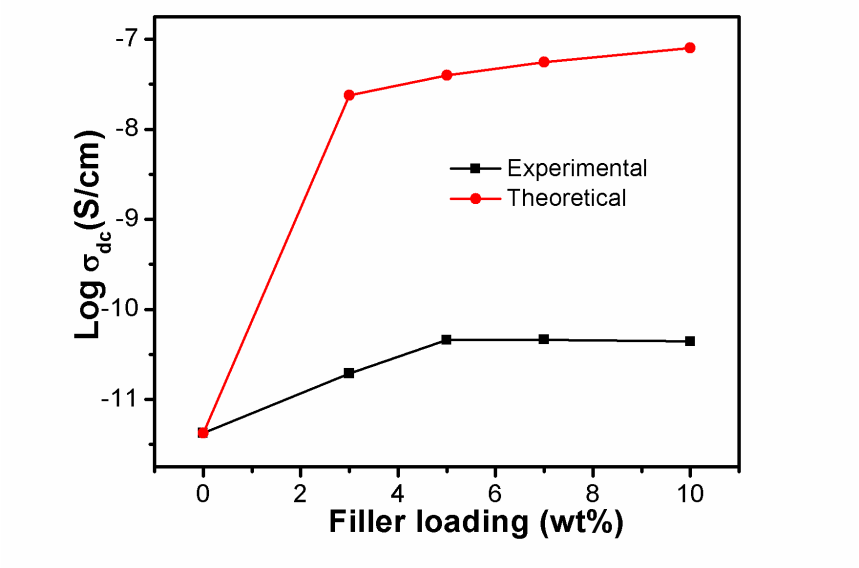

Figure 7.19: Theoretical $\sigma_{d.c}$ obtained from Bueche model and experimental conductivity of PBMA/Nd_2O_3 nanocomposites

7.2.10.2 Scarisbrick Model

Scarisbrick assumed that the conductivity is accompanied by inter-particle contact within the polymer matrix and thus conductivity mainly depends on the amount as well as the arrangement of filler

present in the matrix [152]. The Scarisbrick model can be expressed as the following equations.

$$\frac{\sigma c}{\sigma f} = C^2.\Phi.\Phi[exp(\Phi^{-\frac{2}{3}})] \quad (7.7)$$

$$\frac{\sigma c}{\sigma f} = \Phi.\Phi\left[ex\,p\left(\Phi^{-\frac{2}{3}}\right)\right] (\text{When } C^2 = 1) \quad (7.8)$$

$$\frac{\sigma c}{\sigma f} = 3\ x\ 10^{-3}.\Phi.\Phi[exp(\Phi^{-\frac{2}{3}})] \ (\text{When } C^2 = 3\text{x}10^{-3}) \quad (7.9)$$

where C^2 is the geometric factor, its value defines the dispersion mode of filler in the polymer matrix and also the interface between the polymer matrix and the filler. The value of C^2 lies between 1 and 3 x 10^{-3}. The conductivity ($\sigma_{d.c}$) of PBMA/Nd_2O_3 nanocomposites are calculated using the Scarisbrick model (**equations: 7.7-7.9**) and the comparative graph of theoretical and experimental $\sigma_{d.c}$ is given in **figure 7.20.** From figure, it can be seen that the experimental conductivity is remarkably lower than the theoretical conductivity at the entire loading of Nd_2O_3 nanoparticles for both C^2 values. At lower filler concentrations the theoretical conductivity value and experimental conductivity value shows large deviations compared to the case at higher concentrations. The exact value of C^2 is difficult to find and also in this model the contribution from the polymer matrix does not consider. Therefore the theoretical conductivity using the Scarisbrick model exhibits large deviations from the experimentally determined conductivity for all composites, especially at lower concentrations.

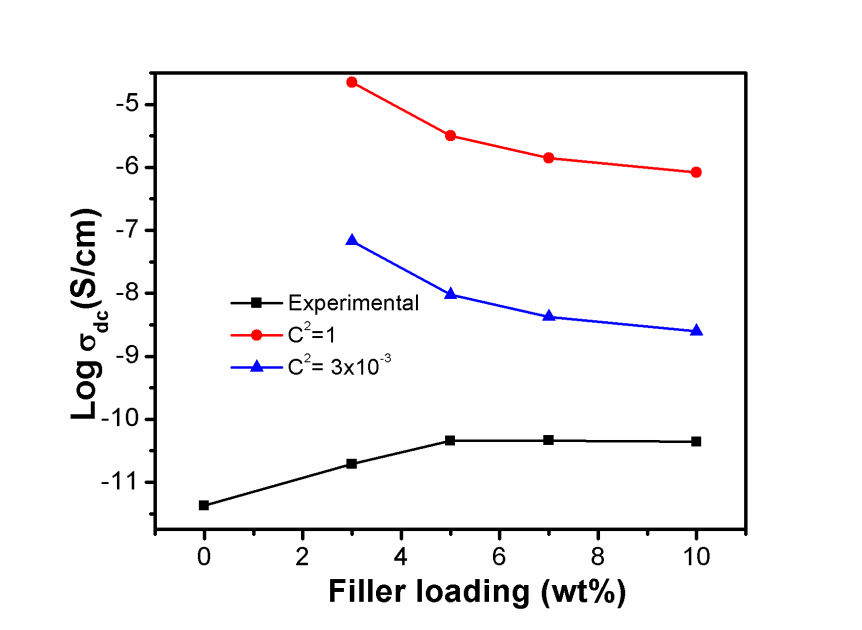

Figure 7.20: Theoretical $\sigma_{d.c}$ obtained from Scarisbrick model and experimental conductivity of PBMA/Nd_2O_3 nanocomposites

7.2.10.3 McCullough Model

McCullough proposed a model for predicting the transport properties of binary systems and can also use for calculating the conductivity polymer composites [150]. The equation is as follows.

$$\sigma c = \sigma p.\Phi p + \sigma f.\Phi f - \left[\frac{\lambda.\Phi p.\Phi f+(\sigma f-\sigma p)^2}{vf.\sigma f+vp.\sigma p}\right] \qquad (7.10)$$

Where λ is the structural factor, indicate the extent of conductive network formation in the polymer matrix and its value differ from 0 to 1, vf and vp are given as

$$vf = (1-\lambda).\Phi f + \Phi p.\lambda \qquad (7.11)$$

$$vp = (1-\lambda).\Phi p + \Phi f.\lambda \qquad (7.12)$$

The theoretical conductivity of PBMA/Nd_2O_3 nanocomposites is determined from the McCullough model (**equations: 7.10-7.12**) for different λ values and the comparative graph of theoretical and experimental conductivity is presented in **figure 7.21.** The theoretical conductivity using the McCullough model greatly depends on the λ values which in turn dependent on filler properties and so the exact value of λ is not known. So to validate the McCullough model the conductivity is calculated for various λ values. Interestingly, in the of PBMA/Nd_2O_3 nanocomposites, the experimental conductivity shows large deviations from that of the theoretical conductivities. So McCullough model also fails in the case of PBMA/Nd_2O_3 nanocomposites.

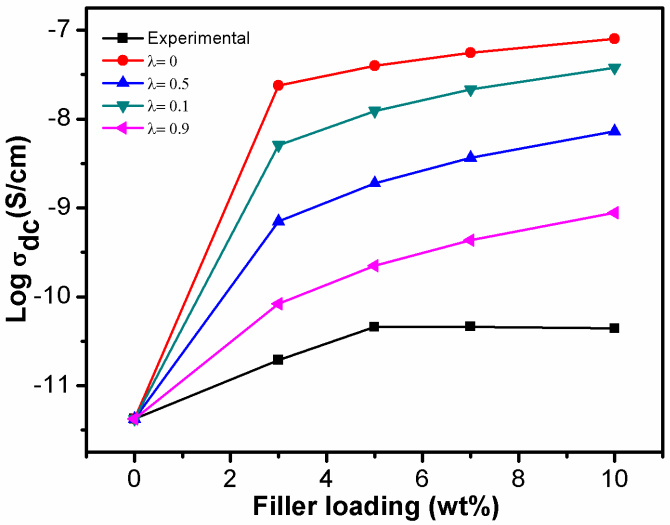

Figure 7.21: Theoretical $\sigma_{d.c}$ obtained from McCullough model and experimental conductivity of PBMA/Nd_2O_3 nanocomposites

7.2.10.4 Proposed Model for PBMA/Nd_2O_3 Composites

The electrical conductivity determined from Scarisbrick, Bueche and McCullough model are fails to explain the conductivity of PBMA/Nd_2O_3 composites because of the difference in conductivity of pure polymer and the nanoparticles. The mismatch between theoretical and experimental conductivity can be overcome by considering the factors affecting the composite properties such as geometry, morphology, aspect ratio, shape and size. Here we suggest a new model by considering the shape factor (S) of the composite system as:

$$log\sigma c = \frac{\Phi p.\log \sigma p + \Phi f.S.log\sigma f}{\Phi p.e^{\Phi f} + \Phi f.S.e^{\Phi p}} \qquad (7.13)$$

The experimental conductivity values are applied to the above proposed equation and the result is given in **figure 7.22**. The resultant conductivity value from proposed model is in good agreement with the experimentally measured values. This finding has been considered encouraging for developing new and innovative thermoplastic composite materials for using augmented tensile strength and nano-electronics devices.

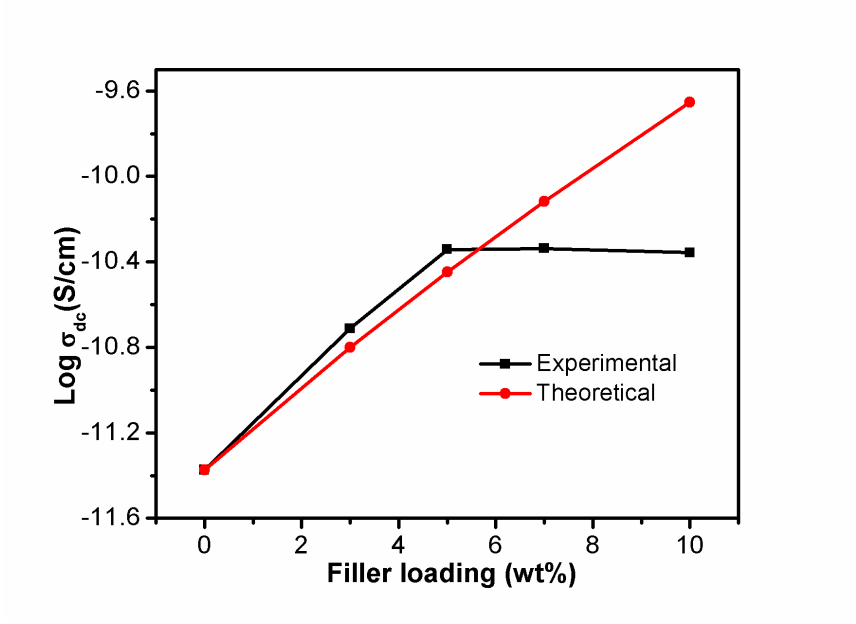

Figure 7.22: Theoretical $\sigma_{d.c}$ obtained from proposed model and experimental conductivity of PBMA/Nd_2O_3 nanocomposites

7.3 Conclusion

The PBMA/Nd_2O_3 nanocomposites were prepared by in situ polymerization method. It was characterized by different analytical techniques. The FT-IR and UV spectra revealed the successful incorporation of Nd_2O_3 nanoparticles in the PBMA matrix. The result from XRD revealed a systematic and ordered arrangement of Nd_2O_3 nanoparticles in the PBMA matrix. The SEM images showed the uniform dispersion of nanoparticles and the TEM images revealed that the size of nanoparticles in the polymer was in nano-regime. The DSC results showed that the prepared composites showed a higher glass transition temperature than pure PBMA. Also, the thermal stability of

nanocomposite was higher than PBMA and the thermal stability increased with the loading of nanoparticles in the polymer. The tensile strength of PBMA composites was substantially enhanced with the loading of nanoparticles, however, the elongation at break decreased with the addition of nanoparticles. The nanocomposite reinforced with 5 wt% Nd_2O_3 nanoparticles showed the highest mechanical strength compared with loading of fillers. The experimental data of the tensile strength were compared with those from the Einstein, Mooney, and Pukanszky models, and were found to be in good agreement with the Pukanszky model indicating the better interfacial interaction between the PBMA and Nd_2O_3 nanoparticles. The effect of loading of Nd_2O_3 on AC conductivity and activation energy of PBMA nanocomposites was studied at different temperatures and frequencies and these properties were substantially improved with the addition of Nd_2O_3 nanoparticles. The AC conductivity of nanocomposites was higher than pure PBMA and the magnitude of conductivity increased with an increase in temperatures. The higher AC conductivity of nanocomposite at higher temperatures was due to the increased segmental movement of composite material. Among the nanocomposites, the 5 wt% composite shows the maximum AC conductivity. The activation energy, as well as exponential parameter calculations, showed that the PBMA/Nd_2O_3 nanocomposites were following the hopping conduction mechanism. The DC conductivity of PBMA was also significantly improved with the addition of Nd_2O_3 nanoparticles. The experimental DC conductivity values were also correlated with the various theoretical

assumptions by Bueche, Scarisbrick and McCullough models. All these model fails to explain the conductivity of composite material and therefore we proposed a new model for theoretical conductivity which fit very well with experimental conductivity.

CHAPTER 8

CONCLUSION AND FUTURE OUTLOOKS

Contents

8.1 Conclusion

The effect of metal oxide nanoparticles on the structural, thermal, mechanical and electrical properties of poly (butylmethacrylate) (PBMA) has been studied in detail. PBMA belongs to the family of acrylate thermoplastic polymers with good flexibility, light weight, transparency, good processability, protection against ultraviolet radiation, good weather stability, high strength, and dimensional stability. Moreover, the combination of polyacrylates with metal oxide nanoparticles results in composites having better electrical property, thermal, and mechanical stability. The electrical conductivity of insulating polymer can be enhanced by proper dispersion of conductive fillers. Recently, there is an increased demand for flexible conductive composite by the incorporation of the relatively small amount (1–15 phr) of conductive fillers, which convert the thermoplastic material into a semi-conductive one. Fillers such as transition as well as rare earth metal oxide nanoparticles are promising reinforcement for developing polymer nanocomposites possessing excellent mechanical and electrical properties. TiO_2, CeO_2 and Nd_2O_3 have been widely used owing to their outstanding properties including good optical properties, better surface properties and thermal and electrical conductivity. Reports showed that incorporation of metal oxide nanoparticles like TiO_2, CeO_2 and Nd_2O_3 into polymer matrix results nanocomposites with excellent conductivity, better mechanical properties and superior structural stability.

In this work, TiO_2, Ce doped TiO_2, Nd doped TiO_2, CeO_2 and Nd_2O_3 nanoparticles were incorporated into PBMA polymer via in situ

polymerization method. The structural and morphological characteristics of developed PBMA nanocomposites were analyzed via FT-IR, UV, XRD, FE-SEM and TEM analysis. The thermal properties were studied by DSC and TGA. The effect of nanoparticle addition on tensile properties was studied in detail. Moreover, the electrical properties like AC and DC conductivity of the developed nanocomposites were studied. Further, various theoretical modeling studies were employed in order to investigate the mechanism behind the enhanced tensile and DC conductivity properties.

The PBMA nanocomposites with different loading of TiO_2 nanoparticles were successfully developed. The FT-IR spectra of the nanocomposites showed the better interface between the PBMA matrix and the TiO_2 filler. The UV studies showed that the nanocomposite with 7 wt% exhibits the maximum absorption and after the absorption intensity was decreasing indicate the maximum limit of homogenous dispersion in the case of 7 wt% loading. At higher loading of fillers the homogenous dispersion was interrupted might be due to the presence of agglomerated particles. The XRD results showed the ordered dispersion and better compatibility between the matrix and filler by increase in percentage crystallinity upon addition of TiO_2 nanoparticles. The morphological studies showed the homogenous dispersion of TiO_2 nanoparticles in the PBMA matrix and the maximum dispersion of filler was observed in 7 wt% loading. The TEM images confirmed the better compatibility between the incorporated TiO_2 nanoparticle and the PBMA matrix. The DSC and TGA studies revealed the enhanced thermal stability of PBMA/TiO_2

nanocomposites than the bare PBMA obviously due to the better interface between the matrix and filler. The PBMA/TiO_2 nanocomposites also showed significant improvement in the tensile properties and here also the 7 wt% loading exhibits the maximum property. Theoretical predictions based on Einstein, Mooney, Guth and Pukanszky equations for tensile properties of composites were carried out and among these models Pukanszky shows close match with the experimental tensile values. The dielectric, AC and DC conductivity of composites also substantially enhanced by the TiO_2 nanoparticle addition. The studies showed that the conductivity of composites increases with loading of nanoparticle (maximum is in 7 wt% loading) and increase in temperature. The DC conductivity of the polymer composites were also predicted using theoretical models based on Bueche, Scarisbrick, McCullough and Mamunya models. In Bueche, Scarisbrick and McCullough models the theoretical value exceeds than that of experimental values. However, Mamunya model exhibits better fit that of experimental conductivity. Thus it can be concluded that the conductivity of PBMA/TiO_2 nanocomposites was mainly governed by the interface between PBMA matrix and the filler.

The effect of Ce doped TiO_2 nanoparticle on the structural, thermal, mechanical and electrical properties of PBMA was systematically studied. The FT-IR, UV-Visible and XRD studies showed the successful and homogenous incorporation of Ce-TiO_2 nanoparticle in the PBMA matrix with better interface between them. The SEM images also revealed the homogenous dispersion and 7 wt% shows the maximum limit. Above 7 wt% the presence of agglomerated

nanoparticles were visible in SEM images. The higher Tg and thermal stability of PBMA/Ce-TiO_2 nanocomposites indicate the favourable thermal properties of composites than the bare PBMA. The nanocomposite shows excellent tensile strength than pure PBMA and the composite with 7 wt% sample shows the maximum tensile strength. The reinforcing nature of Ce-TiO_2 nanoparticles in PBMA was also carried with different theoretical modeling such as Einstein, Mooney and Pukanszky equations. Among these models, Pukanszky model showed better agreement in PBMA/Ce-TiO_2 nanocomposites. The AC conductivity, dielectric properties of the PBMA/Ce-TiO_2 nanocomposites was significantly higher than pure PBMA and these properties increases with filler loading up to 7 wt% and after that it decreases. Further, the AC conductivity of PBMA and all PBMA/Ce-TiO_2 nanocomposites showed direct dependence on the temperature as well as frequency. The activation energy and exponential parameter was determined from temperature dependent AC conductivity studies and the values showed that the PBMA/Ce-TiO_2 nanocomposites follow hopping conduction model. The DC conductivity of all the nanocomposites was higher than pure PBMA and the conductivity increased regularly with the loading of nanoparticles. Various theoretical models were studied based on Scarisbrick, McCullough, Bueche and Mamunya equations to predict the DC conductivity nature of PBMA/Ce-TiO_2 nanocomposites. The conductivity calculated using the thermodynamic model introduced by Mamunya showed the best agreement with that of the experimental data. However, the statistical approaches given by Scarisbrick, McCullough and Bueche models fail to predict the conductivity of PBMA/Ce-TiO_2 nanocomposites. Thus

the prepared PBMA/Ce-TiO_2 nanocomposites showed excellent tensile strength, thermal stability, and electrical properties, and therefore this composite can be used as a promising material for nanoelectronic devices and various electromagnetic shielding.

The change in the structural, thermal and mechanical properties of PBMA with the loading of Nd-TiO_2 nanoparticles was studied. The FT-IR spectra clearly indicated the successful addition of Nd-TiO_2 nanoparticles in the PBMA matrix by the presence of Ti-O vibration peak. The shift in absorption edge of UV-Visible spectra indicated the enhancement in optical properties of PBMA by the addition of Nd-TiO_2 nanoparticles and the 7 wt% loaded sample showed the maximum property. The appearance of crystalline peaks of Nd-TiO_2 in the XRD of PBMA composite shows better compatibility between the matrix and filler. The SEM study further revealed the homogenous distribution of nanoparticles in the polymer matrix. The glass transition temperature (Tg) from DSC and the degradation temperature of nanocomposites from TGA were shifted to higher temperatures and this indicated the enhanced thermal stability of PBMA with the addition of Nd-TiO_2 nanoparticles. The improved tensile strength of composites showed the effective interfacial interaction between the nanoparticle and matrix. The reinforcing nature of nano-filler in PBMA was studied with various theoretical models based on Einstein, Mooney and Pukanszky. Among the models, Pukanszky showed the best agreement with the experimental tensile plots. The AC conductivity of hybrid nanocomposites was increased with increase in loading of nanoparticles as well as with temperature and frequencies.

The parameters such as activation energy and the exponent values were determined and the variations in their value denoted the hopping conduction mechanism present in the PBMA/Nd-TiO_2 nanocomposites. Among the nanocomposites, the 7 wt% sample shows the maximum AC conductivity. The DC conductivity also showed the significant enhancement with loading of nanoparticles. The loading of nanoparticles creates continuous conducting network which facilitate the hopping of charge carriers results in an increase in the DC conductivity. The applicability of DC conductivity was investigated by various theoretical models like McCullough, Bueche, Scarisbrick and Mamunya models. The theoretical conductivity obtained from Mamunya model was more suitable for the experimental conductivity of PBMA/Nd-TiO_2 nanocomposites, suggest that in the case of PBMA/Nd-TiO_2 nanocomposites, there have an effective interfacial interaction between both the components and it was responsible for the improved conducting properties of PBMA nanocomposites than the plane PBMA.

PBMA nanocomposites reinforced with CeO_2 nanoparticles also displayed outstanding mechanical and electrical properties due to the effective dispersion of CeO_2 nanoparticles in the PBMA matrix. The FT-IR spectra showed the better incorporation of nanoparticles and the UV-Visible spectra revealed the effective interfacial interaction of nanoparticles with the PBMA matrix. The appearance of crystalline peaks in PBMA/CeO_2 nanocomposites obtained from the XRD profile showed the more ordered dispersion of nanoparticles in the polymer matrix. The morphologies (from SEM and TEM) of PBMA/CeO_2

nanocomposites clearly showed the homogenous dispersion of nanoparticles. The higher glass transition temperature as well as decomposition temperature showed the enhanced thermal properties of PBMA with the addition of CeO_2 nanoparticles. The addition of CeO_2 nanoparticles increased the tensile property of PBMA by the interfacial interaction between them and the 7 wt% loaded sample shows the maximum. The nanoparticles act as stress relieving sites and therefore the composites exhibits maximum property. The comparison of experimental tensile strength with theoretical models like Einstein, Mooney, Guth, Kerner and Pukanszky equation was carried out and the results shows the Pukanszky model was more applicable in the case of PBMA/CeO_2 nanocomposites. The dielectric, AC conductivity and DC conductivity also showed significant improvement with the loading of CeO_2 nanoparticles. The changes in DC conductivity values of PBMA/CeO_2 nanocomposites were correlated with theoretical models like Bueche, Scarisbrick and McCullough models. The Bueche, Scarisbrick and McCullough model fails to explain the conductivity of polymer composite in the entire loading of fillers. So we proposed a new model for theoretical conductivity, which is in good agreement with the experimentally observed conductivity and therefore this proposed model can be applied to thermoplastic polymers nanocomposite system.

Nd_2O_3 nanocomposites were also introduced into PBMA matrix in different weight percentages and study the changes in structure, morphology, thermal, mechanical and electrical properties were studied systematically. Both FT-IR and UV spectra revealed the

successful incorporation of Nd_2O_3 nanoparticles in the PBMA matrix. The presence of crystalline peaks and the decrease in intensity of amorphous peak in the XRD spectra revealed a systematic and ordered arrangement of Nd_2O_3 nanoparticles in the PBMA matrix. The SEM images showed the uniform dispersion of nanoparticles and the TEM images revealed that the size of nanoparticles in the polymer was in nano-regime. However, in the case of PBMA/Nd_2O_3 nanocomposites the 5 wt% sample showed the maximum limit of homogenous dispersion. Both DSC and TGA results showed the enhanced thermal properties of PBMA composites than bare PBMA by increase in the value of glass transition and degradation temperature respectively. The nanocomposite reinforced with 5 wt% Nd_2O_3 nanoparticles showed the highest mechanical strength compared with other percentages. The experimental data of the tensile strength were compared with those from the Einstein, Mooney, and Pukanszky models, and were found to be in good agreement with the Pukanszky model indicating the better interfacial interaction between the PBMA and Nd_2O_3 nanoparticles. The AC conductivity and activation energy of PBMA nanocomposites was studied at different temperatures and frequencies and these properties were substantially improved with the addition of Nd_2O_3 nanoparticles. The higher AC conductivity of nanocomposite at higher temperatures was due to the increased segmental movement of composite material. Among the nanocomposites, the 5 wt% composite shows the maximum AC conductivity. The activation energy, as well as exponential parameter calculations, showed that the PBMA/Nd_2O_3 nanocomposites were following the hopping conduction mechanism. The DC conductivity of PBMA was also significantly improved with

the addition of Nd_2O_3 nanoparticles. The experimental DC conductivity values were also correlated with the various theoretical assumptions by Bueche, Scarisbrick and McCullough models. These entire models fail to explain the conductivity of composite material and therefore we proposed a new model for theoretical conductivity which fit very well with experimental conductivity.

All the experimental results in this work revealed that the PBMA nanocomposites incorporated with doped and un doped metal oxide nanoparticles are applicable in electronic devices owing to their considerable mechanical and electrical properties.

8.2 Future outlooks

The properties of polymer nanocomposites greatly depend on the type of filler, matrix, the mode of distribution of filler in the matrix and the compatibility between the filler and matrix. So, more systematic studies are further needed for developing polymer composites exhibiting outstanding properties. From this point of view, we pointed some future works to be undertaken.

- Development of nanocomposites using the butylmethacrylate with various functional metal oxide nanoparticles
- Investigate the more suitable nanofillers by examining various types of conducting fillers for developing composites with better properties
- Explore the optical applications of PBMA composites containing TiO_2 and CeO_2 nanoparticles.

- ❖ Detailed study on dielectric constant and dielectric loss at various temperatures
- ❖ Fabrication of copolymers based on butylmethacrylate with other functional monomers
- ❖ Reinforcement of various functional nanoparticles with copolymer based on butylmethacrylate
- ❖ Development of nanocomposites applicable for nanoelectronic devices

REFERENCES

REFERENCES

1. M. E. Avval, P.N. Moghadam, M. M. Baradarani, Polym. Compos. 40 (2018) 730-737.

2. F. Chouli, I. Radja, E. Morallon, A. benyoucef, Polym. Compos. 38 (2017) 254-260.

3. F. Magalhaes, F. C. C. Moura, R. M. Lago, Desalination. 276 (2011) 266-271.

4. T. Otsuka, Y. Chujo, Polym. J. 42 (2010) 58-65.

5. M. S. Zoromba, N. M. Hosn, J. Therm. Anal.Calorim.119 (2015) 605-611.

6. D. K. Koli, G. Agnihotri, R. Purohit, Int. J. Late. Trends Eng. Technol. 2 (2013) 486-496.

7. G. Fredi, A. Dorigato, A. Pegoretti, EXPRESS Polym. Lett. 12 (2018) 349–364.

8. Q. Meng, Y. Gu, L. Luo, S. Wang, M. Li, Z. Zhang, J. Appl. Polym. Sci. 134 (2017) 44832-44842.

9. Y. Gong, G. Yang, J. Mater. Sci. 44 (2009) 4639-4644.

10. N. Yesildag, C. Hopmann, M. Adamy, C. Windeck, AIP Conference Proceedings. 1914 (2017) 150001

11. I. Mohagheghian, G. J. McShane, W. J. Stronge, Procedia. Eng. 10 (2011) 704–709.

12. S. Park, S. He, J. Wang, A. Stein, C. W. Macosko, Polymer. 104 (2016) 1-9.

13. A. U. Chaudhry, V. Mittal, Polym. Eng. Sci. 53 (2013) 78-88.

14. F. Faraguna, P. P€otschke, J. Pionteck, Polymer. 132 (2017) 325-341.

15. S.W. Zhang, S. X. Zhou, Y. M. Weng, L. M. Wu, Langmuir. 21 (2005) 2124-2128.

16. D. Han, Q. Y. Guo, W. B. Zhang, L. X. Liu, Q. Fu, J. Name. 00 (2013) 1-3.

17. M. Ochi, R. Takahashi, A. Terauchi, Polymer. 42 (2001) 5151-5158.

18. S. Mallakpoura, E. Shafiee, Des. Monomers. Polym. 20 (2017) 378-388.

19. J. Pagacz, K. Pielichowski, J. Therm. Anal. Calorim. 111 (2013) 1571-1575.

20. T. A. Taha, J. Mater. Sci: Mater. Electron. 28 (2017) 12108-12114.

21. M.C. Duffy, J. Am. Inst. Conservat. 28 (1989) 67-77.

22. J. Brus, P. Kotlik, Stud. Conserv. 41 (1996) 109-119.

23. S. Paul, Surface Coatings Science and Technology, Wiley, New York, (1996)

24. H.V. Pechmann, O. Röhm, B. Deutschen, C. Gesellschaft, 34 (1901) 427-429.

25. H.U. Moritz, Chem. Eng. Technol. 12 (1989) 71-87.

26. G. Stoev, M. Angelova, J. High. Resolut. Chrom. 10 (1987) 25-26.

27. X. S. Chai, Q.X. Hou, F.J. Schork, J. Chromatogr. 1040 (2004) 163-167.

28. Röhm, Haas US 1 829 208 (W. Bauer) (1931).

29. ICI ltd. US 2 117 321 (R. Hill) (1938).

30. Röhm & Haas US 2 193 742 (O. Röhm and W. Bauer) (1940).

31. I.G. F. Aktiengesellschaft US 2 140 048 (H. Fikentscher and C. Heuck) (1938).

32. M. Do. Amaral, S. V. Es, J.M. Asua, J. Polym. Sci. Part A: Polymer Chemistry, 42 (2004) 3936-3946.

33. J. Trivedi, T. Bhatt, H. Trivedi, Cellulose. Chem. Technol. 48 (2014) 503-514.

34. D. Briesenick, W. Bremser, Prog. Org. Coat. 82 (2015) 26-32.

35. W. Work, K. Horie, M. Hess, R. Stepto, Pure and Applied Chemistry. 76 (2004) 1985-2007.

36. V. C. Jasna, M. T. Ramesan, J. Inorg. Organomet. Polym. 27 (2017) 968–978.

37. R. Verdejo, M. M. Bernal, L. J. Romasanta, F. A. Tapiador, M. A. Lopez-Manchado, J. Cell. Polym. 30 (2011) 45-62.

38. F. P. Schmidt, H. Ditlbacher, U. Hohenester, A. Hohenau, F. Hofer, J. R. Krenn, Nano. Lett. 12 (2012) 780-783.

39. A. Nieto, D. Lahiri, A. Agarwal, Carbon. 50 (2012) 4068-4077.

40. A. Umar, Y. B. Hahn, Nanotechnology. 17 (2006) 2174-2180.

41. X. Liu, N. Wen, X. Wang, Y. Zheng Nanomater. Nanotechnol. 5 (2015) 1-7.

42. H. Zou, S. Wu, Shen, J. Chem. Rev. 108 (2008) 3893-3957.

43. M. R. Vengatesan, V. Mittal Spherical fibrous fill compos. Wiley-VCH Verlag GmbH & Co. KGaA (2016) 1-38.

44. N. L. W. Septiani, B. Yuliarto, Nugraha, H. K. Dipojono, Appl. Phys. A Mater. Sci. Process. 123 (2017) 1-9.

45. X. Lu, D. Chao, J. Chen, W. Zhang, Y. Wei, Mater. Lett. 60 (2006) 2851-2854.

46. N. V. Konduru, R. J. Jimenez, A. Swami, S. Friend, V. Castranova, P. Demokritou, J. D. Brain , R. M. Molina, Part Fibre Toxicol. 12 (2015) 31.

47. S. Paszkiewicz, I. Pawelec, A. Szymczyk, Z. Rosłaniec, Polish. J. Chem. Technol. 17 (2015) 74-81.

48. J. Wan, A. F. Kaplan, J. Zheng, X. Han, Y. Chen, N. J. Weadock, N. Faenza, S. Lacey, T. Li, J. Guo, L. Hu, J. Mater. Chem. A. 2 (2014) 6051-6057.

49. M. M. Shahjamali, M. Salvador, M. Bosman, D. S. Ginger, C. Xue, J. Phys. Chem. C. 118 (2014) 12459-12468.

50. M. Bhattacharya, Materials. 9 (2016) 1-35.

51. R. Stephen, S. Thomas, Rubber nanocomposites. John Wiley & Sons, Ltd; (2010) 1-19.

52. A. P. Kumar, D. Depan, T. N. Singh, R. P. Singh, Prog. Polym. Sci. 34 (2009) 479-515.

53. W. Macyk, K. Szaciłowski, G. Stochel, M. Buchalska, J. Kuncewicz, P. C. Èabuz, Chem. Rev. 254 (2010) 2687-2701.

54. A. J. María, A. Sotto, R. G. del, A. Martínez, S. Molina, S. B. Teli, J. Abajo, J. Memb. Sci. 428 (2013) 131-141.

55. A. C. Matos, C. F. Marques, R. V. Pinto, I. A. C. Ribeiro, L. M. Gonçalves, M. A. Vaz, J. M. F. Ferreira, A. J. Almeida, A. F. Bettencourt, Int. J. Pharm. 490 (2015) 200- 208.

56. Abduljalil, A. Hashim, A. Jewad, Eur. J. Sci. Res. 63 (2011)231-235.

57. J. Ahmed, Y. A. Arfat, C. E. Aguirre, R. Auras. J. Therm. Anal. Calorim. 125 (2016) 205-214.

58. M. A. Bangar, W. Chen, N. V. Myung, Mulchandani, Thin Solid Films. 519 (2010) 964-973.

59. Y. Qi, J. Zhang, S. Qiu, L. Sun, F. Xu, M. Zhu, L. Ouyang, D. Sun, J. Therm. Anal. Calorim. 98 (2009) 533-537.

60. K. Liu, M. Zhong, J. Rare Earths. 28 (2010) 680-683.

61. J. Zhou, Q. Liu, W. Feng, Y. Sun, F. Li, Chem. Rev. 115 (2015) 395-465.

62. M. Majumder, R. B. Choudhary, A. K. Thakur, I. Karbhal, RSC Adv. 7 (2017) 20037-20048.

63. A. Janotti, C. G. Van de Walle, Rep. Prog. Phys. 2 (2009) 126501-126530.

64. D. Vaishnav, R. K. Goyal, IOP Conf. Series Mater. Sci. Eng. 64 (2014) 012016-012025.

65. T. W. Quadri, L. O. Olasunkanmi, O. E. Fayemi, M. M. Solomon, E. E. Ebenso, ACS Omega. 2 (2017) 8421-8437.

66. L. A. Garcı´a-Cerda, L. E. Romo-Mendoza, M. A. Quevedo-Lo´pez, J. Mater. Sci. 44 (2009) 4553-4556.

67. K. Karthik, G. K. Selvan, M. Kanagaraj, S. Arumugam, N. V. Jaya, J. Alloy Comp. 509 (2011) 181-184.

68. B. H. Shambharkar, S. S. Umare, J. Appl. Polym. Sci. 122 (2011) 1905-1912.

69. E. Soleimani, F. B. Niavarzi, J. Mater. Sci: Mater. Electron. 29 (2018) 2392-2405.

70. Y. J. Lim, Y. H. An, N. J. Jo, Nanoscale Res. Lett. 7 (2012) 19-25.

71. D. K. Koli, G. Agnihotri, R. Purohit, IJLTET. 2 (2013) 486-493.

72. S. Rajesh , B. VijayaRamnath , C. Elanchezhian, N. Aravind, V. Vijai Rahul, S. Sathish, Proc. Eng. 97 (2014) 598-606.

73. B. J. Ash, D. F. Rogers, C. J. Wiegand, L. S. Schadler, R. W. Siegel, B. C. Benicewicz, T. Apple, Polym. Compos. 23 (2002) 1014-1025.

74. L. Chen, D. Liu, P. Yang, RSC Adv. 9 (2019) 12793-12800.

75. Y. Zhang, Z. Bakenov, T. Tan, J. Huang, Metals. 8 (2018) 461-471.

76. A. Parveen, A.S. Roy, Adv. Mat. Lett. 4 (2013) 696.

77. A. Chandra, L.S. Turng, S. Gong, D.C. Hall, D.F. Caulfield, H. Yang, Polym. Compos. 28 (2007) 241-250.

78. A. H. Yuwono, B. Liu, J. Xue, J. Wang, H. I. Elim, W. Ji, Y. Li, T. J. White, J. Mater. Chem. 14 (2004) 2978-2987.

79. A.A. Haroun, A.M. Youssef, Synt. Metals. 161 (2011) 2063-2069.

80. C. Hu, Z. Zhang, H. Liu, P. Gao, Z. L. Wang, Nanotechnol. 17 (2006) 5983-5987.

81. M. Kamruddin, P. K. Ajikumar, R. Nithya, G. Mangamma, A. K. Tyagi, R. Baldev, Powder Technol. 161 (2006) 145-146.

82. D. Schubert, R. Dargusch, J. Raitano, S. W. Chan, Biochem. Biophys. Res. Commun. 342 (2006) 86-91.

83. T. J. Brunner, P. Wick, P. Manser, P. Spohn, R. N. Grass, L. K. Limbach, Environ. Sci. Technol. 40 (2006) 4374-4381.

84. X. Lu, D. Zheng, P. Zhang, C. Liang, P. Liu, Y. Tong, Chem. Commun. 46 (2010) 7721-7723.

85. M. Aguirre, E. J. S. Sandoval, M. Johansson, A. Ahniyaz, M. Paulis, J. R. Leiza, J. Mater. Chem. A. 2 (2014) 20280-20287.

86. N. Parvatikar, M. V. N. Ambika Prasad, J. Appl. Polym. Sci. 100 (2006) 1403-1405.

87. P. Latha, K. Prakash, S. Karuthapandian, Res. Chem. Intermed. 44 (2018) 5223-5240.

88. P. Goel, M. Arorab, RSC Adv. 5 (2015) 14974-14981.

89. Z.Guo, H. W. Ng, G. L. Yee, H. H. Thomas, J. Nanosci. Nanotechnol. 9 (2009) 3278-3285.

90. G. Kickelbick, Hybrid Materials: Synthesis, Characterization, and Applications: Wiley-VCH. (2007).

91. E. Ruiz-Hitzky, P. Aranda, M. Darder, M. Ogawa, Chem. Soc. Rev. 40 (2011) 801-828.

92. G. Kickelbick, J. Sol-Gel Sci. Technol. 46 (2008) 281-290.

93. C. S.Wu, H. T. Liao, J. Appl. Polym. Sci. 88 (2003) 966-972.

94. W. Bahloul, V. L. Legaré, G. Seytre, P. Cassagnau, J. Sol-Gel Sci. Technol. 57 (2011) 86-94.

95. W. Bahloul, O. Oddes, V. B. Legaré, F. Mélis, P. Cassagnau, B. Vergnes, AlChE J. 57 (2011) 2174-2184.

96. Ray, M. Okamoto, Prog. Polym. Sci. 28 (2003) 1539-1641.

97. G. Odian, Principles of polymerization. John Wiley & Sons, Inc., Hoboken, New Jersey, fourth ed. (2004).

98. F. Zhang, Y. Wang, C. Chai, Polym. Int. 53 (2000) 1353-1359.

99. H. Hu, X. Wang, J. Wang, L. Wan, F. Liu, H. Zheng, R. Chen, C. Xu, Chem. Phys. Lett. 484 (2010) 247-253

100. M. Hassan, K. R. Reddy, E. Haque, A. I. Minett, V. G. Gomes, J. Colloid Interface Sci. 410 (2013) 43-51.

101. Z. Sedla´kova, J. Plesˇtil, J. B. M. Sˇ louf, P. Holub, Polym. Bull. 63 (2009) 365-384.

102. J. I. Hong, L. S. Schadler, R. W. Siegel, Appl. Phys. Lett. 82 (2003) 1956-1958.

103. Z. M. Dang, L. Z. Fan, S. J. Zhao, C. W. Nan. Mater. Res. Bull. 38 (2003) 499-507.

104. M. Wong, R. Tsuji, S. Nutt, S. J. Su, Soft Matter. 6 (2010) 4482-4490.

105. F. Hussain, M. Hojjati, M. Okamoto, R. E. Gorga, J Compos. Mater. 40 (2006) 1511-1575.

106. M. M. Demir, G. Wegner, Macromol. Mater. Eng. 297 (2012) 838-863.

107. Ö. Tunusoğlu, M. M. Demir, Ind. Eng. Chem. Res. 52 (2013) 13401-13410.

108. A. Anzlovar, Z. C. Orel, M. Zigon, Eur. Polym. J. 46 (2010) 1216-1224.

109. K. L. Wu, S. C. Chou, Y. Y. Cheng, J. Appl. Polym. Sci. 116 (2010) 3111-3117.

110. C. J. Zhou, X. Y. Qiu, Q. X. Zhuang, Z. W. Han, Q. L. Wu, J. Appl. Polym. Sci. 124 (2012) 4740.

111. H. Baniasadi, A. Ramazani, S. Nikkhah, J. Mater. Des. 31 (2010) 76-84.

112. S. Gnanam, V. Rajendran, J. Sol-Gel Sci. Technol. 58 (2011) 62-69.

113. P. Sun, L. Liu, S. C. Cui, J. G. Liu, Catal. Lett. 144 (2014) 2107-2113.

114. M. Bahar, M. Mozaffari, S. Esmaeili, J. Theor. Appl. Phys. 11 (2017) 79-86.

115. M. Farahmandjou, M. Zarinkamar, J. Ultrafine Grained Nanostruct. 48 (2015) 5-10.

116. H. Kavas, M. Gunay, A. Bayal, M.S. Toprak, H. Sozeri, S. Aktas, J. Inorg. Organomet. Polym. 23 (2013) 306-314.

117. M. T. Ramesan, Int. J. Plast. Technol. 19 (2015) 368-380.

118. R. Gangopadhyay, A. De, Chem. Mater. 12 (2000) 608-622.

119. R. F. Mulligan, A. A. Iliadis, P. J. Kofinas, Appl. Polym. Sci. 89 (2003) 1058-1061.

120. S. S. Bhattacharya, S. B. Chaudhari, Int. J. Eng. Res. Dev. 7 (2013) 01-05.

121. J. Jancar, J. F. Douglas, F. W. Starr, S. K. Kumar, P. Cassagnau, A. J. Lesser, S. S. Sternstein, M. J. Buehler, Polymer. 51 (2010) 3321-3590.

122. P. B. Johnson, R. W. Christy, Phys. Rev. B. 16 (1972) 4370-4379.

123. K. Suhailath, P. Jayakrishnan, B. Naufal, P. Periyat, V. C. Jasna, M. T. Ramesan, Adv. Polym. Tech. 37 (2016) 1114.

124. S. Chaudhari, T. Shaikh, P. Pandey, Int. J. Eng. Res. Appl. 3 (2013) 1386-1391.

125. S. K. Kumar, N. Jouault, Macromolecules. 46 (2013) 3199-3214.

126. S. J. Park, M. S. Cho, S. T. Lim, H. J. Cho, M. S. Jhon, Macromol. Rapid. Commun. 24 (2003) 1070-1073.

127. K. Suhailath, M. T. Ramesan, B. Naufal, P. Periyat, V. C. Jasna, P. Jayakrishnan, Polym. Bull. 74 (2016) 671-688.

128. S. Mugundan, G. Rajamannan, N. Viruthagiri, R. Shanmugam, P. Gobi, Appl. Nanosci. 5 (2015) 449–456.

129. A. Shahzada, A. Sharif and S. A. Agnihotry, Bull. Mater. Sci. 30 (2007) 31-35.

130. C. Rameshkumar, S. Sarojini, K. Naresh, R. Subalakshmi, J. Surface Sci. Technol. 33 (2017) 12–18.

131. D. J. Park, T. Sekino, S. Tsukuda, A. Hayashi, T. Kusunose, S. I. Tanaka, J. Solid State Chem. 84 (2011) 2695–2700.

132. N. W. Elshereksi, S. H. Mohamed, A. Arifin, Z. A. M. Ishak, J. Phys. Sci. 25 (2014) 15–27.

133. Y. Zare, Appl. Clay Sci. 115 (2015) 61–66.

134. A. Monfared, A. J. Arani, Appl. Clay Sci. 108 (2015) 1–11.

135. Hemlata, S. N. Maiti, J. Appl. Polym. Sci. 132 (2015) 41381.

136. M. Atai, A. Pahlavan, N. Moin, Dent. Mater. J. 28 (2012) 133-145.

137. A. Einstein, R. Fürth, Dover Publications; 1956.

138. S. Ahmed, F. Jones, J. Mater. Sci. 25 (1990) 4933–4942.

139. E. Guth, J. Appl. Phys. 16 (1945) 20-25.

140. E. Kerner, Proc. Phys. Soc. B. 69 (1956) 808-813.

141. B. Pukanszky, Composites. 21 (1990) 255–262.

142. A. Lazzeri, V. T. Phuong, Compos. Sci. Technol. 93 (2014) 106–113.

143. A. M. K. Aippunny, S. M. Shamsudeen, P. Valparambil, S. Mathew, U. N. Vishwambharan, J. Appl. Polym. Sci. 133 (2016) 43568.

144. M. Subburaj, M. T. Ramesan, P. P. Pradyumnan, AIP Conf Proc 1620 (2014) 541–548.

145. N. J. S. Sohi, S. Bhadra, D. Khastgir, Carbon. 49 (2011) 1349-1361.

146. K. Jonscher, Andrew, J. Phys. D Appl. Phys. 32 (1999) 57-70.

147. M. E. Leyva, G. M. O. Barra, A.C.F. Moreira, B. G. Soares, D. Khastgir, J. Polym. Sci. Polym. Phys. 41 (2003) 2983-2997.

148. M. T. Ramesan, P. Jayakrishnan, J. Inorg. Organomet. Polym. Mater. 27 (2017) 143-153.

149. R. Taherian, ECS J. Solid State Sc. 3 (2014) 26-38.

150. R. L. McCullough, Compos. Sci. Technol. 22 (1985) 3–21.

151. F. Bueche, J. Appl. Phys. 43(1972) 4837–4838.

152. R. M. Scarisbrick, J. Phys. D Appl. Phys. 6 (1973) 2098–2110.

153. E.P. Mamunya, V.V. Davidenko, E.V. Lebedev, Compos. Interfaces. 4 (1996) 169-176.

154. R. Kotsilkova, V. Petkova, Y. Pelovski, J. Therm. Anal. Calorim. 64 (2001) 591–598.

155. M. T. Ramesan, V. Nidhisha, P. Jayakrishnan, Mater. Sci. Semicond. Process. 63 (2017) 253-260.

156. G. M. Joshi, K. Deshmukh, J. Electron. Mater. 43 (2014) 1161-1165.

157. M. T. Ramesan, V. Santhi, J. Mater. Sci. 28 (2017) 18804-18814.

158. S. Chaudhari, T. Shaikh, P. Pandey, Int. J. Eng. Res. Appl. 3 (2013) 1386-1391.

159. M. Khairy, N. H. Amin, R. Kamal, J. Therm. Anal. Calorim. 128 (2017) 1811–1824.

160. A. Chatterjee, J. Appl. Polym. Sci. 118 (2010) 2890–2897.

161. O. U. Rahman, S. S. Ahmad, RSC Adv. 6 (2016) 10584–10596.

162. T. P. Shendea, B. A. Bhanvasea, A. P. Rathodb, D. V. Pinjaric, S. H. Sonawane , Ultrason. Sonochem. 41 (2018) 582–589.

163. N. Shaari, S. H. Tan, A. R. Mohamed, J. Rare Earth. 30 (2012) 651–658.

164. S. Maddila, E. O. Oseghe, S. B. Jonnalagadda, J. Chem. Technol. Biotechnol. 91 (2016) 385–393.

165. S. Sugumaran, C. S. Bellan, Opt. Int. J. Light Electron Opt. 125 (2014) 5128–5133.

166. H. Yuvaraj, W. S. Kim, J. T. Kim, I. P. Kang, Y. S. Gal, S. W. Kim, K. T. Lim, Mol. Cryst. Liq. Cryst. 514 (2009) 355–365.

167. A. H. Yuwono, J. Xue, J. Wang, H. I. Elim, W. Ji, Y. Li, T. White, J Mater Chem. 13 (2003) 1475–1479.

168. T. Sampreeth, M. A. Al-Maghrabi, B. Bahuleyan, M. T. Ramesan, J. Mater. Sci. 53 (2018) 591–603.

169. E. Ndinda, H. Park, K. N. Kim, Kor. J. Mater. Res. 24 (2014) 33- 36.

170. M. S. Gaur, P. K. Singh, A. P. Indolia, P. K. Yadav, A. A. Rogachev, A. V. Rogachev, Ferroelectrics. 510 (2017) 56–70.

171. M. Marinovic, J. Vukovic, K. Jeremic, J. M. Nedeljkovic, Polym.Compos. 30 (2009) 737-742.

172. M. T. Ramesan, V. Santhi, J. Mater. Sci: Mater. Electron. 28 (2017) 18804–18814.

173. A. Laachachi, M. Ferriol, M. Cochez, D. Ruch, J. M. L. Cuesta, Polym. Degrad. Stab. 93 (2008) 1131–1137.

174. O. Takashi, K. Yutaka, J. Made, I. Toru, O. Kikuo, Ind. Eng. Chem. 47 (2008) 2597-2604.

175. A. Lazzeri, V. T. Phuong, Compos. Sci. Technol. 93 (2014) 106-113.

176. S. Y. Zare, RSC Adv. 6 (2016) 57969–57976.

177. Y. Zare, K. Y. Rhee, S. Park, J. Appl. Polym. Sci. 134 (2017) 44869–44875.

178. J. L. Milner, C. Bunget, F. A. Farha, T. Kurfees, V. H. Hammond, J. Manuf. Process. 15 (2013) 219–226.

179. P. Jayakrishnan, M.T. Ramesan, Mater. Chem. Phys. 186 (2017) 513-522.

180. V. C. Jasna, M.T. Ramesan, J. Inorg. Organomet. Polym. 27 (2017) 968-978.

181. M.T. Ramesan, P. Jayakrishnan, T. Sampreeth, P. P. Pradyumnan, J. Therm. Anal. Calorim. 129 (2017) 135-145.

182. P.W. Chen, D.D.L. Chung, J. Electron. Mater. 24 (1995) 47-51.

183. X. Wu, S. Qi, J. He, G. Duan, J. Mater. Sci. 45 (2010) 483-489.

184. C. Lu, Y.W. Mai, J. Mater. Sci. 43 (2008) 6012-6015.

185. F. Lux, J. Mater. Sci. 28 (1993) 285-301.

186. K. Miyasaka, K. Watanabe, E. Jojima, H. Aida, M. Sumita, K. Ishikawa, J. Mater. Sci. 17 (1982) 1610-1616.

187. S. Salimian, M. E. A. Araghi, A. N. Golikand, J. Phys. Chem. Solids. 91 (2016) 170–181.

188. S. T. Navale, G. D. Khuspe, M. A. Chougule, V. Patil, J. Phys. Chem. Solids. 75 (2014) 236–243.

189. S. Kango, S. Kalia, A. Celli, J. Njuguna, Y. Habibi, R. Kumar, Prog. Polym. Sci. 38 (2013) 1232-1261.

190. D.J.Y.S. Pagé, N. Cunningham, N. Chan, G. Carran, J. Kim, J.

Vinyl Addit. Technol. 13 (2007) 91-97.

191. Z. Matusinovic, R. Shukla, E. Manias, C. G. Hogshead, A. Charles, Wilkie, Polym. Degrad. Stabil. 97 (2012) 2481-2486.

192. J.M. Lee, D.S. Kim, Polym. Compos. 28 (2007) 325-330.

193. R. Gangopadhyay, A. De, Chem. Mater. 12 (2000) 608-622.

194. Z. Wei, G. Wang, P. Wang, L. Liu, M. Qi, Polym. Eng. Sci. 52 (2012) 1047-1057.

195. F.S. Shariatmadar, M.M. Nia, Polym. Compos. 33 (2012) 1188-1196.

196. H. Xia, Q. Wang, Chem. Mater. 14 (2002) 2158–2165.

197. Y. Man, L. Mu, Y. Wang, S. Lin, G.L. Rempel, Q. Pan, Polym. Compos. 36 (2015) 8-16.

198. S.M. Khaled, R. Sui, P.A. Charpentier, A.S. Rizkalla, Langmuir. 23 (2007) 3988-3995.

199. L.M. Hamming, R. Qiao, P.B. Messersmith, L. C. Brinson, Compos. Sci. Technol. 69 (2009) 1880.

200. X. Wu, P. Su, H. Liu, L. Qi, J. Rare Earths. 27 (2009) 739-743.

201. G. Gu, Z. Zhang, H. Dang, Appl. Surf. Sci. 221 (2004) 129-135.

202. H. Kim, Y. Wang, M. A. Winnik, Polymer. 35 (1994) 1779-1786.

203. K. Suhailath, M.T. Ramesan, J. Mater. Sci. Mater. Electron. 28 (2017) 13797-13805.

204. A. Bokare, M. Pai, A.A. Athawale, Solar Energy. 91 (2013) 111-119.

205. X.M. Shi, J. Zhang, D.R. Li, S.J. Chen, J. Appl. Polym. Sci. 112 (2009) 2358-2365.

206. H. Yang, W. Jiang, Y. Lu, Mater. Lett. 61 (2007) 2789-2818.

207. F. Yang, G.L. Nelson, J. Appl. Polym. Sci. 91 (2004) 3844-3850.

208. N.W. Elshereksi, S.H. Mohamed, A. Arifin, Z.A. M. Ishak, J. Phys. Sci. 25 (2014) 15-27.

209. M.T. Ramesan, T. Sampreeth, J. Mater. Sci. Mater. Electron. 28 (2017) 16181-16191.

210. M.T. Ramesan, C. Jose, P. Jayakrishnan, T. Anilkumar, Polym. Compos. 39 (2018) 38-45.

211. P.K.C. Pillai, P. Khurana, A. Tripathi, J. Mater. Sci. Lett. 5 (1986) 629-632.

212. R. Punia, R. S. Kundu, S. Murugavel, N. Kishore, J. Appl. Phys. 112 (2012) 113716.

213. B. S. Li, M. S. Toprak, Y. S. Jo, J. Dobson , D. K. Kim, M. Muhammed, Adv. Mater. 19 (2007) 4347-4352.

214. M.T. Ramesan, P. Jayakrishnan, J. Inorg. Organomet. Polym. 27 (2017) 323-333.

215. M. Rahaman, T. K. Chaki, Compos. Sci. Technol. 72 (2012) 1575-1580.

216. Y. P. Mamunya, V.V. Davydenko, P. Pissis, E.V. Lebedev, Eur. Polym. J. 38 (2002) 1887–1897.

217. S. Mallakpour, M. Dinari, J. Therm. Anal. Calorim. 114 (2013) 329-337.

218. R. Nosrati, A. Olad, F. Maryami, Chem. Intermed. 44 (2018) 6219-6237.

219. M.T. Ramesan, K. Nushhat, K. Parvathi, T. Anilkumar, J. Mater. Sci. Mater. Electron. 30 (2019) 13719-13728.

220. Z. Jing, J. Zhan, Adv. Mater. 20 (2008) 4547-4551.

221. L. Song, F. Tang, Z. Xiao, Z. Cao, H. Zhu, A. Li, J. Electron. Mater. 47 (2018) 5896-5904.

222. S. H. Deshmukh, D. K. Burghate, V. P. Akhare, V. S. Deogaonkar, V. T. Deshmukh, M. S. Deshmukh, Bull. Mater. Sci. 30 (2006) 51-56.

223. M. Paulo, Q. Syed, Langmuir. 20 (2004) 3424-3430.

224. S. M. Imran, G. N. Shao, M. S. Haider, N. Abbas, M. Hussain, H. T. Kim, J. Appl. Polym. Sci. 132 (2015) 41800.

225. L. M. Wei, T. Tang, B. T. Huang, J. Polym. Sci. Polym. Chem. 42 (2004) 941-949.

226. Y. Chen, Z. Li, N. Tribol. Int. 82 (2015) 211-217.

227. M. T. Ramesan, P. K. Dilsha, Mater. Res. Express 6 (2019) 105328-105333.

228. J. Hu, M. Chen, L. Wu, Polym. Chem. 2 (2011) 760-772.

229. V.R. Madduluri, B. D. Raju, K.S.R. Rao, Res. Chem. Intermediat. 45 (2019) 2749.

230. A. Miren, J. S. Eric, J. Mats, A. Anwar, P. Maria, R. L. Jose, J. Mater. Chem. A. 2 (2014) 20280-20287.

231. M. Farahmandjou, M. Zarinkamar, J. Ultrafine Grained Nanostruct. 48 (2015) 5-10.

232. N. Z. Yahya, M. Rusop, J. Nanomaterials. 4 (2012) 257-262.

233. S. Manish, K. D. Ashok, K. Partha, U. Elias, H. K. Nam, H. L. Joong, J. Mater. Chem. A.1 (2013) 9792.

234. W. Du, L. Jiang, M. Shi, Z. Yang, X. Zhang, RSC Adv. 9 (2019) 1602-1612.

235. S. K. Chi, M. O. Seung, Electrochim. Acta. 46 (2001) 1323-1331.

236. Z. Wenge, W. Shing-Chung, Compos. Sci. Technol. 63 (2003) 225-235.

237. C. Basavaraja, Y. M. Choi, H. T. Park, D. S. Huh, J. W. Lee, M. Revanasiddappa, S. C. Raghavendra, S. Khasim, T. K.

Vishnuvardhan, Bull. Korean Chem. Soc. 28 (2007) 1104-1108.

238. M.E. Brown, A.K. Galweyl, Proc. Math. Phys. Sci. 450 (1995) 501-512.

239. A.K. Jonscher, Thin Solid Films. 1 (1967) 213-234.

240. A. R. Long, Adv. Phys. 31 (1982) 553-637.

241. P. Mannu, M. Palanisamy, G. Bangaru, S. Ramakrishnan, A. Kandasami, N. Kumar, Appl. Phys. A. 125 (2019) 458.

242. T. Kuilla, S. Bhadra, D. Yaoa, N. H. Kim, S. Bose, J. H. Lee, Progress. Polym. Sci. 35 (2010) 1350-1375.

243. V. Dhand, G. Mittal, K. Y. Rhee, S. J. Park, D. Hui, Composites: Part B. 73 (2015) 166-180.

244. M. K. Poddar, S. Sharma, V. S. Moholkar, Polymer. 99 (2016) 453-469.

245. T. P. Nguyen, Surf. Coat. Tech. 206 (2011) 742-752.

246. M. Kanda, Y. Nishi, Mater. Trans. 50 (2009) 177-181.

247. S. Mallakpour, V. Behranvand, Eur. Polym. J. 84 (2016) 377-403.

248. X. Zhao, L. Lv, B. Pan, W. Zhang, S. Zhang, Q. Zhang, Chem. Eng. J. 170 (2011) 381-394.

249. P. Jayakrishnan, M. T. Ramesan, Polym. Compos. 39 (2018) 2791-2800.

250. N. Salah, S. S. Habib, Z. H. Khan, S. A. Hamedi, S. P. Lochab, J. Lumin. 129 (2009) 192-196.

251. M. Zawadzki, L. K. Epi´nski, J. Alloys Compd. 380 (2004) 255-259.

252. R. Yuvakkumar, S. I. Hong, J. Sol-Gel Sci. Technol.73 (2015) 511-517.

253. J. Wang, Y. Zheng, Y. Kang, A.Wang, Chem. Eng. J. 223 (2013) 632-637.

254. M. K. Poddar, S. Sharma, V. S. Moholkar, Polymer. 99 (2016) 453-469.

255. R. Y. Hong, J. Z. Qian, J. X. Cao, Powder Technol. 163 (2006) 160-168.

256. X. Tong, T. Tang, Q. Zhang, Z. Feng, B. Huang, J. Appl. Polym. Sci. 83 (2002) 446-454.

257. C. Basavaraja, Y. M. Choi, H. T. Park, D. S. Huh, J. W. Lee, M. Revanasiddappa, S. C. Raghavendra, S. Khasim, T. K. Vishnuvardhan, Bull. Korean Chem. Soc. 28 (2007) 1104-1108.

258. A. Navidfar, T. Azdast, A. K. Ghavidel, J. Appl. Polym. Sci. 133 (2016) 43738.

259. B. Sannakki, Anita, Physics Procedia. 49 (2013) 15-26.

260. G. Zhang, D. Brannum, D. Dong, L. Tang, E. Allahyarov, S. Tang, K. Kodweis, J. K. Lee, L. Zhu, Chem. Mater. 28 (2016) 4646-4660.

261. S. J. F. Byrnes, Basic theory and phenomenology of polarons (2008).

262. S. Rajendran, O. Mahendran, K. Krishnaveni, J. New Mat. Electrochem. Systems. 6 (2003) 25-28.

263. T. Y. Suroor, M. A. El-Ziady, Mater. Chem. Phys.77 (2002) 697-703.

264. H. Wolf, M. Willert-Porada, J. Power Sources. 153 (2006) 41-46.

LIST OF PUBLICATIONS

1. K. Suhailath, M. T. Ramesan, B. Naufal, P. Periyat, V. C. Jasna, P. Jayakrishnan, Synthesis, characterisation and flame, thermal and electrical properties of poly (n-butylmethacrylate)/titanium dioxide nanocomposites, Polym. Bull. 74 (2016) 671-688.

2. K. Suhailath, P. Jayakrishnan, B. Naufal, P. Periyat, V. C. Jasna, M. T. Ramesan, Synthesis by in situ free radical polymerization, characterization, and properties of poly (n-butylmethacrylate)/samarium-doped titanium dioxide nanoparticles composites, Adv. Polym. Tech. 37 (2016) 1114.

3. K. Suhailath, M. T. Ramesan, Effect of titanium dioxide nanoparticles on temperature dependent electrical conductivity of poly (n-butylmethacrylate) nanocomposites: Application of different conductivity models, AIP Conference Proceedings. 020035 (2017) 1849.

4. K. Suhailath, M. T. Ramesan, Temperature dependent AC conductivity, mechanical and different DC conductivity modeling of poly (butylmethacrylate)/samarium doped titanium dioxide nanocomposites J. Mater. Sci. Mater. Electron. 28 (2017) 13797.

5. K. Suhailath, M. T. Ramesan, Effect of nano-Ce-doped TiO_2 on AC conductivity and DC conductivity modeling studies of poly (n-butylmethacrylate), J. Elec. Mater. 47 (2018) 6484-6493.

6. K. Suhailath, M. T. Ramesan, Investigations on the structural, mechanical, thermal, and electrical properties of Ce-doped TiO_2/poly (n-butyl methacrylate) nanocomposites, J. Therm. Anal. Calorim. 135 (2019) 2159.

7. K. Suhailath, M. T. Ramesan, Effect of neodymium-doped titanium dioxide nanoparticles on the structural, mechanical, and electrical properties of poly (butylmethacrylate) nanocomposites J. Vinyl Addit. Techn. 25 (2019) 9-18.

8. K. Suhailath, M. T. Ramesan, Theoretical and experimental studies on DC conductivity and temperature dependent AC conductivity of poly (butylmethacrylate)/Nd-TiO_2 nanocomposites, J. Thermoplast. Compos. Mater. 33 (2020) 1061-1077.

9. K. Suhailath, M. T. Ramesan, Effect of ceria nanoparticles on mechanical properties, thermal and dielectric properties of poly (butylmethacrylate) nanocomposites, Polym. Compos. 41 (2020) 2344-2354.

10. K. Suhailath, Meenu Thomas, M. T. Ramesan, Effect of temperature on AC conductivity of poly (butylmethacrylate)/cerium dioxide nanocomposites and applicability of different conductivity modeling studies, Res. Chem. Intermed. (2020) doi: 10.1007/s 11164-020-04107-w

11. K. Suhailath, Meenu Thomas, M. T. Ramesan, Studies on mechanical properties, dielectric behavior and DC conductivity of neodymium oxide/poly (butylmethacrylate) nanocomposites. Polym. Polym. Compos. (2020) doi: 10.1177/0967391120960658.

12. K. Suhailath, B. K. Bahuleyan, M. T. Ramesan, Synthesis, characterization, thermal properties and temperature-dependent AC conductivity studies of poly (butylmethacrylate)/neodymium oxide nanocomposites, J. Inorg. Polym. Mater. (2020) doi: 10.1007/s10904-020-01665-9.

Presentations

1. K. Suhailath and M. T. Ramesan, Effect of titanium dioxide nanoparticles on temperature dependent electrical conductivity of poly (n-butylmethacrylate) nanocomposites: Application of different conductivity models, Optic's 17, A conference on light, NIT Calicut, 9-11th January, 2017

2. K. Suhailath and M. T. Ramesan, Effect of Ce doped TiO_2 nanoparticles on the dielectric properties of poly(n-butyl methacrylate)-National seminar, Frontiers in chemical science FCS-2018, Calicut University, 26-28th February, 2018

3. K. Suhailath and M. T. Ramesan, Preparation and tensile studies of PBMA/TiO_2 nanocomposites, MESMAC International conferences MES Mampad College, 15-17th January, 2019

4. K. Suhailath and M. T. Ramesan, Conductivity studies of poly (butylmethacrylate) (PBMA) based nanocomposites using CeO_2 nanoparticles, 31st Kerala Science Congress, 2-3 February 2019, Kollam

5. K. Suhailath, K. Parvathi, S. S. Menon and M. T. Ramesan, Thermal and Dielectric properties of poly (butylmethacrylate)/Nd-TiO_2 nanocomposites, National seminar, Frontiers in chemical science FCS-2019, Calicut University, 19-21th March, 2019

Book Chapter

1. M.T. Ramesan, K. Suhailath, Role of nanoparticles on polymer composites, Micro and Nano Fibrillar composites (MFCs and NFCs) from polymer blends, Woodhead publishing, Elsevier, ISBN: 978-0-08-101991-7